The Synthesis, Characterisation, and Application of Novel *N*-Ferrocenoyl Peptide Derivatives

To Jojo

Declaration

I hereby certify that this material, which I now submit for assessment on the programme of study leading to the award of Ph.D. is entirely my own work and has not been taken from the work of others save to the extent that such work has been cited and acknowledged within the text of my work,

Signed:_____ ID No:_____

Date:_____

Acknowledgements

Thanks are due first and foremost to Dr. Peter Kenny for his direction, patience, and enthusiasm during the course of this work.

To my fellow members of the Peter Kenny research group, Dave Savage, Frankie Anderson, Paula Kelly, and Steve Alley.

To Dr. John Gallagher for his input and contribution to this work.

Michael Burke, Maurice Burke, Vinnie Hooper, Damien McQuirke and all the technical staff at Dublin City University, for their willingness to assist at a moment's notice.

To my fellow postgraduates Jonathan Rochford, Andrea Dallas, Ian Grey, Mairead Sheridan, and Ger McDermott.

To Darren Walsh and Lorraine Keane for their assistance with the electrochemistry.

Abstract

In recent years, there has been an increasing focus on the design and synthesis of electrochemical biosensors, as they can lead to the analytical determination of biological and organic analytes. As amino acids and peptides play such a diverse role within biological systems, incorporation of a redox active, chromophoric group into these compounds is of particular interest. This coupling is usually carried out as the last step in the preparation of such bioorganometallic compounds, as work the ferrocene moiety can prove sensitive to the conditions employed during peptide synthesis. To this end, novel ***N***-ferrocenoyl mono and dipeptide derivatives, with varying structural motifs, have been prepared using a variety of coupling methods, and the conditions for their preparation optimised. All compounds were characterized by ^{1}H, ^{13}C, 135DEPT and HMQC NMR, I.R., optical rotation, and UV-Vis spectroscopy, as well as cyclic voltammetry. The preparation of asymmetrically di-substituted ferrocene derivatives (**140-146**), without isolation of intermediates, is also reported.

The anion binding abilities of selected compounds is reported, capitalising on the presence of the ^{1}H NMR-detectable amide protons within these compounds, as well as the electroactive ferrocene group. All compounds selected for these studies showed, to varying degrees, downfield chemical shifts in their ^{1}H-NMR spectra in the presence of anions, as well as cathodic shifts in their cyclic voltammograms. The number of amide groups, as well as their relative orientation within the compound, is considered to be of prime importance. The ***N***-ferrocenoyl mono-peptide derivatives are seen to exhibit reversible electrochemical behaviour in the presence of halide ions, while the dipeptides, both mono and 1, 1' disubstituted, bind these anions irreversibly.

Table of Contents

Chapter III: The Synthesis and Characterisation of *N*-Ferrocenoyl Dipeptides

Chapter IV: The Synthesis and Characterisation of 1, 1'-*N*-Ferrocenoyl Symmetric Dipeptides

Chapter I

Literature Survey

1.1: Ferrocene

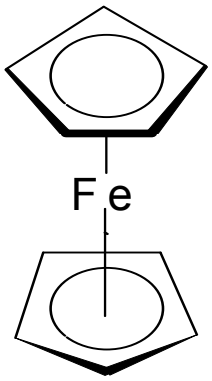

1

Ferrocene (**1**) was first isolated in 1951 by two independent research groups. The orange compound was found to be air-stable, insoluble in water, and had a melting point of 173^0C [1, 2]. These observations precluded the possibility that the bonding within the molecule was purely a result of either C-Fe σ-bonds or ionic interactions. The following year, the correct structure of ferrocene was elucidated, again by two independent groups. Wilkinson concluded that since all the carbons were electronically equivalent, and, as there was only one C-H stretching frequency observed in the I.R. spectrum, all carbons must contribute equally in bonding to the iron atom [2]. X-ray diffraction studies by Fischer and Pfab [3] confirmed the proposed sandwich structure, in which a central iron atom was located between two cyclopentadienyl rings. The aromaticity of the compound was confirmed by Woodward, who performed electrophilic aromatic substitution reactions, such as the Friedel-Crafts acylation with aluminium trichloride, on the compound (ferrocene was found to react 3 x 10^6 times faster than benzene) [4].

The two cyclopentadienyl (Cp) rings of ferrocene may be orientated in two extremes of either an eclipsed (D_{5h}) or staggered (D_{5d}) conformation. The energy of rotation about the Fe-Cp axis is very small (~ 4kJmol^{-1}) and the ground state structures of ferrocene may show either of these conformations.

1.2: The Chemistry of Ferrocene

Ferrocene (as well as other metallocenes) are usually prepared by one of three different synthetic routes. The first of these involves the cracking of dicyclopentadiene (a retro Diels-Alder reaction), followed by deprotonation of the weakly acidic cyclopentadiene with an alkali metal. Treatment with iron (II) chloride then affords ferrocene:

$$FeCl_2 + 2NaC_5H_5 \rightarrow [(\eta^5\text{-}\ C_5H_5)_2Fe]$$

The second method is known as metal vapour synthesis; the reactants are heated to high temperatures, and then brought together on a cold surface:

$$Fe + 2C_5H_6 \rightarrow [(\eta^5\text{-}\ C_5H_5)_2Fe] + H_2$$

Finally, ferrocene can also be prepared via the use of an auxiliary base, which generates the cyclopentadienyl anion *in situ*:

$$FeCl_2 + 2C_5H_6 + 2C_5H_5NH \rightarrow [(\eta^5\text{-}\ C_5H_5)_2Fe] + 2[C_5H_5NH_3]Cl$$

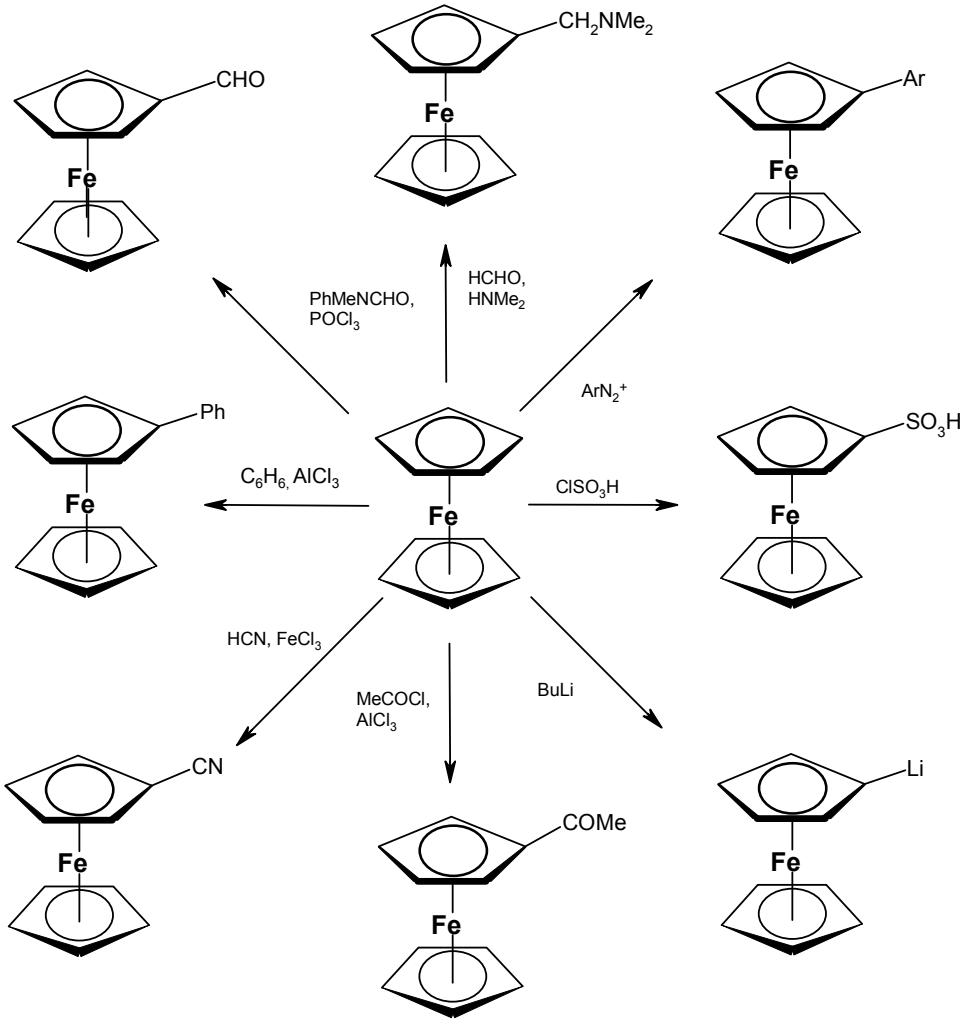

Scheme 1: The organic reactions of ferrocene

Because of its stability, the ferrocene moiety can survive relatively harsh reaction conditions, making a wide range of organic transformations possible (*scheme 1*). Ferrocene, having six

π-electrons delocalised over five atoms, is much more prone to electrophilic substitution than benzene. The ferrocenyl group is also one of the strongest known electron-releasing groups (aminoferrocene is twenty times more basic than aniline). Two main mechanistic routes have been proposed for the electrophilic substitution of ferrocene [5] (*scheme 2*).

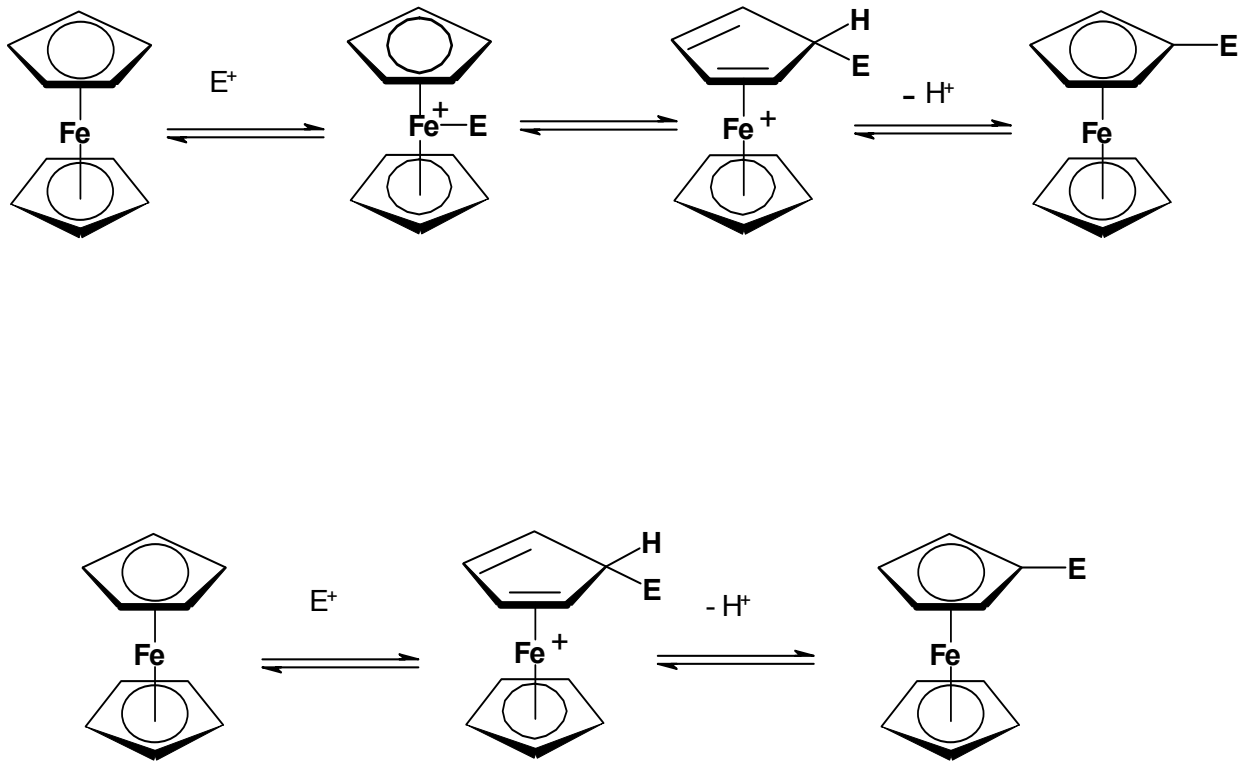

Scheme 2: Two mechanisms for electrophilic substitution of ferrocene

In the first of these, the electrophile interacts with the central iron atom, before being transferred to the aromatic ring with subsequent deprotonation. In the second, electrophilic attack takes place directly at the *exo* face of the ring, with no direct metal participation.

Friedel-Crafts acylation of ferrocene occurs readily, yielding both mono and 1, 1'-disubstituted products. Once acylation has occurred on one ring, the unsubstituted ring is deactivated towards further substitution by a factor of 2 x10^4, illustrating the electronic effects that are passed from one ring to another via the iron centre. The Friedel-Crafts alkylation of

ferrocene is not a useful synthetic method because of poor yields, and the resultant mixture of poly-alkylated products results.

Lithiation of ferrocene also occurs readily, with t-BuLi or n-BuLi the preferred reagents. As the protons of the aromatic rings of ferrocene are weakly acidic, it can be deprotonated by the hydrocarbon portion of the reagent, and the extent of lithiation can be controlled by choice of reaction conditions. The mono-lithiated intermediate can be formed exclusively via treatment of ferrocene with a stoichiometric amount of t-BuLi or i-BuLi, whereas the 1, 1'-disubstituted product is formed when n-BuLi is used in conjunction with *N,N,N′,N′*, tetramethylethylenediamine (TMEDA). No such selectivity is possible with either sodium or potassium reagents.

Unlike benzene, ferrocene can undergo the Mannich reaction with formaldehyde and an amine, and thus is more akin to thiophene than benzene in its reactivity. Another important difference between benzene and ferrocene is the behaviour of the latter in the presence of oxidising agents (*e.g.* NO_2^+, H_2SO_4). The iron centre is quite easily oxidized to the ferricenium ion, and so direct nitration, sulphonation, or halogenation cannot be carried out in a similar manner to benzene [1].

1.3: Electronic Structure of Ferrocene

Ferrocene can be considered as consisting of an Fe^{2+} ion (six d-electrons) bonded to two cyclopentadienyl anions (six π-electrons each), and thus it can be seen that ferrocene obeys the 18-electron rule – all valence electrons are located in bonding or non-bonding orbitals. The anti-bonding orbitals are left unpopulated, and hence the compound is stable.

A more informative picture of the bonding within ferrocene is provided by a molecular orbital diagram (*Fig. 1*), which shows the molecular orbitals which result from the interactions of the ligand and metal orbitals. Symmetry considerations, the relative energies, and overlap integrals of the ligand π-orbitals and the 3d, 4s and 4p orbitals of the central iron can be used to predict which molecular orbitals will be formed.

The lowest-energy orbitals are ligand-based (a_{1g}, a_{2u}), as the metal orbitals with appropriate symmetry requirements ($3d_z^2$/4s, and $4p_z$ respectively) are so much higher in energy. The e_{2g} orbitals remain essentially metal-based ($d_{x^2-y^2}$, d_{xy}), as their δ-overlap with the ligand e_{2g} orbitals is poor. The stability of the ferrocene molecule is largely due to the overlap of the ligand e_{1g} orbitals with the d_{xz} and d_{yz} orbitals of the iron atom, which results in the formation of two strong π-bonds.

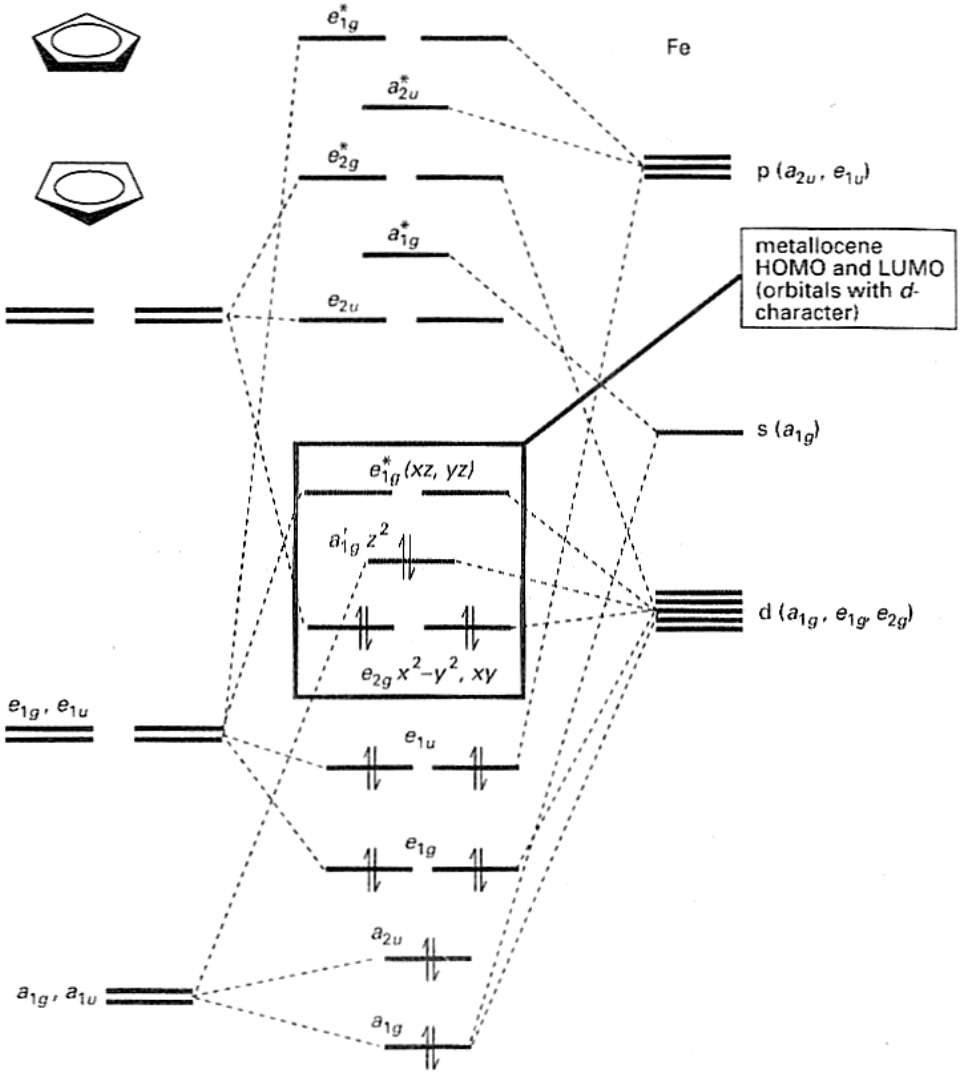

Fig. 1: A qualitative molecular orbital diagram for the ferrocene molecule [1]

The frontier orbitals of ferrocene are the weakly bonding e_{2g}, the non-bonding a'_{1g}, and the weakly anti-bonding, unoccupied e'_{1g} level. Given that these orbitals are similar in energy, it can be seen that deviations from the 18-electron rule are possible (*e.g.* the 16-electron chromocene and the 20-electron nickelocene, both of which are more reactive than ferrocene). Depending on the method employed in calculating the relative energies of the frontier orbitals, the HOMO of ferrocene can be considered as being the a'_{1g} ($3d_z^2$) [6], or the degenerate e_{2g} (d_x^2- $_y^2$, d_{xy}) pair [7]. This becomes important when considering the electronic structures of ferrocene derivatives, along with their spectroscopic and electrochemical

properties (section 1.4). The LUMO of ferrocene is derived from an out of phase π-interaction between the d_{xz}/d_{yz} iron orbitals, and the Cp e_{1g} orbitals [8].

1.4: Electronic Structure of Substituted Ferrocenes

The π-system of the Cp rings can interact with the π-system of a substituent, such as an acyl group, or the highly conjugated systems employed in the study of non-linear optics. The most significant perturbation to the molecular orbitals of ferrocene that occurs upon substitution with another π-system is not to the a'_{1g} (d_{z^2}) metal-based orbital, but to the degenerate e_{2g} ($d_{x^2-y^2}$, d_{xy}) pair. Upon substitution, the most important effect is the energy splitting between the two components of the e_{2g} energy level. One component of this degenerate pair will have the proper nodal characteristics to interact with the substituent-based orbitals, while the other component is non-interacting (*Fig. 2*).

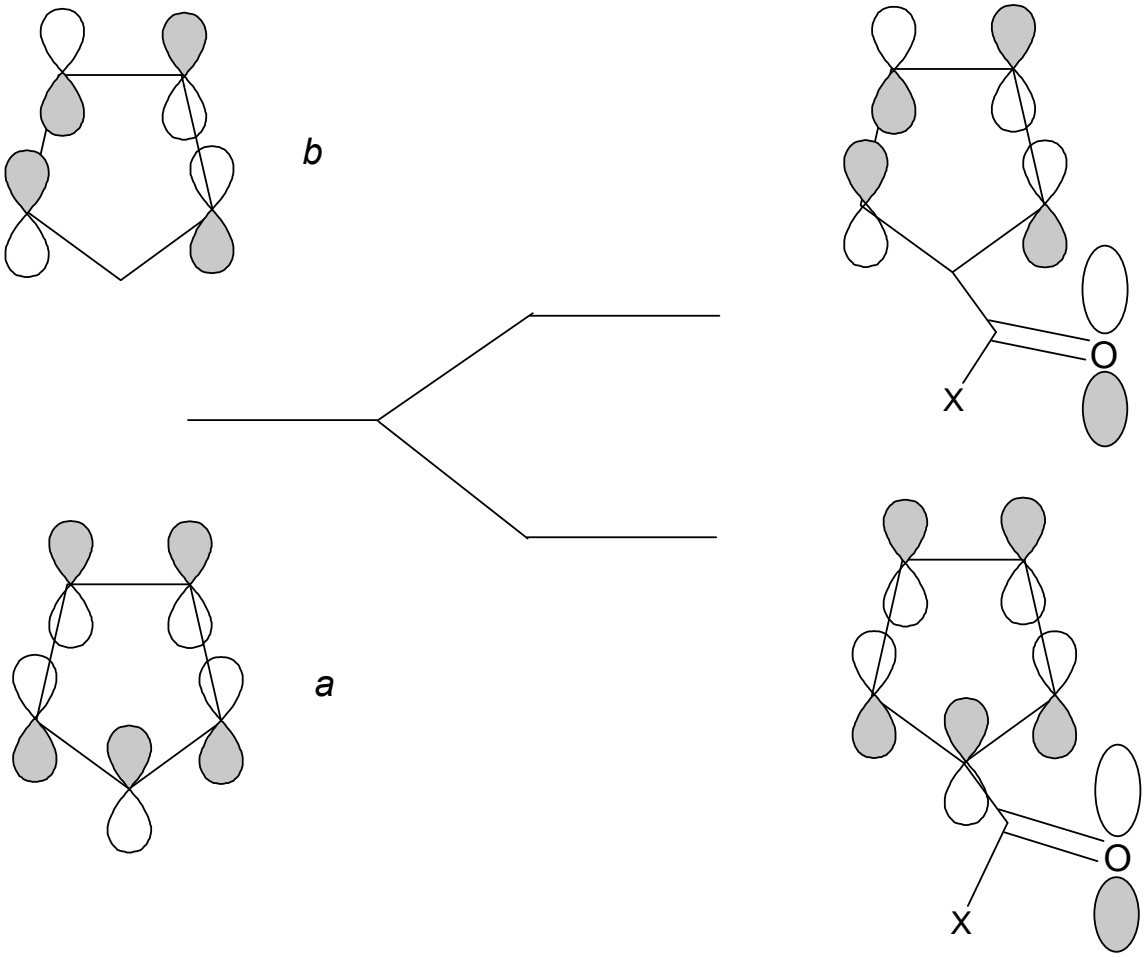

Fig 2: Cp – carbonyl orbital interactions

The ‘b’ component of the ferrocene HOMO has almost zero contribution from the C_1 carbon atom, so overlap with the substituents p_π orbitals is greatly reduced. The 'a' component, however, has significant contribution from the C_1 carbon atom, and is thus stabilised by a contribution from the carbonyl oxygen p_π orbital. In ferrocene carboxaldehyde, ferrocene carboxylic acid, and ferrocene carboxamide, these two components are split by 0.046, 0.082, and 0.065 eV respectively. (other Cp-based, lower energy degenerate pairs of orbitals are split even more upon acylation of a Cp ring). The non-interacting 'b' component of the e_{2g} energy level now becomes the HOMO of the substituted system.

Co-planarity of the Cp ring and substituent π-system will maximise their overlap, and for simple carbonyl-substituted systems such as ferrocene carboxylic acid, deviations from co-planarity (the ‘twist’ angle) in the solid state have been shown to be < 6° [8]. However, when more bulky substituents are introduced, these deviations become more pronounced. The isopropyl amide derivative (**2**), has a twist angle of 16.7^0 [9], while the macrocyclic system (**3**), has a twist angle of 50.2° [10]. Even at this large distortion from co-planarity, *ca*. 60% of the orbital overlap is maintained.

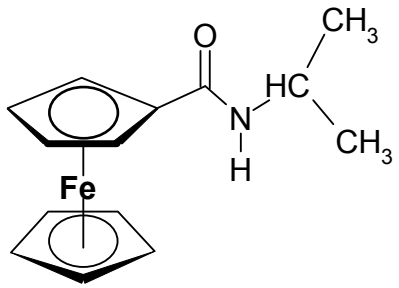

2

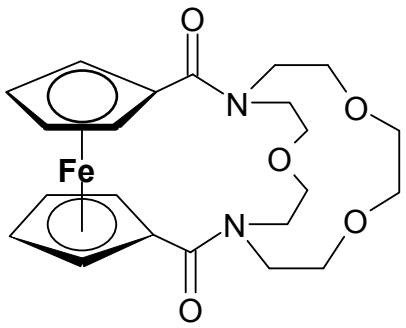

3

Variations in the half wave potentials of ferrocene derivatives have proven to be an extremely sensitive technique in investigating the electronic effects of substituents on the frontier orbitals of ferrocene. The presence of the electron-withdrawing acyl group, with its relatively low-lying LUMO, has the effect of lowering the energy of the ferrocene HOMO, making the molecule more difficult to oxidize [11], and there are consistent reports in the literature of mono-substituted amide ferrocenene derivatives with anodic shifts of their $E_{1/2}$ values in the +150-250mV range (vs. Fc/Fc^+). For 1, 1’-disubstituted ferrocene amides, this anodic shift becomes even more pronounced [12].

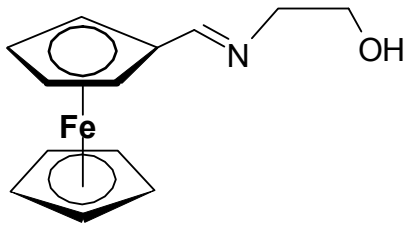

4

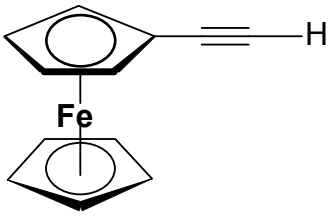

5

For ferrocenes with an sp^3 carbon substituent, such as the ferrocene alkyl-amines prepared by Hess *et al*. [13], there is very little difference in the reported $E_{1/2}$ values vs. the Fc/Fc^+ redox couple (< 20mV), indicating a far lesser degree of perturbation to the ferrocene frontier orbitals. Other conjugated ferrocene systems, such as the ferrocenyl-imine compounds synthesized by Lopez *et al*. (**4**) [14] and the alkynyl derivatives prepared by Nolte's group (**5**) [15], also display anodic shifts in their cyclic voltamogramms relative to the ferrocene/ferricenium cation redox couple, but to a lesser extent, as these groups are not as electron-withdrawing as acyl-substituted systems.

1.5: Applications of Ferrocene

Because of the well defined electrochemical and spectroscopic behaviour, chemical stability and low toxicity of ferrocene, it has found applications in areas such as anion sensing, asymmetric catalysis, as a mediator between redox enzymes and electrodes, as liquid crystalline materials, and in materials with high second harmonic generation efficiencies for non-linear optics. The incorporation of a ferrocene moiety into biomolecules is currently an area of intense research activity. Owing to the ease with which electrophilic aromatic substitution can occur on the cyclopentadienyl rings, a vast array of ferrocene derivatives have been reported in the literature since it was first discovered over fifty years ago.

1.5.1: Ferrocene and Asymmetric Catalysis

During the last twenty years, there has been an increasing use of ferrocene derivatives as chiral auxiliaries in homogenous asymmetric catalysis, both in research and on an industrial scale. The ferrocene moiety offers many advantages in this respect. A chiral, redox-active ligand is, in theory, capable of acting as a chiral auxiliary in an organic transformation, with

subsequent decomplexation of the ligand upon electrochemical oxidation, thus facilitating the catalytic cycle. Due to its bulkiness, a ferrocene nucleus adjacent to a stereogenic centre can improve stereoselectivity via steric hindrance, and nucleophilic substitution reactions at positions vicinal to the ferrocene group are highly favoured, and take place with retention of configuration [16]. To this end, a number of interesting ferrocene containing ligands have been prepared.

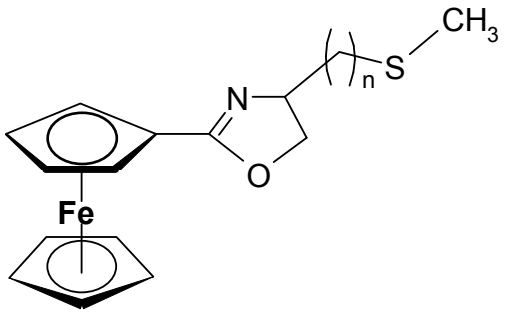

6 *n = 1*
7 *n = 2*

Two such ligands (**6**, **7**), have been synthesised by Chesney et al. (derived from L-(S-methyl)-cysteine and L-methionine respectively), and were shown to be particularly effective in palladium-catalysed substitution reactions of allylic acetate with diethyl malonate [17]. The ligand derived from L-methionine proved to be more effective in transferring chirality than that derived from S-methyl-L-cysteine, probably due to the extra methylene group between the donor atoms which co-ordinate to the palladium atom. The effect of this is to bring the asymmetric environment closer to the allyl species, as shown in the transition states (*Figs. 3 and 4*).

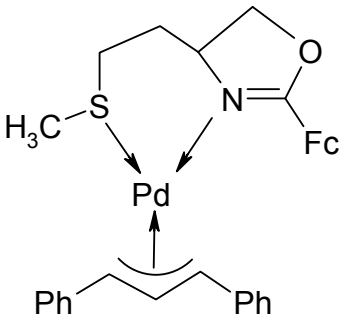

Fig. 3: Transition state of methionine oxazoline ligand

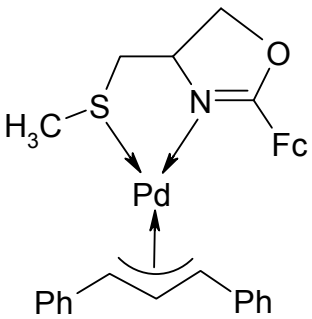

Fig. 4: Transition state of S-methyl cysteine oxazoline ligand

Depending on the solvent used, enantiomeric excesses of > 93% were obtained with the methionine-derived ligand.

Recently, Gonzales reported the synthesis of palladium complexes with chiral ferrocenyl-thiazolidines, again utilizing S-donor atoms derived from L-cysteine. The arrangements of the ligands (**8**) in the complex is similar to those described for other palladium (II) complexes of the type [Pd(η^3-C_3H_5)(Br)(L)] which have catalytic activity [18].

The Schiff-base derivatives prepared by Lopez (**4**, section 1.4), have also proved to be effective donors in palladium and platinum complexes, and the group synthesized a di-μ-chloro-bridged cyclopalladated complex (**9**) [14].

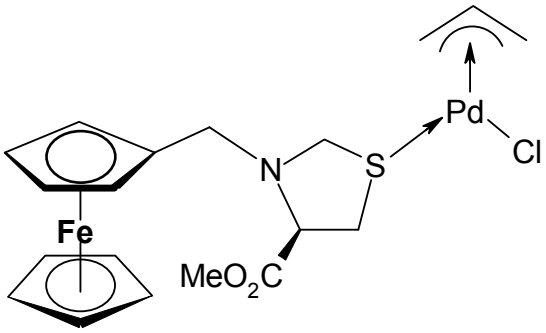

8

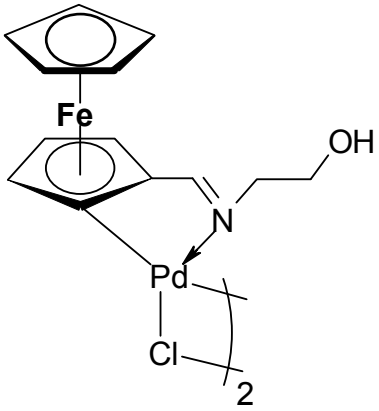

9

Orthometallation is a common feature of heterobimetallic systems incorporating a ferrocene moiety. This process involves the chelation-controlled, regioselective C-H activation with a metallation reagent, resulting in the formation of a new metal-carbon bond [19]. The cyclometallation of ferrocene results in the formation of planar, cyclometallated derivatives, which have great potential in the area of asymmetric catalysis [20].

Finally, optically pure cyclopalladated ferrocenylimines have been found to be particularly effective in the resolution of racemic mixtures of α-amino acids. When the cyclopalladated dimeric complex (*scheme 3*) was employed as a resolving agent, the resolution of several mixtures of racemic amino acids was successfully performed via chromatography (the reverse process was also carried out, with enantiomerically pure amino acids being used to resolve racemic mixtures of cyclopalladated ferrocene-containing compounds) [21].

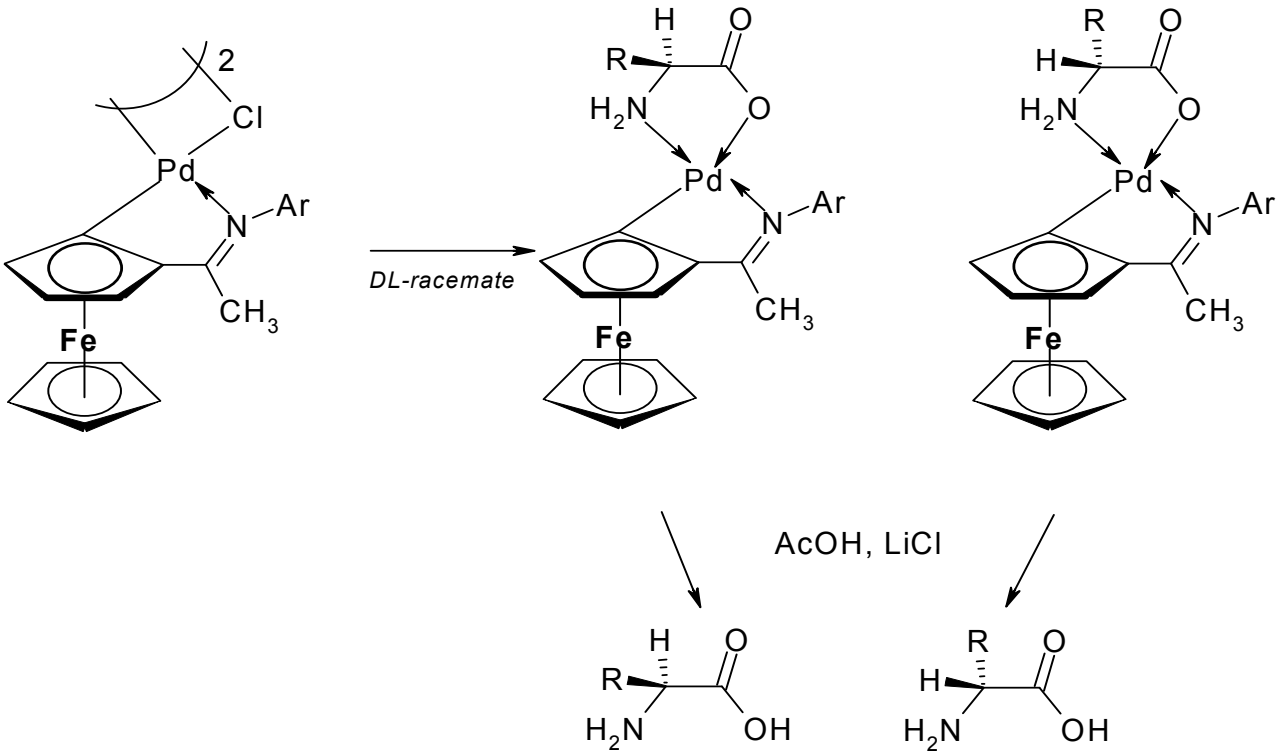

R = $CH_2CH_2CH_2CH_3$ (norleucine), $CH_2CH(CH_3)_2$ (leucine), CH_2Ph (phenylalanine)

Scheme 3: Optical resolution of amino acids with cyclopalladated complex

1.5.2: Anionic Sensors Incorporating Ferrocene Units

The design of ferrocene-based anion receptors is another area of current intense research [22, 23]. In biological processes, the majority of enzyme substrates are negatively charged [24]. Therefore, an understanding of the interactions which bind the guest and host molecule together, has potential application in the design of drugs capable of mimicking those interactions. Alzheimer's disease has been linked to anion-binding enzymes, and cystic fibrosis is known to be caused by a misregulation of chloride channels. From an environmental point of view, pollutants such as phosphate and nitrate anions need to be continually monitored [25].

The first metallocene-based anion receptors reported in the literature were based on the cobaltocenium cation, which were capable of binding anions such as halides, via favourable electrostatic interactions. Electrochemically, the Cp_2Co/Cp_2Co^+ redox couple showed significant cathodic shifts upon anion complexation, with the complexed anion stabilizing the positively charged cobalt centre, thus making it harder to reduce [26].

Neutral, ferrocene containing secondary amides have no inherent electrostatic interaction with guest anionic species, and their complexed forms have lower stability than their cobaltocenium analogues. However, the anion-receptor interactions can be modulated via oxidation to the ferricenium cation, at which point electrostatic interactions can be 'switched on' [27]. The oxidation of ferrocene in the vicinity of the amide group increases the acidity of the amide proton, making hydrogen-bonding stronger, and thus there is a synergy between ion-paring and H-bonding interactions [28]. Thermodynamic studies have shown ΔH^0 for the complexation is favourable, as the formation of H-bonds is energy releasing, while ΔS^0 is unfavourable, due to the association of two species in solution, and a loss of conformational freedom. Favourable ΔH^0 and unfavourable ΔS^0 is a common feature of anion recognition in biological processes [29].

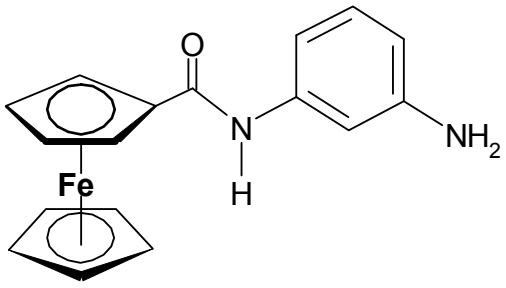

10

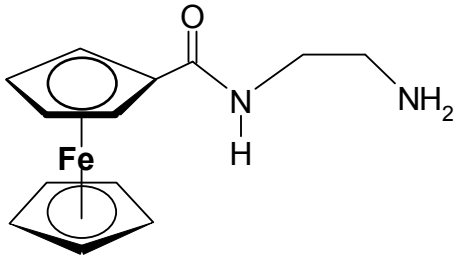

11

Ferrocene containing molecules which have the ability to bind and electrochemically sense anionic substrates range from the relatively simple ones first designed by Beer and co-workers [30] (**10, 11**), to larger, more complex molecules, such as ferrocene-metalloporphyrin receptors, which bind anions via a Lewis acidic zinc centre [31]. Dendrimers containing up to eighteen ferrocene units have been prepared [32], as have lower-rim polysubstituted ferrocene-containing calixarenes [33], with the aim of increasing ion selectivity.

The amide receptor (**10)** was found to selectively bind dihydrogen phosphate, even in the presence of a ten fold excess of hydrogen sulphate and chloride ions, while the amide receptor (**11)**, with its more basic amine functionality, was found to selectively bind the more acidic HSO_4^- anion. Cathodic shifts of over 200mV were observed upon complexation with anionic guests.

Finally, the binding of guests by a ferrocene containing molecule has also found application in the area of chirality sensing. Tsukube and co-workers prepared a ferrocene carboxylic acid-crown ether conjugate (**12**) [34], which is capable of binding the protonated form of certain unprotected α-amino acids. The protonated amine is bound by the crown ether ring, while the carboxylic acid group can form two-point hydrogen bonding with the carboxyl group of the guest. Via CD spectroscopy, the chirality of the guest could be determined.

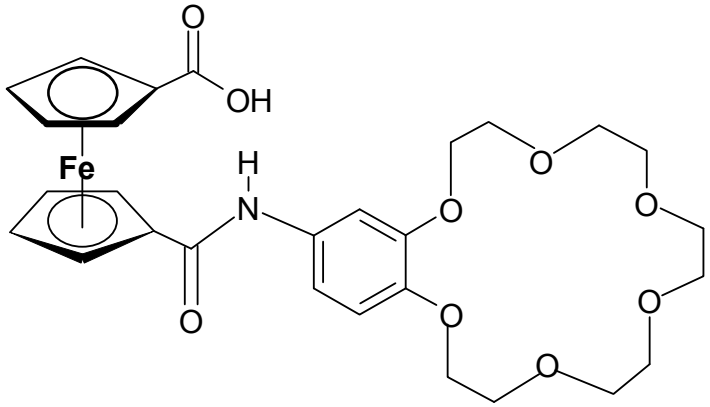

12

1.5.3: Ferrocene Containing Molecules for Second Order Non-Linear Optics

The interest in materials with large second-order optical non-linearities stems from their potential application in telecommunications, optical computing, and optical information processing. In such materials, there is no linear relationship between the induced dipole moment, and the applied electric field, providing the field is of high enough intensity (as is the case with lasers). The induced dipole moment is given by the equation:

$$\mu^* = \alpha\varepsilon + 1/2\beta\varepsilon^2$$

- where μ^* is the induced dipole moment, α is the polarizability of the molecule, ε is the electric field strength, and β is the first hyperpolarizability [35]. Large hyperpolarizabilities are associated with molecules that have large differences between the ground state and excited state dipole moments, and a small energy gap between the ground and excited state [36]. Organic chromophores which fulfil these criteria, the so-called 'push-pull' systems, have donor-acceptor moieties separated by conjugated bridges, for example (E)-4-(methoxy)-4'-nitrostilbene [37].

In the last ten years, there has been a substantial amount of work devoted to molecules incorporating a ferrocene group with potential NLO responses. Ferrocene derivatives are particularly suitable to function as a donor in these materials, owing to the presence of metal to ligand charge transfer bands (MLCT) in the visible region, the relatively low redox potential, and the enhanced electron delocalisation in π-substituted systems.

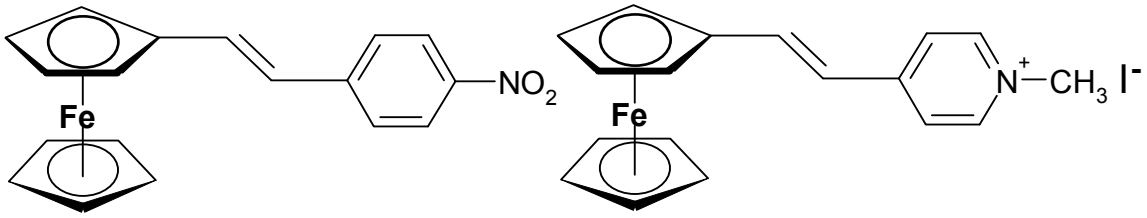

13 **14**

Among the first ferrocene derivatives to exhibit large hyperpolarizabilities were those prepared by Calabrese and co-workers at DuPont, trans-1-ferrocenyl-2-(4-nitrophenyl) ethylene (**13**) and trans-1-ferrocenyl-2-(*N*-methylpyridinum) ethylene iodide **(14)**, which displayed second-harmonic generation (SHG) 62 and 220 times greater than that of urea [8]. It should be noted that these results were obtained using dc electric field induced second harmonic generation (EFISH). The alternative method, the Kurtz second harmonic powder generation test gives zero SHG if the material crystallizes in a centrosymmetric space group [37]. In no other area of metallocene chemistry do electronic structure and quantum chemical calculations take on such importance as in the area of non-linear optics. Extended Huckel molecular orbital calculations assign the HOMO of these ferrocene derivatives as being the iron-based a'_{1g} ($3d_{z^2}$) orbital [38]. The LUMO of these conjugated systems is largely located around the nitrogen atom. Hence, electron density is significantly redistributed in the excited state relative to the ground state, illustrating the suitability of ferrocene as a donor moiety in NLO materials [39]. Conjugation also has the effect of lowering the HOMO-LUMO energy gap, with the band observed circa. 440 nm for simple ferrocene (in acetonitrile) being bathochromically shifted to 550 nm for the nitrophenyl derivative **13** [40].

1.5.4: Liquid Crystals Incorporating Ferrocene

The liquid crystal (mesogenic) state represents a discrete state of matter (the mesophase) lying between the solid and liquid states. A crystal has a defined shape, and its physical properties are anisotropic because the molecules (or ions) are ordered in terms of their position and orientation. The molecules of a liquid lack this positional and orientational order, and hence its physical properties are isotropic. Liquid crystals have the fluid characteristics of liquids, but also a degree of positional and translational order, reminiscent of solids [41].

Liquid crystals can be divided into two broad categories, thermotropic and lyotropic. Thermotropic mesogens change phase upon heating or cooling, with the solid phase melting to the mesophase (the melting point), and, at a higher temperature, forming the isotropic liquid (the clearing point). Some mesogens exhibit polymorphism – they have more than one mesophase, depending on temperature. Lyotropic phases are formed by molecules in a solvent (generally water), and the appearance of the mesophase is concentration dependent.

Thermotropic mesogens can be classed as calamitic (rod-like) or discotic (disk-like). Rod-like thermotropic mesogens can themselves be sub-divided into nematics (where the molecules align themselves in a roughly parallel fashion), and smectic (where the mesogens form layers), which is a more ordered arrangement than the nematic phase [42].

The study of the incorporation of metals into liquid crystals (resulting in what are known as metallomesogens) is now a well established area of materials chemistry, with many potential applications resulting from the polarizable electron density around a metal atom (such as molecular electronics, magnetic/electrical switches, conductors and optical devices) [43].

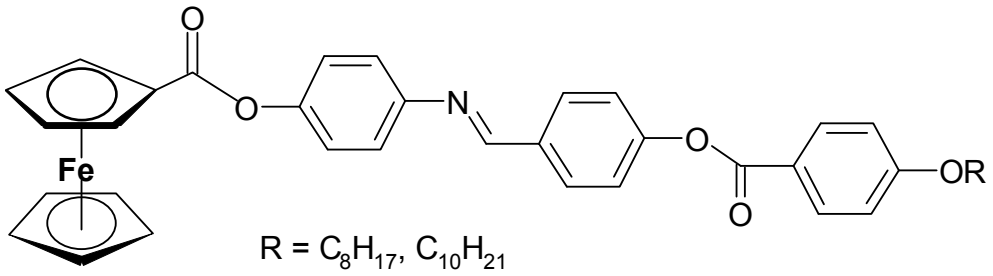

15

Other important advantages include stereochemistry not found in organic mesogens, and the possibility of paramagnetic materials. The main disadvantage of metallomesogens is their

tendency to decompose upon heating, and hence the chemically robust ferrocene moiety is a suitable candidate for incorporation into these materials. The first ferrocene-containing mesogen to appear in the literature were the ferrocenyl imines, prepared by Malthete *et al*. (**15**), which formed a stable nematic liquid crystal phase upon heating [43].

Deschenaux *et al*. have investigated the thermotropic liquid crystal properties of both 1, 1' and 1, 3- disubstituted ferrocenyl systems, examples of which are **16** and **17** [44, 45].

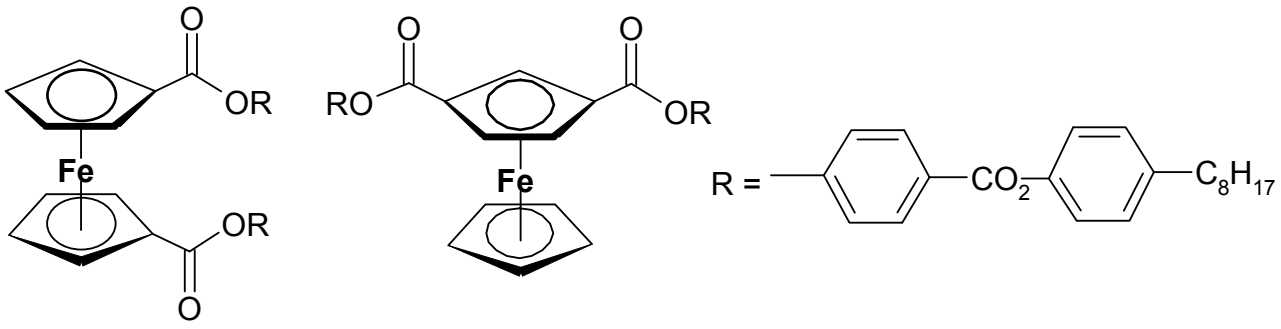

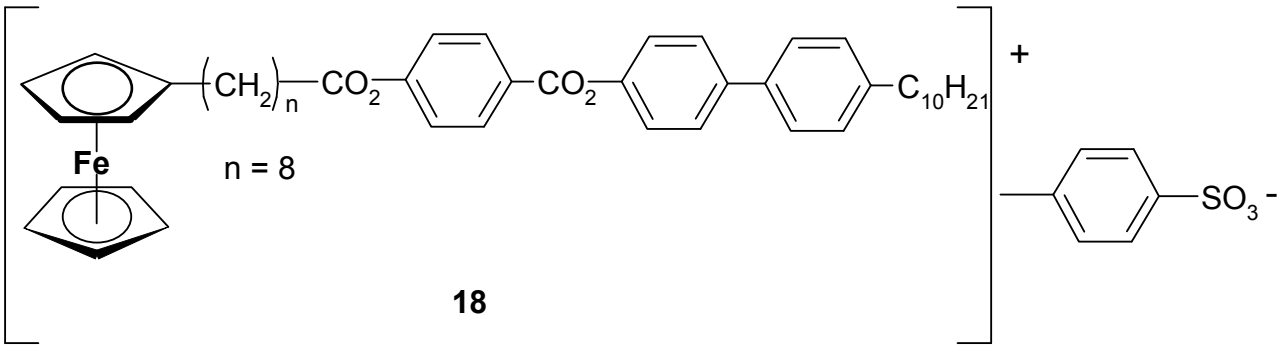

Interestingly, none of the 1, 1' disubstituted ferrocenyl systems exhibited any mesogenic behaviour upon heating, instead melting into an isotropic liquid. However, the 1, 3-disubstituted systems gave rise to wide nematic phases of over 60^0C in some cases. The same research group have used the well-defined redox behaviour of ferrocene to induce mesomorphism via chemical oxidation. Prior to treatment with silver tosyolate, the ferrocene derivative (**18**) displayed no mesogenic behaviour.

Ferrocene containing polymers are attractive materials, as they combine the unique chemical properties of ferrocene with the low thermal expansion and processibility. Thus, polymeric materials incorporating ferrocene units into both the backbone and side chain have

been prepared. Liu *et al*. have synthesized functionalised liquid crystalline polymers from silicon-bridged ferrocenophane monomer units (**19**). The introduction of the ferrocene moiety has also been shown to induce mesomorphism into an otherwise non-mesogenic polymer (**20**) [46].

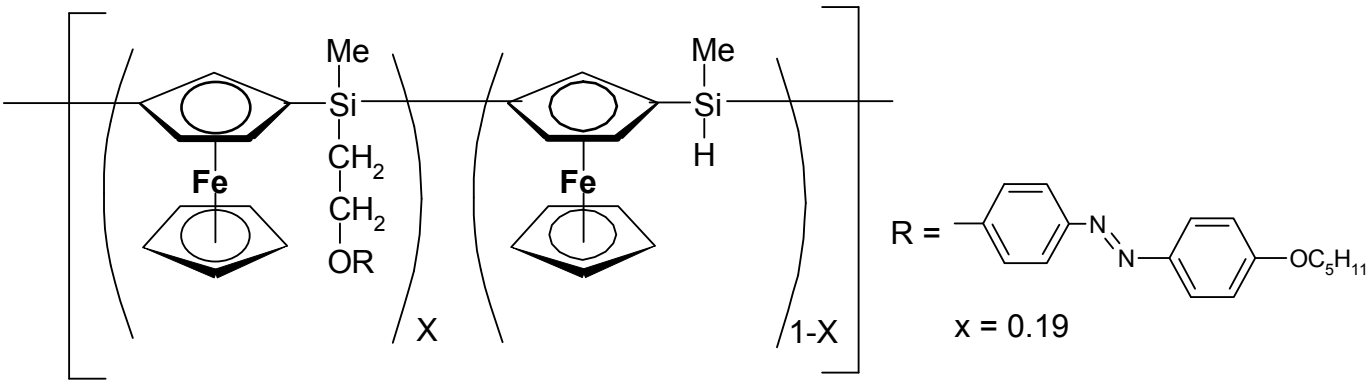

19

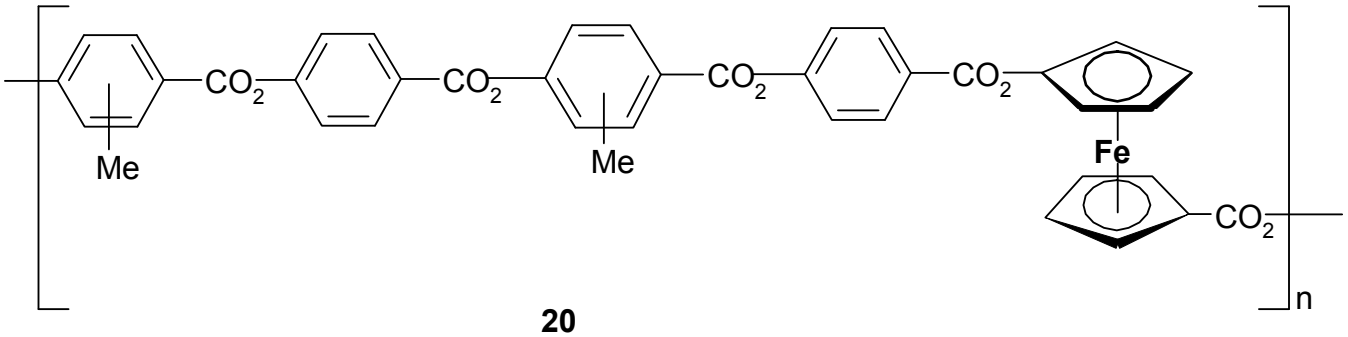

20

Finally, Galyamaldinov *et al*. reported the first example of a heterobimetallic liquid crystalline material [47], the ferrocene/copper salicylaldimine complex (**21**).

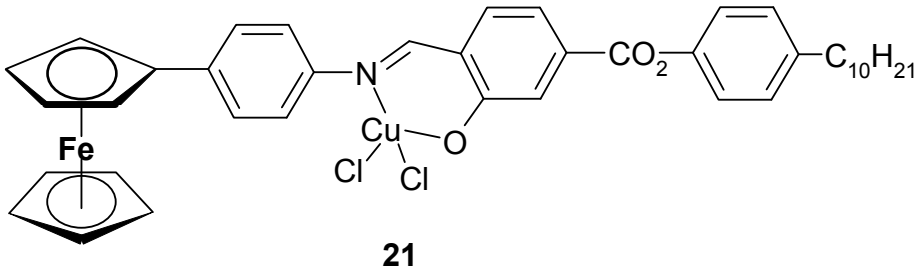

21

1.5.5: Bioorganometallic Chemistry of Ferrocene Derivatives

Bioorganometallic chemistry is currently of interest to many research groups, and incorporates areas ranging from inorganic to medicinal chemistry [48]. It takes advantage of the unique chemical and spectroscopic properties of organometallic compounds, for the incorporation into, or detection of, biomolecules. Organometallic carbonyl compounds, for example, when covalently bound to a biologically active substrate, can be detected via infrared spectroscopy, providing a safer alternative to conventional radioactive markers. Thus, ferrocene has been incorporated into a number of biomolecules, such as amino acids and peptides, steroid derivatives, and sugar molecules (ferrocene derivatives of amino acids and peptides will be discussed in section 1.7).

The difficulty in controlling pathogenic organisms with antibiotics has risen dramatically in the last few decades. Mycobacterial resistance to anti-tuberculosis agents is particularly worrying, as tuberculosis results in three million deaths worldwide annually. Therefore, there is an urgent need for the design of new drugs with new modes of action. The ferrocene moiety is particularly suited to this task, owing to its low toxicity and chemical stability [49].

The steroidal (N-ferrocenylmethyl) amine derivative (**22**) synthesised by Krieg *et al*. was tested *in vitro* for antimicrobial activity against a broad spectrum of test organisms (fungi, mycobacteria, etc.), and shown to be extremely effective against each microorganism.

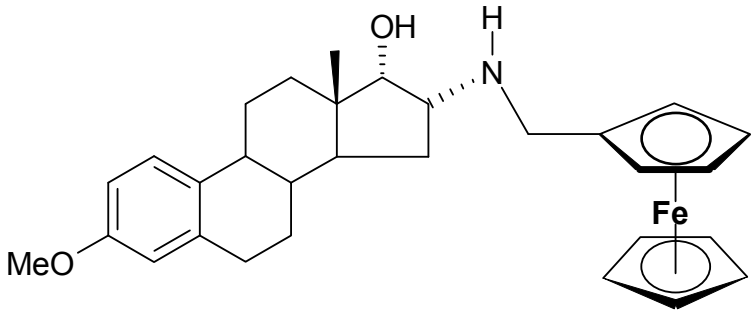

22

The three standards used in these experiments, rifampicin, isoniazid and ciproflaxacin, were observed to have a different pattern of activity, and did not cover the range of organisms as did the 16-(ferrocenylmethyl) amino estratrienes. The authors attribute these observations to a different mode of action to that of known drugs. The penicillin-ferrocene derivative (**23**) prepared by Edwards *et al*., is another compound that displays significant antibacterial activity [50].

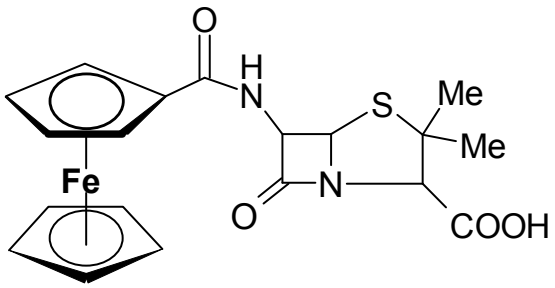

23

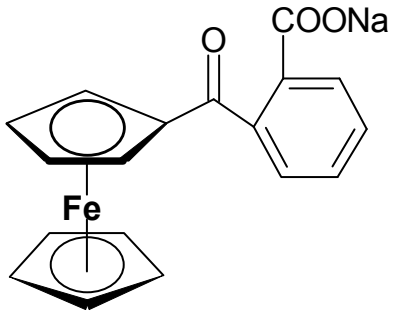

24

The ferrocenoyl derivative (**24**) is one of the few ferrocene-containing compounds to have been used in pharmaceutical treatment of illnesses, having been patented in the USSR, and marketed under the trade name ferrocenone. It has been employed in the treatment of various conditions, including iron deficiency anemia, and infection of the nasopharynx [51].

Ferrocenyl amines have also been shown to have antiproliferative properties against a variety of carcinomas and tumours [52]. Cisplatin analogues with ferrocenylamine ligands of the type **25,** have been prepared by Duffy and co-workers [53]. This study highlighted the relationship between the toxicology of ferrocenyl amines and their basicity. *N*-alkyl ferrocenyl amines were observed to protonate and oxidise to their ferricenium analogues more readily than *N*-aryl ferrocenyl amines. Protonation competes with complexation to the Pt(II) center, and the reduced biological activity of the ***N***-alkyl species *in vitro* is attributed to their propensity to protonate [54].

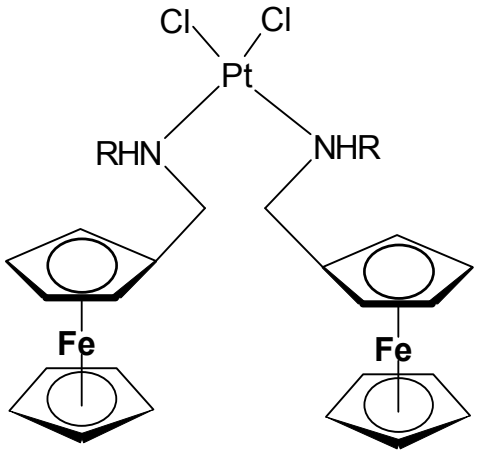

25

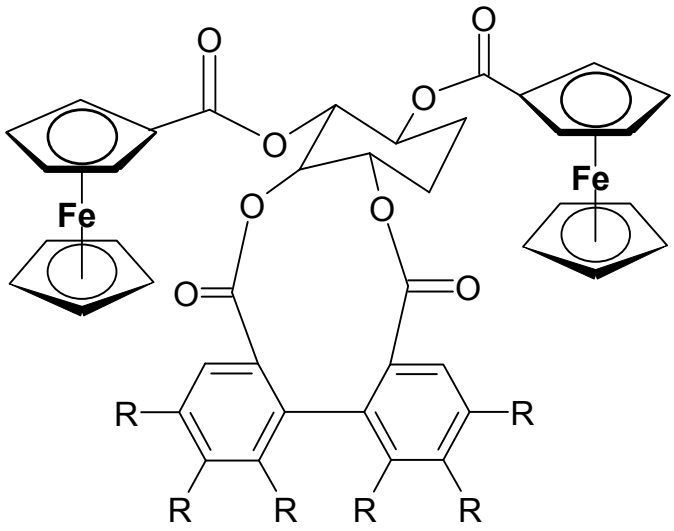

26

Ferrocenoyl saccharide derivatives (**26)** have been prepared by Itoh and co-workers [55], as glucosides are known to be effective in the area of antimalarial action and DNA binding ability in cancer cells [56].

Ferrocene has also served as a redox active moiety in the determination of blood glucose levels in diabetes patients [57], in the selective recognition of nucleotides [58], and in the redox modification of enzymatic co-factors [59].

1.6: Amino Acids and Peptides

All proteins can be considered as being polymers of α-amino acids. These molecules are centred around a tetrahedral (α) carbon atom (*Fig. 5*), to which is attached a carboxyl group, an amine functionality, and a hydrogen atom. The fourth substituent is unique to each individual amino acid, and serves a variety of structural and/or functional roles when incorporated into a protein. Of the twenty commonly occurring amino acids, all have an asymmetric α-carbon (with the exception of the achiral glycine), and are found in the L-form. Threonine and isoleucine also possess additional chiral centres.

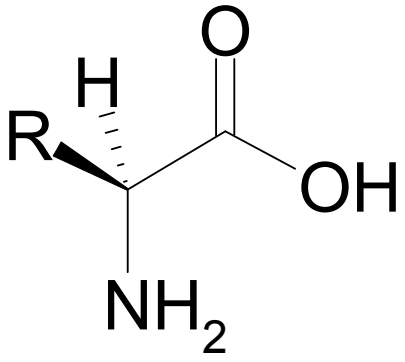

Fig. 5: general structure of L-amino acids

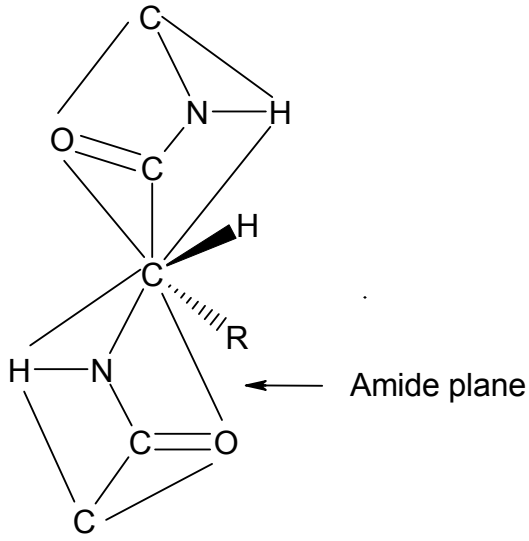

Fig. 6: Planarity of amide group(s)

Other less common amino acids are also found in minor amounts in proteins, and usually result from modification of the R-group after incorporation into the peptide chain (e.g. hydroxyproline) [60].

Free amino acids are ionic compounds in the solid state, with a protonated amine group, and a deprotonated carboxyl group, which accounts for their high melting points, large dipole

moments, and water solubility [61]. In addition to the ionisable amine and carboxyl groups, five amino acids (lysine, arginine, histidine, aspartic and glutamic acid), have charged R-groups at physiological pH, and tend to be located on the surface of globular proteins, thus aiding in their solubility. In the early 1950s, Pauling and Corey formulated two rules concerning the structure of proteins, from their crystallographic studies of low molecular weight peptides. The first of these was that the amide groups always prefer planarity, i.e. the C-N peptide bond, and the four atoms to which they are directly attached, lie in the same plane (*Fig. 6*). The planarity of the amide group is due to the fact that resonance stabilization is maximized when the p-orbitals of the amide C, N, and O atoms lie in the same plane (*fig. 7*).

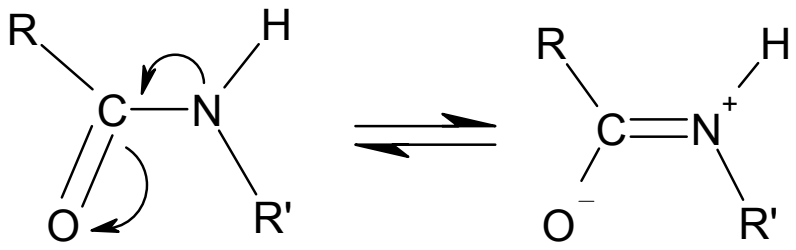

Fig. 7: Resonance forms of the peptide bond

The second rule was that the partially deshielded amide protons and the carbonyl oxygen atoms always form the maximum number of hydrogen bonds. Thus, regular, repeating patterns of hydrogen bonding, such as the α-helix and the β-pleated sheet, are formed. These two rules mean that the conformational freedom of peptide backbones is greatly reduced. The higher orders of structure (tertiary and quaternary) imposed by individual amino acid side chains, serve to bring an ordered structure to physiologically active proteins, providing specific sites for molecular recognition, electron transfer, etc.

1.6.1: The Synthesis of Peptides

In living systems, the synthesis of peptide chains is an intricate, enzymatically controlled process, the order of amino acids being determined by the order of nucleotides in the corresponding messenger RNA template. In the absence of such a highly ordered, chemically selective environment, the formation of a peptide chain of predetermined sequence requires multi-step synthetic procedures, namely protection, activation, and coupling.

Modern peptide synthesis employs one of two principal methods: solution and solid phase synthesis. Merrifield's method for the synthesis of peptides on an insoluble polymeric support (for which he was awarded the 1984 Nobel prize) has proved so successful that most peptides are now prepared in this manner. Briefly, the ***C***-terminal of an ***N***-protected amino acid is anchored to the polymeric resin, usually via the formation of an ester or an amide bond. Repetitive cycles of deprotection, followed by coupling then affords the peptide, with subsequent cleavage from the resin [62]. This is the reverse of the ribosomal process in nature, where chain elongation takes place from the ***N***-terminal.

Solid phase peptide synthesis offers several advantages over solution phase synthesis, namely speed of preparation, the possibility of automation, and near quantitative yields. Solution phase synthesis is still the preferred method, however, for large-scale synthesis, and enables isolation of intermediates, as well as the synthesis of cyclic peptides [63].

1.6.1.1: Activation

An amine and a carboxyl group can only react to form an amide bond at elevated temperatures, which would inevitably induce side reactions in complex peptides [64]. Therefore, one of these functional groups must be activated for peptide synthesis. Increasing the nucleophilicity of the amine with an electron-donating substituent (such as a t-Butyl group) has the disadvantage of decreasing the rate of ***N***-acylation, due to steric hindrance. Therefore, activation in peptide synthesis has been confined to increasing the electrophilicity of the carboxyl carbon atom with an electron-withdrawing group. One of the earliest examples of such activation is the azide method of Curtis, still widely used in peptide chemistry today.

Conversion of the carboxyl group to the acid chloride results in what is known as over activation – acid chlorides are powerful acylating agents, and can react with nucleophiles other than amines, e.g. hydroxy groups. Therefore, an activating group must make the carboxyl group sufficiently reactive towards amines, while remaining inert towards less reactive nucleophiles found in amino acid side chains. Many examples of carboxyl-activating groups have appeared in the literature over the years, with conversion to the azide, acid anhydride, and active ester being among the most widely used methods.

1.6.1.2: Protection

In order for peptide synthesis to occur, there should be only one nucleophile available for acylation, and therefore one of the amino groups must be blocked. Similarly, the carboxyl group of the other amino acid must be protected from activation. In addition to these α-functional groups, several amino acid side chains have functional groups that can potentially interfere with peptide bond formation. Therefore, protecting groups must be carefully chosen for all reactive groups not directly involved in coupling, which renders them inert under coupling conditions, and can be cleaved without affecting the newly formed peptide bond.

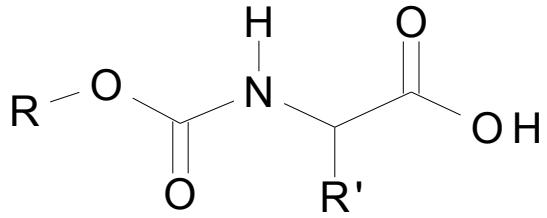

27

An amine group cannot be protected via acylation, as removal of the protecting group via acid/base hydrolysis would result in cleavage of the peptide bonds as well. Formation of a urethane-type bond (**27**), however, allows for facile removal of the protecting group under mild conditions, leaving the amide bond(s) intact. In 1932, Bergman and Zervas introduced the benzyloxycarbonyl (or 'Z' group) [65], which is easily removed via catalytic hydrogenation and/or acidolysis, and is still widely used in peptide synthesis today. The most popular urethane-type protecting group in peptide chemistry today is probably the tertbutyloxycarbonyl (or 't-Boc') group.

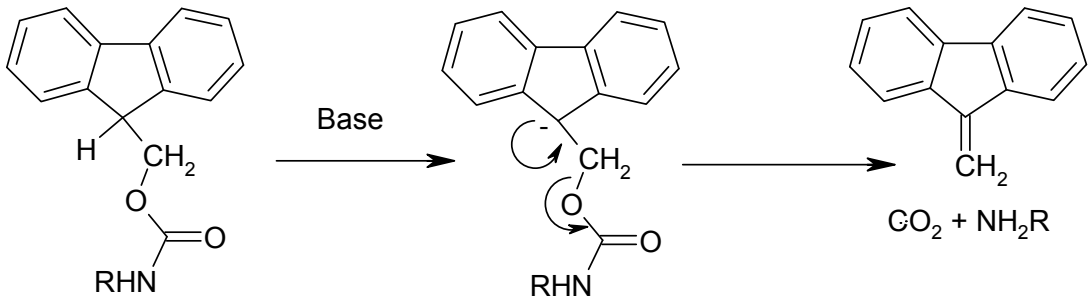

Scheme 4: Removal of the Fmoc group

Other ***N***-blocking groups currently employed in peptide synthesis include the p-toluene sulfonylurea (Tonsil, Toss) group (which can be removed by reduction with sodium in liquid

ammonia), and the 9-fluorenylmethoxy carbonyl (Fmoc), which is cleaved by a process of β-proton abstraction in the presence of weak bases (*scheme 4*).

The most widely used procedure in the protection of the α-carboxyl group is conversion to the ester. Thus, methyl, ethyl, t-butyl and aryl esters have all been employed in peptide synthesis. Alkyl esters, while relatively straightforward to prepare, must be removed by saponifiation, which can lead to unwanted side reactions, particularly in larger peptides. The most worrying of these is the possibility of racemisation, which is particularly common in peptides with ***S***-benzyl cysteine residues. Benzyl esters have an advantage in this respect, being easily cleaved by catalytic hydrogenation. Ethyl esters, substituted on their β-carbon atom with an electron-withdrawing group, can be easily cleaved in base by β-proton abstraction. Phenyl esters are readily removed in dilute base, but they do have some weak active ester character, and are liable to nucleophilic attack by a free amine group.

The need for protection of side chain functional groups varies with each individual amino acid, and with the conditions employed in peptide synthesis. For instance, the sulfhydryl group of cysteine must be protected, irrespective of the coupling conditions, as it is an excellent nucleophile, and can compete with amines for acylation, or else be oxidized by air to form disulfides. ***S***-alkylation with benzyl or trityl groups is the most widely used methods of sulfhydryl protection. The ε-amino group of lysine, or the δ-amino group of the less common ornithine, are similar in reactivity to their α-amino groups, and are therefore readily acylated under normal coupling conditions. Selective acylation of the side chain amino group can be achieved via the formation of a Cu(II) complex of the amino acid (which effectively blocks the amino group), followed by introduction of a tosyl group (*scheme 5*).

The side chain carboxyl groups of aspartic and glutamic acid are sometimes left unprotected in coupling reactions, although this can lead to undesirable side reactions, such as the formation of anhydrides, leading to branching of the peptide chain. Most often, the diester of these amino acids is prepared, followed by selective saponification of one of the ester groups [65] (*scheme 6*). Protection of the hydroxy groups of serine, threonine and tyrosine is optional, and depends on the coupling conditions. In the presence of bases, deprotonation of the hydroxy group can occur, generating nucleophiles which can react in the presence of activated species such as anhydrides.

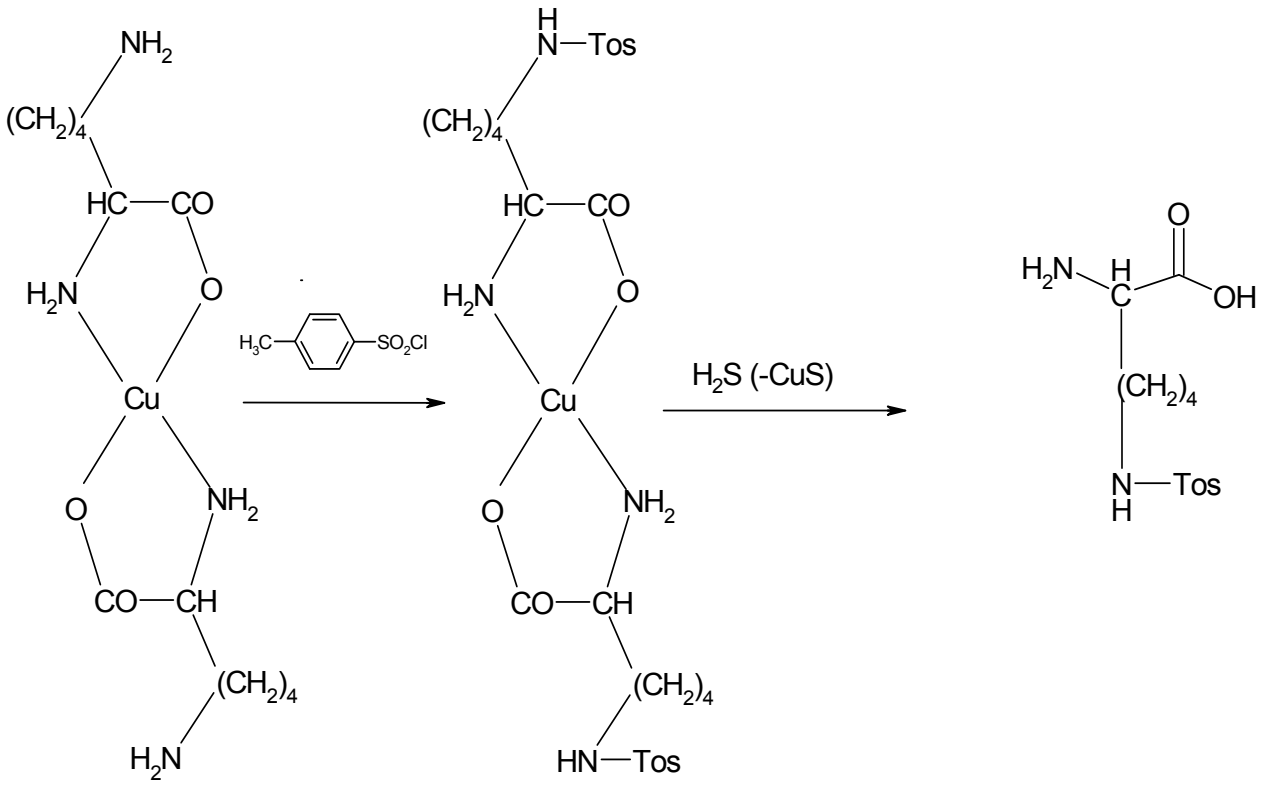

Scheme 5: Selective protection of the lysine ε-amino group

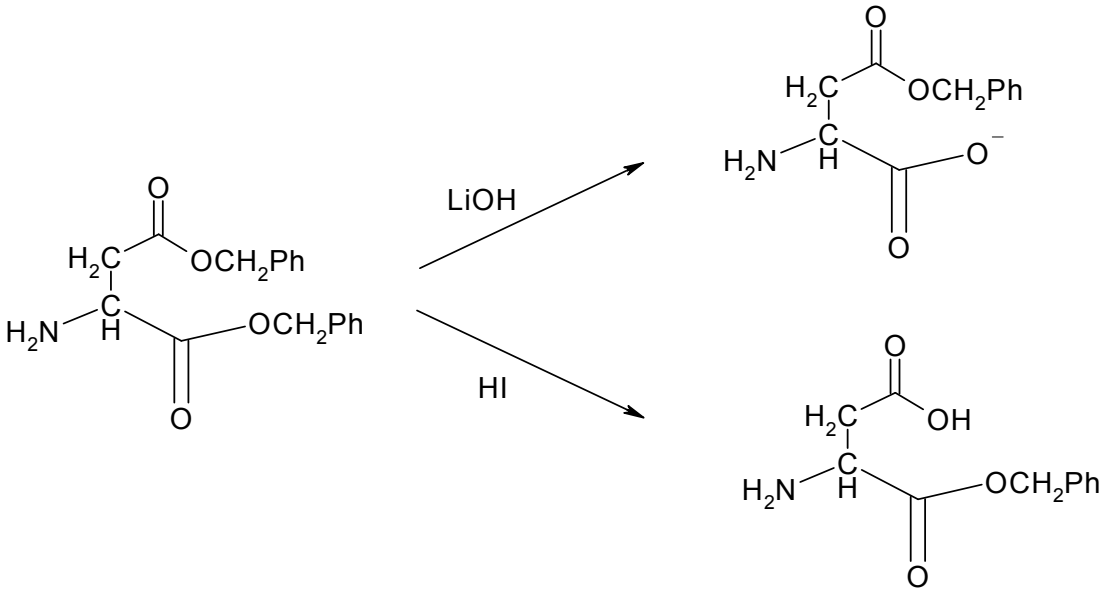

Scheme 6: The selective deprotection of the carboxyl groups of aspartic acid

Of the three, serine can most effectively compete with amines for acylation, while the sterically hindered secondary alcohol of threonine is the least reactive. Protection is also optional in the case of the indole and imidazole rings of tryptophan and histidine respectively, the carboxamide groups of glutamine and asparagine, and the thioether of methionine.

1.6.1.3: Coupling

Formation of a peptide bond is a bimolecular dehydration reaction between a free amine and a free carboxyl group. Carbodiimides are powerful dehydrating agents, and have become the most widely used coupling reagent in peptide chemistry, the most popular being dicyclohexylcarbodiimide (DCC). In such reactions, activation of the carboxyl group occurs through nucleophilic addition to the cumulated double bond of the diimide. Nucleophilic attack by amines is generally too slow to compete. Addition results in the formation of the O-acylisourea intermediate, which is prone to nucleophilic attack from a free amino group to give the coupled product (*scheme 7*), from another carboxy group, which affords the reactive anhydride, or from an auxiliary nucleophile, which results in the formation of an active ester.

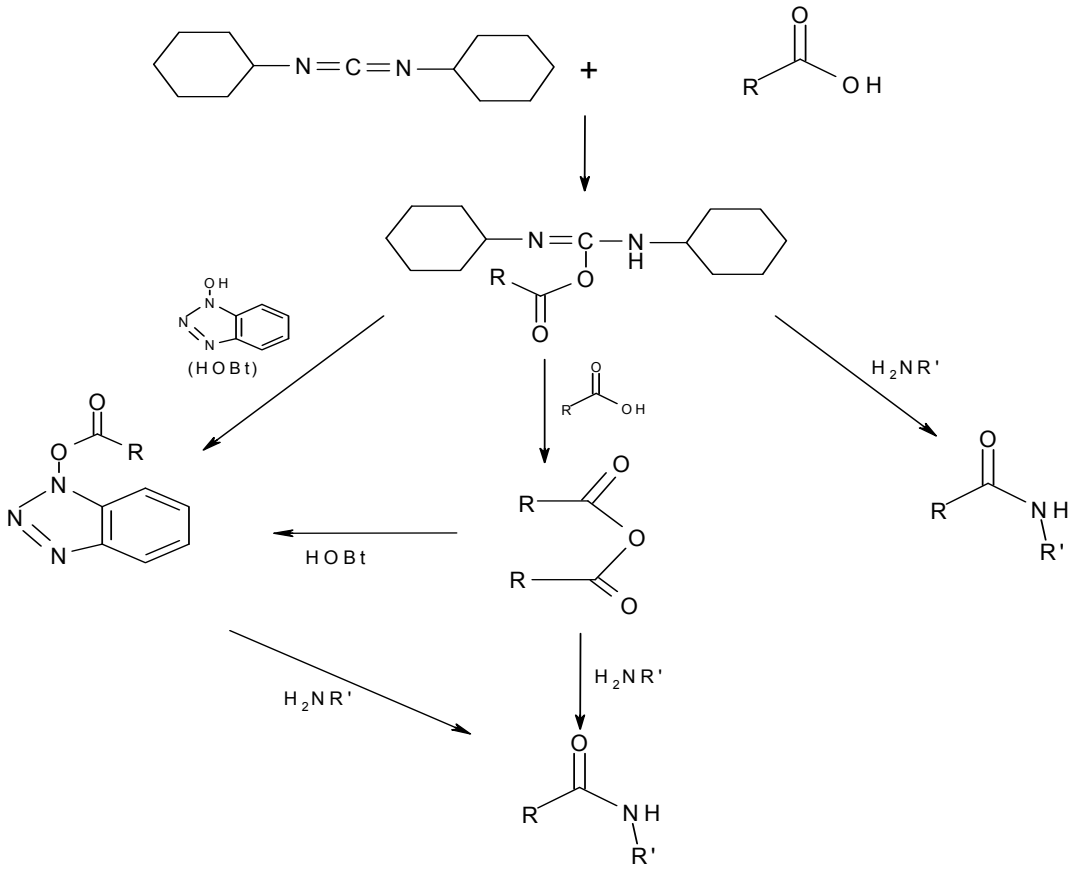

Scheme 7: DCC/HOBt coupling protocol

The problem of side reactions, particularly racemisation of the carboxy terminal residue, can be overcome by the use of these auxiliary nucleophiles. The first of these was *N*-hydroxysuccimide, which, although still used occasionally in peptide synthesis today, has largely been replaced by 1-hydroxybenzotriazole (HOBt). Although several mechanistic studies have been performed on the DCC/HOBt system, it is still not clear how much each pathway contributes to the overall coupling reaction. Two other such additives, 3-hydroxy-4-oxo-3, 4-dihydro-1, 2, 3- benzotriazine (HODhbt, **28**) and 1-hydroxy-7-azabenzotriazole (HOAt, **29**) have also found widespread use as auxiliaries due to their effectiveness at reducing racemisation.

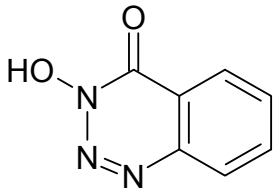

28

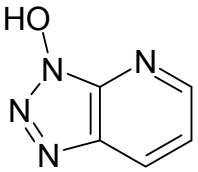

29

Although acylphosphonium salts have been used in coupling reactions since the late sixties, it was not until several years later that their use became widespread, with the introduction of Castro's 1-H-benzotriazol-1-yloxy-tris (dimethylamino) phosphonium hexafluorophospate (BOP) reagent [66]. A disadvantage of using this reagent is the formation of the toxic by-product, hexamethylphosphorotriamide. Thus, other acylphosphonium salts, such as PyBOP, have been developed, which form less toxic by-products. The mechanism for the action of the BOP reagent is outlined in *scheme 8*.

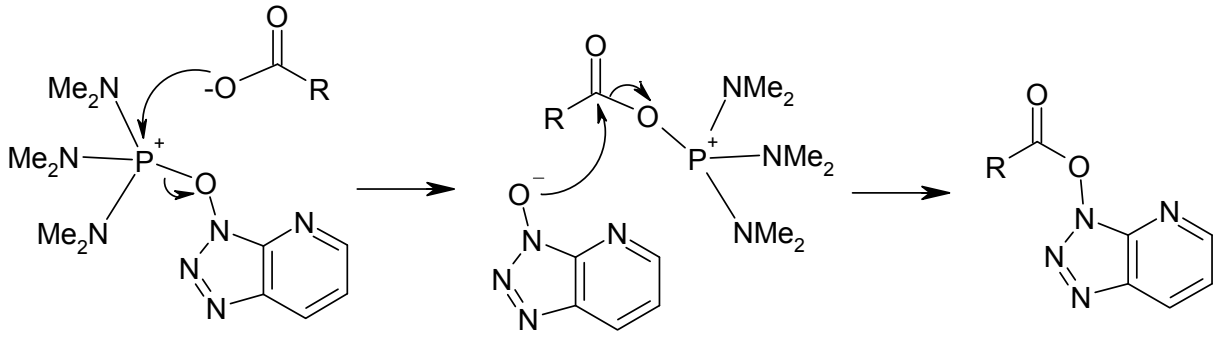

Scheme 8: Formation of the active ester with BOP

Uronium salts were introduced a decade after phosphonium salts, the most popular of which are O- (1H-benzotriazol-1-yl)-*N, N, N', N*' -tetramethlyuronium tetrafluoroborate (TBTU, **30**), and HATU, (**31**), which is based upon the HOAt additive.

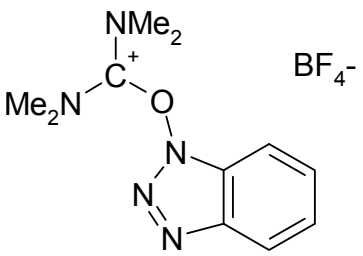

30

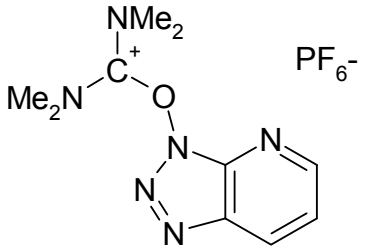

31

The biggest drawback in employing these reagents is their tendency to react with free amine groups, unlike carbodiimides or phosphonium salts, which is why the ***N***-protected amino acid must be pre-activated with the uronium salt before the addition of the free amine, and the use of excess uronium salt must be avoided [67].

Mixed anhydrides have long been used in peptide synthesis. The most obvious problem they present is that of regioselectivity, as nucleophilic attack of the free amine group must occur at the correct carbonyl carbon atom. This problem can be addressed by treatment of the ***N***-protected amino acid with carboxylic acids that are severely sterically hindered. Thus, mixed anhydrides prepared with isovaleroyl chloride or pivaloyl chloride can ensure that nucleophilic attack occurs at the correct site [68] (*scheme 9*).

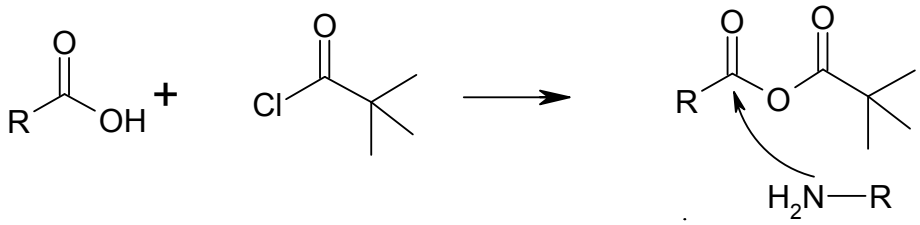

Scheme 9: Regiospecificity using mixed anhydrides

Mixed carbonic anhydrides are another popular choice of coupling reagent, and their regioselectivity is due to electronic rather than steric effects. The carbonyl carbon atom, which is not from the ***N***-protected amino acid, is flanked by two electron-releasing oxygen

atoms, thus decreasing its electrophilicity. Isobutyl chloroformate is probably the most popular choice of reagent for this kind of chemistry [69] (*Scheme 10*).

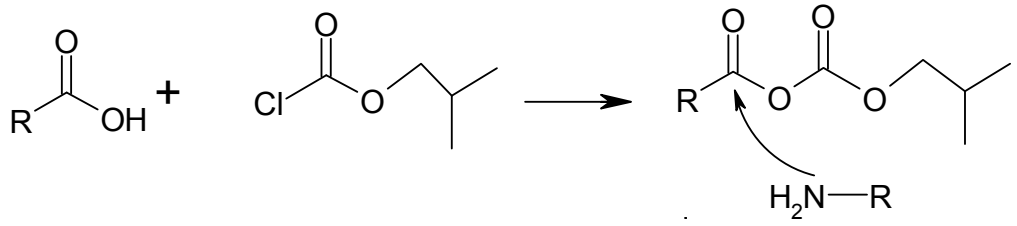

Scheme 10: Regiospecificity using carbonic anhydrides

Mixed carbonic anhydrides can also be generated *in situ* with coupling reagents such as 1-ethoxycarbonyl-2-ethoxy-1, 2-dihydroquinoline (EEDq) [70], (*scheme 11*). Reagents of this type are very slow to react with amines, but react readily with carboxylic acids, and the anhydride undergoes subsequent aminolysis rapidly.

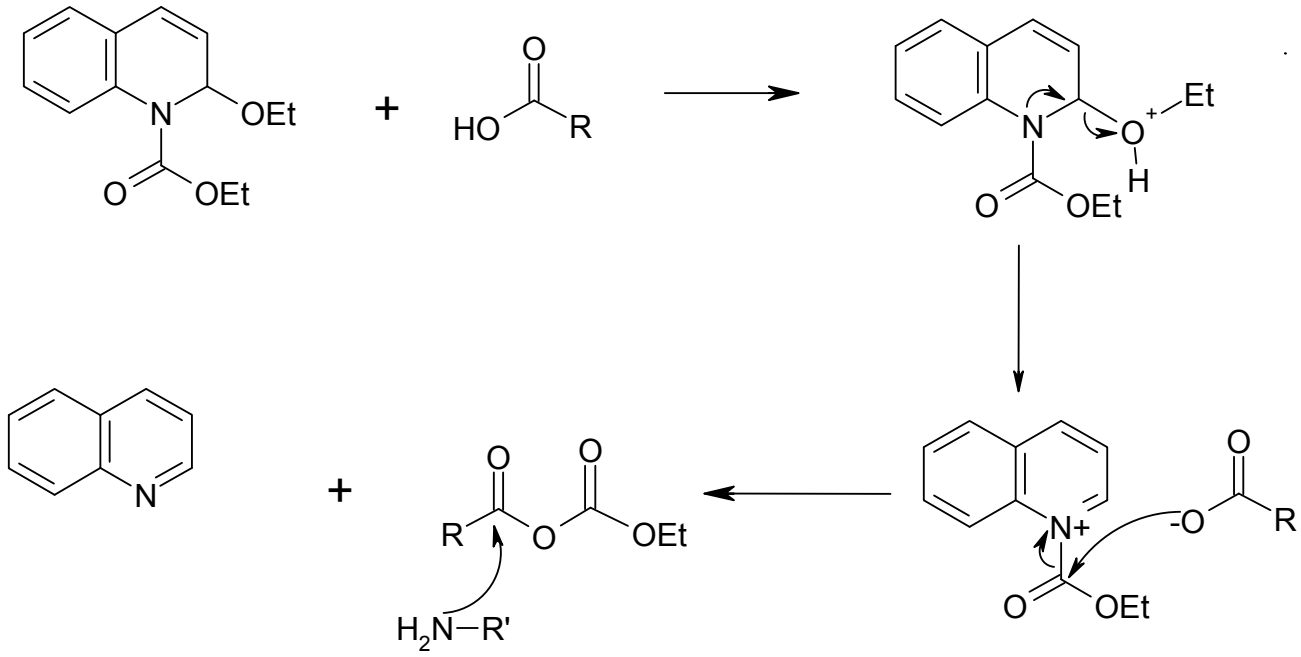

Scheme 11: In situ generation of mixed carbonic anhydrides

1.6.2: Amino Acids as Ligands

Transition metals frequently function as co-factors in enzyme catalysed reactions, and known metalloproteins such as ferredoxins, cytochromes, and blue copper proteins number

several hundred. The metal cation can be held in an enforced stereochemistry, which can help bind or activate substrates in enzymatically catalysed reactions (*see p. 21*). Amino acid residues can coordinate to a metal cation via donor atoms from the peptide backbone or side chain heteroatoms. The ***N***-terminal amine, deprotonated amide, and carbonyl oxygen atoms from the peptide backbone can all function as donor atoms, while side chain donors include the imidazolic nitrogen of histidine, the carboxylate groups of glutamic and aspartic acid, and the sulphur atoms of methionine and cysteine.

Sulphur donor atoms are among the most common binding sites of proteins [71]. In iron-sulphur proteins, iron atoms are coordinated tetrahedrally by the thiol groups of cysteine residues and inorganic sulfide atoms. Such iron-sulphur clusters are common in redox enzymes (**32**). In the blue copper proteins, both cysteine sulphur atoms, and the thioether group of methionine are used to coordinate a Cu^{2+} ion. Being a 'soft' donor atom, sulphur shows a great affinity towards the late transition elements, with the thioethers of methionine and S-methyl cysteine being particularly selective towards Pd (II) and Pt (II) ions [72].

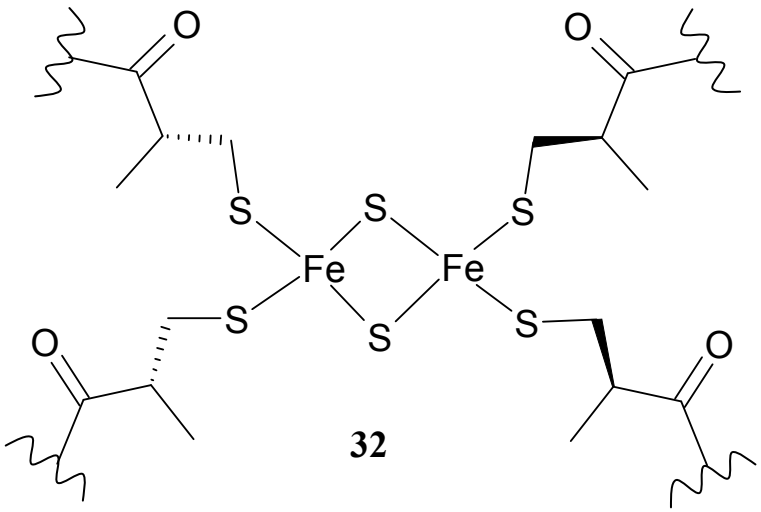

32

Methionine has been used as an inhibitor of the nephrotoxicity of the anti-cancer drug cisplatin, and indeed one of the metabolites of the drug is the complex $[Pt(L\text{-}Met)_2]$ [73]. The use of cisplatin has, however, been limited by the toxic side effects. These side effects result from the coordination of the Pt (II) ion to cysteine sulfhydryl residues in the kidney, and the formation of the Pt-S bonded species is thought to have a significant role in the toxicity and transport of the drug [74]. Cisplatin is also ineffective against gastrointestinal tumours, owing to the excess of chloride ions in this region, which are able to bind to the platinum centre [75]. Hence, many methionine and S- methyl cysteine-Pt (II) and Pd (II) cisplatin analogues have

been synthesised, and their anti tumour properties investigated. These ligands may not be replaced so easily by chlorides, thus increasing the effectiveness of the drug.

Calaf and co workers synthesised complexes of the type $[M(Cl)_2(L\text{-}MetOMe)]$, (M = Pt, Pd) [76] (**33**). The platinum complex was shown *in vitro* to bind to consecutive DNA bases, the two chloride ions being substituted by two molecules of nucleotide, coordinated via the N(7) atom of guanine, and the N(3) atom of cytosine.

The palladium complex (**34)** incorporating L-methionine methyl ester and the immunoregulatory agent levamisole (LMS) of the formula $[(LMS)_2Pd(L\text{-}Met)]$ was prepared by Nijasure and co-workers, and this was also shown to have antitumour activity [77].

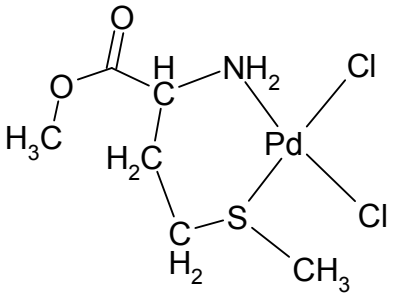

33

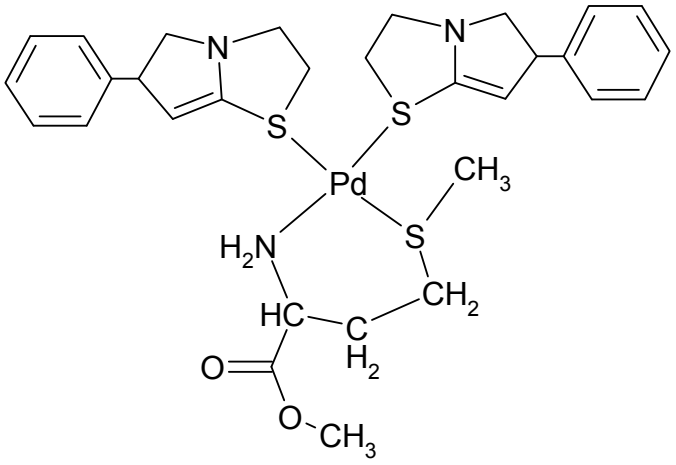

34

Finally, an interesting study was carried out by Sheldrick and co workers, in which several di-peptides of aromatic amino acids (H-Tyr-Trp-OH, H-Trp-Tyr-OH, H-Trp-Phe-OH, H-Phe-Tyr-OH) were reacted with $[(\eta^6\text{-cymene})Ru(acetone)_3]$, producing compounds of the type **35** and **36** [78]. In order to ensure η^6-co-ordination of the ruthenium atom to the aromatic side chains of these amino acids, these compounds were prepared under strongly acidic conditions (neat trifluoroacetic acid) to prevent competitive η^6-co-ordination from the amine and carboxylate groups. Under these conditions, it was found that co-ordination of the ruthenium atom occurred in a chemospecific manner, in order of electron-donating ability, with the indole ring of the tryptophan side chain being the most favoured, followed by the phenol group of tyrosine, and finally the phenyl group of phenylalanine. This was found to be the case irrespective of whether the amino acids were found at the ***C***- or ***N***-terminal of the dipeptides.

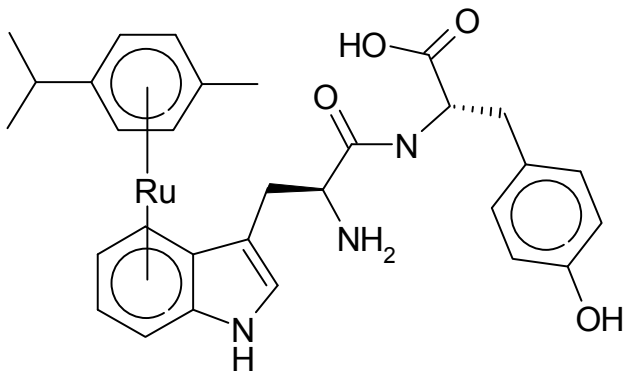

35

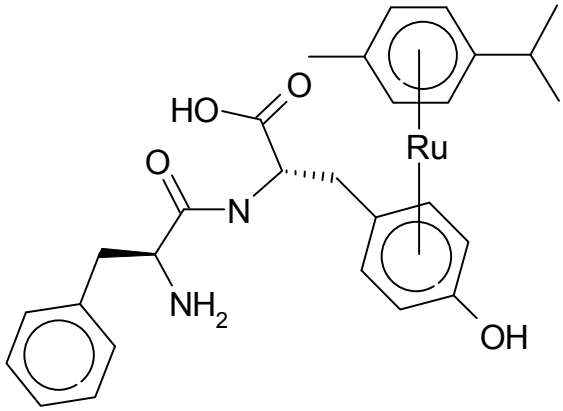

36

However, when an analogous series of compounds was prepared from the reaction of the same dipeptides with [(η^5-Cp*)Ir(acetone)$_3$], kinetic studies showed an initial preference for co-ordination at the C-terminal of the dipeptide, and a mixture of products of the type **37** and **38** were obtained.

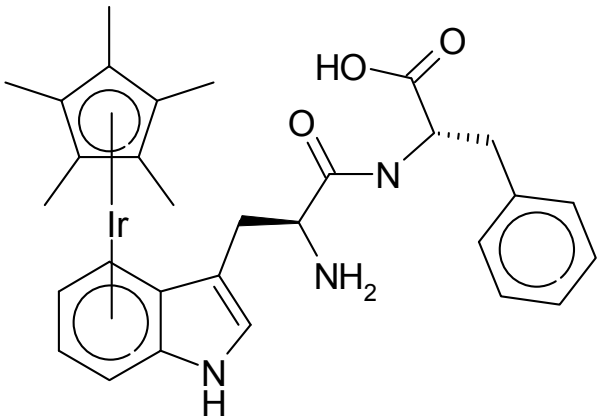

37

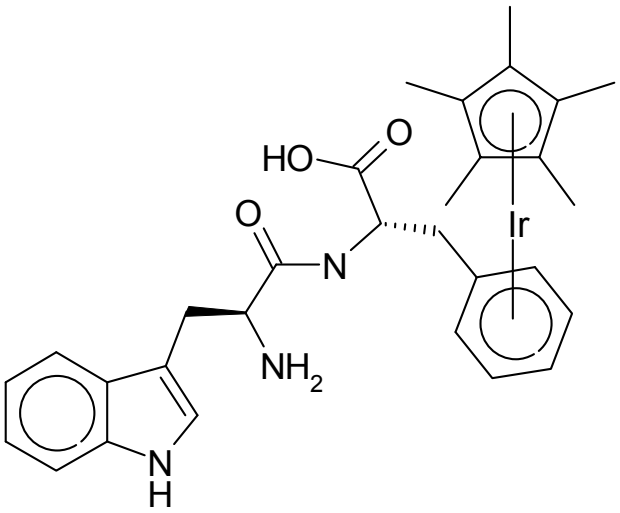

38

1.7: Ferrocene Derivatives of Amino Acids

The first example of an amino acid modified with a ferrocene group was reported as far back as 1957, in an attempted synthesis of DL-alanine [79]. In 1987, Degani and Heller employed the ferrocene moiety as a redox relay, by modifying the protein glucose oxidase, with several ferrocene units. Thus, the enzyme could interact with metal electrodes [59]. In the previous

year, Eckert and co-workers had used the lipophilic ferrocene moiety to increase the solubility of peptides in organic solvents, and to facilitate their chromatographic purification [80]. Since then, an increasing number of amino acid derivatives of ferrocene have been reported in the literature, taking advantage of the self-assembling properties of peptides, and the well defined electrochemical and spectroscopic properties of ferrocene, in areas such as the study of electron transfer processes in proteins [81], the development of supramolecular 'smart' materials [82], asymmetric catalysis [83], and in bioorganometallic chemistry, which is the main focus of this section.

Following on from the work of Degani and Heller, Shinohara *et al*. modified several proteins, including bovine serum albumin (BSA) and the biotin-binding protein avidin, with ferrocene units [84]. The modified proteins were then adsorbed on an SnO_2 electrode, together with fructose dehydrogenase (FDH), and the sensor response of the electrode for fructose was investigated via chronoamperometry. The co-adsorption of Fc-BSA enhanced the response current significantly. This suggests that the Fc-BSA functioned as an electron-transferring interface. Direct modification of FDH with ferrocene units had the effect of denaturing the protein.

The use of chemically modified metalloproteins to investigate electron transfer within peptides has been the focus of much attention in recent years. The variable redox potential of the ferrocene moiety makes it ideally suited to this task. It has been determined by Kraatz *et al*. that the redox behaviour of the ferrocenoyl group is sensitive not only to individual amino acid side chains, but also to the number of residues attached [85]. The electrochemistry of a series of oligoprolines, Fc-Pro_n-oBz (n = 1-4) (**39**) was investigated, and it was found that elongation of the peptide chain resulted in a cathodic shift in the redox potential of the ferrocenoyl group.

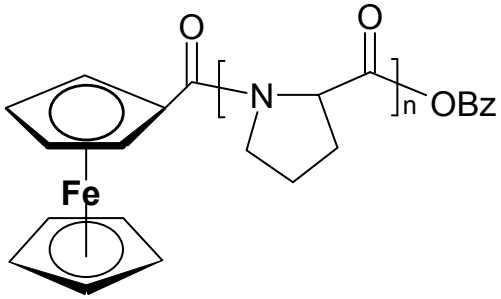

39

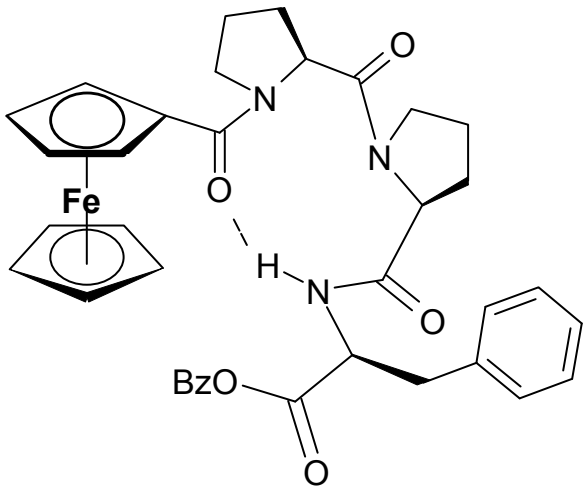

40

When n = 3, one full turn of the polyproline – II helix was complete, and elongation of the chain to n = 4 caused no further shift in redox potential. When n > 3, all the carbonyl groups point towards the ester carbonyl of the peptide chain, thereby creating a permanent dipole within the molecule. Such alignments are thought to play a major role in influencing electron transfer rates within peptides [86], yet since the Fc group is at the positive end of the dipole, the cathodic shift with increasing chain length is counterintuitive. The authors tentatively attribute this effect to the directional character of a carbonyl oxygen p-orbital perpendicular to the Cp-amide plane.

Interestingly, when the third proline residue was replaced by phenylalanine, a β- turn was induced in the peptide, owing to the presence of the amide proton on the third residue, which formed a hydrogen bond with the ferrocenoyl oxygen (**40**). An anodic shift of ca. 30mV of the ferrocenoyl group was observed, illustrating the ability of ferrocene to distinguish between different structural motifs present in small peptide chains.

The electron transfer between the enzyme ribonuclease reductase (RNR) and modified, water-soluble ferrocenes (**41**, **42**) has been investigated by Liu *et al*. [87]. The enzyme R-2 sub-unit consists of a μ-oxo-bridged binuclear Fe (III) site, and a tyrosyl radical. Electron transfer is believed to occur in the following manner:

$$Fe_2^{III}, Tyr^{\cdot} + e^- \rightarrow Fe^{III}Fe^{II}, Tyr^{\cdot} + H^+ \rightarrow Fe_2^{III}, Tyr^-$$

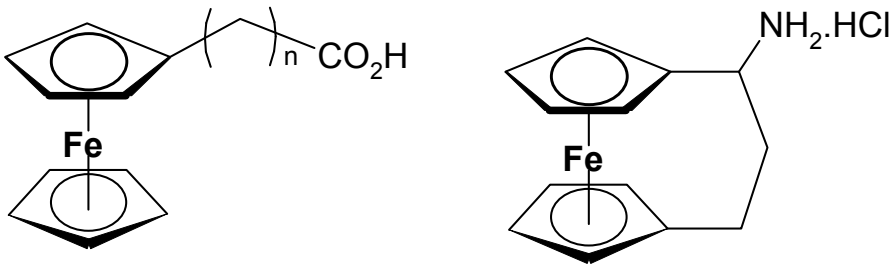

n = 6, 8, 10

41 **42**

It was found that the ferrocene derivatives were strong enough oxidizing agents to reduce the tyrsoyl radical, but not the Fe^{III} atom, unlike organic radical substrates. The authors attribute this to the difficulty of ferrocene in transferring electrons from its orbitals to the Fe^{III} atom.

Kraatz *et al*. have also investigated the change in the redox potential of ferrocene-containing peptides, via H-bonding with substrates. The ferocenoyl derivative Fc-LF-OMe showed a 30mV shift in redox potential upon binding 3-aminopyrazole, due to the β-sheet conformation induced in the molecule (**43**) [88].

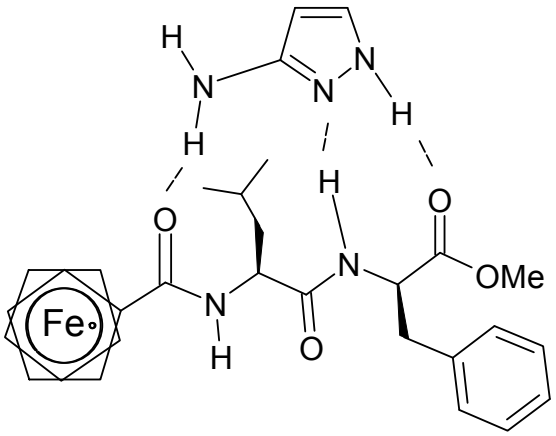

43

Kenny *et al*. investigated the anion-binding properties of three *N*-ferrocenoyl glycine ester derivatives (benzyl, ethyl, and methyl). While the choice of ester was shown not to be crucial, all three were shown to bind $H_2PO_4^-$ strongly [89].

The same group subsequently prepared six novel *N*-ferrocenoyl dipeptide ester derivatives, with the least sterically hindered Fc-GG-OMe (**44**) producing the most sensitive electrochemical response in anion binding studies [90]. Bulky R groups are thought to hinder close interaction of the substrate and the amide proton [91]. The group is currently developing these compounds by altering the stereochemical environment vicinal to the amide proton, by incorporating a phenyl spacer between the ferrocene moiety and the amide group (**45**) [92].

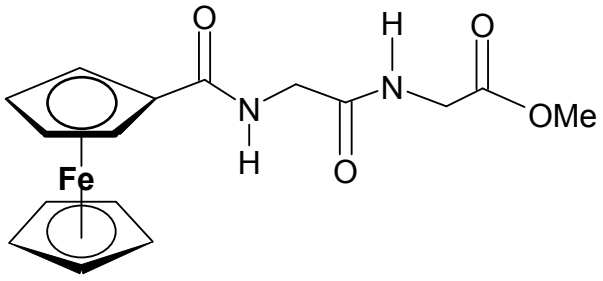

44

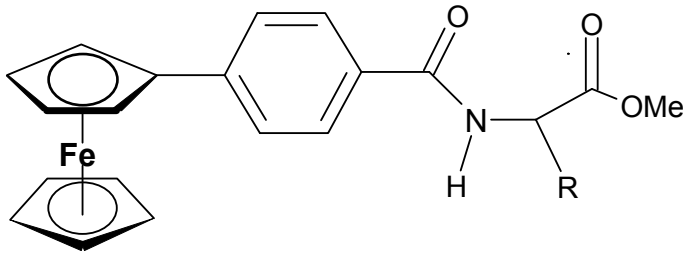

45

The fields of supramolecular science and crystal engineering are concerned with the development of advanced materials, capable of performing complicated tasks on the molecular level [93]. Due to their potential application as molecular conducting devices, superconductors, and molecular memory devices, several groups have taken advantage of the self-organizing properties of ferrocene containing peptides, to construct multi-centred charge transfer compounds. The peptide backbone is employed to control the spatial arrangement of the ferrocene redox centres.

The group of Hirao has investigated the self-assembling properties of ferrocene bearing podand dipeptide chains, e.g. (L-Ala-L-Pro-OMe) (**46**). They found that, due to two *intra*-molecular hydrogen bonds, and hydrophobic interactions of the proline residues, the molecules adopted a helical arrangement in the solid state, with one turn of the helix per 14.91Å [94]. There was a stacking effect observed, with the proline residues forming hydrophobic columns, and the ferrocene groups forming redox-active columns.

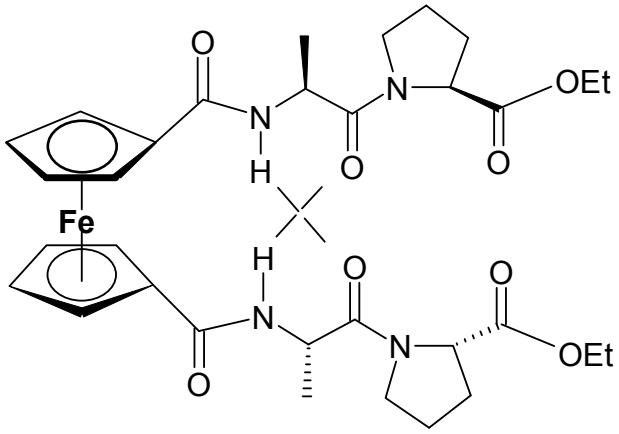

46

The mono substituted derivative, in the absence of these *intra*molecular H-bonds, formed intermolecular, H-bonded seven-membered rings. Because of the *intra*-molecular H-bonding,

the di-substituted derivative was found to crystallize in the 1, 1'-configuration of the substituents. In the absence of an amide proton, as in the di-substituted oligoprolines prepared by Kraatz *et al*. (*see p. 34*), no *intra*-molecular H-bonding is possible, and the molecule adopts a 1, 3' conformation in the solid state, to minimize steric interactions of the substituents.

A novel 21 amino acid peptide with the sequence $(Leu\text{-}Lys\text{-}Leu\text{-}Leu\text{-}Leu\text{-}Lys\text{-}Leu)_3$, incorporating six ferrocenoyl groups attached to the lysine side chains, was recently synthesized by Wieckowska and co-workers (**47**). The peptide was found to preserve the α-helix, with the ferrocene groups being aligned one on top of the other. There was also evidence from electrochemical studies of communication between the individual redox centres [95].

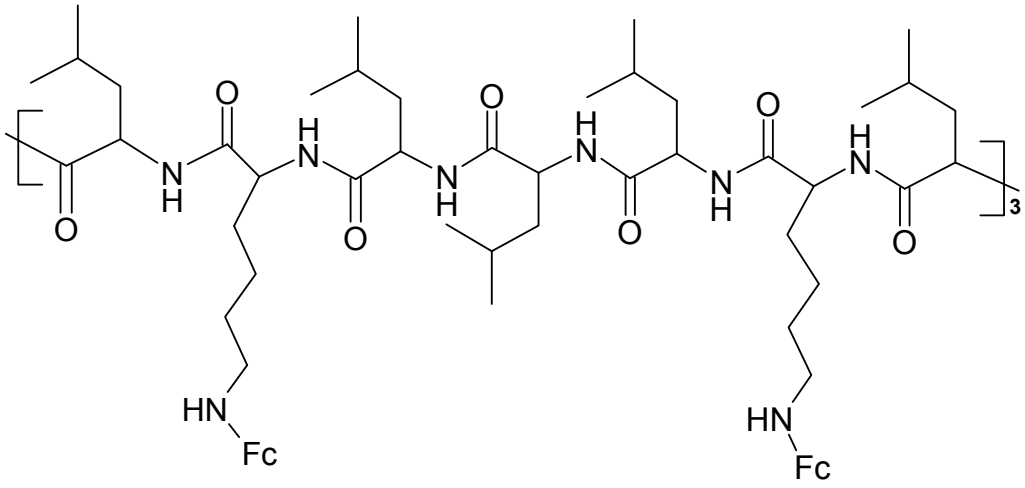

47

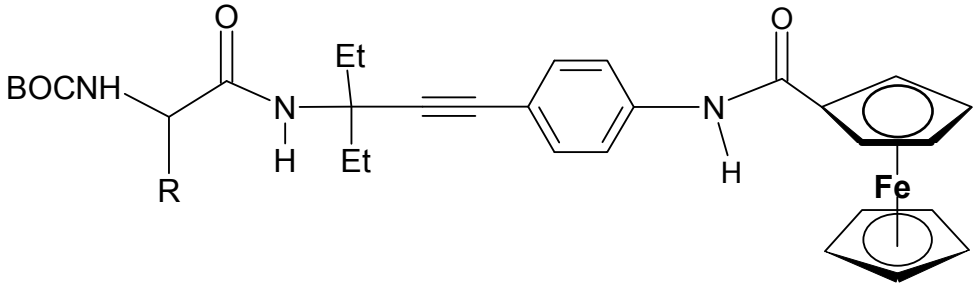

48

In their work on linking organometallic moieties to biomolecules, Nolte *et al*. have prepared several ferrocene containing alkynyl peptides (**48**), thus providing a synthetic method for the selective labelling of the C-terminal of peptides. The same group also produced the heterobimetallic compound (**49**), using benzoic acid chromium tricarbonyl, under mild peptide coupling conditions, thus allowing labelled biomolecules to be detected via infra-red spectroscopy [96].

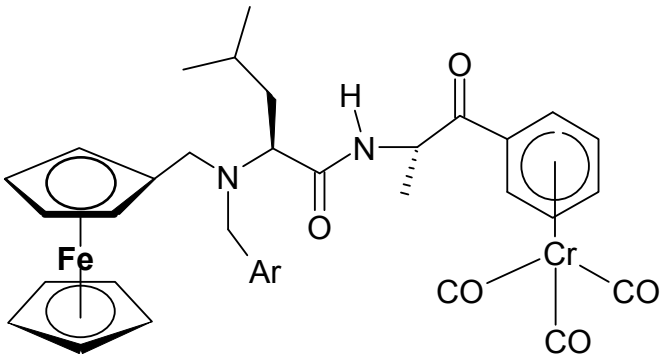

49

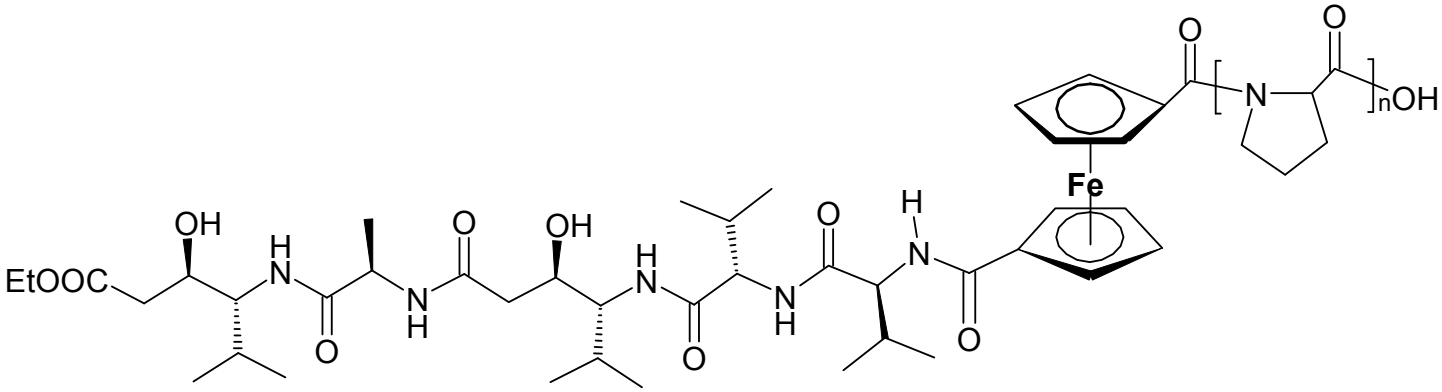

50

Xu *et al*. have recently prepared the asymmetrically di-substituted ferrocenoyl peptide (**50**) as a potential biosensor – one ring is substituted with an oligoproline chain, the other with a pentapeptide, containing the uncommon amino acid statine. This pentapeptide is known to be a potent inhibitor of aspartic proteases, such as HIV-1 protease. The electrochemical response of this molecule towards aspartic proteases is under investigation [97].

Ferrocene has an inter-cyclopentadienyl ring separation of circa 3.3Å, which is close to the N-O separation for the hydrogen bond in a β-sheet (an important secondary structural feature of peptides), and this fact has been exploited by Herrick and co-workers, who prepared the proline and valine derivatives of 1, 1'-ferrocene carboxylic acid (**51** and **52** respectively) [98].

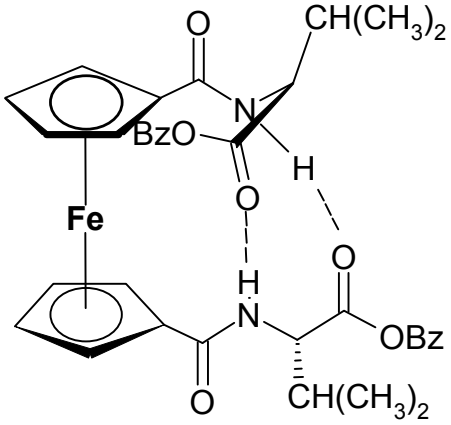

51

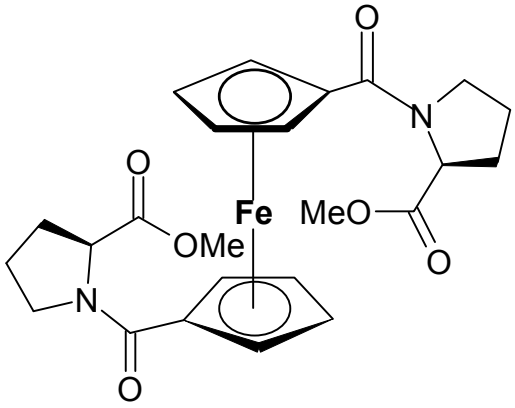

52

The spectroscopic data from this work showed that the ferrocene skeletal unit could indeed be used to induce an ordered, β-sheet-like conformation in **53**, with symmetrical hydrogen bonding occurring in an anti-parallel fashion, between the amide proton and the oxygen atom of the ester group. Use of the ferrocene moiety also proved successful in overcoming the problem of aggregation in solution associated with other β-sheet mimetics [99].

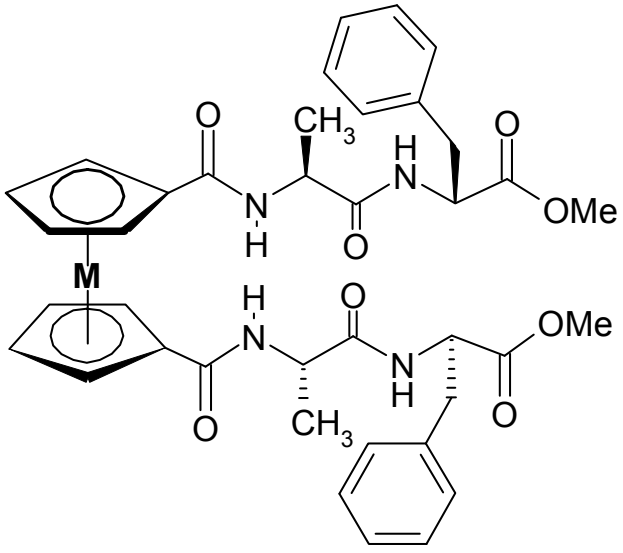

M = Fe (53), Co^{+} (54)

This observation was further investigated by Weyhermuller *et al*., who investigated the influence of a positive charge on the β-sheet conformation by preparing a series of ferrocene-peptide derivatives, along with their cobaltocenium analogues (**53** and **54** respectively) [100]. By preparing the positively charged cobaltocenium compounds, the difficulty in isolating the one-electron oxidized ferricenium derivative could be overcome.

The authors concluded that the proximity of the positively charged cobalt atom had minimal effect on intra-molecular hydrogen bonding which is responsible for the stability of the β-sheet, while recognizing that the symmetrical nature of the organometallic peptides prepared, coupled with their exclusive use of non-polar, uncharged amino acids, may have influenced their findings.

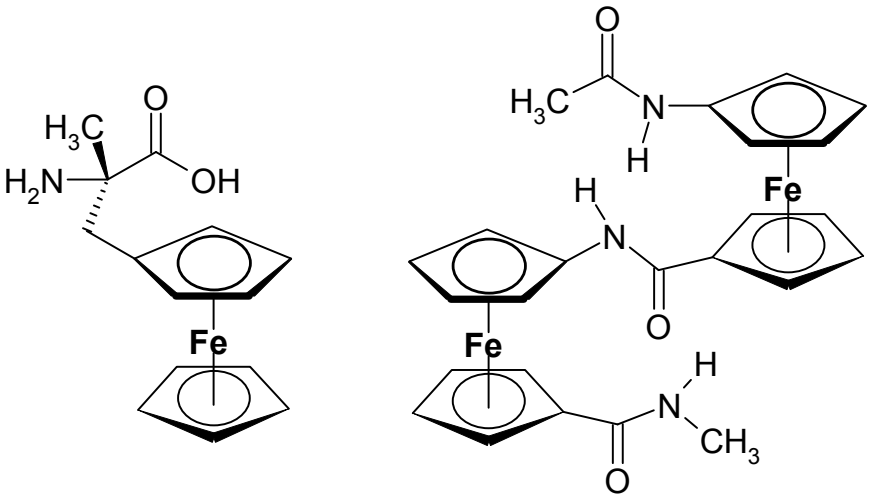

55 **56**

The ferrocene moiety has also been incorporated into amino acids at non-terminal positions. Kira and co-workers prepared the novel ferrocenyl amino acid (**55**) [101]. The amino acid is free to undergo peptide chemistry at both the N and C termini. In polypeptides containing this residue, e.g. $(Ferala)_2$-$(Glu(OBz))_4$, a right-handed helix was still adopted, despite the bulky ferrocenyl group.

Okamura and co-workers prepared the novel peptide containing skeletal ferrocenoyl groups (**56**), in which the three amide planes were found to stack one over another in the solid state. This is indicative of the conformational freedom afforded by the two rotary cyclopentadiene rings of ferrocene [102].

Finally, the group of Frejd *et al*. used the ferrocene moiety to prepare an analogue of the opioid pentapeptide Leu-(5)-enkaphalin, in a multi-step synthetic procedure, in which the tetrapeptide subunit Tyr-$(Gly)_2$-Phe was replaced with a cyclic ferrocenyl-containing subunit, to afford the pentapeptide (**57**). The study of the interaction of biomolecules with membrane-bound receptors is a difficult process to replicate *in vitro*, particularly when the parent pentapeptide has such a high degree of conformational freedom [103]. The receptor selectivity towards enkephalins is, however, thought to be dependent on the relative orientation of the aromatic residues of tyrosine and phenylalanine. The two cyclopentadiene rings of the ferrocenyl group effectively replaces these two phenyl rings, and thus functions as a 'constraining' unit, while still allowing a certain degree of conformational freedom of the peptide backbone. Hence, the peptide is still able to adopt a conformation similar to that adopted *in vivo*.

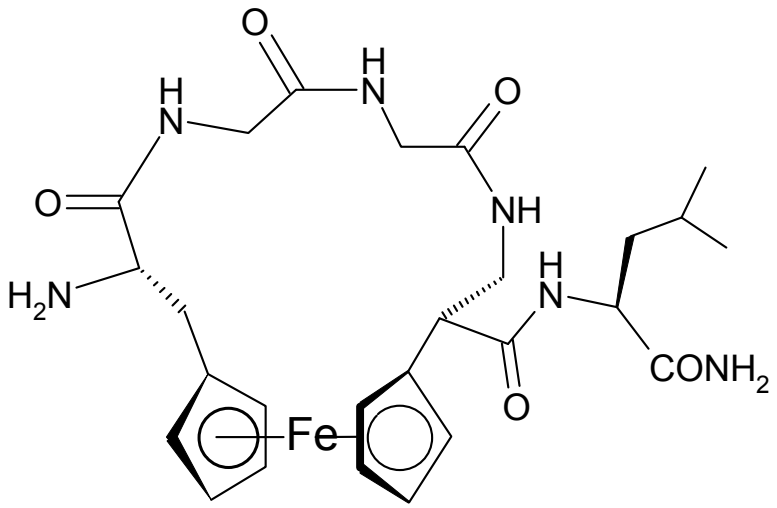

57

1.8: References

1) Metallocenes, N.J. Long, (*1998), Blackwell sciences.*
2) G. Wilkinson, *J. Am. Chem. Soc., 74,* (1952), *6146.*
3) F.A.Cotton, G. Wilkinson*, Advanced Inorganic Chemistry, 5th ed., Wiley-Interscience.*
4) G. Wilkinson, R.B. Woodward, M. Rosenblum, M.C. Whiting, *J. Am. Chem. Soc., 556, (1952), 11.*
5) A. Tongi, T. Hayashi, *Ferrocenes, VCH, Wienhiem, (1993).*

6) L. Lin , A. Berces, H.B.Kraatz, *J. Organometallic Chem.,* 556, *(1998)*, *11.*

7) S. Barlow, R.S. Marder, *J. Chem. Soc. Chem. Comm., (2000), 1555.*

8) J.C. Calabrese, L.T. Cheng, J.C. Green, S.R. Marder, W. Tam *J. Am. Chem. Soc. 113,(1991), 7227.*

9) P.D. Beer, M.I. Ogden, D.B. Crowe, B. Main, *J. Chem. Soc. Dalton Trans., (1993), 2107.*

10) M.C. Grossel, M.R. Goldspink, J.A. Hirljiac, S.C. Watson*., Organometallics, 10, (1991), 851.*

11) J.C. Green, *Struct. Bond., 43, (1981), 37.*

12) H.B. Kraatz, Y. Xu, P. Saweckzko, *J. Organometallic Chem.,637-639, (2001), 335.*

13) A. Hess, O. Brosch, T. Weyhermuller, N.M. Nolte, *J. Organometallic Chem., 589, (1999), 75.*

14) C. Lopez*,* A. Caubret, X. Solans, M. Font-Bardia*., J. Organometallic Chem., 598, (2000), 87.*

15) O. Brosch*,*T. Weyhermuller, N.M. Nolte*, Inorg. Chem., 38, (1999), 5308.*

16) G.W. Gokel, D.Marquading, I. Kugi *, J. Org. Chem., 37, (1972), 3052*

17) M.R. Bryce, A. Chesney, R.W.J. Chubb, A.S. Batstanov, J.A. Howard*., Tetrahedron, Asymmetry, 8, (1997), 2337.*

18) A. Gonzales, J.R. Granell, C. Lopez, *J. Organometallic Chem., 637-639, (2001),116.*

19) A.D. Ryabov, *Chem. Rev., 90, (1990), 403.*

20) Y. Wu, X.L. Cui, C.X. Du, W.L. Wang, R.Y. Guo, R.F. Chen *J. Organometallic Chem., 637-639, (2001), 27.*

21) X.L. Cui, Y.J. Wu, L.R. Yang*., Chin. Chem. Lett., 10, (1999), 127.*

22) R.H. Crabtree*,* K. Kavallieratos, S. Wang, *Inorg. Chem., 38, (1999), 5184.*

23) P.D. Beer, Z. Chen, A.R. Goulden, S.E. Stokes, *J. Chem,soc., Chem. Comm., (1992), 270.*

24) P.D. Beer, *Inorg. Chem., 36, (1997), 2112.*

25) P.D. Beer*, Co-Ord. Chem. Rev., 205, (2000), 131.*

26) P.D. Beer, *J. Organometallic Chem., 375, (1989), 240.*

27) J.E. Kingston, L. Ashford, P.D. Beer, M.G.B. Drew, *J. Chem. Soc., Dalton Trans., (1999), 251.*

28) C. Valerio, J.L. Fillaut, C. Valero, J. Ruiz, J. Guitlard, D. Austruc*, J. Am. Chem. Soc., 119, (1997), 2588.*

29) M.S. Searle, D.H. Williams*, J. Am. Chem. Soc., 114, (1992), 10690.*

30) P.D. Beer, S.W. Dent, T. Wear*, J. Chem. Soc., Faraday Trans., 92, (1996), 97.*

31) P.D. Beer, M.G.B. Drew, R. Jagessar, *J. Chem. Soc., Dalton Trans.,(1997), 881.*

32) D. Austruc, C. Valerio, J.L. Fillaut*., J. Am. Chem. Soc., 119 (1997), 2588.*

33) P.A. Gale, Z. Chen, M.G.B. Drew, J.A. Heath, P.D.Beer*., Polyhedron 17, (1998), 405.*

34) H. Tsukube, H. Fukui, S. Shinoba, *Tett. Lett., 42, (2001), 7583.*

35) P.W. Atkins, *Phsyical Chemistry, 5th Ed., Oxford University Press, (1994).*

36) S.K. Pal, A. Krishnan, P.K. Das, A.G. Samuelson, *J. Organometallic Chem.,604, (2000), 248.*

37) M. Malaun R. Kowallick, A. McDonagh, M. Marcaicion*., J. Chem Soc., Dalton Trans., (2001), 3025.*

38) S. Barlow*,* S.R. Marder*, J. Chem. Soc., Chem. Comm., (2000), 248.*

39) T.D. Turbitt, W.E. Watts, *J. Chem. Soc., (1971), 177.*

40) S.R. Marder, J.W. Perry, W.P. Schaefer, B.G. Tiemann*., Organometallics, 10, (1991), 1896.*

41) D.W. Bruce*, J. Chem. Soc. Dalton. Trans, (1993), 2983.*

42) A.M. Giroud-Godquin, P.M. Maitlis, *Agnew. Chem. Int. Eng. Ed., 30, (1991), 375.*

43) J. Malthete, J. Billard, *Mol. Cryst. Liq. Crys. 34, (1996), 117.*

44) R. Deschaneux, J.L. Marendez, *J. Chem. Soc. Chem. Comm., (1991), 909.*

45) R. Deschaneux, M. Schweissgath, A.M. Levehut, *J. Organometallic Chem., 548, (1997), 49.*

46) X.H. Liu, D.W. Bruce, I. Manners, *J. Chem. Soc. Chem. Comm., (1997), 290.*

47) I. Galyamaldinov, I. Kostics, U. Scholten, *J. Chem. Soc. Chem. Comm., (1990), 439.*

48) G. Jaouen, A. Vessieres, I. Butler*, Acc. Chem. Res., 26, (1993), 361.*

49) R. Krieg, R. Wyrwa, U. Mallmann, H. Gorls, B. Schonecker*, Steroids, Vol. 63, (1998).*

50) E.I. Edwards, R. Epton, G. Marr*, J. Organometallic Chem., 168, (1979), 259.*

51) A.N. Nesmeyanov, N.S. Kocketkova, *Russ. Chem. Rev., 43, (1974), 710.*

52) B. Longato, B. Corrain, G. Bonora, G. Pillone*, Inorg. Chim. Acta, 137, (1987), 75.*

53) N.W. Duffy, J. Harper, P. Ramini, R.R. Bandarage, B.H. Robinson, J Simpson*., J. Organometallic Chem.,564, (1998), 125.*

54) N.W. Duffy*,* B.H. Robinson, J. Simpson, *Inorg. Chem., 13, (1994), 511.*

55) T. Itoh, S. Shirakami, N. Ishida, Y. Nakao, T. Yoshida, H.S. Kim*, Chem. Lett., (1998), 979.*

56) H. Tamura, M. Miwa*., Chem. Lett., (1977), 1177.*

57) F.A. Armsrong, H.A. Hill, N.J. Walton*., Acc. Chem. Res., 21, (1988), 40.*

58) O. Brosch, T. Weyhermuller, N.M. Nolte*, Eur. J. Inorg. Chem., (2000), 323.*

59) Y. Degani, A. Heller, *J. Phys. Chem., 91, (1987), 1285.*

60) G. Zubay, *Biochemistry, 3rd ed., WCB Publishers, (1993).*

61) M. Jones, *Organic Chemistry, (1997), W.W. Norton and Co.*

62) R.B. Merryfield, *J. Am. Chem. Soc., 85, (1963), 2149.*

63) P.L. Williams, *Chemical Approaches to the Synthesis of Peptides, CRC press, (1997), 95.*

64) M. Bodansky*,* A. Bodansky*, Principles of Peptide Synthesis, 2nd ed., Springer-Verlay, (1993).*

65) G. Gavine, G. Kenner, R.C. Shepherd, *J. Am. Chem. Soc., 91, (1969), 5669.*

66) J. Coste, J. le-Nyuyen, B. Castro*, Tett. Lett., 31, (1991), 305.*

67) S.C. Story, J.V. Aldrich*, Int. J. Pept. Protein. Res., 43, (1994), 29.*

68) J.R. Vaughan, A. Osato, *J. Am. Chem. Soc., 73, (1951), 5553.*

69) G. Stravropoulos, K. Kkaragiannis,*Int. J. Pept. Protein. Res., 45, (1995), 908.*

70) B. Bellau, G. Malik, *J. Am. Chem. Soc., 90, (1968), 1651.*

71) B. Boka, Z. Nagy, K. Varnagy, I. Sovago, *J. Inorg. Biochem., 83, (2001), 77.*

72) L. D. Pettit, M. Bezer, *Co-Ord. Chem. Rev., 61, (1985), 97.*

73) P.S. Murdoch, J. D. Randford, P.J. Sadler, S.J. Barners-Price*, Inorg Chem, 32, (1993), 2249.*

74) J. Redijk, *Chem. Rev., 99,(1999), 2499.*

75) M.P. Hacker, E.B. Douple, I.H. Krakoff, *Platinum Coordination Complexes in Cancer Chemotherapy, Nijhoff, Boston, (1984).*

76) M. Calaf*,* A. Caubet, V. Moreno, M.F. Bardiu, X. Solans, *J. Inorg. Biochem., 59, (1995), 63.*

77) A.M. Nijasure, V.N. Joshi, A.D. Sawant*, J. Inorg. Biochem., 73, (1999), 109.*

78) R. Stodt, S. Gencaslan, A. Frodl, C. Schmidt, W. Sheldrick, *, Inorg. Chimica Acta, (2003), Article in Press.*

79) M. D. Rausch, M. Vogel, and H. Rosenberg, *J. Org. Chem., 900-903, 1957, 22.*

80) H. Eckhart.,C. Seidel*, Agnew Chem, Int. Ed. Eng., 25, (1986), 159.*

81) H.B. Kraatz, J. Lusztyk, G.D. Enright, *Inorg. Chem., 36, (1997), 2400.*

82) T. Moriuchi, A. Nomoto, K. Yoshida, T. Hirao, *J. Organometallic Chem., 589, (1999), 50.*

83) W. Bauer, K. Polborn, W. Beck*, J. Organometallic Chem., 579, (1999), 296.*

84) Y. Xu, H.B. Kraatz*., Tetrahedron Lett., 42, (2001), 75.*

85) H. Shinohara, T. Kusaka, E. Yokoto, R. Monden, *Inorg. Chim. Acta, 137, (1987), 75.*

86) M. A. Fox, E. Galoppini, *J. Am. Chem. Soc., 118, (1996), 2299.*

87) A. Liu, D.N. Lesse, J.C. Swarts, A.G. Sykes*, Inorg. Chim. Acta, 337, (2002), 83.*

88) P. Sawecko, H.B. Kraatz, *Co-Ord. Chem. Rev., 190-192, (1999), 185.*

89) J.F. Gallagher, P.T.M. Kenny, M.J. Sheehy, *Inorg. Chem. Comm., 2, (1999), 200.*

90) J.F. Gallagher, P.T.M. Kenny, M.J. Sheehy, *Inorg. Chem. Comm., 2, (1999), 329.*

91) D. L. Stone, D. K. Smith, *Polyhedron, 22, (2003), 763.*

92) D. Savage, J. F. Gallagher, Y. Ida, P.T.M. Kenny, *Inorg. Chem. Comm., 5, (2002), 1034.*

93) H.B. Kraatz, D.M. Leek, A. Houman, G.D. Enright*, J. Organometallic Chem., 589, (1999), 38.*

94) T. Moriuchi, A. Nomoto*.,* T. Hirao, S. Yamazaki, *J. Organometallic Chem., 637, (2001), 75.*

95) A. Wieckowska *,* R. Bilewicz, A. Misicka, M. Pietraszkiewicz, *Chem. Phys. Lett., 350, (2001), 447.*

96) J. Schnert, A. Hess, N.M. Nolte, *J. Organometallic Chem., 637-639, (2001), 349.*

97) H.B. Kraatz, Y. Xu, P. Saweczko, *J. Organometallic Chem., 637-639, (2001), 335.*

98) R. Herrick, R. Jarret, T. Curran, D. Dragoli, M. Flaherty, S. Lindeyberg, R. Slate, L. Thornton, *Tett. Lett., 37, (1996), 5289.*

99) D. Osterman, R. Mora, F. Kezdy, E. Kaiser, S. Meridith, *, J. Am. Chem. Soc., 106, (1984), 6845.*

100) D. Staveren, T. Weyhermuller, N. Metzler-Nolte, *Dalton Trans., (2003), 210.*

101) M. Kira*, Chem. Lett., (1997), 89.*

102) T. Okamura*,*H. Tsukube, H. Fukui, *Inorg. Chem., 36, (1998), 6731.*

103) S. Maricic*,* U. Berg, T. Frejd, *Tetrahedron, 58, (2002), 3085.*

Chapter II

The Synthesis and Characterisation of *N*-Ferrocenoyl Amino Acids

2.1: Introduction

Following the discovery of ferrocene more than fifty years ago, a vast array of derivatives have been prepared and characterized. Among the first reactions carried out on ferrocene were lithiation using n-butyl lithium, arylation using diazonium salts, and Friedel-Crafts acylation with acid halides and aluminium trichloride. The last of these reactions was instrumental in confirming the aromaticity of the compound. Thus, the well-established organic chemistry of ferrocene has allowed its incorporation into many organic compounds [1], among them biomolecules such as amino acids and peptides.

The work undertaken in this project is a continuation of the research performed by Michael J. Sheehy under the supervision of Dr. Peter Kenny. In this work, it was found that ***N***-ferrocenoyl glycine mono and di-peptide derivatives had anion-binding properties, with particular selectivity being displayed towards $H_2PO_4^-$ (*fig. 1*) [2]. Altering the molecular geometry by incorporating extra methylene spacers into both the peptide backbone, and/or the side chain can not only increase the lipophilicity of the molecule, but also may induce selectivity towards other anionic substrates.

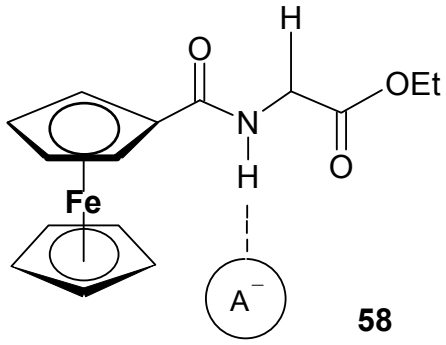

58

*Fig. 1: Anion binding mode of **N**-Ferrocenoyl glycine ester (**58**);*

Anion binding may be dependant on the steric accessibility of the amide proton, as amino acid derivatives with bulkier side chains, such as ***N***-ferrocenoyl phenylalanine, exhibited only small perturbations in their N-H chemical shifts during ^{1}H-NMR anion titration studies [2, 3]. Therefore, tailoring of the chemical environment vicinal to the amide proton is envisaged to alter the anion-binding abilities of these molecules.

The electrochemical and spectroscopic behaviour and chemical stability of ferrocene has resulted in its many different areas of research other than anion sensing, such as asymmetric

catalysis, bioorganometallic chemistry, supramolecular chemistry, in liquid crystalline materials, and in materials for non-linear optics, with the incorporation of a ferrocene moiety into biomolecules currently an area of intense research activity [4]. Modifying a biologically active substrate with one or more ferrocene units allows for the possibility of studying these labelled compounds, given the previously mentioned electrochemical and spectroscopic properties of ferrocene. Amino acids are logical candidates for such modification, given that they fulfil such diverse roles in biological systems.

The chirality of amino acids would make the area of asymmetric catalysis an obvious choice for application of ferrocene peptide derivatives, while their self-assembling properties opens up possibilities in the field of supramolecular chemistry. Ferrocene-peptide derivatives have also been shown to be effective in selective anion recognition.

While there have been an increasing number of ferrocene derivatives of amino acids and peptides since Degani and Heller employed the ferrocene moiety as a redox relay in the enzyme glucose oxidase, few have exploited the presence of potential donor atoms in the amino acid side chain. This is surprising, as side chain donor atoms play an important role in the co ordination of metal ions in biological systems [5]. ***N***-Ferrocenoyl derivatives of amino acids such as L-methionine and L-histidine can provide a possible route towards heterobimetallic systems, given the co-ordinating properties of the hetero-atoms in the side chains of these amino acids. Previous work in the area of ***N***-ferrocenoyl peptides has suggested that the ferrocene moiety is electrochemically sensitive not only to the number of residues attached, but also to the individual side chains [6]. With this in mind, novel ***N***-ferrocenoyl peptides have been prepared with potential application in several diverse areas of current research.

2.2: The Synthesis of Amino Acid Esters

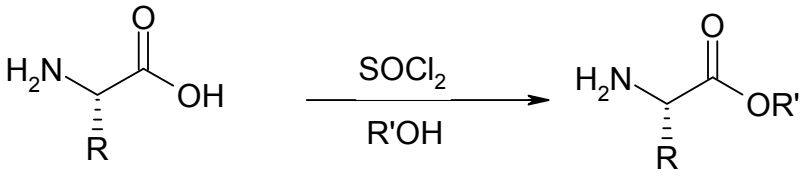

Scheme 1: The esterification of amino acids using a solution of thionyl chloride in the appropriate alcohol.

Esterification of amino acids was accomplished using the long established thionyl chloride procedure, which afforded the amino acid esters as white solids in quantitative yields (*scheme 1*).

The reaction of L-glutamine and L-asparagine under these conditions resulted in esterification of the carboxamide groups in the side chain, yielding L-glutamic acid diethyl ester and L-aspartic acid dimethyl ester respectively (*scheme 2*).

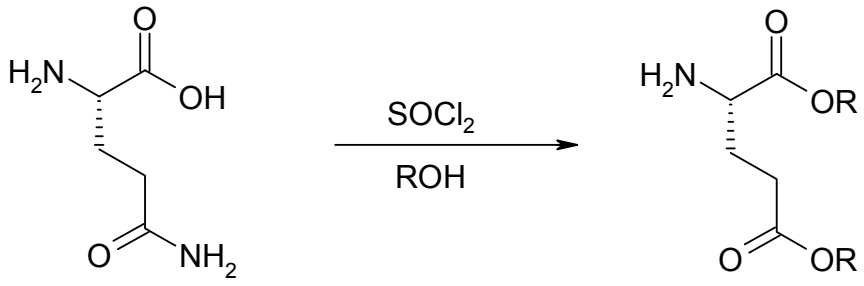

Scheme 2: The attempted esterification of L-glutamine, using the thionyl chloride protocol. The carboxamide functionality, also proved susceptible to esterification under these conditions.

2.3: Synthesis of Ferrocene Carboxylic Acid

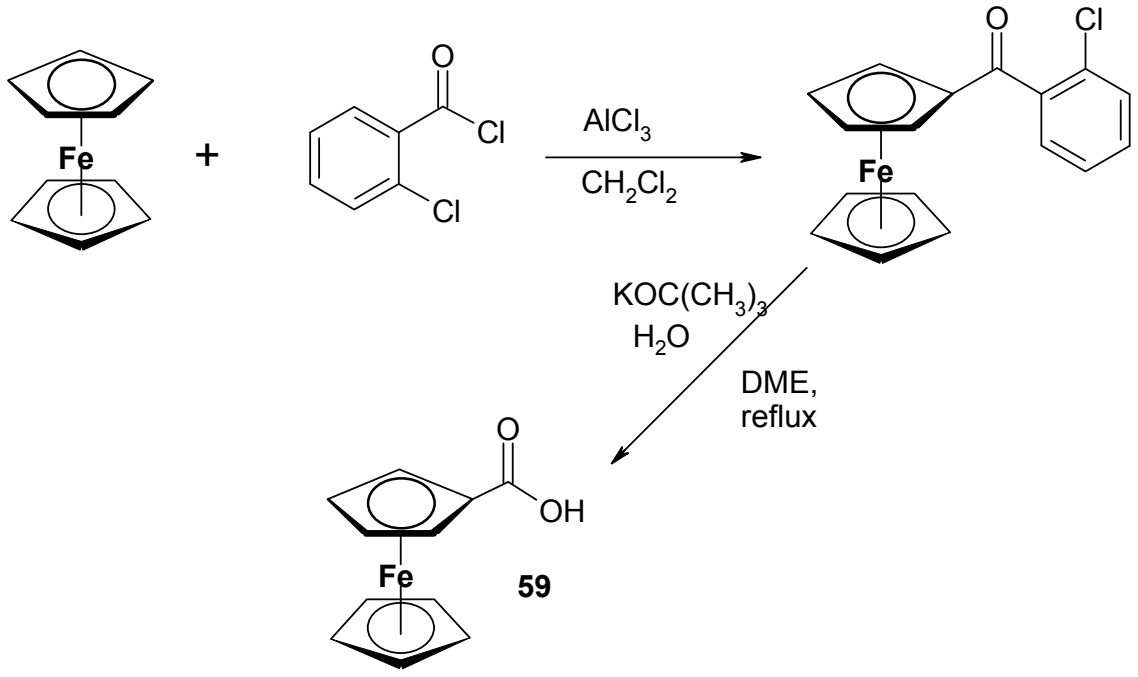

*Scheme 3: Synthesis of ferrocene carboxylic acid (**59**)*

Ferrocene carboxylic acid was prepared using the method of Reeves *et al.* [7], affording the acid as a fine yellow/brown powder in very good yield (70-80%). However, instead of drying the product under vacuum, removal of residual water was accomplished by drying the acid for 6 hours at 80°C.

2.4: Synthesis of *N*-Ferrocenoyl Amino Acid Derivatives

Several routes were employed during the preparation of the ***N***-ferrocenoyl amino acid derivatives, in order to optimize the conditions best suited to their synthesis. As the project evolved, consistent yields of over 80% were achieved using synthetic route 1. Several of these compounds were selected to undergo subsequent peptide chain elongation to afford ***N***-ferrocenoyl dipeptide derivatives, which are discussed in chapter 3.

2.4.1: Synthetic Route 1

Synthetic route 1 is a modification of the procedure used by Kraatz *et al*. [8, 9], which employs dicyclohexylcarbodiimide (DCC) as the coupling reagent, as well as the auxiliary nucleophile 1-hydroxybenzotriazole (HOBt), which forms an air-stable active ester intermediate with ferrocene carboxylic acid. The reactions were followed by TLC analysis at all times. The synthesis of **70** is typical of this synthetic route, and is shown in *scheme 4*. Column chromatography, using a 2:1 hexane/ethyl acetate mobile phase proved the only satisfactory method of purification, affording complete separation of the target molecules from intermediate **60**.

As can be seen from *table 1*, 24 hours was found to be the optimum time at which to quench the reaction. Given the reduced stability of ferrocene compounds in chlorinated solvents [10], it is likely that longer reaction times would result in product decomposition.

Reaction Time (Hrs)	12	18	24	36	48	60
Yield **70**	26	40	72	66	57	32
Yield **60**	41	23	11	12	8	n/d

*Table 1: The % yields of **60** and **70** isolated after varying reaction times during the preparation of **70** using synthetic route 1.*

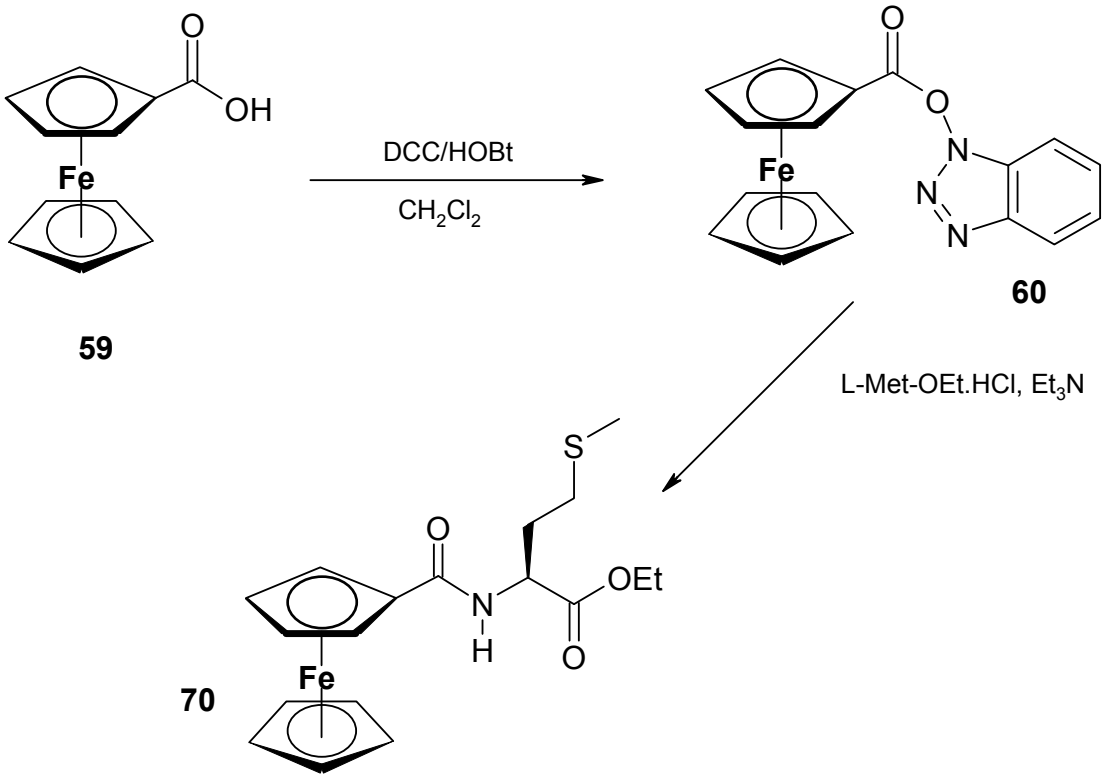

*Scheme 4: The preparation of **N**-ferrocenoyl methionine ethyl ester (**70**), using the DCC/HOBt protocol.*

2.4.2: Synthetic Route 2

Carbonyldiimidazole (CDI), like DCC, is another coupling reagent that has long been employed in peptide synthesis [11]. Indeed, the imidazolic adduct of ferrocene, **61**, first prepared by Imrie *et al*. [12], is a synthetic intermediate that has recently been used to prepare a large array of ferrocene compounds. It is, however, less stable than the Fc-OBt intermediate, and required storage at temperatures < 5 ºC. Compounds **62**, **65**, **68**, **70** and **73**, having previously been prepared according to route 1, were also synthesised using the CDI protocol, and on a similar scale.

As was the case when the DCC/HOBt protocol was employed, the only satisfactory method of work-up was column chromatography, again using 2:1 hexane/ethyl acetate mobile phase, allowing complete separation from the ferrocene-imidazole intermediate. Purification by

recrystallizations from various solvent combinations did not completely remove traces of **61**, and had a negative impact upon yields.

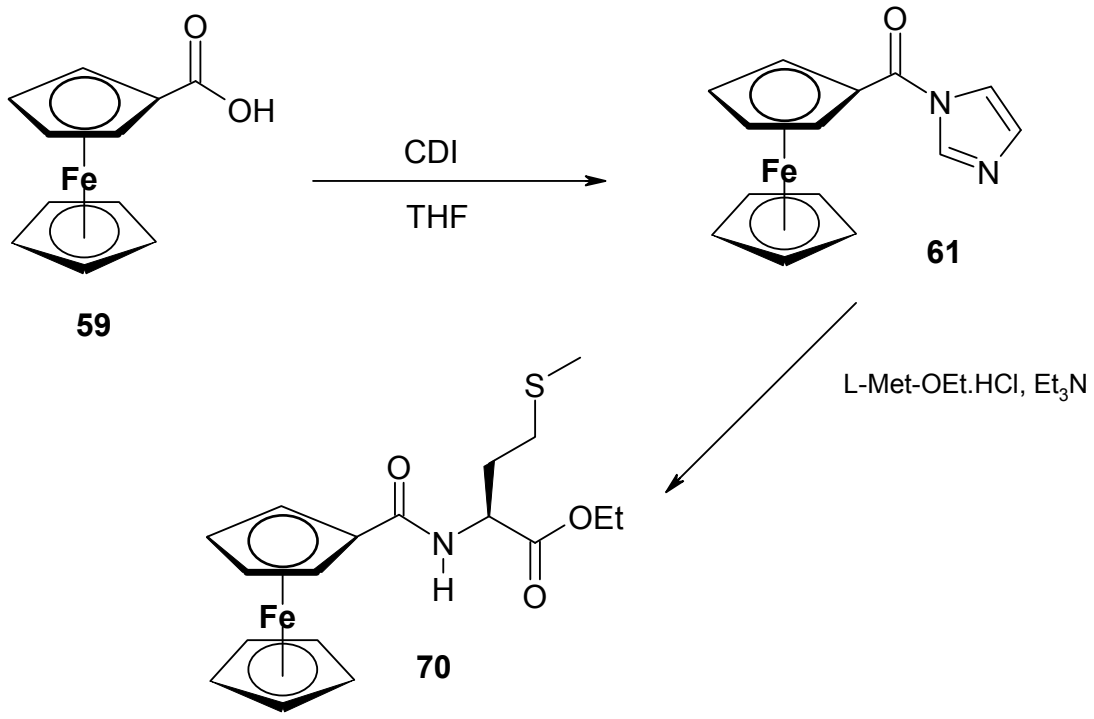

*Scheme 5: The preparation of **70** using CDI as a coupling reagent. Ferrocenoyl imidazolide, **61**, was also isolated during work up.*

2.4.3: Synthetic Route 3

Tetramethyluronium tetrafluoroborate (TBTU) is the most popular of the newer uronium salt coupling reagents [13], although considerably more expensive than either DCC or CDI. Compounds **65**, **68**, **70**, **73**, and **78** were prepared using this protocol. The synthesis of **70** is shown in *scheme 6*.

Mechanistically, the TBTU reagent is thought to function via the formation of an *O*-benzotriazole adduct with the free acid [14], as is the case when the DCC/HOBt protocol is employed. This proved to be the case when **65**, **68**, **70**, **73**, and **78** were prepared in this manner, as varying quantities of the ferrocenoyl-*O*-benzotriazole adduct were isolated during

Purification. This in turn necessitated the use of column chromatography during the purification of the target compounds. For comparative purposes, *table 2* is included, and summarizes the yields of several compounds using the various coupling reagents.

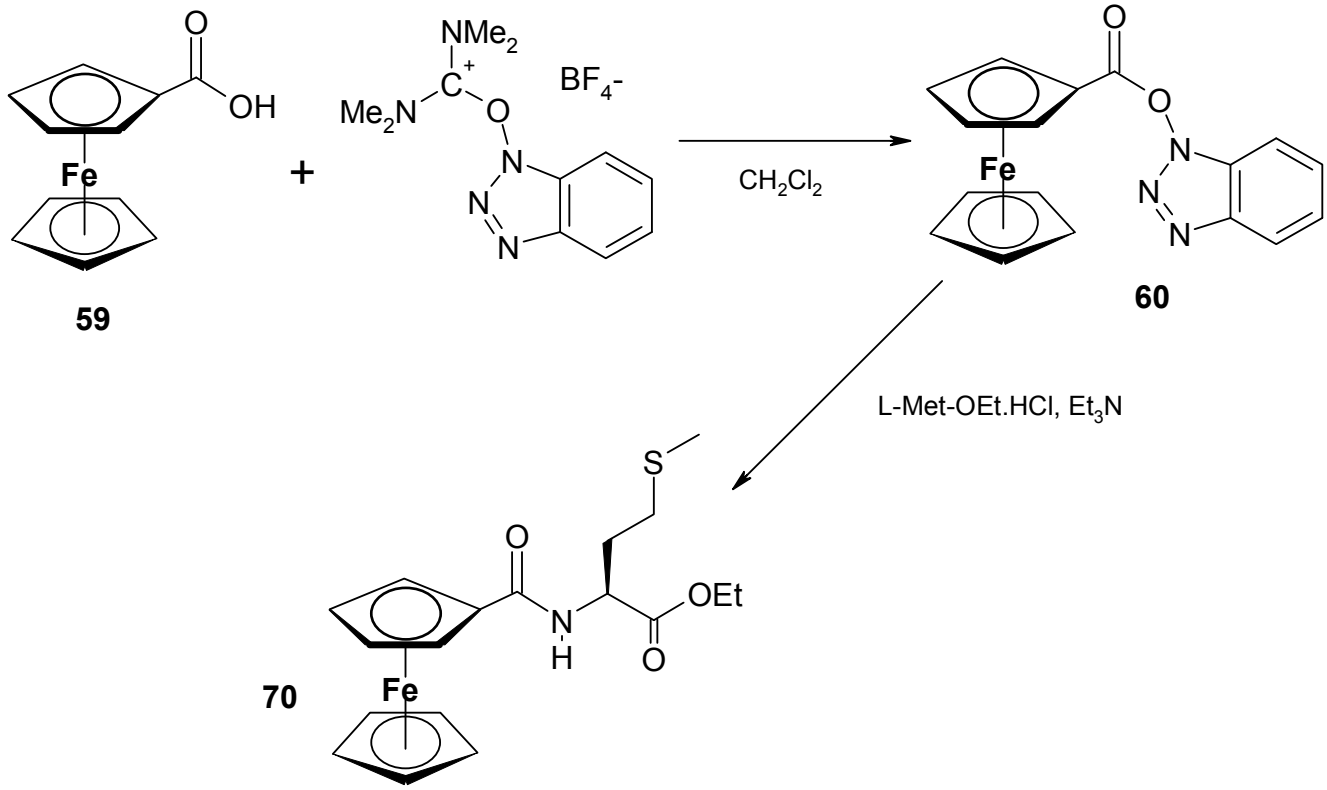

*Scheme 6: Synthesis of **70** using TBTU as the coupling reagent.*

Compound	DCC (DCM)	CDI (THF)	TBTU (DMF)
62	69	67	N/A
65	72	65	69
68	82	79	77
70	70	60	72
73	69	55	75
78	68	N/D	60

Table 2: The % yields of selected compounds using the various coupling reagents and solvents.

2.4.4: Synthetic Route 4

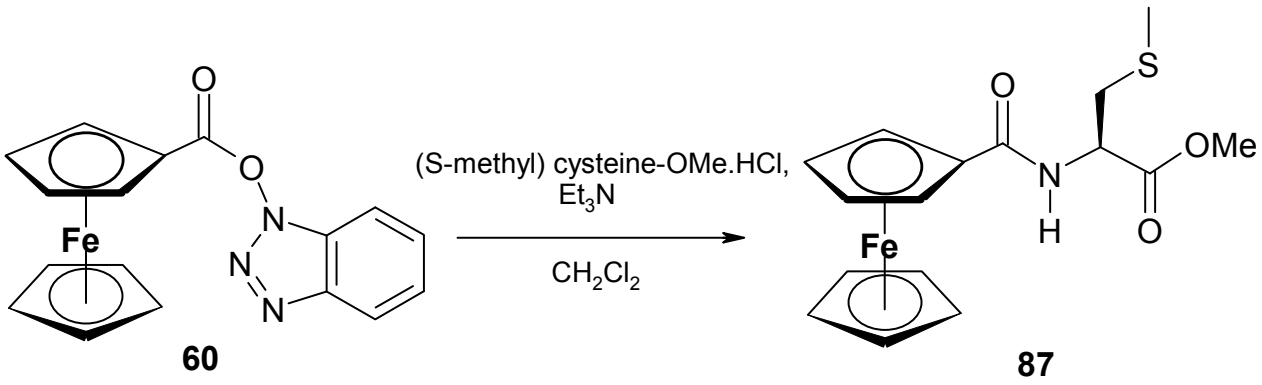

*Scheme 7: Preparation of **87** using the Fc-OBt active ester.*

Compounds **62**-**89**, whether prepared by route 1 or 3, were all found to contain varying amounts of the Fc-OBt intermediate **60** during column chromatography. It was deemed prudent to retain all samples of this active ester, as it could be subsequently employed in the preparation of both mono- and di- ***N***-ferrocenoyl peptides. The preparation of **87** with Fc-OBt is shown in *scheme 7*.

From *table 2*, it can be seen that the more expensive TBTU coupling reagent offers very little advantage over the well-established DCC/HOBt protocol. The yields recorded for compounds **62**, **65**, **68**, **70**, and **73** were all lower when CDI was employed, although this could be because of the solvent used (THF). Synthetic route 1 afforded the ***N***-ferrocenoyl amino acid derivatives in varying yields (43% in the cases of **80** to 82% in the case of **68**), and are summarised in *table 3*. These yields would appear to depend on several factors, including the solubility of the individual amino acid ester (largely dependant on the polarity of the amino acid's side chain) in DCM, and the stoichiometry of the coupling reaction (the dihydrochloride salts of the amino acid esters of L-lysine, L-ornithine and L-histidine, were observed to react more slowly).

In all cases, work up of the desired compounds was most effectively achieved by silica gel column chromatography using a mobile phase of 2:1 hexane/ethyl acetate. Not only did this method tend to avoid the losses incurred during multiple recrystallizations, but it also afforded complete separation of the ***N***-ferrocenoyl amino acid ester from the active intermediates ***N***-ferrocenoyl-O-benzotriazole active ester **60**, (which itself could then be employed in synthetic route 4), and **61**.

Compound	Name	M.P. (ºC)	Yield (%)
62	***N*-ferrocenoyl-L-2-aminobutyric acid ethyl ester**	116-118	69
63	***N*-ferrocenoyl-L-norvaline ethyl ester**	124-126	63
64	***N*-ferrocenoyl-L-norleucine ethyl ester**	142-144	72
65	***N*-ferrocenoyl-L-phenylglycine methyl ester**	118-120	72
66	***N*-ferrocenoyl-L-valine methyl ester**	124-125	61
67	***N*-ferrocenoyl-L-glutamic acid diethyl ester**	128-129	67
68	***N*-ferrocenoyl -L-aspartic acid dimethyl ester**	123-125	82
69	***N*-ferrocenoyl -(S-benzyl)-L-cysteine ethyl ester**	126-128	65
70	***N*-ferrocenoyl-L-methionine ethyl ester**	122-124	70
71	***N*-ferrocenoyl -L-threonine ethyl ester**	113-115	71
72	***N*-ferrocenoyl-L-serine methyl ester**	128-130	74
73	***N*-ferrocenoyl-L-tyrosine methyl ester**	140-143	69
74	***N*-ferrocenoyl-L-histidine methyl ester**	162-164	49
75	***N*-ferrocenoyl-L-tryptophan methyl ester**	111-113	67
76	***N*-ferrocenoyl-α-isoaminobutyric acid ethyl ester**	139-140	64
77	***N*-ferrocenoyl-(1S, 2R)-(+)-norephedrine**	153-155	71
78	***N*-Ferrocenoyl -D-methionine-ethyl ester**	123-125	66
79	***N*-ferrocenoyl-(N^{ε}-Fc)-L-lysine methyl ester**	228-230	49
80	***N*-ferrocenoyl -(N^{im}-Fc)-L-histidine methyl ester**	181-183	43
81	***N*-ferrocenoyl -β-alanine methyl ester**	128-130	70
82	***N*-ferrocenoyl-γ-aminobutyric acid-ethyl ester**	110-111	70
83	***N*-ferrocenoyl-(1S, 2R)-(+)-ephedrine**	138-139	71
84	***N*-ferrocenoyl-(1S, 2S)-(+)-pseudoephedrine**	131-132	72
85	***N*-ferrocenoyl–sarcosine ethyl ester**	63-65	59
86	***N*-ferrocenoyl-L-thyroxine methyl ester**	134-137	69
87	***N*-ferrocenoyl-(S-methyl)-L-cysteine methyl ester**	119-122	74
88	***N*-ferrocenoyl-valeric acid methyl ester**	130-131	68
89	***N*-ferrocenoyl-(N^{δ}-Fc)-L-ornithine methyl ester**	201-204	60

*Table 3: % Yields and melting points of **N-ferrocenoyl amino acid derivatives.***

Even after column chromatography, some of those compounds prepared by route 1 were observed to contain residual amounts of ***N***, ***N***' dicyclohexylurea, the presence of which could be confirmed by the presence of a doublet in the ^{1}H-NMR spectrum in d^6 DMSOcirca 5.5 ppm. However it could readily be removed by recrystallization from acetone.

All compounds were characterized using ^{1}H, ^{13}C, 135DEPT and HMQC NMR, I.R., and UV-Vis spectroscopy, as well as mass spectrometry and optical rotary analysis, and melting point determination. In all cases, the half-wave potentials were also recorded, and these will be discussed both in this chapter and at length in chapter VI.

2.5: ^{1}H-NMR Spectra of *N*-Ferrocenoyl Amino Acids

Molecular conformation of any peptide is critical in determining its biological activity, and this in turn is largely dependant on the number and strength of hydrogen bonds formed in solution. Both α-helices and β-sheets, two important features of the secondary structure of proteins, are formed as a result of hydrogen bonding between amide protons and the oxygen atom of another amide group. ^{1}H-NMR spectroscopy is an invaluable method of determining the solution state conformation adopted by compounds such as these. Specifically, amide protons which form hydrogen bonds generally show resonances at 7.5 ppm or greater when recorded in a polar solvent [16, 17]. All spectra were recorded in the H-bonding solvent DMSO-d^6, and, where deemed necessary, $CDCl_3$.

2.5.1: ^{1}H-NMR Spectra of 62

The ^{1}H-NMR spectrum of **62**, ***N***-ferrocenoyl-L-2-aminobutyric acid ethyl ester, is shown in *fig. 2*, and is a typical example of those ***N***-ferrocenoyl amino acid derivatives possessing a chiral α-carbon atom. The methyl groups of the side chain and ethyl ester group appear in the spectrum as triplets at 0.95 and 1.21 ppm, respectively, with the two protons of the methylene group of the side chain being observed as a multiplet *ca.* 1.8 ppm, and the complexity of this signal is enhanced by geminal coupling of these protons, as their proximity to the chiral centre results in them being magnetically non-equivalent.

The presence of this chiral centre is responsible for many of the distinctive features of the spectrum, as it renders otherwise similar protons in magnetically non-equivalent environments. For example, the two *ortho*-hydrogen atoms on the substituted Cp ring appear as two sharp

singlets at 4.85 and 4.93 ppm, presumably as a result of their proximity to different substituents on the α-carbon atom.

The *meta*-protons are observed as a slightly broadened singlet at 4.36 ppm, and the unsubstituted Cp ring is observed as a singlet at 4.21 ppm. The hydrogen located on the α-carbon, being adjacent to both the amide hydrogen and a methylene group, is observed as a multiplet in the 4.24-4.30 region.

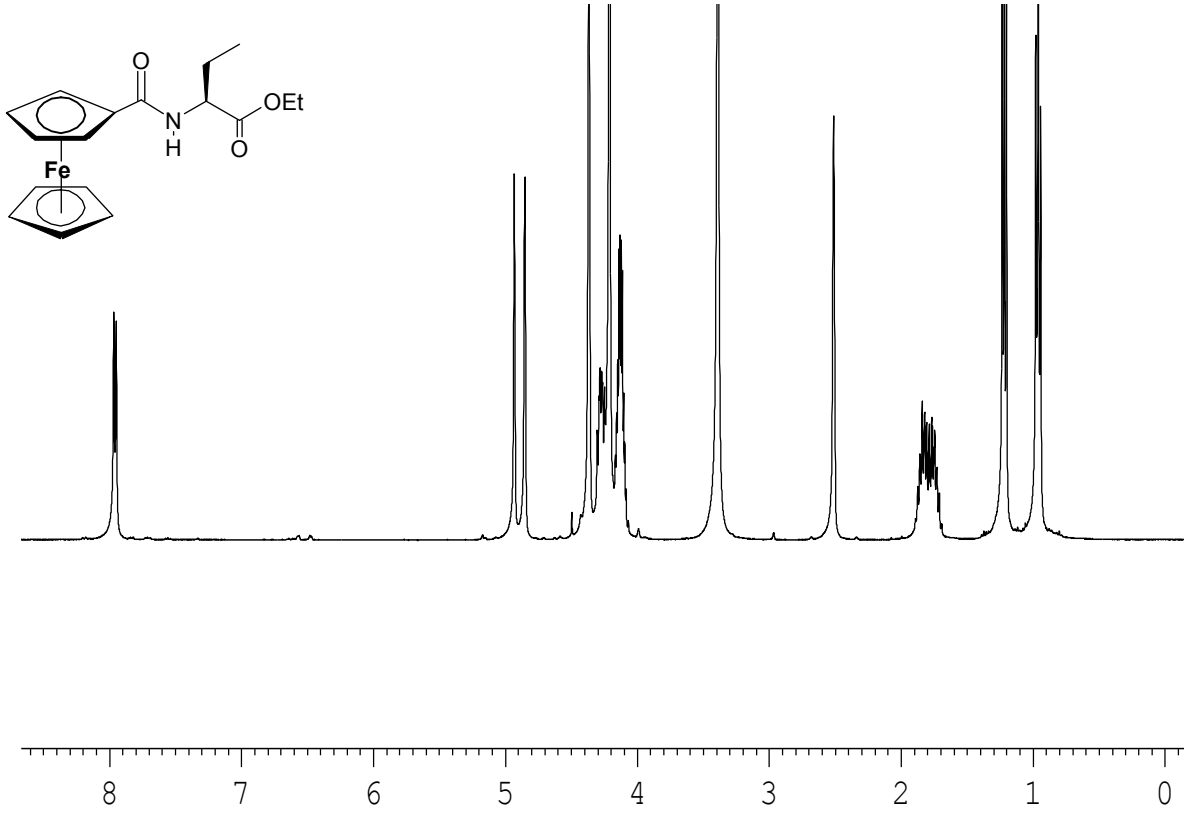

*Fig. 2: The ^{1}H-NMR spectrum of compound **62** in d^{6} DMSO.*

The amide hydrogen is observed as a doublet (J = 7.6 Hz), due to coupling with the α-hydrogen, and its position in the spectrum at *ca*. 7.9 ppm is indicative of a hydrogen-bonding interaction with the solvent. Non-hydrogen-bonded amide protons generally show resonances

between 5.5 and 7.0 ppm, and this is observed to be the case when the ^{1}H-NMR spectrum of **62** is recorded in $CDCl_3$, where the amide hydrogen is observed as a doublet at *ca*. 6.3 ppm (J = 7.0 Hz).

2.5.2: ^{1}H-NMR Spectra of 79 and 89

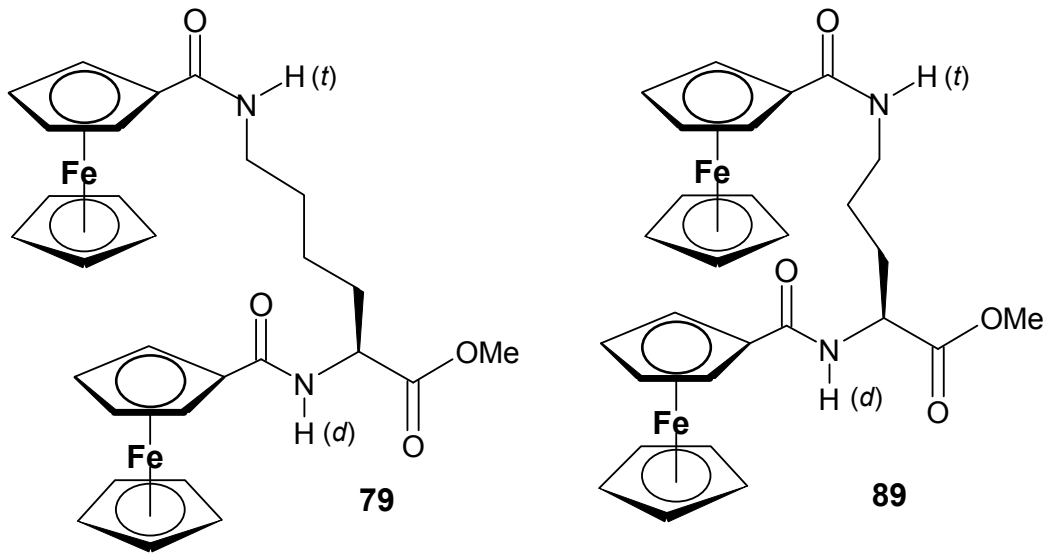

*Fig. 3: Compounds **79** (left) and **89**, **N**-ferrocenoyl-(**N**$^{\varepsilon}$-Fc)-L-lysine methyl ester and **N**-ferrocenoyl-(**N**$^{\delta}$-Fc)-L-ornithine methyl ester respectively. Each has two amide protons which appear in the ^{1}H-NMR spectrum as doublets (d), or triplets (t.)*

Compounds **79** and **89**, ***N***-ferrocenoyl-(N$^{\varepsilon}$-Fc)-L-lysine methyl ester and ***N***-ferrocenoyl-(N$^{\delta}$-Fc)-L-ornithine methyl ester respectively, are unusual in that they both have additional ferrocenoyl groups attached to their side chains. The ^{1}H-NMR spectrum of **79** in *d*^{6} *DMSO* (*fig. 4*) shows the presence of two unsubstituted Cp rings, at 4.14 and 4.23 ppm, each signal integrating for five protons. In addition, two different amide proton resonances are observed, a doublet (J = 7.6 Hz) for the amide group adjacent to the chiral centre at 7.98 ppm, and a triplet (J = 5.4 Hz) for the side chain amide proton at 7.83 ppm. The substituted Cp ring adjacent to the chiral carbon atom shows two sharp singlets for the *ortho*- protons. The *ortho*-protons of the

substituted Cp ring on the side chain, which are in magnetically equivalent environments, appear as a singlet integrating for two protons at 4.80 ppm.

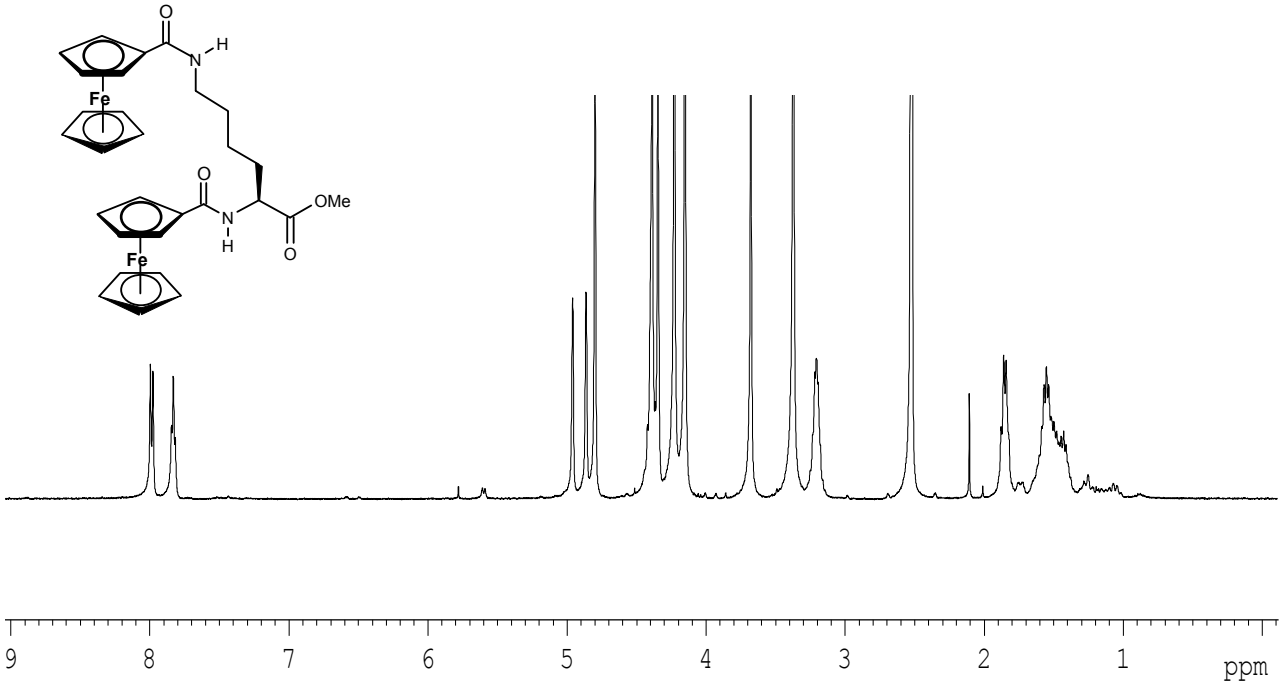

*Fig. 4: The ^{1}H-NMR spectrum of compound **79** in d^{6} DMSO.*

The ^{1}H-NMR spectrum of **79** (*fig. 5*), recorded in $CDCl_3$, is quite revealing in terms of the conformation adopted by this compound in non-polar solution. The doublet observed for the amide proton adjacent to the chiral centre appears at 6.50 ppm, whereas the triplet observed for the amide proton on the side chain appears at 7.62 ppm, indicating that the latter proton forms a hydrogen bond with either the oxygen atom of the other amide group, or else the oxygen atom of the ester group. Certainly, from a spatial point of view, either conformation would appear possible. The ^{1}H-NMR spectrum of **89** in $CDCl_3$ shows amide hydrogen resonances at 6.42 ppm (*doublet*), and 7.01 ppm (*triplet*). This would suggest that compound **89** does not form an intra-molecular hydrogen bond in $CDCl_3$, perhaps due to the fact that it's side chain is a methylene group shorter than that of **79**.

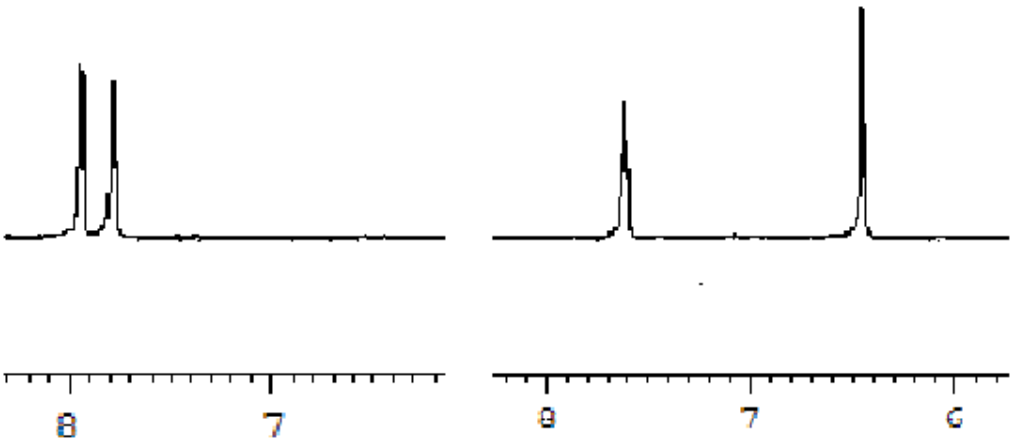

*Fig. 5: The amide protons in the ^{1}H-NMR spectrum of **79** recorded in d^{6} DMSO (left) and $CDCl_3$.*

2.5.3: ^{1}H-NMR Spectra of 81, 82 and 88

The achiral compounds **81**, **82**, and **88** all have an extended peptide backbone due to the presence of extra methylene groups between their amide and ester functionalities (*fig. 6*). These compounds have amide protons which appear as triplets in their ^{1}H-NMR spectrum, due to coupling to the neighboring methylene protons, with chemical shifts similar to the amide protons of the other ***N***-ferrocenoyl amino acid derivatives. Another noticeable feature of their spectra is that the *ortho*-protons of the substituted Cp ring no longer appear as two sharply defined singlets, as, in the absence of a chiral centre, they are magnetically equivalent. The ^{1}H-NMR spectrum of **81** is shown in *fig. 7*.

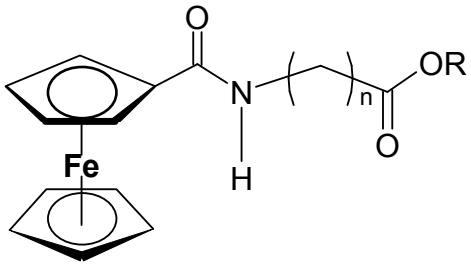

Compound	R =	n =
81	Me	2
82	Et	3
88	Me	4

*Fig. 6: The structures of compounds **81**, **82**, and **88**.*

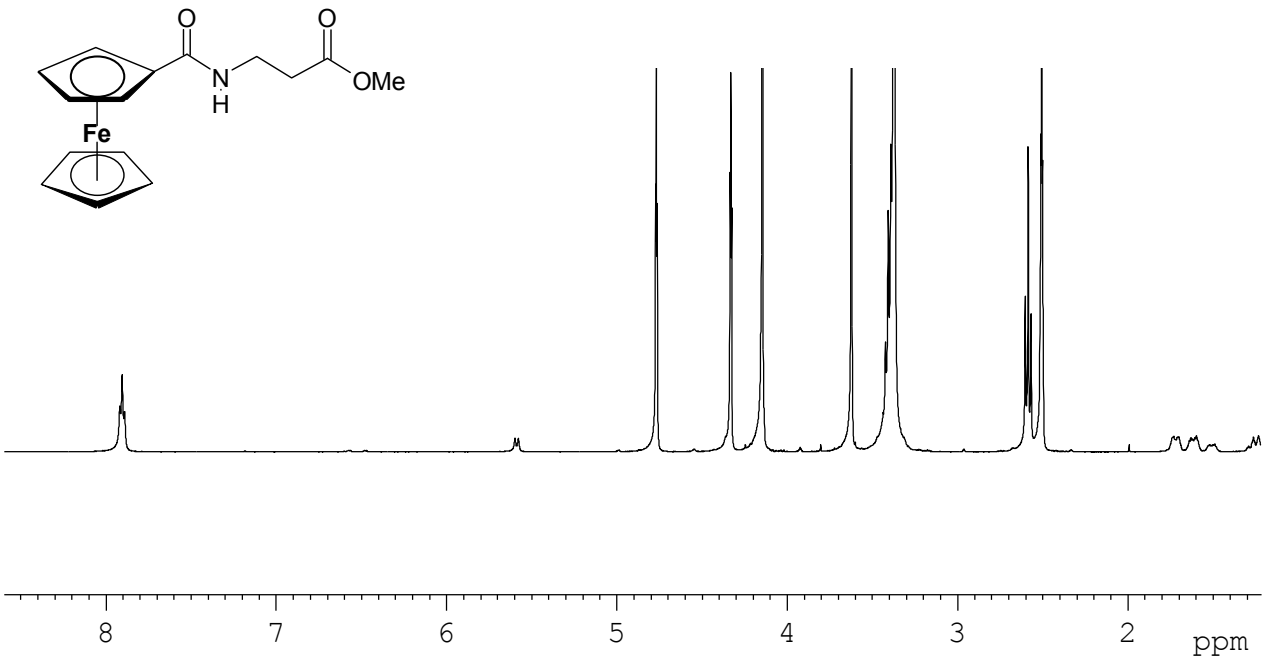

*Fig. 7: The [1]H-NMR spectrum of compound **81** in d[6] DMSO.*

The presence of these extra methylene groups naturally affords a greater degree of conformational freedom to the peptide backbone. This effect becomes noticeable when the ^{1}H-NMR spectrum of **81**, **82**, and **88** are recorded in the non-hydrogen bonding solvent, $CDCl_3$. The amide protons of both **81** and **82** both appear as broadened singlets, with chemical shifts of 6.26 and 6.29 ppm respectively. A dramatic contrast is observed in the spectrum of **88**, where a resonance for the amide proton is observed at 7.71ppm (*fig. 8*).

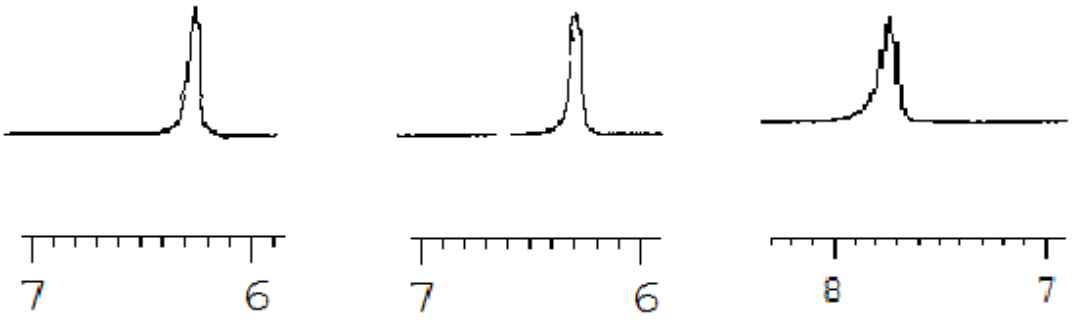

*Fig. 8: Amide proton signals in the [1]H-NMR spectrum of **81** (left), **82** (centre), and **88**, recorded in $CDCl_{3..}$*

The four methylene groups between the amide and ester moieties allow the molecule to adopt a stable conformation in $CDCl_3$, where a hydrogen bonding interaction between the amide hydrogen and the oxygen atom of the ester group is established.

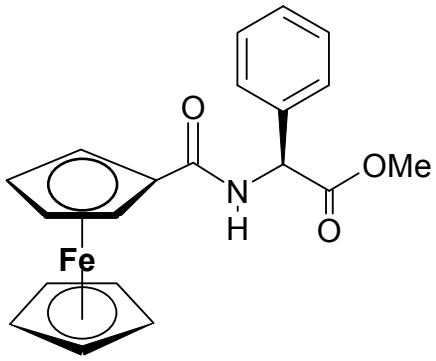

*Fig. 9: Compound **65**, **N**-ferrocenoyl-L-phenylglycine methyl ester.*

Compound **65** (*fig. 9*), the ***N***-ferrocenoyl derivative of the uncommon amino acid L-phenylglycine, has a side chain which consists of a phenyl group. Therefore, the hydrogen located on the α-carbon is effectively in the benzylic position, and is observed as a doublet at 5.62 ppm, which is a downfield shift of over 1 ppm when compared to similar compounds with alkyl side chains. The amide proton experiences a greater downfield shift in d^6 DMSO than any of the other ***N***-ferrocenoyl amino acid derivatives, being observed at 8.47 ppm. A summary of these ^{1}H-NMR results is given in *table 4*.

Compound	**N-H**	**$Cp_{unsub.}$**	**H_{ortho}**	**H_{meta}**	**H_{α}**
62	7.95(d)	4.21	4.85, 4.93	4.36	4.24-4.30
63	7.97(d)	4.02	4.84, 4.92	4.36	4.32-4.36
64	7.97(d)	4.2	4.85, 4.92	4.36	4.32-4.36
65	8.47(d)	4.19	4.80, 4.91	4.37	5.62 (d)
66	7.84(d)	4.19	4.91, 4.96	4.37	4.22-4.26
67	8.03(d)	4.26	4.83, 4.89	4.38	4.37-4.42
68	8.25(d)	4.2	4.80, 4.81	4.38	4.73-4.80
69	8.16(d)	4.23	4.85, 4.87	4.38	4.57-4.63

Compound	N-H	$Cp_{unsub.}$	H_{ortho}	H_{meta}	H_{α}
70	8.03(d)	4.22	4.84, 4.90	4.38	4.49-4.55
71	7.46(d)	4.23	4.84, 4.92	4.38-4.44	4.38-4.44
72	7.84(d)	4.23	4.81, 4.89	4.38	4.45-4.50
73	8.02(d)	4.03	4.78, 4.81	4.33	4.55-4.61
74	8.13(d)	4.65	4.78	4.35	4.63-4.67
75	7.99(d)	3.98	4.78	4.32	4.72
76	7.83(s)	4.21	4.58	4.34	4.11-4.16
77	7.49(d)	3.98	4.74, 4.75	4.28	4.11-4.16
78	8.03(d)	4.27	4.87, 4.90	4.37	4.49-4.84
79	7.98(d)	4.23	4.86, 4.96	4.34	4.39-4.42
	7.83(t)	4.15	4.80	4.34	
80	8.13(d)	4.07	4.84	4.39	4.77-4.84
		4.25	4.96	4.73	
81	7.90(t)	4.17	4.77	4.33	-
82	7.82(t)	4.13	4.77	4.31	-
83	-	4.02	4.68	4.28	4.26
84	-	4.02	4.68	4.28	4.37
85	-	4.26	4.69	4.42	-
86	8.15(d)	3.99	4.71, 4.88	4.35	4.64-4.69
87	8.16(d)	4.23	4.84, 4.86	4.38	4.57-4.62
88	7.96(t)	4.15	4.78	4.33	-
89	8.13(d)	4.15	4.85, 4.92	4.33	4.37-4.41
		4.21	4.79	4.37	

*Table 4: ^{1}H-NMR Chemical shifts (ppm), of **N**-ferrocenoyl amino acid derivatives in d^{6}* DMSO

2.6: ^{13}C-NMR Spectra of *N*-Ferrocenoyl Amino Acid Derivatives

The ^{13}C-NMR spectrum of the ***N***-ferrocenoyl amino acid derivatives, recorded in d^{6} DMSO, show a large degree of consistency in terms of their ferrocenoyl resonances, with the *ortho*, *meta*, and unsubstituted Cp ring carbon atoms occurring within a narrowly defined region (68-71 ppm).

Similarly, the *ipso*-carbon of the substituted Cp ring appears consistently in the 75-77 ppm region. The amide carbonyl carbons are observed *ca*. 169 ppm, while the ester carbonyl carbons appear *ca*. 172 ppm. A signal in the 50-60 ppm region is also observed for those compounds which possess a chiral α-carbon atom, its chemical shift being largely a function of the side chain of the individual amino acid used. Those compounds which have an α-methylene group instead of a tertiary chiral carbon show resonances in the 30-40 ppm region.

An important distinction can be drawn between these chiral compounds and achiral compounds **76**, **81**, **82**, **86** and **88** in terms of their pattern of ferrocenoyl resonances. All chiral compounds show two signals for the *ortho*-carbons of the substituted Cp ring, and most also show two signals for the *meta*-carbons, while the achiral compounds show only one signal for these carbons. Also, the *ipso*-carbon of the substituted Cp ring of the achiral compounds tends to appear at a slightly more downfield position in the spectrum.

2.6.1: ^{13}C-NMR Spectrum of 62

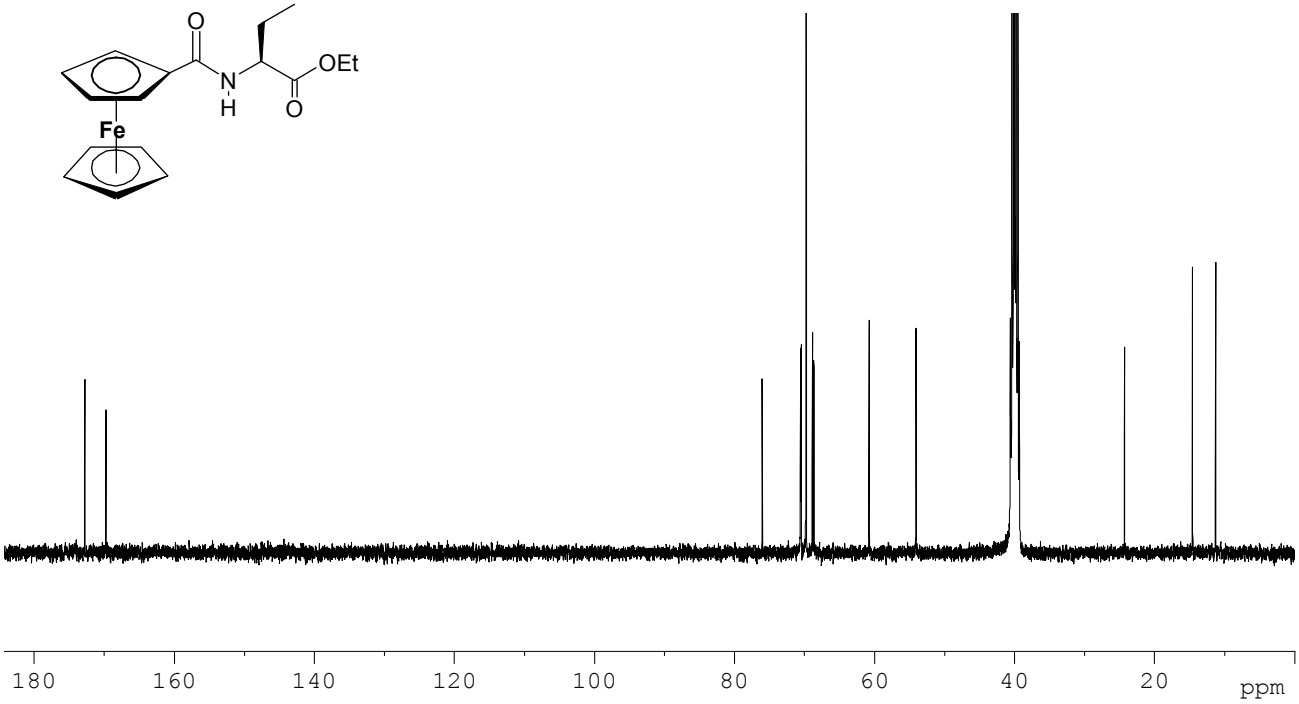

*Fig. 10: The ^{13}C-NMR spectrum of compound **62***

The ^{13}C-NMR spectrum of **62** recorded in d^6 DMSO, (*fig. 10*), is typical of those ***N***-ferrocenoyl amino acid derivatives possessing a chiral α-carbon atom. Two signals for the methyl groups of both the side chain and ester group appear at 11.2 and 14.5 ppm, with another two signals for the adjacent methylene groups appear at 24.2 and 60.7 ppm, while a signal for the α-carbon is present at 54 ppm. Two narrowly separated signals are observed for the *ortho*-carbon atoms on the substituted Cp ring in the 68.5-69 ppm region. This feature of the spectrum is presumably as a consequence of the chiral centre, which caused the *ortho*-protons to appear as two individual signals in the ^{1}H-NMR spectrum. A single signal for the unsubstituted Cp ring in the 69.5–70 ppm region, and two signals for the *meta*-carbon atoms in the 70–71 ppm region (these signals were unambiguously assigned by the 2-D HMQC spectrum).

The resonance for the *ipso*-carbon on the substituted Cp ring is consistently observed in the 75–76 ppm region, the amide carbon atom signal is observed at 169.7 ppm, and the ester carbon at 173 ppm. These quaternary carbons are, as expected, absent from the 135DEPT spectrum (*fig. 11*), while the two methylene carbons appear as negative peaks.

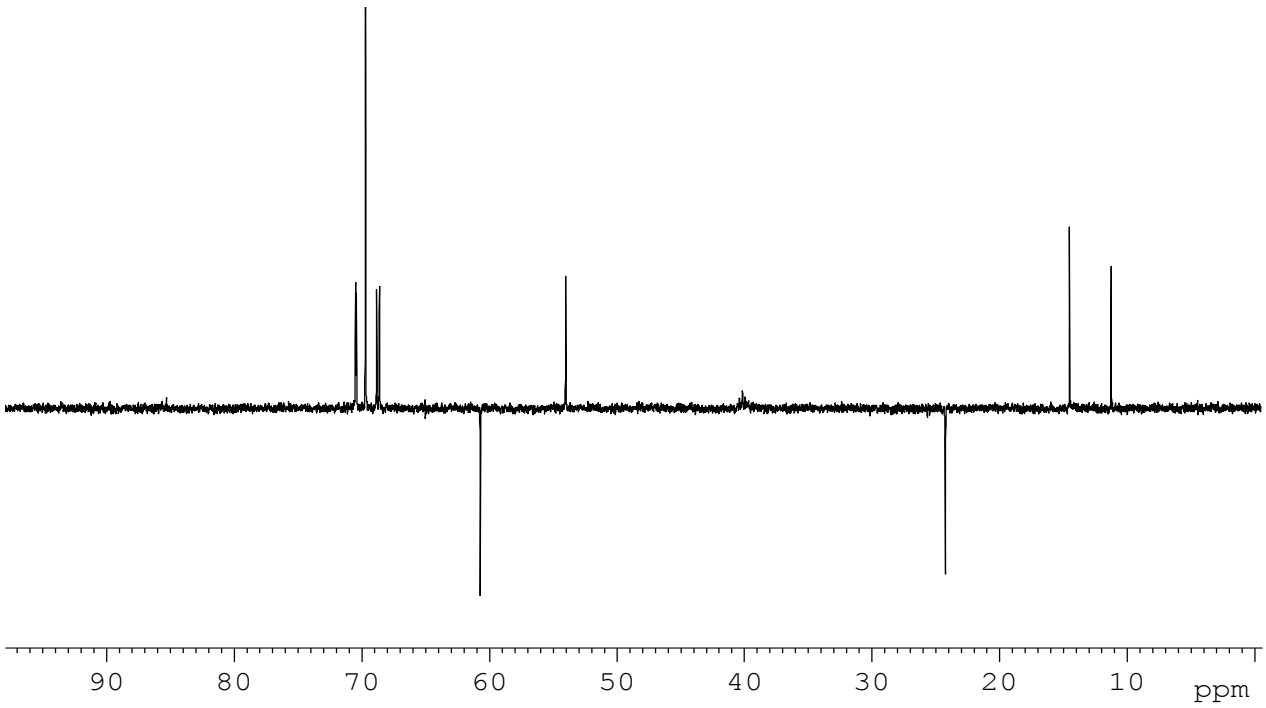

*Fig. 11: The 135DEPT spectrum of compound **62***

2.6.2: ^{13}C-NMR Spectrum of 81

The ^{13}C-NMR spectrum of **81** recorded in d^6 DMSO is shown in *fig. 12*, and is typical of the achiral ***N***-ferrocenoyl amino acid derivatives, in that only one signal is observed for each of the *ortho*- and *meta*-carbons of the substituted Cp ring. The two methylene groups appear at 34.3 and 35.5 ppm, and are observed as negative peaks in the 135DEPT spectrum (*fig. 13)*. The chemical shifts of the unsubstituted ring (69.7 ppm), amide carbonyl (169.4 ppm), and ester carbonyl carbons (172.3 ppm) are typical of all the ***N***-ferrocenoyl amino acid derivatives discussed in this chapter, and are independent of any chirality within the molecule. The *ipso*-carbon on the substituted Cp ring is observed at 76.7 ppm, which is a downfield shift of approximately 1 ppm compared to compounds with a chiral α-carbon atom. A summary of the ^{13}C-NMR data for compounds **62**-**89** is given in *table 5*.

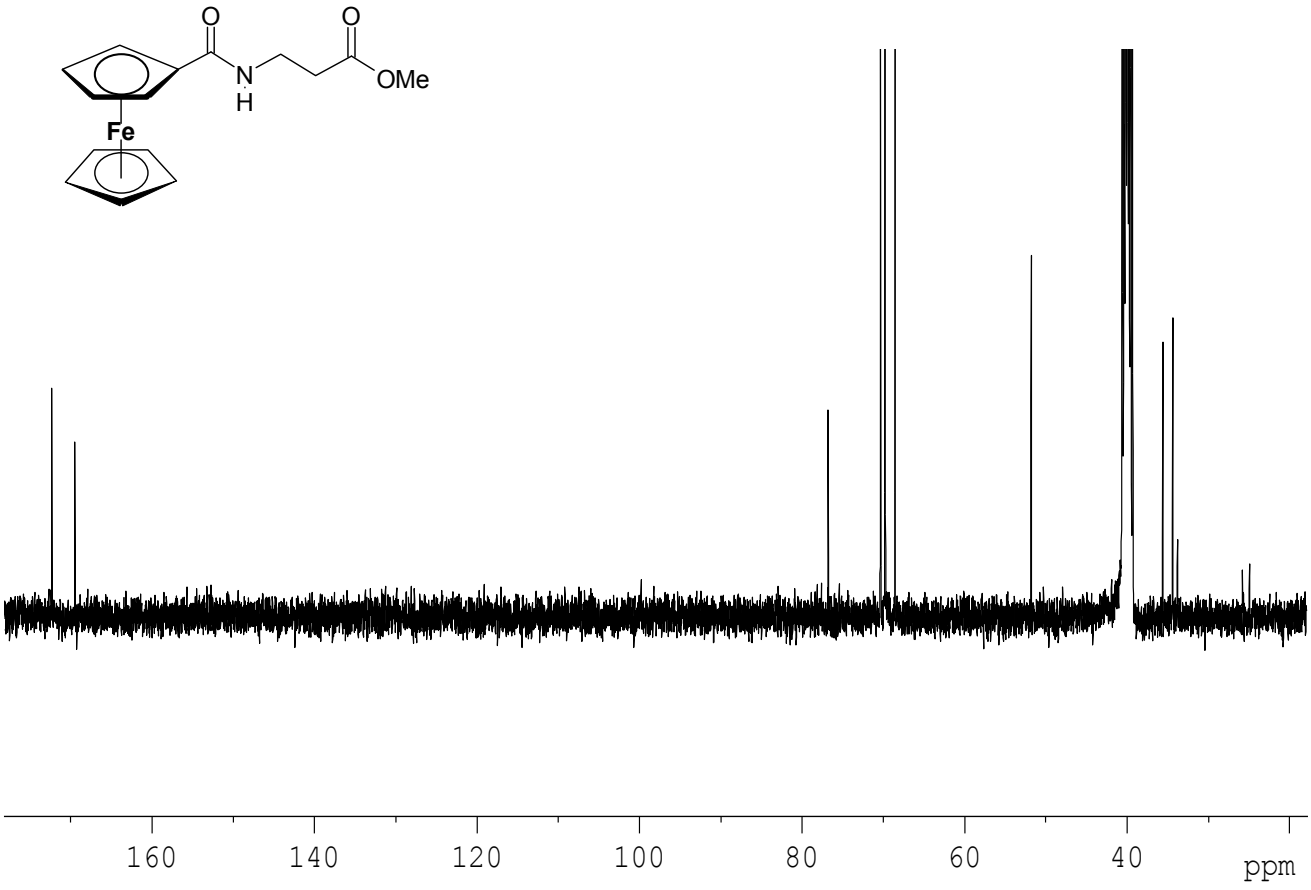

*Fig. 12: The ^{13}C-NMR spectrum of compound **81***

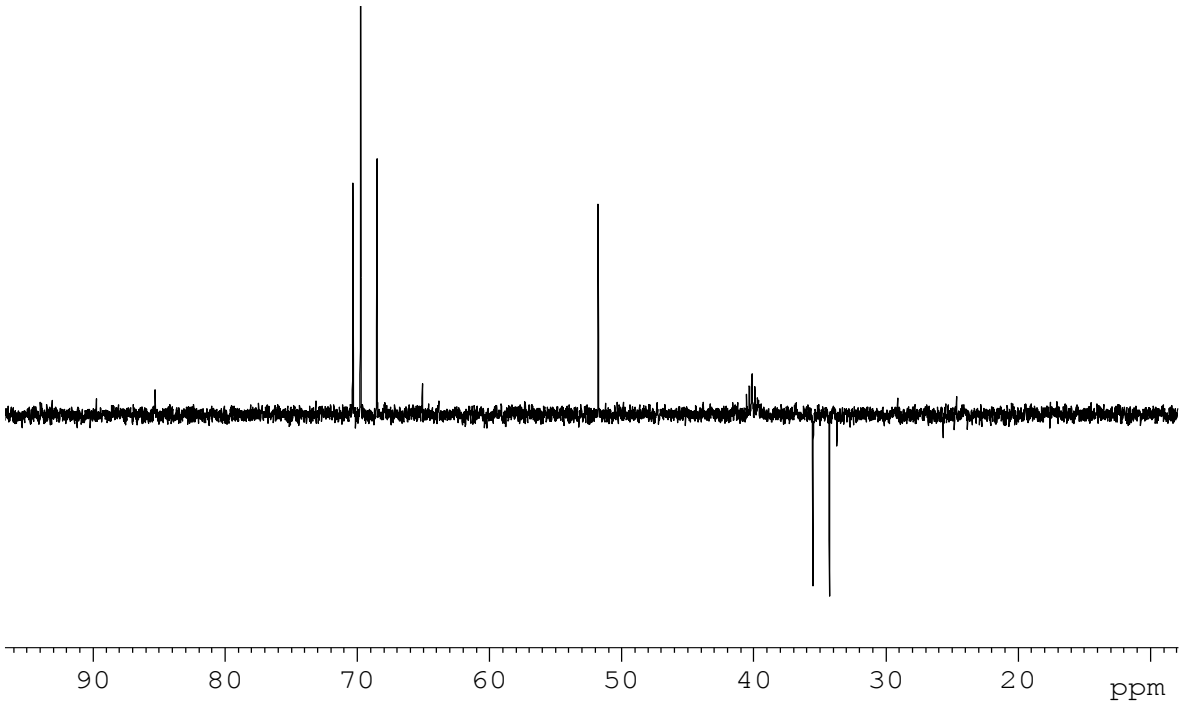

*Fig. 13: The 135DEPT spectrum of compound **81***

Compound	$C=O_{amide}$	$C=O_{ester}$	$Cp_{unsub.}$	C_{ortho}	C_{meta}	C_{ipso}
62	169.74	172.78	69.71	68.61, 68.81	70.43, 70.50	75.97
63	169.76	173.00	69.71	68.62, 68.81	70.44, 70.51	75.92
64	169.63	172.96	69.70	68.64, 69.70	70.43, 70.50	75.99
65	169.61	171.63	69.73	68.89, 68.94	70.59, 70.66	75.51
66	169.86	172.84	69.68	68.75, 68.93	70.49, 70.59	75.85
67	169.85	172.34, 172.64	69.73	68.62, 68.75	70.50, 70.57	75.76
68	169.51	171.10, 171.81	69.80	68.03, 68.60	70.65	75.14
69	169.67	171.35	69.33	68.83, 68.73	70.59, 71.05	75.78
70	169.87	172.60	69.74	68.64, 68.77	70.57	75.90
71	169.96	171.23	69.78	68.67, 68.70	70.55, 70.60	75.95
72	169.72	171.65	69.81	68.50, 68.86	70.52, 70.75	75.83
73	169.57	172.99	69.69	68.35, 68.80	70.40, 70.44	75.81
74	169.58	172.71	69.74	68.47, 68.60	70.49, 70.73	75.85
75	169.57	173.17	69.61	68.43, 68.71	70.38, 70.42	75.83
76	168.78	174.32	69.68	68.76	70.38	76.11

Compound	$C{=}O_{amide}$	$C{=}O_{ester}$	$Cp_{unsub.}$	C_{ortho}	C_{meta}	C_{ipso}
77	168.55	-	69.93	68.04, 68.82	70.11, 70.15	76.94
78	169.81	172.58	69.73	68.64, 68.78	70.49, 70.55	75.85
79	169.19	173.40	69.63	68.64, 68.63	70.16, 70.45	75.90
	169.76		69.72	68.84	70.51	77.17
80	168.83	172.70	69.70	68.50, 68.93	70.60, 71.90	75.63
	169.69		70.73			71.54
81	169.42	172.29	69.69	68.47	70.27	76.69
82	169.25	173.06	69.62	68.45	70.19	77.06
83	169.39	-	69.79	70.17	71.38	78.67
84	169.39	-	69.79	70.17	71.38	78.65
85	169.79	170.64	69.78	70.45	71.29	76.12
86	169.81	172.46	69.77	68.34, 68.94	70.35, 70.83	75.68
87	169.74	171.96	69.82	68.69	70.58, 70.61	75.73
88	169.06	173.67	69.62	70.13	68.43	77.23
89	169.55	173.28	69.66	68.45, 68.49	70.23, 70.51	75.79
	170.01		69.75	68.72	70.58	76.99

*Table 5: ^{13}C-NMR Chemical shifts (ppm), of **N**-ferrocenoyl amino acid derivatives in d^6* DMSO

2.7: Infra-Red Spectra of *N*-Ferrocenoyl Amino Acid Derivatives

Infrared spectra can provide valuable information regarding both the *inter*- and *intra*-molecular hydrogen bonding interactions of these compounds. The C=O ester and C=O amide bands, when recorded as KBr discs, are consistently observed in the 1740 and 1620 cm^{-1} region in the solid state respectively. When the spectra are recorded as thin film CH_2Cl_2 solutions, these values are generally increased by *ca.* 25 cm^{-1}. For compounds with tertiary amide groups (**83**, **84**, **85**), the amide band is observed at slightly lower wavenumbers.

The contrast between the N-H stretch vibrations recorded in the solid state and in solution can be quite revealing in terms of the molecular conformations adopted by these compounds. Wavenumbers lower than 3400 cm^{-1} are diagnostic of hydrogen bonded amide protons, and the solid-state spectra (KBr) of these compounds show N-H stretches in the 3250 – 3350 cm^{-1} region.

This is to be expected, as hydrogen bonds would be largely responsible for the coherence of these compounds in the solid state. Infrared spectra of compounds **79** and **88**, recorded in CH_2Cl_2, show N-H stretching vibrations below 3400 cm^{-1}, indicating that these compounds form intra-molecular hydrogen bonds in non polar solution [16]. This observation is in agreement with the ^{1}H-NMR data recorded for these compounds, where **79** and **88** showed amide proton resonances above 7.5 ppm when recorded in $CDCl_3$.

The infrared spectrum of **88**, recorded as a thin film methylene chloride solution, shows an N-H stretch at 3361 cm^{-1}, which is indicative of a hydrogen-bonded amide proton, with the carbonyl oxygen of the ester group acting as a donor. As mentioned in section 2.5.3, this conformation would appear to be inaccessible to compounds **81** and **82**, due to their shorter peptide backbone (these compounds show υ_{N-H} stretches at 3422 and 3404 cm^{-1} respectively). These results have further implications when these compounds are employed in anion binding studies, and are discussed at length in chapter VI.

As was mentioned in section 2.5.2, compound **79** showed an amide proton resonance at 7.62 ppm (triplet) when recorded in $CDCl_3$, and also shows an N-H stretch at 3361 cm^{-1} when recorded as a thin film methylene chloride solution. Both these observations are indicative of a hydrogen-bonded amide proton. A summary of the infra-red data for compounds **62-89** is given in *table 6*.

Compound	**υ_{N-H}(KBr)**	**υ_{COOR}(KBr)**	**υ_{CONR}(KBr)**	**υ_{N-H} (CH_2Cl_2)**
62	3274	1746	1629	3418
63	3276	1751	1626	3417
64	3274	1748	1625	3414
65	3394	1735	1642	3421
66	3332	1742	1629	3409
67	3290	1735	1638	3402
68	3304	1735	1628	3409
69	3238	1748	1626	3412
70	3268	1752	1628	3414
71	3317	1723	1609	3402
72	3341	1738	1610	3408
Compound	**υ_{N-H}(KBr)**	**υ_{COOR}(KBr)**	**υ_{CONR}(KBr)**	**υ_{N-H} (CH_2Cl_2)**

73	3355	1724	1609	3410
74	3387	1750	1639	3422
75	3324	1747	1628	3409
76	3333	1736	1635	3411
77	3364	-	1607	-
78	3267	1751	1628	3413
79	3287	1743	1626	3401, 3361
80	3298	1758	1645	3407
81	3303	1735	1624	3422
82	3289	1734	1625	3404
83	-	-	1607	-
84	-	-	1578	-
85		1744	1603	-
86	3350	1739	1613	3411
87	3294	1753	1631	3407
88	3303	1738	1621	3373
89	3292	1745	1626	3414

*Table 6: Infrared bands of **N**-ferrocenoyl amino acid derivatives (cm^{-1}) (KBr). The N – H stretch, recorded in CH_2Cl_2, is also included.*

2.8: UV-Vis Spectra of *N*-Ferrocenoyl Amino Acid Derivatives

The UV-Vis spectra of the compounds discussed in this chapter are largely invariant, with two low energy bands being observed in the 440 and 300 nm range, indicating that the nature of the amino acid substituent has negligible impact on the electronic properties of the ferrocenoyl moiety. Similarly consistent results were obtained when the extinction coefficients of these compounds were calculated, with results being in the 200 A.U. range, which is typical of values for these types of compounds.

An unexpected compound was isolated during the preparation of **74, *N*-**ferrocenoyl-L-histidine methyl ester, whereby a second ferrocenoyl derivative of L-histidine methyl ester, **80** (***N*-**ferrocenoyl-(N^{im}-Fc)-L-histidine methyl ester), was isolated (*fig. 14*). **80** is the only ***N*-**

ferrocenoyl amino acid derivative whose UV-Vis spectrum differs substantially from the others, where the low energy bands are bathochromically shifted to 345 and 460 nm respectively. This would suggest that there is some degree of conjugation between the imidazolic and cyclopentadienyl aromatic systems via the sp^2 amide carbon atom.

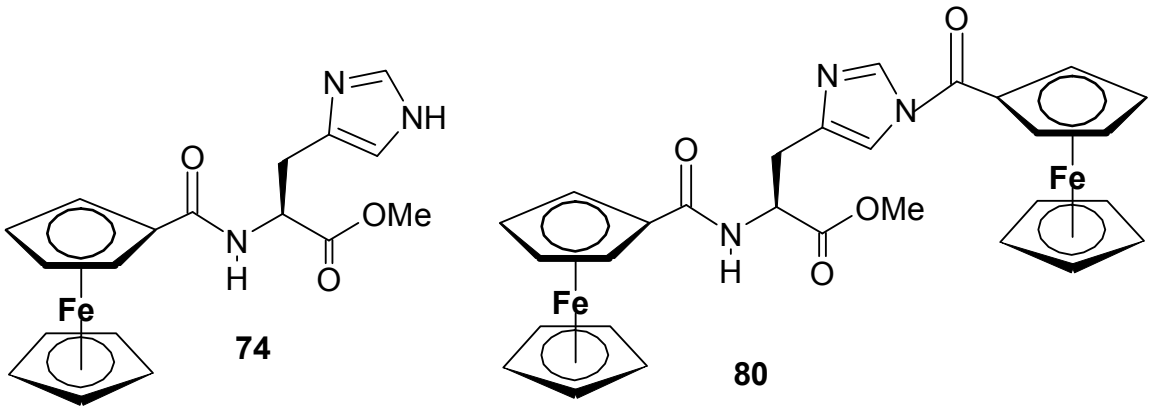

*Fig 14: Compounds **74** (left) and **80** (right), L- histidine methyl ester derivatives.*

2.9: Cyclic Voltammograms of *N*-Ferrocenoyl Amino Acid Derivatives

Cyclic voltammograms of all compounds were recorded in acetonitrile, using the ferrocene/ferricenium couple as an internal redox standard. Each exhibited a reversible, one-electron peak, due to the oxidation of the ferrocenoyl group to the ferricenium cation. Half-wave potentials of the compounds bearing an amide proton ranged from 170 mV in the case of **77**, to 202 mV in the case of **68**. However, in compounds where the amide proton is replaced by a methyl group (**83**, **84**, **85**), significant cathodic shifts are observed. For the ***N***-ferrocenoyl sarcosine (**81**) derivative, the half wave potential recorded was 156 mV, while the ***N***-ferrocenoyl derivatives of ephedrine (**83**) and pseudoephedrine (**84**) displayed redox potentials of 117 and 108 mV respectively. It has been previously noted that sterically constrained ferrocene-amide derivatives have lower redox potentials than unconstrained analogues. This cathodic shift is illustrated in *fig. 15*, where the structure of the two ferrocenoyl derivatives differs only by substitution of the amide proton in **77** with a methyl group in **83**.

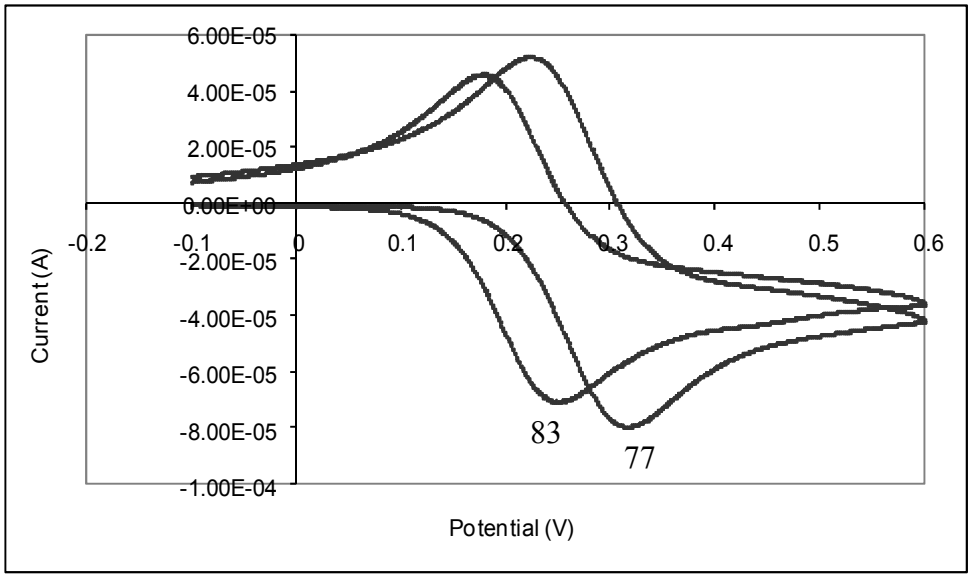

*Fig 15: Cyclic voltammograms of compounds 77 and **83** recorded in CH_3CN.*

This can be explained by the fact that the bulky amide substituents, such as a methyl group, can cause deviations from co-planarity between the amide group and the substituted Cp ring, and hence the overlap between these two π-systems is decreased. This decreased overlap has the effect of lessening the electron-withdrawing capability of the amide group. Thus, the energy of the ferrocene HOMO orbital is not lowered as much, making oxidation to the ferricenium cation easier [15].

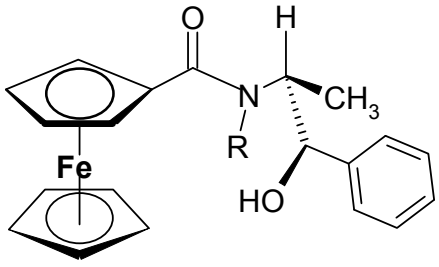

R = H **77**
R = CH_3 **83**

*Fig. 16: Compounds 77 and **83**.*

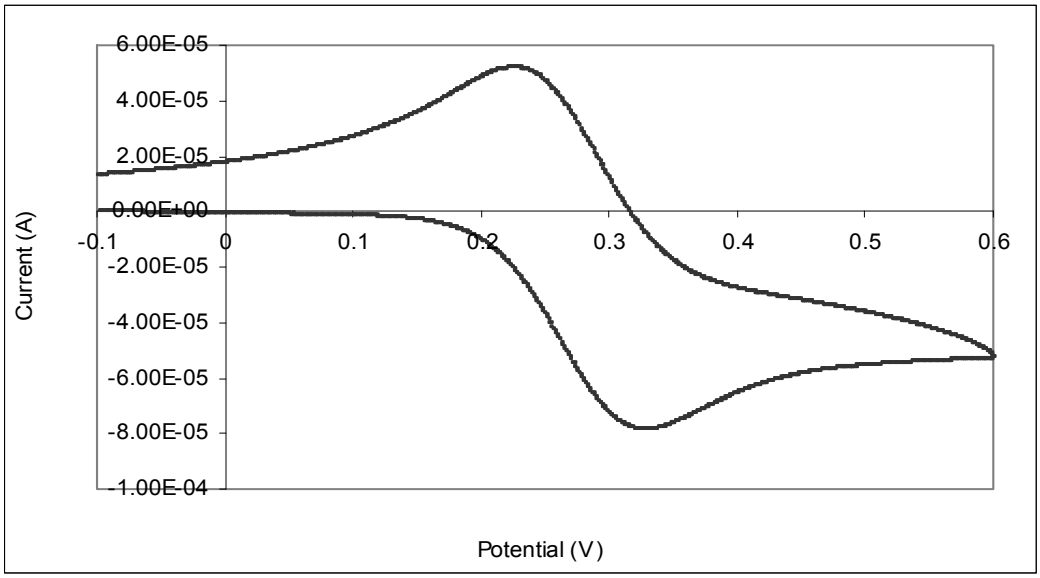

*Fig. 17: Cyclic voltammogram of **79**, displaying only one oxidation/reduction peak, despite the presence of two ferrocenoyl groups.*

A summary of both the electrochemical and UV-Vis data for compounds **62-89** is given in *table 7*.

Compound	λ_{max} (nm)	ε (M^{-1} cm^{-1})	$[\alpha]_D^{20}$	$E_{1/2}$(mV)
62	443, 306	200	-42	186
63	441, 303	220	-37	187
64	440, 304	191	-39	176
65	445, 305	202	-52	199
66	444, 306	201	-50	189
67	443, 306	204	-44	190
68	443, 306	202	-39	202
69	443, 304	214	-77	196
70	446, 306	200	-58	182
71	439, 306	199	-50	190
72	440, 306	193	-40	190
73	445, 305	204	-9	192
74	445, 305	195	-39	190
75	440	222	-47	187
76	442, 305	196	-	179

Compound	λ_{max} (nm)	ε (M^{-1} cm^{-1})	$[\alpha]_D^{20}$	$E_{1/2}$(mV)
77	442, 304	209	34	170
78	445, 305	212	59	188
79	440, 305	199	-43	177
80	460, 345	440	-47	184
81	439, 304	179	-	175
82	446, 301	181	-	169
83	445	180	34	117
84	440	189	36	108
85	445, 305	209	-	156
86	443, 305		-21	170
87	442, 304		-	169
88	442, 302	212	-	160
89	441, 307	161	-22	188

*Table 7: Electrochemical, UV-Vis and optical rotation data of compounds **62-89**. All ε values refer to lowest energy band.*

The cyclic voltammograms of **79**, **80** and **89**, surprisingly, do not differ substantially from those observed for compounds of the other ***N***-ferrocenoyl amino acid derivatives, in that only one distinct oxidation and reduction peak is observed for each compound, despite the presence of two ferrocenoyl groups, as illustrated in *fig. 17*. Even when a slower scan rate was employed (0.02V/sec), neither oxidation nor reduction waves could be resolved into two discernable peaks.

2.10: Conclusions

Coupling of ferrocene carboxylic acid to the hydrochloride salts of various amino acid esters (and β-amino alcohols in the case of **77**, **83**, and **84**) was effected using various well established coupling reagents (dicyclohexylcarbodiimide, carbonyldiimidazole, O- (1H-benzotriazol-1-yl) - ***N, N, N', N***', -tetramethyluronium tetrafluoroborate). Compounds **65**, **68**, **70** and **73** were prepared using all three routes, and while all proved effective, it was found that CDI resulted in slightly lower yields than the other two reagents. This may be partially explained by the suggestion that the active ester formed when employing CDI, **61**, is more prone to decomposition

than the active ester **60**, which is formed when DCC and TBTU is employed. From an economic standpoint, DCC would appear the more attractive option. The optimum reaction time was determined to be 24 hours for the purpose of maximizing yields when DCC was employed, although longer reaction times have been reported in the literature [18].

Compounds **79** and **89** were formed in a 2:1 stoichiometric reaction of ferrocene carboxylic acid with L-lysine methyl ester and L-ornithine methyl ester respectively, the amine groups on their side chains proving just as reactive as their α-amino groups when using the DCC/HOBt coupling protocol. No mono-***N***-acylated product was isolated during the work-up of either of these compounds. Compound **80** was formed in a similar manner, and resulted from reaction of ferrocene carboxylic acid with both the α-amino group and the imidazolic ring of L-histidine methyl ester.

All ***N***-ferrocenoyl amino acid derivatives possessing an α-chiral carbon showed the same basic pattern of resonances in their ^{1}H-NMR spectra, with two sharply defined, one-proton singlets being observed for the *ortho*-protons of the substituted Cp ring, a two-proton singlet for the *meta*-protons, and a five-proton singlet for unsubstituted Cp ring. In the absence of a chiral centre, these *ortho*-protons appear either as slightly broadened singlets (**82**, **88**), or doublets with weak coupling to the *meta*-protons (**76**, **81**). The amide protons, when recorded in the hydrogen-bonding solvent d^6 DMSO, appear in the 7.5-8.5 ppm range, and in the 6.0-6.5 range when recorded in the non-polar solvent $CDCl_3$. The exceptions to this general trend are **79** and **88**, which appear to adopt a stable, hydrogen-bonded conformation in non-polar solution. This is in agreement with the $\upsilon_{N\text{-}H}$ stretch vibrations observed in the IR spectra when recorded in dichloromethane, in which only **79** and **88** show bands below 3400 cm^{-1}.

All compounds show a reversible, one-electron peak in their cyclic voltammograms, due to the oxidation of the ferrocenoyl group to the ferricenium cation. This proved to be the case even with **79**, **80**, and **89**, all of which incorporate two ferrocenoyl groups in different chemical environments. Slowing of the scan rate from 0.1V/sec to 0.02V/sec did not result in resolution of the voltammogram into two separate oxidation or reduction peaks. Compounds with tertiary amide groups (**83**, **84** and **85**) showed cathodic shifts relative to those compounds with secondary amide groups.

.

2.11: Experimental

Ferrocene carboxylic acid (59)

7.0g (0.05mol) anhydrous aluminium chloride was added to a solution of ferrocene (9.3g, 0.05mol) and 2-chlorobenzoyl chloride (8.8g, 0.1mol) in dry dichloromethane under nitrogen at 0ºC. After 30mins, the reaction was raised to room temperature, and allowed to proceed for two hours. The reaction was once again cooled to 0ºC, and 100mls water was added. After stirring for a further 30mins, the layers were allowed to separate, and the aqueous layer extracted with 10mls water. The organic layers were combined, dried over magnesium sulphate, and the solvent removed *in vacuo*, yielding a viscous red oil which solidified after 10mins.

The 2-Chlorobenzoyl ferrocene was then added to a solution of potassium tert-butoxide (18.2g, 0.16mol) and water (0.88mls, 0.5mol) in 1,2-dimethoxyethane. The reaction was then refluxed under nitrogen for 3hrs, cooled, and added to 500mls water. The solution was then washed with diethyl ether, and the organic layer back extracted with 10% sodium hydroxide. The aqueous layers were combined, and acidified to pH 2 using conc. HCl, causing the title product to precipitate as a fine yellow/brown powder. The product was then dried at for 6 hours at 80°C.

Yield 9.2g, 80%, m.p. 223-225°C (lit 224-225°C) [2].

^{1}H-NMR (400MHz) δ ($CDCl_3$): 4.24 (5H, s, *unsub*. Cp ring), 4.44 (2H, br. s, H_{meta} Cp ring), 4.84 (2H, br. s, H_{ortho} Cp ring), 12.04 (1H, br. s, FcCOO<u>H</u>).

***N*-ferrocenoyl-OBt (60).**

All coupling reactions between ferrocene carboxylic acid and amino acid esters, using the DCC/HOBt protocol yielded varying amounts of the title product during column chromatography on silica gel, using a mobile phase of 2:1 hexane/ethyl acetate. It was isolated as an air-stable, dark red crystalline solid.

m.p. 135-137°C.

^{1}H-NMR (400MHz) δ ($CDCl_3$): 4.47 (5H, s, *unsub*. Cp ring), 4.70 (2H, br. s, H_{meta} Cp ring), 5.11 (2H, br. s, H_{ortho} Cp ring), 7.45-7.59 (3H, m, ArH), 8.11-8.14 (1H, m, ArH).

***N*-ferrocenoyl-imidazole (61)**

Coupling reactions between ferrocene carboxylic acid and amino acid esters, using CDI as the coupling reagent, yielded varying amounts of the title product during column chromatography on

silica gel, using a mobile phase of 2:1 hexane/ethyl acetate. It was invariably eluted before the ***N***-ferrocenoyl amino acid derivatives, and isolated as a dark red solid (typically 10 – 20%).
m.p. 118-119°C, (lit 121-122°C) [12].
^{1}H-NMR (400MHz) δ ($CDCl_3$): 4.28 (5H, s, *unsub*. Cp ring), 4.52 (2H, br. s, H_{meta} Cp ring), 4.90 (2H, br. s, H_{ortho} Cp ring), 7.18 (1H, br. s, $H_{imidazole}$), 7.73 (1H, br. s, $H_{imidazole}$), 8.47 (1H, br. s, $H_{imidazole}$).

N-Ferrocenoyl Amino Acid Esters

Route 1, General procedure:

0.35g (2.5mmol) of 1-hydroxybenzotriazole, 0.4mls (2.5mmol) of triethylamine, 0.6g (3.0mmol) of dicyclohexylcarbodiimine, and 2.5mmol of the corresponding amino acid ester hydrochloride salt* were added to a slurry of 0.57g (2.5mmol) of ferrocene carboxylic acid in dichloromethane (30mls), at 0°C. After 30 mins, the mixture was raised to room temperature, and stirring was continued for 48 hrs. The precipitated ***N***, ***N*** - dicyclohexylurea was filtered off, and the solvent evaporated *in vacuo*, and the crude product was purified by silica gel column chromatography using a mobile phase of 2:1 hexane/ethyl acetate.
*1.25 mmol was used in the case of **79**, **80** and **89**.

Route 2, General procedure:

0.4mls (2.5mmol) of triethylamine, 0.49g (3.0mmol) of carbonyldiimidazole, and 2.5mmol of the corresponding amino acid ester hydrochloride salt were added to a slurry of 0.57g (2.5mmol) of ferrocene carboxylic acid in dry tetrahydrofuran (30mls) at 0°C. After 30 mins, the mixture was raised to room temperature, and stirring was continued for 24 hrs. The solvent evaporated *in vacuo*, and the crude product was purified by silica gel column chromatography using a mobile phase of 2:1 hexane/ethyl acetate.

Route 3, General procedure:

0.4mls (2.5mmol) of triethylamine, and 0.83g of O- (1H-benzotriazol-1-yl) - ***N, N, N', N***', - tetramethyluronium tetrafluoroborate (2.5mmol) was added to a slurry of 0.57g (2.5mmol) of ferrocene carboxylic acid in dimethylformamide (30mls) at ambient temperature. After 30 mins,

2.5mmol of the corresponding amino acid ester hydrochloride salt was added, and stirring was continued for 24 hrs. The solvent evaporated *in vacuo*, and the crude product was purified by silica gel column chromatography using a mobile phase of 2:1 hexane/ethyl acetate.

Route 4, General procedure:

0.4mls (1.2mmol) of triethylamine and 2.5mmol of the corresponding amino acid ester hydrochloride salt were added to a solution of **60** (0.87g, 2.5mmol), in dichloromethane (30mls). Stirring was continued for 24 hrs, and the solvent evaporated *in vacuo*. The crude product was purified by silica gel column chromatography using a mobile phase of 2:1 hexane/ethyl acetate.

_N_-ferrocenoyl-L-2-aminobutyric acid ethyl ester (62)

0.42g of L-2-aminobutyric acid ethyl ester hydrochloride was used in the syntheses.

Yields: Route 1, 0.26g, (69%). Route 2, 0.25g, (67%), orange microcrystalline solid. m.p. 116-118°C

$E_{1/2}$ = 0.186V (Vs. Fc/Fc+), $[\alpha]_D^{20}$ = – 42° (EtOH), UV-Vis (λ_{max}) (EtOH): 266, 306, 443 nm (ε = 200 M^{-1} cm^{-1}), I.R. υ_{max} (KBr): 3274, 3090, 2976, 1746, 1629, 1543, 1299, 1187, 1025, 820 cm^{-1}.

^{1}H-NMR (400MHz) δ (*d*^{6} DMSO): 0.95 (3H, t, *J* = 7.2 Hz, NHCH($CH_2C\underline{H}_3$)), 1.21 (3H, t, *J* = 7.2 Hz, $OCH_2C\underline{H}_3$), 1.72-1.87 (2H, m, NHCH($C\underline{H}_2CH_3$), 4.10 (2H, q, *J* = 7.2 Hz, -$OC\underline{H}_2CH_3$), 4.21 (5H, s, *unsub*. Cp ring), 4.24-4.30 (1H, m, NHC<u>H</u>-), 4.36 (2H, s, H_{meta} Cp ring), 4.85 (1H, s, H_{ortho} Cp ring), 4.93 (1H, s, H_{ortho} Cp ring), 7.95 (1H, d, *J* = 7.6 Hz, N<u>H</u>CH-).

^{13}C-NMR (100 MHz) δ (*d*^{6} DMSO): 11.21, 14.49, 24.22, (-ve DEPT), 54.01, 60.71 (-ve DEPT), 68.61, 68.81, 69.71, 70.43, 70.50, 75.97, 169.74, 172.78

_N_-ferrocenoyl-L-norvaline ethyl ester (63)

0.45g of L-norvaline ethyl ester hydrochloride was used in the synthesis.

Yield 0.56g, (63%), orange micro-crystalline solid. m.p. 124-126°C.

$E_{1/2}$ = 0.187V (Vs. Fc/Fc+), $[\alpha]_D^{20}$ = -37° (EtOH), UV-Vis (λ_{max}) (EtOH): 264, 303, 441 nm (ε = 220 M^{-1} cm^{-1}), I.R. υ_{max} (KBr): 3276, 1751, 1626, 1536, 1380, 1190, 1028, 819 cm^{-1}.

^{1}H-NMR (400MHz) δ (*d*^{6} DMSO): 0.91 (3H, t, *J* = 7.2 Hz, -$CH_2CH_2C\underline{H}_3$), 1.21 (3H, t, *J* = 7.2 Hz, -$OCH_2C\underline{H}_3$), 1.39-1.48 (2H, m, -$CH_2C\underline{H}_2CH_3$), 1.72-1.77 (2H, m, -$C\underline{H}_2CH_2CH_3$), 4.02

(5H, s, *unsub*. Cp ring), 4.12 (2H, q, J = 7.2 Hz, -OC$\underline{H}_2$CH$_3$), 4.32-4.36 (1H, m, NHC$\underline{H}$-), 4.36 (2H, s, H_{meta} Cp ring), 4.84 (1H, s, H_{ortho} Cp ring), 4.92 (1H, s, H_{ortho} Cp ring), 7.97 (1H, d, J = 7.6 Hz, N$\underline{H}$CH-).

^{13}C-NMR (100 MHz) δ (d^6 DMSO): 13.78, 14.48, 19.27 (-ve DEPT), 32.78 (-ve DEPT), 52.06, 60.74 (-ve DEPT), 68.62, 68.81, 69.71, 70.44, 70.51, 75.92, 169.76, 173.00.

_N_-ferrocenoyl-L-norleucine ethyl ester (64)

0.49g of L-norleucine ethyl ester hydrochloride was used in the synthesis.

Yield 0.66g, (72%), orange microcrystalline solid. m.p. 142-144°C.

$E_{1/2}$ = 0.176V (Vs. Fc/Fc+), $[\alpha]_D^{20}$ = –39° (EtOH), UV-Vis (λ_{max}) (EtOH): 260, 304, 444 nm (ε = 191 M^{-1} cm^{-1}), I.R. υ_{max} (KBr): 3274, 3089, 2956, 2362, 2341, 1748, 1625, 1540, 1187 cm^{-1}.

^{1}H-NMR (400MHz) δ (d^6 DMSO): 0.88 (3H, t, J = 7.2 Hz, CH$_2$CH$_2$CH$_2$C$\underline{H}_3$), 1.21 (3H, t, -OCH$_2$C$\underline{H}_3$, J = 7.2 Hz), 1.30-1.42 (4H, m, -CH$_2$C$\underline{H}_2$C$\underline{H}_2$CH$_3$), 1.73-1.79 (2H, m, -C$\underline{H}_2$CH$_2$CH$_2$CH$_3$), 4.14 (2H, q, J = 7.2 Hz,-OC$\underline{H}_2$CH$_3$), 4.20 (5H, s, *unsub.* Cp ring), 4.32-4.36 (3H, m, NHC$\underline{H}$- + 2H_{meta} Cp ring), 4.85 (1H, s, H_{ortho} Cp ring), 4.96 (1H, s, H_{ortho} Cp ring), 7.96 (1H, d, J = 7.6 Hz, N$\underline{H}$CH-,).

^{13}C-NMR (100 MHz) δ (d^6 DMSO): 14.20, 14.49 , 22.02 (-ve DEPT), 28.25 (-ve DEPT), 30.25 (-ve DEPT), 52.28, 60.73 (-ve DEPT), 68.64, 68.79, 69.70, 70.43, 70.50, 75.99, 169.63, 172.96.

_N_-ferrocenoyl-L-phenylglycine methyl ester (65)

0.51g of L-phenylglycine methyl ester hydrochloride was used in the syntheses.

Yields: Route 1, 0.68g, (72%). Route 2, 0.61g, (65%). Route 3, 0.6g, (69%), orange-red crystalline solid. m.p. 118-120°C.

$E_{1/2}$ = 0.199V (Vs. Fc/Fc+), $[\alpha]_D^{20}$ = – 52° (EtOH), UV-Vis (λ_{max}) (EtOH): 265, 305, 445 nm (ε = 202 M^{-1} cm^{-1}), I.R. υ_{max} (KBr): 3394, 3125, 2947, 1735, 1642, 1509, 1325, 1268,1176, 105, 817 cm^{-1}.

^{1}H-NMR (400MHz) δ (d^6 DMSO): 3.68 (3H, s, -OC$\underline{H}_3$), 4.19 (5H, s, *unsub*. Cp ring), 4.37 (2H, s, H_{meta} Cp ring), 4.91 (1H, s, H_{ortho} Cp ring), 5.00 (1H, s, H_{ortho} Cp ring), 5.62 (1H, d, J = 7.0 Hz, NHC$\underline{H}$-), 7.35-7.48 (5H, m, ArH), 8.47 (1H, d, J = 7.0 Hz, N$\underline{H}$CH-).

^{13}C-NMR (100 MHz) δ (d^6 DMSO): 52.57, 56.70, 68.89, 68.94, 69.73, 70.59, 70.66, 75.51, 128.45, 128.60, 128.87, 131.89, 169.61, 171.63.

***N*-ferrocenoyl-L-valine methyl ester (66)**

0.42g of L-valine methyl ester hydrochloride was used in the synthesis.

Yield 0.5g, (61%), orange microcrystalline solid. m.p. 124-125°C.

$E_{1/2}$ = 0.189V (Vs. Fc/Fc+), $[\alpha]_D^{20}$ = –50° (EtOH), UV-Vis (λ_{max}) (EtOH): 260, 306, 444 nm (ε = 201 M^{-1} cm^{-1}), I.R. υ_{max} (KBr): 3332, 2963, 1742, 1629, 1377, 1306, 1200, 993 cm^{-1}.

^{1}H-NMR (400MHz) δ (*d*^{6} DMSO): 0.93 (3H, d, (CH(C<u>H</u>$_3$)$_2$), *J* = 6.8 Hz)), 0.98 (3H, d, *J* = 6.8 Hz,-CH(C<u>H</u>$_3$)$_2$), 2.13-2.20 (1H, m, NHCH(C<u>H</u>(CH$_3$)$_2$), 3.66 (3H, s, -OC<u>H</u>$_3$), 4.19 (5H, s, *unsub*. Cp ring), 4.22-4.26 (1H, m, NHC<u>H</u>-), 4.37 (2H, s, H_{meta} Cp ring), 4.91 (1H, s, H_{ortho} Cp ring) 4.96 (1H, s, H_{ortho} Cp ring), 7.84 (1H, d, N<u>H</u>CH-, *J* = 7.6 Hz).

^{13}C-NMR (100 MHz) δ (*d*^{6} DMSO): 19.45, 19.60, 29.60, 51.98, 58.35, 68.75, 68.93, 69.68, 70.49, 70.59, 75.85, 169.86, 172.84.

***N*-ferrocenoyl-L-glutamic acid diethyl ester (67)**

0.60 g of L-glutamic acid diethyl ester hydrochloride was used in the synthesis.

Yield 0.69g, (67%), orange microcrystalline solid. m.p. 128-129°C.

$E_{1/2}$ = 0.190V (Vs. Fc/Fc+), $[\alpha]_D^{20}$ = -44° (EtOH), UV-Vis (λ_{max}) (EtOH): 268, 306, 443 nm (ε = 204 M^{-1} cm^{-1}), I.R. υ_{max} (KBr): 3290, 3097, 2930, 1735, 1638, 1561, 1381, 1213, 1191, 1106 cm^{-1}.

^{1}H-NMR (400MHz) δ (*d*^{6} DMSO): 1.14-1.30 (6H, m, OCH$_2$C<u>H</u>$_3$), 1.89-2.01 (1H, m, NHCH(C<u>H</u>$_2$CH$_2$-)), 2.08-2.15 (1H, m, NHCH(C<u>H</u>$_2$CH$_2$-)), 2.44 (2H, t, *J* = 7.4 Hz, NHCH(CH$_2$C<u>H</u>$_2$-)), 4.03-4.06 (4H, m, -OC<u>H</u>$_2$CH$_3$), 4.26 (5H, s, *unsub*. Cp ring), 4.37-4.42 (3H, m, 2H_{meta} CP ring + NHC<u>H</u>-), 4.83 (1H, s, H_{ortho} Cp ring), 4.80 (1H, s, H_{ortho} Cp ring), 8.03 (1H, d, *J* = 7.6 Hz, N<u>H</u>CH-).

^{13}C-NMR (100 MHz) δ (*d*^{6} DMSO): 14.42, 26.02 (-ve DEPT), 33.70 (-ve DEPT), 51.63, 60.13 (-ve DEPT), 60.92 (-ve DEPT), 68.62, 68.75, 69.73, 70.50, 70.57, 75.76, 169.85, 172.34, 172.64.

***N*-ferrocenoyl-L-aspartic acid dimethyl ester (68)**

0.49g of L-aspartic acid dimethyl ester hydrochloride was used in the syntheses.

Yields: Route 1, 0.76g, (82%). Route 2, 0.73g, (79%). Route 3, 0.71g, (77%), orange microcrystalline solid. m.p. 123-125°C.

$E_{1/2}$ = 0.202V (Vs. Fc/Fc+), $[\alpha]_D^{20}$ = -43° (EtOH), UV-Vis (λ_{max}) (EtOH): 265, 306, 443 nm (ε = 204 M^{-1} cm^{-1}), I.R. υ_{max} (KBr): 3304, 1735, 1628, 1537, 1309, 1230, 818 cm^{-1}.

^{1}H-NMR (400MHz) δ (*d*^{6} DMSO): 2.81 (1H, dd, J_a = 8.8 Hz, J_b = 8.0 Hz, NHCH(C<u>H</u>$_2$-), 2.94-2.99 (1H, m, NHCH(C<u>H</u>$_2$-), 3.63 (3H, s, -OC<u>H</u>$_3$), 3.66 (3H, s, -OC<u>H</u>$_3$), 4.20 (5H, s, *unsub.* Cp ring), 4.38 (2H, s, C_{meta} Cp ring), 4.73-4.80 (1H, m, NHC<u>H</u>-), 4.80(1H, s, H_{ortho} Cp ring), 4.81 (1H, s, H_{ortho} Cp ring), 8.25 (1H, d, *J* = 8.0 Hz, N<u>H</u>CH-).

^{13}C-NMR (100 MHz) δ (*d*^{6} DMSO): 33.69 (-ve DEPT), 49.11, 52.04, 52.27, 68.03, 68.60, 69.80, 70.65, 75.14, 169.51, 171.10, 171.81.

_N_-ferrocenoyl -(S-benzyl)-L-cysteine ethyl ester (69)

0.50g of (S-benzyl)-L-cysteine ethyl ester hydrochloride was used in the synthesis.

Yield 0.73g, (65%), orange microcrystalline solid. m.p. 126-128°C.

$E_{1/2}$ = 0.196V (Vs. Fc/Fc+), $[\alpha]_D^{20}$ = –77° (EtOH), UV-Vis (λ_{max}) (EtOH): 269, 304, 443 nm (ε = 214 M^{-1} cm^{-1}), I.R. υ_{max} (KBr): 3238, 1748, 1626, 1536, 1219, 1183, 1105, 817, 703 cm^{-1}.

^{1}H-NMR (400MHz) δ (*d*^{6} DMSO): 1.21 (3H, t, *J* = 7.2 Hz, (-OCH$_2$C<u>H</u>$_3$), 2.51-2.90 (2H, m, NHCH(C<u>H</u>$_2$SCH$_2$Ph), 3.80 (2H, s, -SC<u>H</u>$_2$Ph), 4.12 (2H, q, *J* = 7.2 Hz, -OC<u>H</u>$_2$CH$_3$), 4.23 (5H, s, *unsub*. Cp ring), 4.38 (2H, s, H_{meta} Cp ring), 4.57-4.63 (1H, m, NHC<u>H</u>-), 4.85 (2H, s, H_{ortho} Cp ring), 7.25-7.34 (5H, m, ArH), 8.16 (1H, d, *J* = 8.0 Hz, N<u>H</u>CH-).

^{13}C-NMR (100 MHz) δ (*d*^{6} DMSO): 14.32, 32.00 (-ve DEPT), 35.36 (-ve DEPT), 51.92, 61.16 (-ve DEPT), 68.83, 68.73, 69.33, 70.59, 71.05, 75.78, 127.26, 128.75, 129.30, 138.49, 169.67, 171.35.

_N_-ferrocenoyl-L-methionine ethyl ester (70)

0.53g of L-methionine ethyl ester hydrochloride was used in the syntheses.

Yields: Route 1, 0.68g, (70%). Route 2, 0.58g, (60%). Route 3, 0.70g, (72%), orange microcrystalline solid. m.p. 122-124°C.

$E_{1/2}$ = 0.179V (Vs. Fc/Fc+), $[\alpha]_D^{20}$ = -58° (EtOH), UV-Vis (λ_{max}) (EtOH): 266, 306, 446 nm (ε = 200 M^{-1} cm^{-1}), I.R. υ_{max} (KBr): 3268, 2917, 1752, 1628, 1541, 1221, 1182, 1024, 821 cm^{-1}.

^{1}H-NMR (400MHz) δ (*d*^{6} DMSO): 1.22 (3H, t, *J* = 7.2 Hz, -OCH$_2$C<u>H</u>$_3$), 2.01-2.07 (5H, m, -C<u>H</u>$_2$SC<u>H</u>$_3$), 2.51-2.63 (2H, m, -C<u>H</u>$_2$CH$_2$SCH$_3$), 4.13 (2H, q, *J* = 7.2 Hz, -OC<u>H</u>$_2$CH$_3$), 4.22 (5H,

s, *unsub*. Cp ring), 4.38 (2H, s, C_{meta} Cp ring), 4.49-4.55 (1H, m, NHC<u>H</u>-), 4.84 (1H, s, H_{ortho} Cp ring), 4.90 (1H, s, H_{ortho} Cp ring), 8.03 (1H, d, *J* = 7.6 Hz, N<u>H</u>CH-).

^{13}C-NMR (100 MHz) δ (*d*^{6} DMSO): 14.47, 14.93, 30.29 (-ve DEPT), 51.32, 60.95 (-ve DEPT), 68.64, 68.77, 69.74, 70.57, 75.90, 169.87, 172.60.

_N_-ferrocenoyl -L-threonine ethyl ester (71)

0.46g of L-threonine ethyl ester hydrochloride was used in the synthesis.

Yield 0.64g, (71%), orange-red crystalline solid. m.p. 113-115°C.

$E_{1/2}$ = 0.190V (Vs. Fc/Fc+), $[\alpha]_D^{20}$ = – 50° (EtOH), UV-Vis (λ_{max}) (EtOH): 264, 306, 439 nm (ε = 199 M^{-1} cm^{-1}), I.R. υ_{max} (KBr): 3103, 3317, 2976, 2933, 1723, 1609, 1546, 1380, 1104, 1027, 824 cm^{-1}.

^{1}H-NMR (400MHz) δ (*d*^{6} DMSO): 1.14 (3H, d, *J* = 6.2 Hz, -CH(OH)C<u>H</u>$_3$), 1.22 (3H, t, *J* = 7.2 Hz, -OCH$_2$C<u>H</u>$_3$), 4.11-4.22 (3H, m, -OC<u>H</u>$_2$CH$_3$, + NHCH(C<u>H</u>(OH)CH$_3$)), 4.23 (5H, s, *unsub*. Cp ring), 4.38-4.44 (3H, m, H_{meta} Cp ring + NHC<u>H</u>(CH(OH)-), 4.84 (1H, s, H_{ortho} on Cp ring), 4.92 (1H, s, H_{ortho} Cp ring), 4.99 (1H, d, *J* = 7.6 Hz, -CH(O<u>H</u>)CH$_3$), 7.46 (1H, d, *J* = 8.8 Hz, N<u>H</u>CH-).

^{13}C-NMR (100 MHz) δ (*d*^{6} DMSO): 14.48, 20.71, 58.56, 60.28 (-ve DEPT), 66.74, 68.67, 68.70, 69.78, 70.55, 70.60, 75.95, 169.96, 171.23.

_N_-ferrocenoyl-L-serine methyl ester (72)

0.39g of L-serine methyl ester hydrochloride was used in the synthesis.

Yield 0.61g, (74%), orange-red crystalline solid. m.p. 128-130°C.

$E_{1/2}$ = 0.190V (Vs. Fc/Fc+), $[\alpha]_D^{20}$ = – 43° (EtOH), UV-Vis (λ_{max}) (EtOH): 268, 305, 440 nm (ε = 193 M^{-1} cm^{-1}), I.R. υ_{max} (KBr): 3426, 3341, 2932, 2362, 2343, 1738, 1610, 1542, 1177, 1074 cm^{-1}.

^{1}H-NMR (400MHz) δ (*d*^{6} DMSO): 3.67 (3H, s, -OC<u>H</u>$_3$), 3.73-3.78 (2H, m, -CH(C<u>H</u>$_2$OH)), 4.23 (5H, s, *unsub*. Cp ring), 4.38 (2H, s, H_{meta} Cp ring), 4.45-4.50 (1H, m, NHC<u>H</u>(CH$_2$OH)), 4.81 (1H, s, H_{ortho} Cp ring), 4.89 (1H, s, H_{ortho} Cp ring), 5.08 (1H, t, *J* = 6.0 Hz, -CH$_2$O<u>H</u>), 7.84 (1H, d, *J* = 7.2 Hz, N<u>H</u>CH-).

^{13}C-NMR (100 MHz) δ (*d*^{6} DMSO): 52.19, 55.34, 61.43 (–ve DEPT), 68.50, 68.86, 69.81, 70.52, 70.75, 75.83, 169.72, 171.65.

***N*-ferrocenoyl-L-tyrosine methyl ester (73)**

0.64g of L-tyrosine methyl ester hydrochloride was used in the syntheses.

Yields: Route 1, 0.67g, (69%). Route 2, 0.53g, (55%). Route 3, 0.73g, (75%), orange-red crystalline solid. m.p. 140-143°C.

$E_{1/2}$ = 0.192V (Vs. Fc/Fc+), $[\alpha]_D^{20}$ = -9° (EtOH), UV-Vis (λ_{max}) (EtOH): 265, 305, 445 nm (ε = 204 M^{-1} cm^{-1}), I.R. υ_{max} (KBr): 3355, 1724, 1609, 1551, 1520, 1436, 1315, 1225, 1109 cm^{-1}.

^{1}H-NMR (400MHz) δ (*d*^{6} DMSO): 2.89-2.96 (1H, m, NHCH(C$\underline{H}_2$PhOH), 3.02-3.06 (1H, m, NHCH(C$\underline{H}_2$PhOH), 3.65 (3H, s, -OC$\underline{H}_3$), 4.03 (5H, s, *unsub*. Cp ring), 4.33 (2H, s, H_{meta} Cp ring), 4.55-4.61 (1H, m, NHC$\underline{H}$-), 4.78 (1H, s, H_{ortho} Cp ring), 4.81 (1H, s, H_{ortho} Cp ring), 6.68 (2H, d, *J* = 8.8 Hz, ArH), 7.12 (2H, d, *J* = 8.8 Hz, ArH), 8.02 (1H, d, *J* = 8.0 Hz, N$\underline{H}$CH-), 9.22 (1H, s, phenolic OH).

^{13}C-NMR (100 MHz) δ (*d*^{6} DMSO): 35.73 (-ve DEPT), 52.24, 54.20, 68.35, 68.80, 69.69, 70.40, 70.44, 75.81, 115.37, 128.19, 130.32, 156.27, 169.57, 172.99.

***N*-ferrocenoyl-L-histidine methyl ester (74)**

0.61g of L-histidine methyl ester dihydrochloride was used in the synthesis.

Yield 0.47g, (49%), orange-red crystalline solid. m.p. 162-164°C.

$E_{1/2}$ = 0.190mV (Vs. Fc/Fc+), $[\alpha]_D^{20}$ = -58° (EtOH), UV-Vis (λ_{max}) (EtOH): 260, 305, 445 nm (ε = 195 M^{-1} cm^{-1}), I.R. υ_{max} (KBr): 3387, 2954, 1750, 1639, 1561, 1511, 1381, 819, 763 cm^{-1}.

^{1}H-NMR (400MHz) δ (*d*^{6} DMSO): 3.03 (2H, s, NHCH(C$\underline{H}_2$-)), 3.64 (3H, s, -OC$\underline{H}_3$), 4.11 (5H, s, *unsub.* Cp ring), 4.35 (2H, s, H_{meta} Cp ring), 4.63-4.67 (1H, m, NHC$\underline{H}$-), 4.78 (2H, s, H_{ortho} Cp ring), 6.92 (1H, s, $H_{imidazole}$), 7.62 (1H, s, $H_{imidazole}$), 8.15 (1H, d, *J* = 7.6 Hz, N$\underline{H}$CH-), 11.20 (1H, s, N$\underline{H}_{imidazole}$).

^{13}C-NMR (100 MHz) δ (*d*^{6} DMSO): 29.52 (-ve DEPT), 51.84, 52.21, 68.47, 68.60, 69.74, 70.49, 70.73, 75.85, 115.55, 127.40, 130.07, 135.45, 169.58, 172.71.

***N*-ferrocenoyl-L-tryptophan methyl ester (75)**

0.64g of L-tryptophan methyl ester hydrochloride was used in the synthesis.

Yield 0.72g, (67%), orange-red crystalline solid. m.p. 111-113°C.

$E_{1/2}$ = 0.187V (Vs. Fc/Fc+), $[\alpha]_D^{20}$ = -47° (EtOH), UV-Vis (λ_{max}) (EtOH): 270, 444 nm (ε = 222 M^{-1} cm^{-1}), I.R. υ_{max} (KBr): 3324, 3260, 2932, 1747, 1628, 1542, 1440, 1274, 1218, 1176, 1107, 1044 cm^{-1}.

^{1}H-NMR (400MHz) δ (*d*^{6} DMSO): 3.20-3.28 (2H, m, NHCH(C$\underline{H}_2$-), 3.67 (3H, s, -OC$\underline{H}_3$), 3.98 (5H, s, *unsub.* Cp ring), 4.32 (2H, s, H_{meta} Cp ring), 4.72 (1H, m, NHC$\underline{H}$-), 4.79 (2H, s, H_{ortho} Cp ring), 7.01-7.07 (2H, m, H_{indole}), 7.26 (1H, s, H_{indole}), 7.33 (1H, d, *J* = 7.6 Hz, H_{indole}), 7.60 (1H, d, *J* = 7.6 Hz, H_{indole}), 7.99 (1H, d, *J* = 8.0 Hz, N$\underline{H}$CH-), 10.09 (1H, s, N-H_{indole}).

^{13}C-NMR (100 MHz) δ (*d*^{6} DMSO): 26.93 (-ve DEPT), 52.66, 53.28, 68.43, 68.71, 69.61, 70.38, 70.42, 75.83, 110.40, 111.84, 118.38, 118.79, 121.32, 124.09, 127.37, 136.50, 169.57, 173.17.

_N_-ferrocenoyl-α-isoaminobutyric acid ethyl ester (76)

0.42g of α-isoaminobutyric acid ethyl ester hydrochloride was used in the synthesis.

Yield 0.57g, (64%), orange solid. m.p. 139-140°C.

$E_{1/2}$ = 0.179V (Vs. Fc/Fc+), UV-Vis (λ_{max}) (EtOH): 267, 305, 440 nm (ε = 196 M^{-1} cm^{-1}), I.R. υ_{max} (KBr): 3333, 2989, 2937, 1737, 1636, 1523, 1301, 1149 cm^{-1}.

^{1}H-NMR (400MHz) δ (*d*^{6} DMSO): 1.17 (3H, t, *J* = 6.8 Hz, -OCH$_2$C$\underline{H}_3$), 1.43 (6H, s, NHC(C$\underline{H}_3$)$_2$-), 4.06 (2H, q, *J* = 6.8 Hz, -OC$\underline{H}_2$CH$_3$), 4.21 (5H, s, *unsub*. Cp ring), 4.34 (2H, d, J = 1.6 Hz, H_{meta} Cp ring), 4.85 (2H, d, *J* = 1.6 Hz, H_{ortho} Cp ring), 7.83 (1H, s, N$\underline{H}$C(CH$_3$)$_2$-).

^{13}C-NMR (100 MHz) δ (*d*^{6} DMSO): 14.42, 25.47, 25.70, 55.47, 60.48 (-ve DEPT), 68.76, 69.68, 70.38, 76.11, 168.78, 174.32.

_N_-ferrocenoyl-(1S, 2R)-(+)-norephedrine (77)

0.47g of (1S, 2R)-(+)-norephedrine hydrochloride was used in the synthesis.

Yield 0.64g, (71%), orange-red crystalline solid. m.p. 153-155°C.

$E_{1/2}$ = 0.170V (Vs. Fc/Fc+), $[\alpha]_D^{20}$ = +34° (EtOH), UV-Vis (λ_{max}) (EtOH): 268, 304, 442 nm (ε = 209 M^{-1} cm^{-1}), I.R. υ_{max} (KBr): 3364, 3288, 3042, 2980, 1607, 1552, 1444, 1327, 1199, 1002, 821, 701 cm^{-1}.

^{1}H-NMR (400MHz) δ (*d*^{6} DMSO): 1.11 (3H, d, *J* = 6.4 Hz, NHCH(C$\underline{H}_3$)-, 3.98 (5H, s, *unsub.* Cp ring), 4.11-4.16 (1H, m, NHC$\underline{H}$(CH$_3$)-, 4.28 (2H, s, H_{meta} Cp ring), 4.61-4.64 (1H, m, NHCH(CH$_3$),C$\underline{H}$OH), 4.72 (1H, s, H_{ortho} Cp ring), 4.75 (1H, s, H_{ortho} Cp ring), 5.51 (1H, d, *J* =

4.0 Hz, -CHO<u>H</u>Ph), 7.20 (1H, d, *J* = 7.2 Hz, ArH), 7.33 (2H, m, ArH), 7.42 (2H, d, *J* = 7.6 Hz, ArH), 7.49 (1H, d, *J* = 8.8 Hz, N<u>H</u>CH-).

^{13}C-NMR (100 MHz) δ (*d*^{6} DMSO): 16.35, 50.67 (NH<u>C</u>H(CH_3), 68.04, 68.82, 69.93, 70.11, 70.15, 75.22, 76.94, 126.88, 127.16, 128.15, 144.29, 168.55.

_N_-ferrocenoyl -D-methionine-ethyl ester (78)

0.53g of D-methionine ethyl ester hydrochloride was used in the synthesis.

Yield 0.64g, (66%), orange microcrystalline solid. m.p. 123-125°C.

$E_{1/2}$ = 0.188V (Vs. Fc/Fc+), $[\alpha]_D^{20}$ = +74° (EtOH), UV-Vis (λ_{max}) (EtOH): 260, 305, 445 nm (ε = 212 M^{-1} cm^{-1}) nm, I.R. υ_{max} (KBr): 3267, 2917, 2362, 1751, 1628, 1538, 1219, 1182, 1024, 821 cm^{-1}.

^{1}H-NMR (400MHz) δ (*d*^{6} DMSO): 1.22 (3H, t, *J* = 6.8 Hz, -OCH$_2$C<u>H</u>$_3$), 2.03 (2H, t, *J* = 6.8 Hz, -C<u>H</u>$_2$SCH$_3$), 2.07 (3H, s, -CH$_2$SC<u>H</u>$_3$), 2.50-2.64 (2H, m, -C<u>H</u>$_2$CH$_2$SCH$_3$), 4.13 (2H, q, *J* = 6.8 Hz, -OC<u>H</u>$_2$CH$_3$), 4.27 (5H, s, *unsub*. Cp ring), 4.37 (2H, s, H_{meta} Cp ring), 4.49-4.84 (1H, m, NHC<u>H</u>-), 4.87 (1H, s, H_{ortho} Cp ring), 4.90 (1H, s, H_{ortho} Cp ring), 8.03 (1H, d, *J* = 8.0 Hz, N<u>H</u>CH-).

^{13}C-NMR (100 MHz) δ (*d*^{6} DMSO): 14.47, 14.93, 30.31 (-ve DEPT), 30.34 (-ve DEPT), 51.33, 60.93 (-ve DEPT), 68.64, 68.78, 69.73, 70.49, 70.55, 75.85, 169.81, 172.58.

_N_-ferrocenoyl-(N$^{\varepsilon}$-Fc)-L-lysine methyl ester (79)

0.29g of L-lysine methyl ester dihydrochloride was used in the synthesis.

Yield 0.36g, (49%) orange microcrystalline solid. m.p. 228-230°C.

$E_{1/2}$ = 0.177V (Vs. Fc/Fc+), $[\alpha]_D^{20}$ = – 43° (EtOH), UV-Vis (λ_{max}) (EtOH): 265, 305, 440 nm (ε = 199 M^{-1} cm^{-1}), I.R. υ_{max} (KBr): 3287, 3081, 2867, 2365, 1743, 1626, 1560, 1542, 1376, 1297, 1107 cm^{-1}.

^{1}H-NMR (400MHz) δ (*d*^{6} DMSO): 1.30-1.55 (4H, m, CH$_2$C<u>H</u>$_2$C<u>H</u>$_2$CH$_2$NH-Fc), 1.84-1.86 (2H, m, NHCH(C<u>H</u>$_2$CH$_2$CH$_2$-), 3.19-3.22 (2H, m, CH$_2$C<u>H</u>$_2$NH-Fc,), 3.67 (3H, s, -OC<u>H</u>$_3$), 4.15 (5H, s, *unsub*. Cp ring), 4.23 (5H, s, *unsub*. Cp ring), 4.34 (2H, s, H_{meta} Cp ring), 4.39-4.42 (3H, m, 2H_{meta} Cp ring + NHC<u>H</u>(CH$_2$CH$_2$CH$_2$-)), 4.80 (2H, s, H_{ortho} Cp ring), 4.86 (1H, s, H_{ortho} Cp ring), 4.96 (1H, s, H_{ortho} Cp ring), 7.82 (1H, t, *J* = 5.4 Hz, CH$_2$CH$_2$N<u>H</u>-Fc), 7.98 (1H, d, *J* = 7.6 Hz, N<u>H</u>CH-).

^{13}C-NMR (100 MHz) δ (*d*^{6} DMSO): 23.42 (-ve DEPT), 29.38 (-ve DEPT), 30.37 (-ve DEPT), 38.59 (-ve DEPT), 52.16, 52.40, 68.64, 68.63, 68.84, 69.63, 69.72, 70.16, 70.45, 70.51, 75.90, 77.17, 169.19, 169.76, 173.40.

_N_-ferrocenoyl -(N^{im}-Fc)-L-histidine methyl ester (80)

0.31g of L-histidine methyl ester dihydrochloride was used in the synthesis.

Yield 0.32g, (43%), orange-red crystalline solid. m.p. 181-183°C.

$E_{1/2}$ = 0.184mV (Vs. Fc/Fc+), $[\alpha]_D^{20}$ = -50° (EtOH), UV-Vis (λ_{max}) (EtOH): 270, 345, 460 nm (ε = 440 M^{-1} cm^{-1}), I.R. υ_{max} (KBr): 3298, 3168, 2952, 2368, 1758, 1688, 1645, 1526, 1440, 1382, 1250, 824, 756 cm^{-1}.

^{1}H-NMR (400MHz) δ (*d*^{6} DMSO): 3.10 (2H, d, *J* = 7.2 Hz, NHCH(C<u>H</u>$_2$-)), 3.36 (3H, s, -OC<u>H</u>$_3$), 4.07 (5H, s, *unsub*. Cp ring), 4.36 (2H, s, H_{meta} Cp ring), 4.25 (5H, s, *unsub*. Cp ring), 4.73 (2H, s, H_{meta} Cp ring), 4.77-4.84 (3H, m, 2H_{ortho} Cp ring + NHC<u>H</u>-), 4.96 (2H, s, H_{ortho} Cp ring), 7.71 (1H, s, $H_{imidazole}$), 8.13 (1H, d, *J* = 8.0 Hz, N<u>H</u>CH-), 8.44 (1H, s, $H_{imidazole}$).

^{13}C-NMR (100 MHz) δ (*d*^{6} DMSO): 29.52 (-ve DEPT), 51.84, 52.41, 68.50, 68.93, 69.70, 70.60, 70.73, 71.54, 71.73, 71.90, 73.43, 75.63, 115.55, 135.35, 137.35, 168.83, 169.69, 172.70.

_N_-ferrocenoyl -β-alanine methyl ester (81)

0.35g of β-alanine methyl ester hydrochloride was used in the synthesis.

Yield 0.55g, (70%), orange solid. m.p. 128-130°C.

$E_{1/2}$ = 0.175V (Vs. Fc/Fc+), UV-Vis (λ_{max}) (EtOH): 304, 439 nm (ε = 179 M^{-1} cm^{-1}), I.R. υ_{max} (KBr): 3303, 2926, 1735, 1624, 1504, 1326, 1206, 1171 cm^{-1}.

^{1}H-NMR (400MHz) δ (*d*^{6} DMSO): 2.60 (2H, t, *J* = 6.6 Hz, NHCH$_2$<u>C</u>H$_2$-), 3.41-3.44 (2H, m, NHC<u>H</u>$_2$CH$_2$-), 3.62 (3H, s, -OC<u>H</u>$_3$), 4.17 (5H, s, *unsub*. Cp ring), 4.33 (2H, d, *J* = 2.0 Hz, H_{meta} Cp ring), 4.77 (2H, d, *J* = 2.0 Hz, C_{ortho} Cp ring), 7.90 (1H, t, *J* = 5.6 Hz, N<u>H</u>CH$_2$CH$_2$-).

^{13}C-NMR (100 MHz) δ (*d*^{6} DMSO): 34.28 (-ve DEPT), 35.51 (-ve DEPT), 51.72, 68.47, 69.69, 70.27, 76.69, 169.42, 172.29.

_N_-ferrocenoyl-γ-aminobutyric acid-ethyl ester (82)

0.42g of γ-aminobutyric acid ethyl ester hydrochloride was used in the synthesis.

Yield 0.60g, (70%), orange solid. m.p. 110-111°C.

$E_{1/2}$ = 0.169V (Vs. Fc/Fc+), UV-Vis (λ_{max}) (EtOH): 268, 301, 446 nm (ε = 181 M^{-1} cm^{-1}), I.R. υ_{max} (KBr): 3289, 2932, 2376, 1734, 1625, 1511, 1379, 1306, 1185, 816 cm^{-1}.

^{1}H-NMR (400MHz) δ (*d*^{6} DMSO): 1.16 (3H, t, *J* = 6.8 Hz, $OCH_2C\underline{H}_3$), 1.74 (2H, m, $NHCH_2C\underline{H}_2$-), 2.34 (2H, br s, $NHCH_2CH_2C\underline{H}_2$-), 3.18 (2H, s, $NHC\underline{H}_2CH_2$-), 3.59 (s, 3H, -OCH_3), 4.04 (2H, q, *J* = 6.8 Hz, -$OC\underline{H}_2CH_3$), 4.13 (5H, s, *unsub*. Cp ring), 4.31 (2H, s, H_{meta} Cp ring), 4.77 (2H, s, H_{ortho} Cp ring), 7.82 (1H, t, *J* = 5.6 Hz,, $N\underline{H}CH_2CH_2$-).

^{13}C-NMR (100 MHz) δ (*d*^{6} DMSO): 14.48, 25.17 (-ve DEPT), 31.31 (-ve DEPT), 38.28 (-ve DEPT), 60.12 (-ve DEPT), 68.45, 69.62, 70.19, 77.06, 169.25, 173.06.

_N_-ferrocenoyl-(1S, 2R)-(+)-ephedrine (83)

0.50g of (1S, 2R)-(+)-ephedrine hydrochloride was used in the synthesis.

Yield 0.67g, (71%), dark red crystalline solid. m.p. 138-139°C.

$E_{1/2}$ = 0.117mV (Vs. Fc/Fc+), $[\alpha]_D^{20}$ = +34° (EtOH), UV-Vis (λ_{max}) (EtOH): 265, 307, 445 nm (ε = 180 M^{-1} cm^{-1}), I.R. υ_{max} (KBr): 3369, 3088, 2982,1607,1495,1457, 1103, 1053, 821 cm^{-1}.

^{1}H-NMR (400MHz) δ (*d*^{6} DMSO): 1.20 (3H, s, $N(CH_3)CH(C\underline{H}_3)$-), 2.78 (1H, s, $N(C\underline{H}_3)CH$-),3.03 (2H, s, $N(C\underline{H}_3)CH$-), 4.02 (5H, s, *unsub*. Cp ring), 4.26 (1H, s, $N(CH_3)C\underline{H}(CH_3)$-), 4.28 (2H, s, H_{meta} Cp ring), 4.55 (1H, s, -$C\underline{H}$(OH)Ph), 4.68 (2H, s, H_{ortho} Cp ring), 5.50 (1H, d, *J* = 4.0 Hz, -CH(O$\underline{H}$)Ph), 7.09-7.41 (5H, m, ArH).

^{13}C-NMR (100 MHz) δ (*d*^{6} DMSO): 13.27, 32.68, 55.27, 69.79, 70.17, 71.38, 75.02, 75.67, 126.83, 127.41, 128.15, 144.26, 169.39.

_N_-ferrocenoyl-(1S, 2S)-(+)-pseudoephedrine (84)

0.50g of (1S, 2S)-(+)-pseudoephedrine hydrochloride was in the synthesis.

Yield 0.68g, (72%), orange solid. m.p. 131-132°C.

$E_{1/2}$ = 0.108mV (Vs. Fc/Fc+), $[\alpha]_D^{20}$ = +36° (EtOH), UV-Vis (λ_{max}) (EtOH): 260, 307, 444 nm (ε = 189 M^{-1} cm^{-1}), I.R. υ_{max} (KBr): 3445, 3090, 2375,1576, 1452,1406, 1036, 818 cm^{-1}.

^{1}H-NMR (400MHz) δ (*d*^{6} DMSO): 1.20 (3H, s, $N(CH_3)CH(C\underline{H}_3)$-), 2.78 (1H, s, $N(C\underline{H}_3)CH$-), 3.03 (2H, s, $N(C\underline{H}_3)CH$-), 4.02 (5H, s, *unsub.* Cp ring), 4.28 (2H, s, H_{meta} Cp ring), 4.37 (1H, s, $N(CH_3)C\underline{H}(CH_3)$-), 4.55 (1H, s, -$C\underline{H}$(OH)Ph), 4.68 (2H, s, H_{ortho} on Cp ring), 5.50 (1H, d, *J* = 4.8 Hz, -CH(O$\underline{H}$)Ph), 7.09-7.41 (5H, m, ArH).

^{13}C-NMR (100 MHz) δ (*d*^{6} DMSO): 13.27, 32.68, 55.27, 69.79, 70.17, 71.38, 75.02, 78.67, 126.83, 127.41, 128.15, 144.26, 169.39.

_N_-ferrocenoyl–sarcosine ethyl ester (85)

0.38g of sarcosine ethyl ester hydrochloride was used in the synthesis.

Yield 0.48g, (59%) orange-red solid. m.p. 63-65°C.

$E_{1/2}$ = 0.156V (Vs. Fc/Fc+), UV-Vis (λ_{max}) (EtOH): 268, 305, 445 nm (ε = 209 M^{-1} cm^{-1}), I.R. υ_{max} (KBr): 3080, 2920, 1744, 1603, 1499, 1298, 1203, 1098, 763 cm^{-1}.

^{1}H-NMR (400MHz) δ (*d*^{6} DMSO): 1.22 (3H, t, *J* = 7.0 Hz, -$OCH_2C\underline{H}_3$), 3.33 (3H, s, $N(C\underline{H}_3)CH_2$-), 4.10-4.52 (4H, m, $N(CH_3)C\underline{H}_2$- + -$OC\underline{H}_2CH_3$), 4.25 (5H, s, *unsub*. Cp ring), 4.42 (2H, s, H_{meta} Cp ring), 4.69 (2H, s, C_{meta} Cp ring).

^{13}C-NMR (100 MHz) δ (*d*^{6} DMSO): 14.43, 38.17, 50.83 (-ve DEPT), 60.28 (-ve DEPT), 69.78, 70.45, 71.29, 76.12, 169.79, 170.64.

_N_-ferrocenoyl-L-thyroxine methyl ester (86)

0.82g of L-thyroxine methyl ester hydrochloride was used in the synthesis.

Yield 0.69g (69%), orange solid, m.p. 140-143°C.

$E_{1/2}$ = 0.190V (Vs. Fc/Fc+), $[\alpha]_D^{20}$ = -11° (EtOH), UV-Vis (λ_{max}) (EtOH): 270, 305, 441 nm (ε = 200 M^{-1} cm^{-1}), I.R. υ_{max} (KBr): 3350, 1739, 1613, 1526, 1520, 1433, 1400, 1222, 1083, 909, 823 cm^{-1}.

^{1}H-NMR (400MHz) δ (*d*^{6} DMSO): 2.99-3.05 (1H, m, -NHCH($C\underline{H}_2$-)),3.16-3.20 (1H, m, -NHCH($C\underline{H}_2$-)), 3.66 (3H, s, $OC\underline{H}_3$), 3.99 (5H, s, *unsub*. Cp ring), 4.35 (2H, s, H_{meta} Cp ring), 4.64-4.69 (1H, m, -NHC$\underline{H}$-), 4.77 (1H, s, H_{ortho} Cp ring), 4.81 (1H, s, H_{ortho} Cp ring), 7.04 (1H, s, ArH), 7.19 (1H, s, ArH), 7.93 (1H, s, ArH), 7.97 (1H, s, ArH), 8.15 (1H, d, *J* = 8.0 Hz, -N$\underline{H}$CH-), 9.23 (1H, s, ArOH).

^{13}C-NMR (100 MHz) δ (*d*^{6} DMSO): 34.52 (-ve DEPT), 52.34, 68.34, 68.94, 69.77, 70.35, 70.83, 75.68, 125.38, 125.68, 141.01, 141.09, 150.43, 151.36, 169.81, 172.46.

_N_-ferrocenoyl-(S-methyl)-L-cysteine methyl ester (87)

0.46g of (S-methyl)-L-cysteine methyl ester hydrochloride was used in the syntheses.

Yields: Route 1, 0.67g (74%). Route 4, 0.81g (90%)*, orange solid, m.p. 136-139°C

$E_{1/2}$ = 0.183mV (Vs. Fc/Fc+), $[\alpha]_D^{20}$ = -48° (EtOH), UV-Vis (λ_{max}) (EtOH): 260, 304, 444 nm (ε = 195 M^{-1} cm^{-1}), I.R. υ_{max} (KBr): 3294, 2925, 2363, 1753, 1631, 1530, 1222, 818 cm^{-1}.

^{1}H-NMR (400MHz) δ (*d*^{6} DMSO): 2.11 (3H, s, -SC<u>H</u>$_3$), 2.89 (1H, dd, J_a = 10.0 Hz, J_b = 13.6 Hz, -C<u>H</u>$_2$SCH$_3$), 2.97 (1H, dd, J_a = 4.8 Hz, J_b = 13.6 Hz, -C<u>H</u>$_2$SCH$_3$), 3.68 (3H, s, OC<u>H</u>$_3$), 4.23 (5H, s, *unsub*. Cp ring), 4.38 (2H, s, H_{meta} Cp ring), 4.57-4.62 (1H, m, -NHC<u>H</u>-), 4.84 (1H, s, H_{ortho} Cp ring), 4.86 (1H, s, H_{ortho} Cp ring), 8.16 (1H, d, *J* = 8.0 Hz, -N<u>H</u>CH-).

^{13}C-NMR (100 MHz) δ (*d*^{6} DMSO): 15.33, 33.69 (-ve DEPT), 51.76, 52.45, 68.69, 69.82, 70.58, 70.61, 75.73, 169.74, 171.96.

*Based on the input of **56**.

_N_-ferrocenoyl-valeric acid methyl ester (88)

0.42g of valeric acid methyl ester hydrochloride was used in the syntheses.

Yields: Route 1, 0.58g (68%). Route 3, 0.51g, (60%). Route 4, 0.78g, (91%)*, orange solid, m.p 121-124°C.

$E_{1/2}$ = 0.149V (Vs. Fc/Fc+), UV-Vis (λ_{max}) (EtOH): 262, 304, 440 nm (ε = 191 M^{-1} cm^{-1}), I.R. υ_{max} (KBr): 3303, 2950, 1738, 1621, 1537, 1292, 1170, 817 cm^{-1}.

^{1}H-NMR (400MHz) δ (*d*^{6} DMSO): 1.49-1.61 (4H, m, -NHCH$_2$C<u>H</u>$_2$C<u>H</u>$_2$CH$_2$CO-), 2.36 (2H, t, *J* = 7.2 Hz, -CH$_2$C<u>H</u>$_2$CO-), 3.15-3.20 (2H, m, -NHC<u>H</u>$_2$CH$_2$-), 3.62 (3H, s, -OC<u>H</u>$_3$), 4.15 (5H, s, *unsub*. Cp ring), 4.33 (2H, s, H_{meta} Cp ring), 4.78 (2H, s, H_{ortho} Cp ring), 7.96 (1H, t, *J* = 5.6 Hz, -N<u>H</u>CH-).

^{13}C-NMR (100 MHz) δ (*d*^{6} DMSO): 22.30 (-ve DEPT), 29.23 (-ve DEPT), 33.61 (-ve DEPT), 38.50 (-ve DEPT), 51.55, 68.43, 69.62, 70.13, 77.23, 169.06, 173.67.

*Based on the input of **56**.

_N_-ferrocenoyl-(N$^\delta$-Fc)-L-ornithine methyl ester (89)

0.27g of L-ornithine methyl ester dihydrochloride was used in the synthesis.

Yield 0.39g (60%), orange crystalline solid, m.p. 201-204°C.

$E_{1/2}$ = 0.188V (Vs. Fc/Fc+), $[\alpha]_D^{20}$ = – 22° (EtOH), UV-Vis (λ_{max}) (EtOH): 265, 307, 441 nm (ε = 161 M^{-1} cm^{-1}), I.R. υ_{max} (KBr): 3292, 2877, 2365, 1745, 1626, 1555, 1370, 1256, 1100 cm^{-1}.

^{1}H-NMR (400MHz) δ (*d*^{6} DMSO): 1.63-1.74 (2H, m, -CH$_2$C<u>H</u>$_2$CH$_2$NHCO-), 1.69-1.84 (2H, m, -C<u>H</u>$_2$CH$_2$CH$_2$NHCO-), 3.20-3.25 (2H, m, -CH$_2$CH$_2$C<u>H</u>$_2$NHCO-), 3.64 (3H, s, OC<u>H</u>$_3$), 4.15

(5H, s, *unsub*. Cp ring), 4.21 (5H, s, *unsub*. Cp ring), 4.33 (2H, br. s, H_{meta} Cp ring), 4.37 (2H, br. s, H_{meta} Cp ring), 4.37-4.41 (1H, m, -NHC<u>H</u>-), 4.79 (2H, s, H_{ortho} Cp ring), 4.85 (1H, s, H_{ortho} Cp ring), 4.92 (1H, s, H_{ortho} Cp ring), 7.91 (1H , t, J = 5.6 Hz, -N<u>H</u>CH_2-), 8.13 (1H, d, J = 7.6 Hz, -N<u>H</u>CH-).

^{13}C-NMR (100 MHz) δ (d^6 DMSO): 26.74 (-ve DEPT), 28.06 (-ve DEPT), 38.49 (-ve DEPT), 52.19, 52.45, 68.45, 68.49, 68.72, 69.66, 69.75, 70.23, 70,51, 70.58, 75.79, 76.99, 169.55, 170.01, 173.28.

2.12: References

1) N.J. Long, *Metallocenes*, *Blackwell sciences,* (*1998)*

2) M. Sheehy, *The Design and Synthesis of Novel Peptide Derivatives as Malarial Protease Inhibitors and Electrochemical Anion Sensing Receptors, Ph.D. Thesis, DCU, (1999)*

3) D. L. Stone, D. K. Smith, *Polyhedron Lett., 22, (2003), 763*.

4) A. Hess, O. Broch, T. Wheymuller, N.M. Nolte, *J. Organometallic Chem., 589, (1999), 75.*

5) G. Zubay , *Biochemistry, 3rd ed., WCB Publishers, (1993)*

6) H.B. Kraatz, J. Lusztyk, G.D. Enright, *Inorg. Chem., 36, (1997), 2400*

7) P.C. Reeves*., Org. Syn., 56, (1977), 28.*

8) Y. Xu, H.B. Kraatz*., Tetrahedron Lett., 42, (2001), 75.*

9) P. Saweczko, H.B. Kraatz, *Co-ord. Chem. Rev., 190-192, (1999), 185.*

10) A. Tongi, T. Hayashi, *Ferrocenes, VCH, Wienhiem, (1993).*

11) M. Bodansky*,* A. Bodansky*, Principles of Peptide Synthesis, 2nd ed., Springer-Verlay, (1993).*

12) C. Imrie, L. Cook, D. Levendis, *J. Organometallic Chem.,637-639, (2001), 266.*

13) S.C. Story, J.V. Aldrich*, Int. J. Pept. Protein. Res., 43, (1994), 29.*

14) P.L. Williams, *Chemical Approaches to the Synthesis of Peptides, CRC press, (1997), 95.*

15) L. Lin, A. Berces, H.B.Kraatz, *J. Organometallic Chem.,* 556, (1998), *11*

16) D.H. Williams, I. Fleming, *Spectroscopic Methods in Organic Chemistry, 4th ed., McGraw-Hill, (1989)*.

17) C.N. Kirsten, T.H. Schrader, *J. Am. Chem. Soc., 119, (1997), 12061.*

18) J.F. Gallagher, P.T.M. Kenny, M.J. Sheehy, *Inorg. Chem. Comm., 2, (1999), 200.*

Chapter III

The Synthesis and Characterisation of *N*-Ferrocenoyl Dipeptides

3.1: Introduction

While there have been a growing number of reports of ferrocene di- and polypeptide derivatives in the literature in recent years, few have been prepared by exposing the ferrocene moiety to the normal cycles of protection/deprotection encountered in standard peptide synthesis. In the majority of cases, this methodology has been avoided via the addition of the ferrocene group to a pre-prepared peptide, i.e. at the final step of peptide chain elongation. Of those reports of chain elongation involving the ferrocene group, low overall yields and problems with purification are common [1, 2]. In addition, the ferrocene group has been shown to be entirely unsuitable to several standard peptide reactions, for example acidolysis and the Merryfield synthesis [3].

The group of Kraatz et al. were able to prepare the dipeptide ferrocenoyl-(proline)$_2$-OBz by hydrogenation of the ***N***-ferrocenoyl-L-proline benzyl ester to give the free acid, followed by DCC/HOBt coupling to H-pro-OBz.HCl (*scheme 1*) [4].

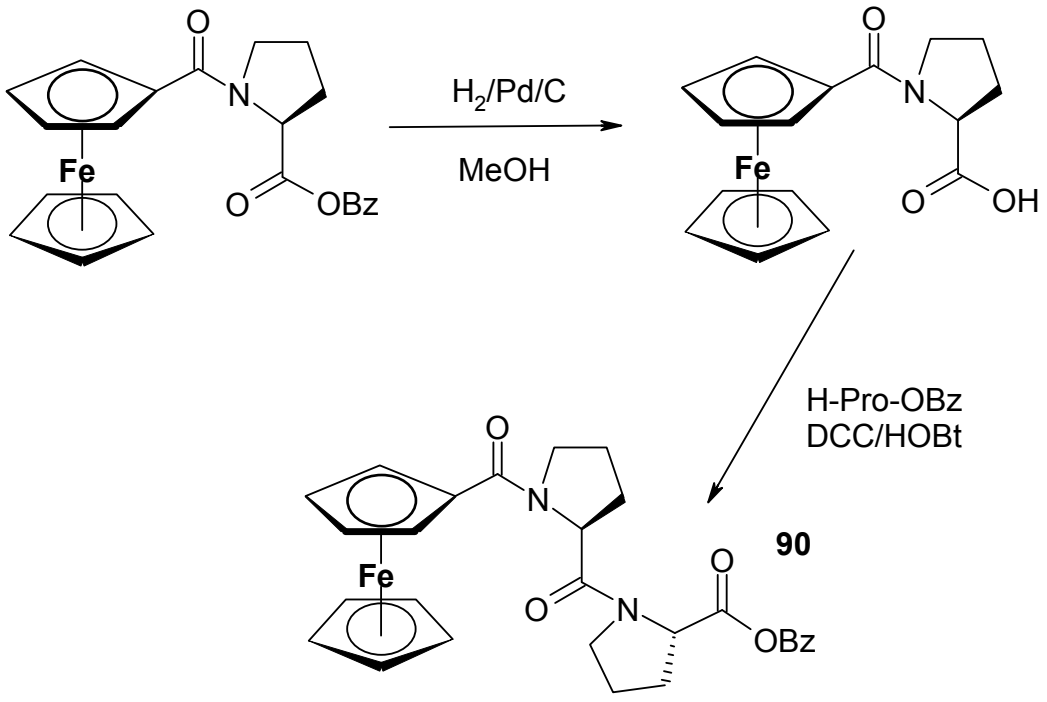

*Scheme 1: Preparation of **90** via catalytic hydrogenation of benzyl ester.*

The starting material for this reaction, ***N***-ferrocenoyl-L-proline benzyl ester, was itself prepared from ferrocene carboxylic acid and proline benzyl ester, using the DCC/HOBt coupling protocol.

Although the authors of this publication report a 65% yield for the final coupling step of the preparation of **90**, the overall yield based on the input of ferrocene carboxylic acid works out at < 55%, assuming quantitative recovery of the free acid after catalytic hydrogenation of the benzyl ester.

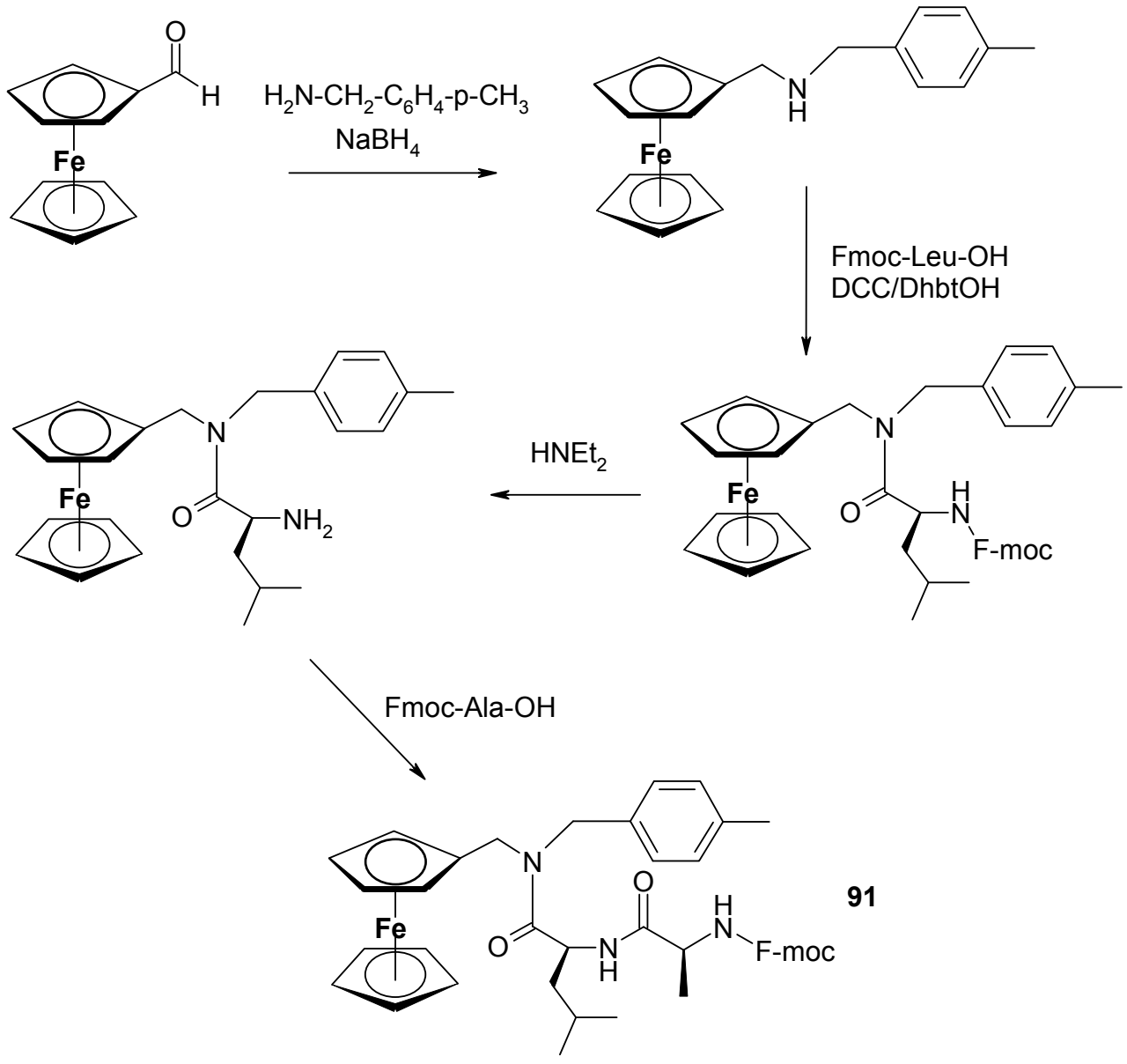

*Scheme 2: Preparation of **91** via removal of Fmoc protecting group.*

Nolte *et al*. have prepared the dipeptide **91** via removal of the ***N***-protecting Fmoc group in the presence of the ferrocene moiety to yield the free amine, which enabled the molecule to undergo chain elongation [5]. Interestingly, when the BOC-protecting group was used for this purpose, its removal using TFA resulted in the degradation of the ferrocene group (*scheme 2*). Based on the initial input of ferrocene aldehyde, the authors report an overall yield of ca. 50%.

Another approach was adopted by Kenny *et al*., who used the enzyme α-chymotrypsin to hydrolyse the methyl ester of the ***N***-ferrocenoyl phenylalanine derivative, to yield the free acid, which could then be coupled to other amino acid esters to yield compounds such as **92** (*scheme 3*) [6].

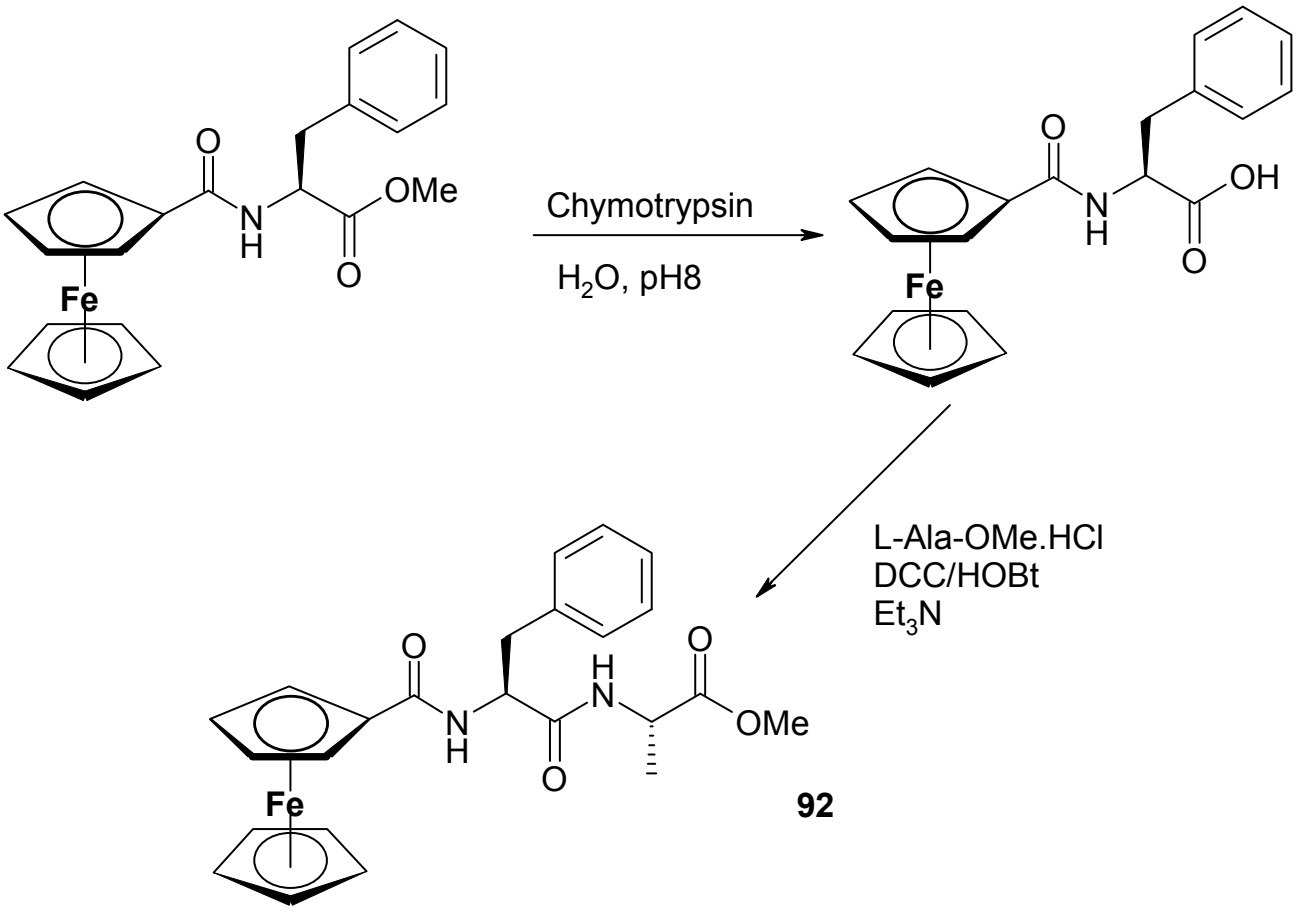

*Scheme 3: Preparation of **92** via α-chymotrypsin catalysed hydrolysis of the methyl ester.*

The obvious drawback with this methodology is that the action of α-chymotrypsin is limited to amino acids which have aromatic side chains (phenylalanine, tyrosine, tryptophan).

With this in mind, several synthetic routes were employed in attempting to synthesize compounds **103-111**. In order to compare the suitability of each of these synthetic routes, compound **103**, ***N***-ferrocenoyl-((S-methyl) L-cysteine)$_2$ methyl ester was prepared by each of these methods.

3.2: Synthesis of Dipeptides

Four different dipeptides (**93-96**) were prepared with a view to synthesizing the ***N***-ferrocenoyl monosubstituted dipeptides discussed in this chapter. All were prepared using the DCC/HOBt coupling protocol, i.e. by reacting an ***N***-BOC protected amino acid with an amino acid ester, followed by cleavage of the BOC protecting group by TFA (*scheme 4*). The dipeptide, ((S-methyl) L-cysteine)$_2$ methyl ester was also isolated as the hydrobromide salt, and was prepared via cleavage of the BOC group by hydrobromic acid in a solution of acetic acid.

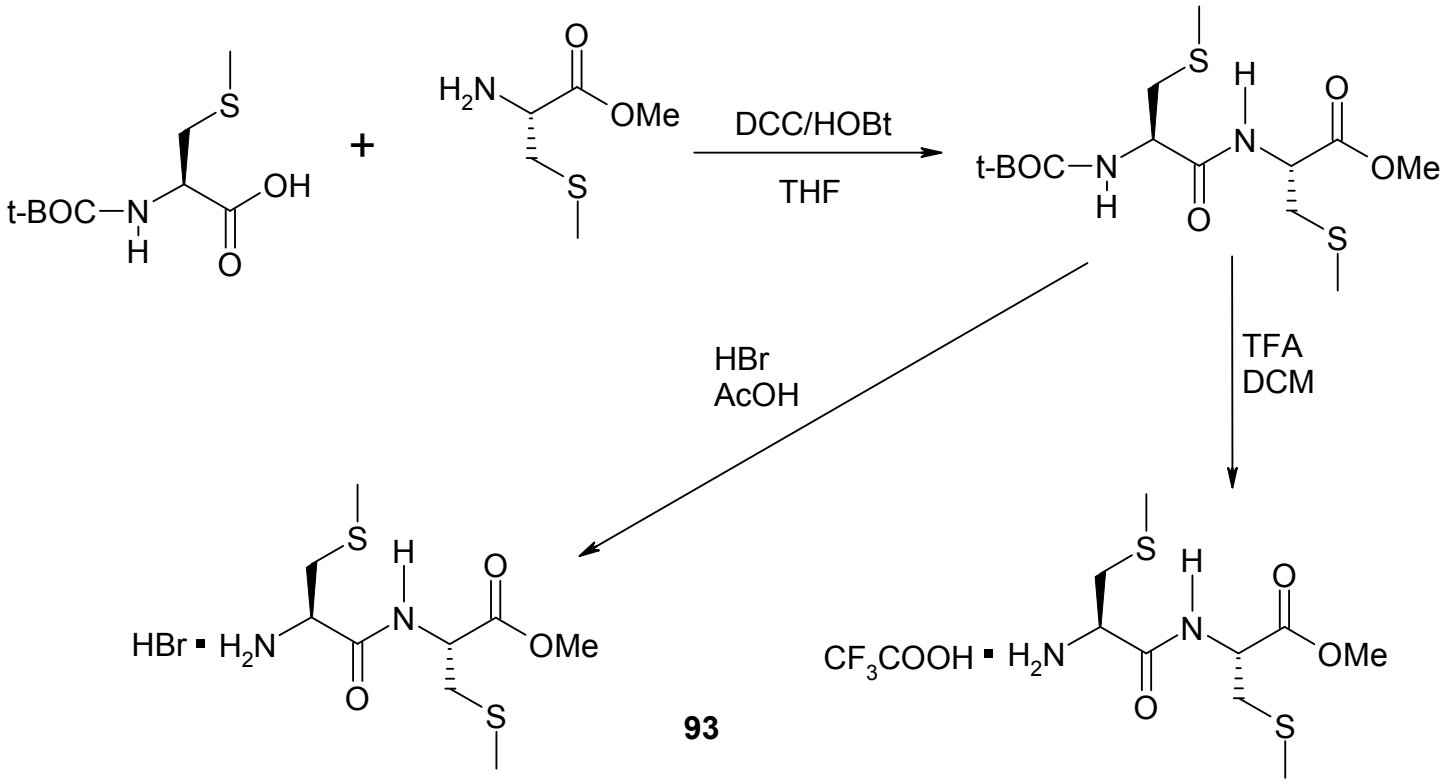

*Scheme 4: Preparation of the dipeptide **93**, using the DCC/HOBt protocol, followed by TFA or HBr cleavage of the BOC protecting group.*

Almost identical ^{1}H-NMR spectra were obtained for the different salts of the dipeptide **93**, irrespective of the method of BOC removal. The formation of the dipeptide was confirmed by ^{1}H-NMR spectroscopy, with the appearance of a signal for the amide proton at ca. 8.1 ppm. All the desired dipeptide esters were recovered in 70-80% yield after deprotection of the ***N***-terminal.

3.3: Synthesis of *N*-Ferrocenoyl Monosubstituted Dipeptides

3.3.1: Synthetic Route 1

The first attempt at synthesizing compound **103** involved reaction of the TFA salt of the ((S-methyl) L-cysteine)$_2$ methyl ester dipeptide with ferrocene carboxylic acid, employing the same DCC/HOBt conditions which had been used successfully in the synthesis of the ***N***-ferrocenoyl amino acid derivatives. This methodology gave the desired ***N***-ferrocenoyl dipeptide derivative in yields < 20%. It was thought that this was due to the difficulty in removing residual TFA from the reaction mixture following the deprotection step, as it is well know that acidic conditions can drastically interfere with coupling reactions. However, even after strenuous attempts at removing any TFA were made (exposure of the reaction mixture to high vacuum for prolonged periods, neutralization with excess triethylamine), coupling of the deprotected dipeptide with ferrocene carboxylic acid still failed to yield **103** in yields any greater than 20%. The synthetic procedure is shown in *scheme 5*.

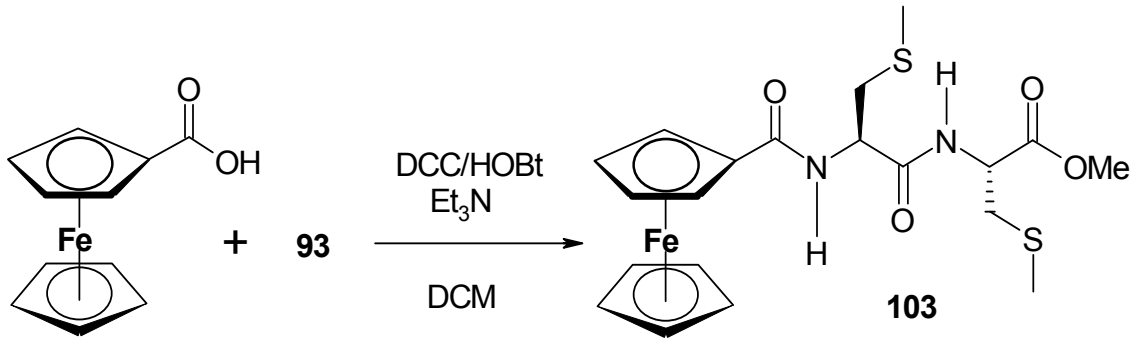

*Scheme 5: The preparation of **103** via reaction of the TFA dipeptide salt, **93**, with ferrocene carboxylic acid.*

3.3.2: Synthetic Route 2

It was subsequently decided to employ a different coupling reagent for the final step of the synthesis of **103**, in order to determine whether yields could be increased in this fashion. CDI was the reagent chosen, and the coupling reaction was carried out using THF as a solvent. Both these methods failed to increase the yield of **103** to any great extent**,** again producing the desired compound in a yield of 23%.

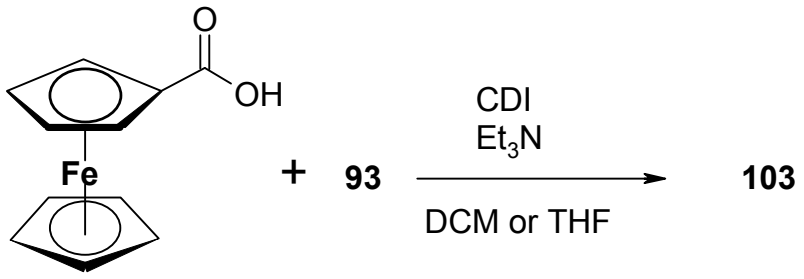

*Scheme 6: The preparation of **103** via use of CDI as the coupling reagent*

3.3.3: Synthetic Route 3

It was noted from column chromatography of the reaction mixtures from both of the previous two synthetic routes that the activated form of ferrocene carboxylic acid, i.e. ferrocenoyl-OBt, **60**, from route one and ***N***-ferrocenoyl imidazole, **61**, from route 2, were not formed in significant quantities (5 and 8% respectively recovered from the reaction mixtures). Inhibition of the formation of these intermediates, therefore, may have been a limiting factor in the preparation of **103**. It was therefore decided to employ a convergent synthetic strategy, by isolation of the ferrocenoyl-benzotriazole active ester, and to react this with the triflouroacetate salt of the freshly prepared dipeptide, **93**. The ferrocene-imidazole adduct, **61**, was deemed unsuitable for this purpose, as it is known to be unstable above 5°C [7], and preparation of **103** was not attempted using this particular synthon. The reaction would also be easier to follow by TLC, as there would be no further intermediates between the conversion of ferrocenoyl-benzotriazole active ester, **60**, to the target molecule **103**.

This strategy was slightly more successful than the previous two routes, affording **103** in a 31% yield (based on ferrocene carboxylic acid input). Changing the solvent from dichloromethane to

THF had a slightly deleterious effect on the yield, **103** being recovered after column chromatography in *ca*. 28% yield.

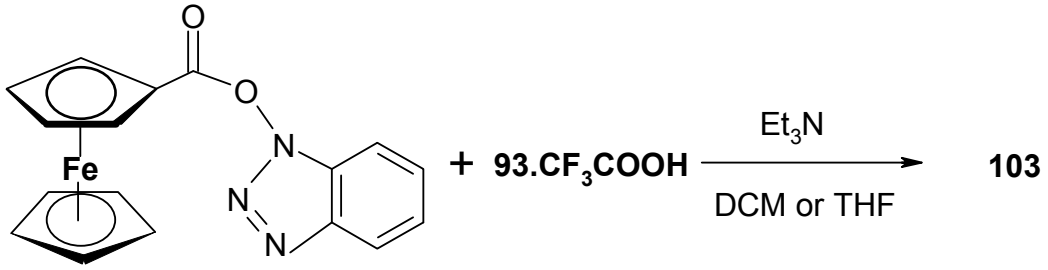

*Scheme 7: The preparation of **103** by reaction of **93** with the active ester **60**.*

Although this was a definite improvement on the first two strategies, it had become apparent that residual TFA was still an issue. Therefore, it was decided to employ different synthetic strategies in which the use of TFA could be avoided.

3.3.4: Synthetic Route 4

In order to avoid usage of TFA for cleavage of the t-BOC protecting group from the ***N***-terminal of the dipeptide, a solution of hydrobromic acid in acetic acid was employed for this purpose. The ***N***-ferrocenoyl-O-benzotriazole intermediate, **60**, was then reacted with the hydrobromide salt of the dipeptide **93** in DCM.

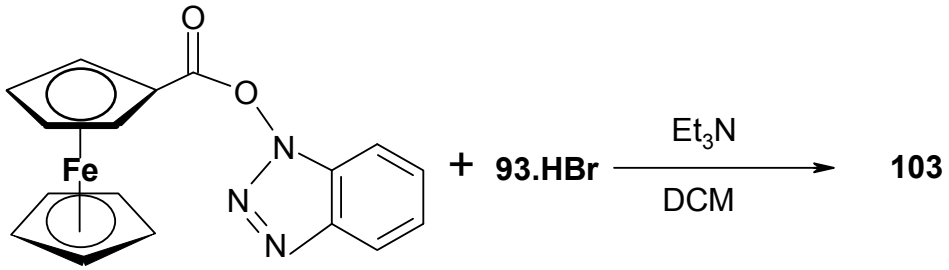

*Scheme 8: The preparation of **103** by reaction of the **93** with the active ester **60**.*

This strategy proved to be the most successful to date, and for the first time, yields of over 40% were recorded for **103**. However, it was clear that there was still significant room for improvement.

All strategies employed to date had relied upon cleavage of the protecting group from the ***N***-terminal of the dipeptide, in acidic solution. Subsequent coupling to ferrocene carboxylic acid, in turn, appeared to be inhibited to a large extent. The most likely explanation for this was the presence of residual acid from the deprotection step. In order to remove the need for this step, several alternative strategies were investigated.

3.3.5: Synthetic Route 5

It was decided to attempt to synthesize the ***N***-ferrocenoyl dipeptide by coupling two amino acids sequentially to ferrocene carboxylic acid, thereby removing the need for ***N***-terminal protection.

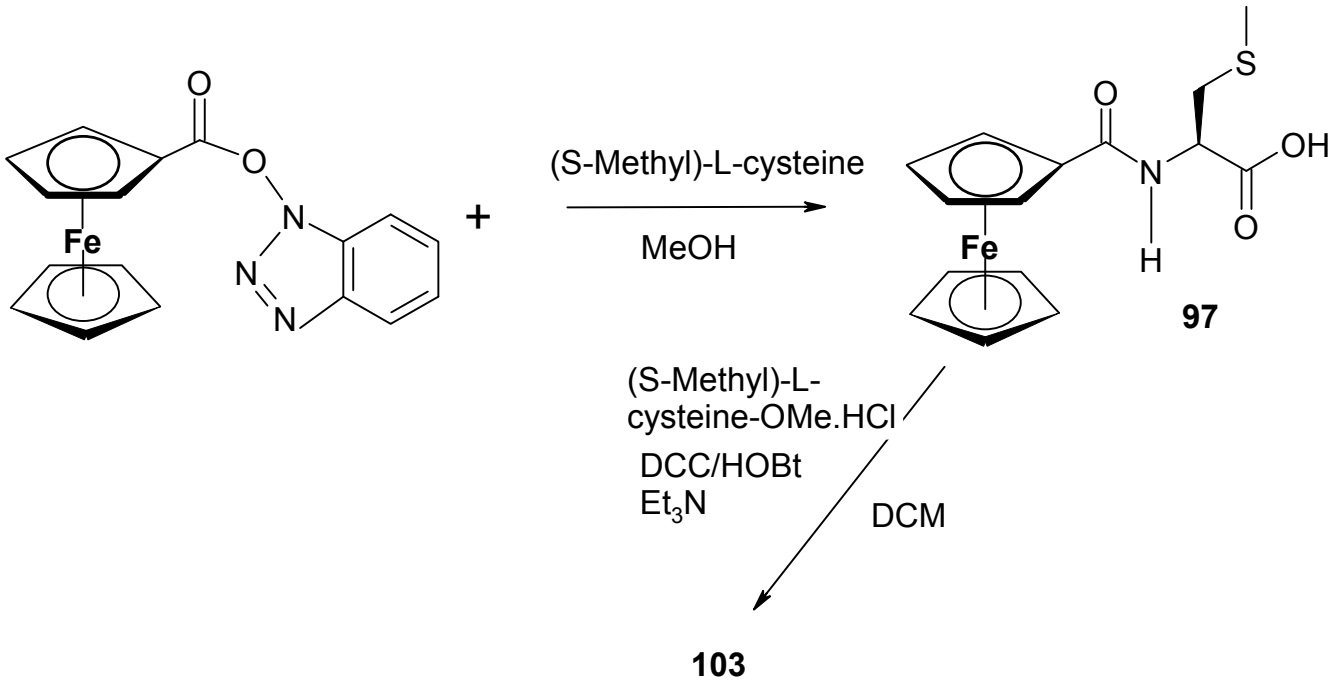

*Scheme 9: The preparation of **103** by reaction of the unprotected amino acid with the active ester **60**.*

The first of these synthetic routes involved reaction of the active ester, ***N***-ferrocenoyl-O-benzotriazole, with the unprotected form of (S-methyl) L-cysteine. As the carboxyl group on the

ferrocene moiety had already been activated, protection of the carboxyl group of L- cysteine was rendered unnecessary.

When the reaction was carried out in DCM, the ***N***-ferrocenoyl amino acid, **97**, was not formed in any appreciably quantity. This could no doubt be attributed to the extremely low solubility of the zwitterionic free amino acid in DCM. This situation was only slightly improved upon by changing the solvent to the more polar absolute methanol, which resulted in the formation of **103** in a 14% yield. Subsequent coupling of **97** to (S-methyl) L-cysteine methyl ester in DCM led to the formation of **103** in an overall yield of 12%. It was clear that this particular method, although circumventing the need for column chromatography, was inferior to the previous methods in terms of maximizing yield. Replacing absolute methanol with DMF, ethanol, or ethyl acetate failed to yield **103** in any appreciable quantity. It became obvious that the solubility of the free amino acid was too low in organic solvents to be of use. It therefore became apparent that protection of the ***C***-terminal of the amino acid would be necessary, i.e. replacing the carboxylate group with a less polar functional group, in order to increase solubility in organic solvents. This, in turn, would necessitate exposure of the ferrocenoyl moiety to reaction conditions appropriate for the removal of the ***C***-terminal protecting group. To this end, several further synthetic routes were investigated.

3.3.6: Synthetic Route 6

As discussed in section 3.1, previous work in this particular area involved synthesis of the ***N***-ferrocenoyl amino acid ester, followed by conversion of the ester group to the free acid via enzyme-catalysed hydrolysis. The enzyme employed for this purpose was α-chymotrypsin, whose action is limited to amino acid residues which have aromatic side chains, i.e. tyrosine, tryptophan, and phenylalanine. Obviously, this method would be of little use in any attempted synthesis of **103**. Alkyl esters, while excellent protecting groups for the ***C***-terminal of peptide chains, are notoriously difficult to remove, and can result in a host of unwanted side reactions, not least of which is racemization [8]. Therefore, it was decided to use the freshly prepared benzyl ester form of (S-methyl) L-cysteine to synthesize the ***N***-ferrocenoyl amino acid ester, followed by palladium catalysed hydrogenation of the benzyl group to form the free acid, which could then undergo further peptide chain elongation. The synthesis is outlined in *scheme 10*.

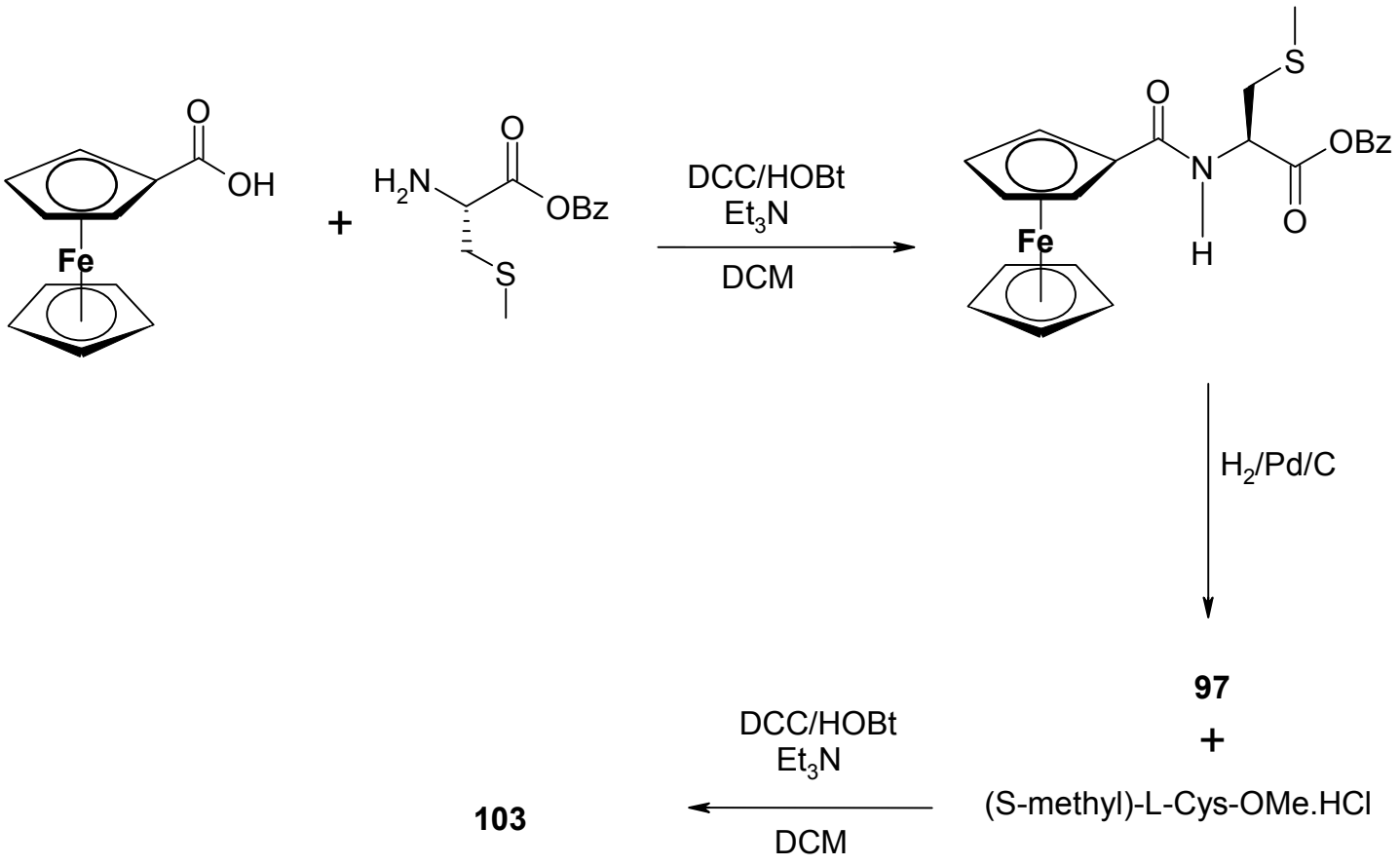

*Scheme 10: Preparation of **103** via catalytic hydrogenation of* the ***N***-ferrocenoyl *benzyl ester.*

This synthetic route proved to be the most successful to date, affording **103** in an overall yield of 52%, which is comparable to previous work in this area. The main drawback with this particular route, however, was the difficulty in recovering the ***N***-ferrocenoyl-(S-methyl)-L-cysteine free acid from the catalytic hydrogenation mixture, which resulted in losses of around 20%. The final step of the procedure, i.e. the coupling of (S-methyl)-L-cysteine methyl ester to **97** was accomplished in a yields > 80% and, more importantly, allowed **103** to be isolated without the need for column chromatography.

3.3.7: Synthetic Route 7

Cleavage of alkyl esters from the ***C***-terminal of peptide chains can result in unwanted side reactions. Saponification of the ester group would also necessitate exposure of the ferrocenoyl

moiety to basic aqueous conditions, which could potentially lead to decomposition, and the formation of iron (III) hydroxide salts. Previous attempts at saponification of ***N***-ferrocenoyl amino acid esters via refluxing in aqueous sodium carbonate had led to the decomposition of the ferrocenoyl moiety [6]. Although ferrocene is one of the more chemically robust organometallic compounds, it was clear that if the saponification route were to be a viable alternative to the previous routes, much milder conditions would have to be employed.

The first attempt at hydrolysis involved the addition of ***N***-ferrocenoyl-L-methionine methyl ester to a 0.5M solution of sodium hydroxide at room temperature under nitrogen, followed by neutralization of the reaction mixture with 0.5M HCl, which led to the precipitation of the ***N***-ferrocenoyl-L-met free acid in yields *ca*. 30% after drying. (*scheme 11*).

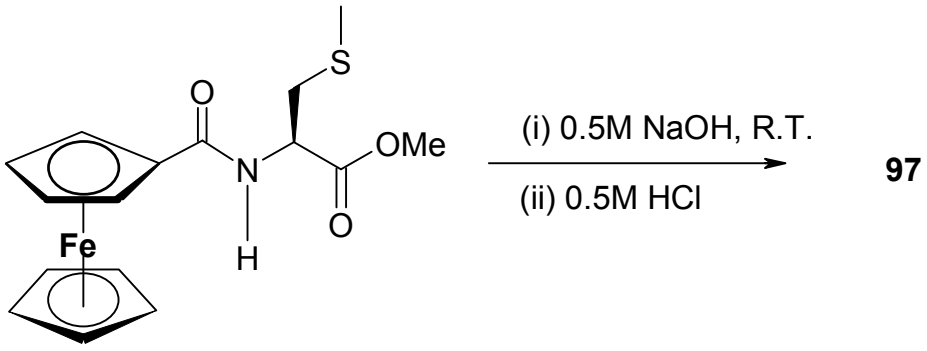

*Scheme 11: Saponification of the ester **87** with 0.5M NaOH.*

Upon examination, the filtrate had the green colour characteristic of iron III hydroxide. This is not surprising, as oxidation of aqueous Fe (II) complexes is known to occur more rapidly in basic solution [9]. Obviously, the ferrocene group was proving too sensitive for these reaction conditions. What was encouraging however was the NMR spectrum of the free acid, which showed only one signal for the amide proton, suggesting that racemization had not taken place. Repetition of the procedure at 0ºC did not result in an increased yield of **97**.

It had become clear that, as decomposition of the ferrocene group was occurring even at 0 ºC, a lower concentration of sodium hydroxide would have to be employed in order to prevent this degradation, while at the same time ensuring complete saponification of the ester group.

When the hydrolysis was repeated for a third time, **87** was slurried in a 0.1M solution of sodium hydroxide at 0ºC, followed by neutralization by 0.1M HCl. Although the reaction time was considerably longer than was the case when 0.5M sodium hydroxide was used, it was found that the free acid could be recovered almost quantitatively after drying. Again, the NMR spectrum of the free acid gave no evidence of racemization having occurred. Subsequent coupling of the free acid to (S-methyl)-L-cysteine under standard coupling conditions yielded **103** in an overall yield of 64%. The full synthesis of **103** is given in *scheme 12*.

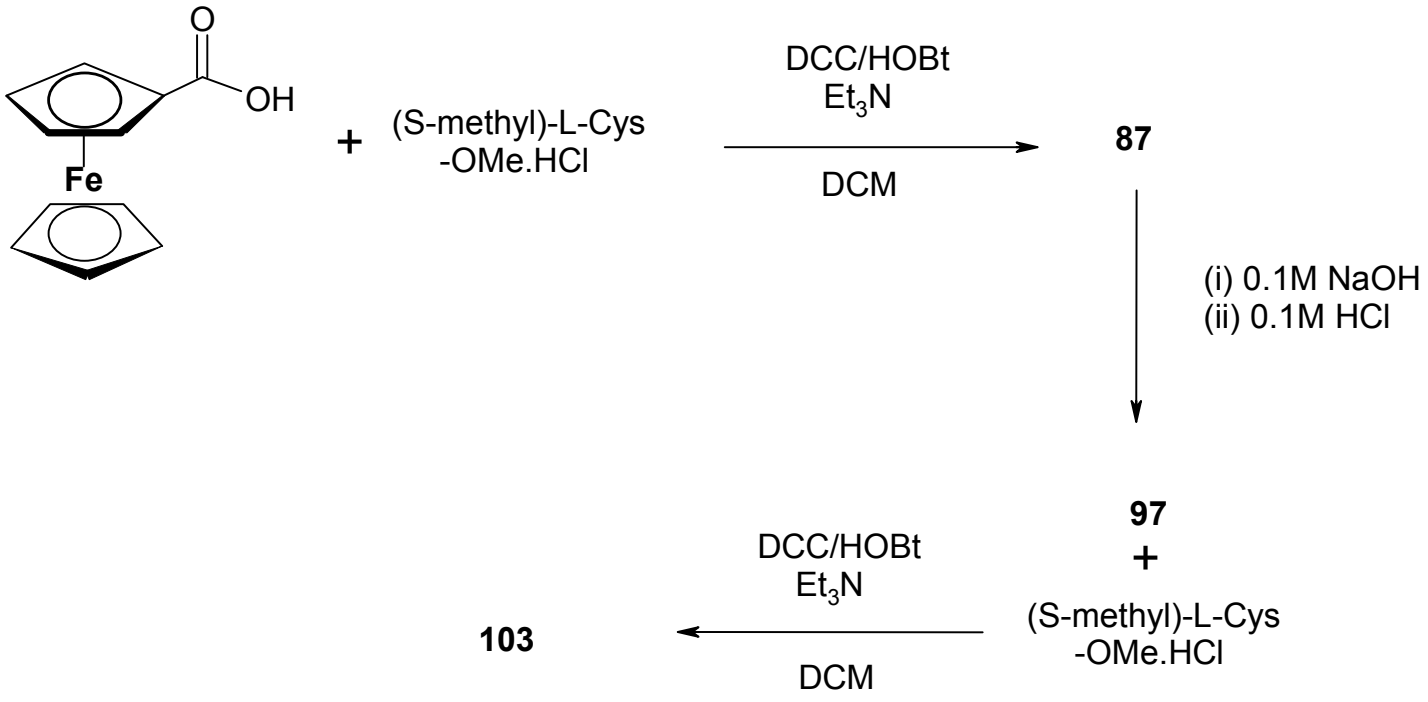

*Scheme 12: Preparation of **103*** via saponification of **87**.

A summary of the yields of compounds **103-111** is given in *table 1*, with all compounds being prepared via synthetic route 7. It is important to note that these yields are based on the initial inputs of ferrocene carboxylic acid, and not on the final coupling reaction. All compounds were recovered in yields < 50%, which compares very favourably with any literature values recorded for compounds of this type [10, 11].

Compound	Name	M.P. (ºC)	Yield (%)
103	***N***-ferrocenoyl-((S-methyl) L-cysteine)$_2$ methyl ester	119-120	62
104	***N***-ferrocenoyl-(S-methyl)-L-cysteine-L-aspartic acid dimethyl ester	131-133°	59
105	***N***-ferrocenoyl-(L-methionine)$_2$ methyl ester	119-120	62
106	***N***-ferrocenoyl-L-methionine-L-tyrosine methyl ester	119-120	63
107	***N***-ferrocenoyl-L-methionine-L-threonine methyl ester	138-141	60
108	***N***-ferrocenoyl-L-tyrosine-(S-methyl)-L-cysteine methyl ester	121-125	57
109	***N***-ferrocenoyl -(β-alanine)$_2$ methyl ester	150-151	58
110	***N***-ferrocenoyl-(γ-aminobutyric acid)$_2$ methyl ester	150-151	60
111	***N***-ferrocenoyl-(valeric acid)$_2$ methyl ester	154-155	52

*Table 1: % Yields and melting points of the **N**-ferrocenoyl monosubstituted dipeptide derivatives.*

3.4: ^{1}H-NMR Spectra of *N*-Ferrocenoyl Monosubstituted Dipeptides

In common with the previously discussed ***N***-ferrocenoyl amino acid derivatives, compounds **103-111** also show a signal for the unsubstituted Cp ring integrating for five protons in the 3.96 - 4.21 ppm range, and the *meta*-protons of the substituted Cp ring also appear as a similar broadened singlet in the 4.3 – 4.4 ppm range. However, in all cases where there is a chiral centre adjacent to the ferrocenoyl group, the *ortho*-protons of the substituted Cp ring do not appear as sharp singlets, but rather as a broadened singlet integrating for two protons. This is an unexpected result, as there are no further chemical modifications made to the ferrocenoyl moiety relative to the ***N***-ferrocenoyl mono peptide derivatives, and one would expect a similar pattern of signals to be recorded. This observation is discussed further in section 3.4.1.

Compounds **103-111** also, as expected, show the presence of two individual amide proton signals in the 7.7 – 8.7 ppm range, although, as will be discussed in subsequent sections, the presence of heteroatoms in the side chains of the individual amino acids have a bearing on the

spectra recorded. Compounds **103-108** also show the presence of two α-protons, which appear as multiplets in the 4.3 – 4.8 ppm range, although these signals are convoluted in the case of **108**.

The amide protons of the achiral compounds **109-111** show an interesting pattern of amide proton signals, ranging from two clearly defined triplets in the case of **108**, to a convoluted multiplet in the case of **111**. These protons also appear at slightly lower ppm compared to their chiral counterparts. These observations will be discussed further in section 3.4.2. A summary of the ^{1}H-NMR data obtained for these compounds is given in *table 2*.

Compound	**N-H**	**$Cp_{unsub.}$**	**H_{ortho}**	**H_{meta}**	**H_{α}**
103	7.85 (d)	4.20	4.72	4.35	4.52
	8.56 (d), 8.67 (d)				4.72
104	7.85 (d)	4.21	4.86	4.37	4.62-4.71
	8.56 (d), 8.64 (d)				
105	7.76(d), 7.79(d)	4.18	4.89	4.36	4.41-4.46
	8.41(d), 8.45(d)				
106	7.72 (d), 7.76 (d)	4.17	4.88	4.34-4.44	4.34-4.44
	8.28 (d), 8.36 (d)				4.54-4.59
107	7.86 (d)	4.14-4.19	4.89	4.36	4.30-4.32
	7.92 (d)		4.91		4.61-4.65
108	7.76 (d)	3.96	4.70-4.74	4.30	4.51-4.54
	8.56 (d)				4.70-4.74
109	7.79 (t)	4.15	4.76	4.32	-
	8.05 (t)				
110	7.83 (t)	4.15	4.77	4.35	-
	7.89 (t)				
111	7.76-7.80 (m)	4.15	4.76	4.33	-

*Table 2: The ^{1}H-NMR chemical shifts (ppm) of the **N**-ferrocenoyl monosubstituted dipeptide derivatives recorded in d^{6} DMSO.*

3.4.1: ^{1}H-NMR Spectra of 103 and 104

The ^{1}H-NMR spectrum of **103** is shown in *fig. 1*. Two closely grouped singlets are observed at 2.07 and 2.16 ppm, each integrating for three protons, which correspond to the two methyl groups of the thioether side chains, with the two multiplets in the 2.72 – 2.82 ppm range corresponding to the two methylene groups of the side chains. A singlet integrating for three protons, corresponding to the methyl ester group appears at 3.6 ppm.

A singlet, integrating for five protons, of the unsubstituted Cp ring (4.20 ppm), as well as the singlet (2H) of the meta-protons of the substituted Cp ring (4.35 ppm), appear in roughly the same region in the spectrum as was observed for the ***N***-ferrocenoyl-(S-methyl)-cysteine amino acid derivative, **87**. Two multiplets, each integrating for one proton and corresponding to the two α-protons, appear *ca*. 4.5 and 4.7 ppm.

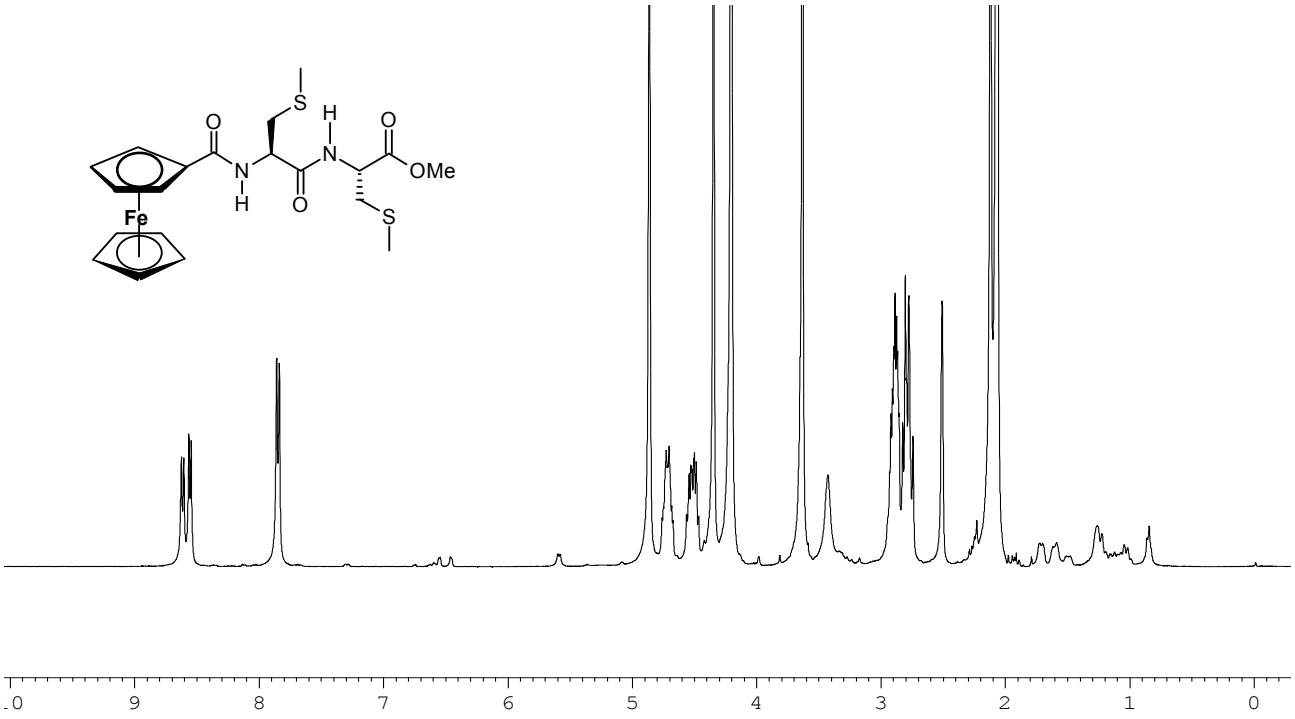

*Fig. 1: The ^{1}H-NMR Spectrum of **103** in d^{6} DMSO.*

There is, however, an interesting contrast between **87** and **103**, in terms of the appearance of the *ortho*-protons of the substituted Cp ring in their respective spectra. This can be seen in *fig. 2*,

where the *ortho*-protons of **87** appear as two sharp singlets, whereas these protons appear as a slightly broadened singlet in the case of **103**.

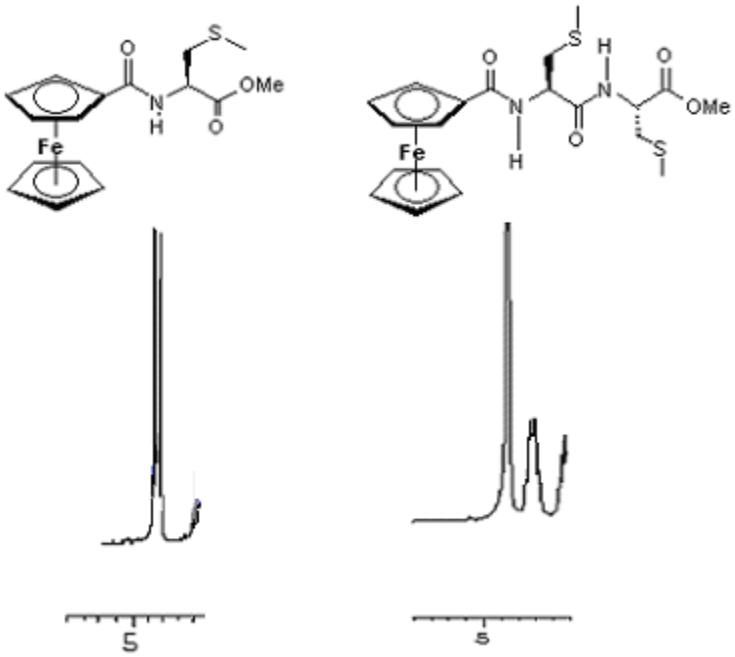

*Fig. 2: The contrast between the ortho-protons of **87** (left, two sharp singlets), and **103** (right, one broadened singlet).*

One possible explanation for this is that the longer dipeptide chain may have a more fluxional nature in solution, thus lessening the defined nature of the *ortho*-proton signals. Although no low temperature studies are possible in d^6 DMSO, the idea that more than one conformation may be present in solution at ambient temperature can be further investigated via inspection of the amide-proton signals.

The doublet at 7.85 ppm in the ^{1}H-NMR spectrum of **103**, (J = 8.0 Hz), is typical of the amide signals observed in the spectra of the ***N***-ferrocenoyl amino acid derivatives. The other amide signal is however observed further downfield as two individual doublets, each with J = 8.0 Hz, and between them integrating for one proton. At first it was feared that the splitting of the amide signal was due to racemization of one of the chiral centres, although this signal pattern was seen to be the case, irrespective of the synthetic route employed. In order to determine whether loss of chiral purity had taken place, high temperature ^{1}H-NMR spectra of **103** were recorded, and can be seen in *fig. 3*. The two individual components of the amide signal are seen to converge at

80°C, which would strongly suggest the presence of two individual conformers in d^6 DMSO solution at ambient temperature.

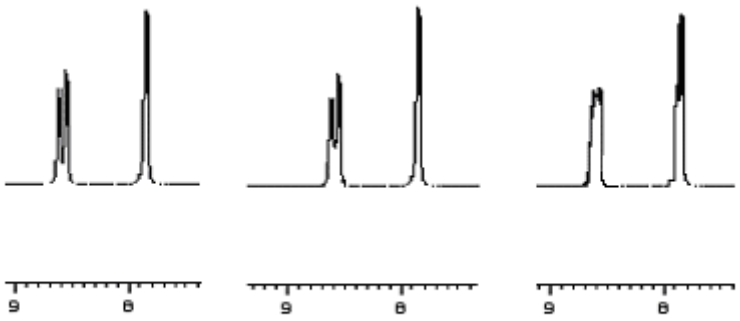

*Fig. 3: The amide protons of **103** recorded at ambient temperature (left), 50°C (centre), and 80°C (right).*

While the amide protons of the dipeptide do form *inter*-molecular hydrogen bonds with the solvent, they could also form an *intra*-molecular hydrogen-bonding interaction with the sulphur atoms of the cysteine side-chain, providing these bonds were spatially accessible. It is informative to compare the amide signals of **103** with ***N***-ferrocenoyl-(S-methyl)-L-cysteine-L-aspartic acid dimethyl ester, **104**. These two compounds differ only in terms of the side chain of their ***C***-terminal residue.

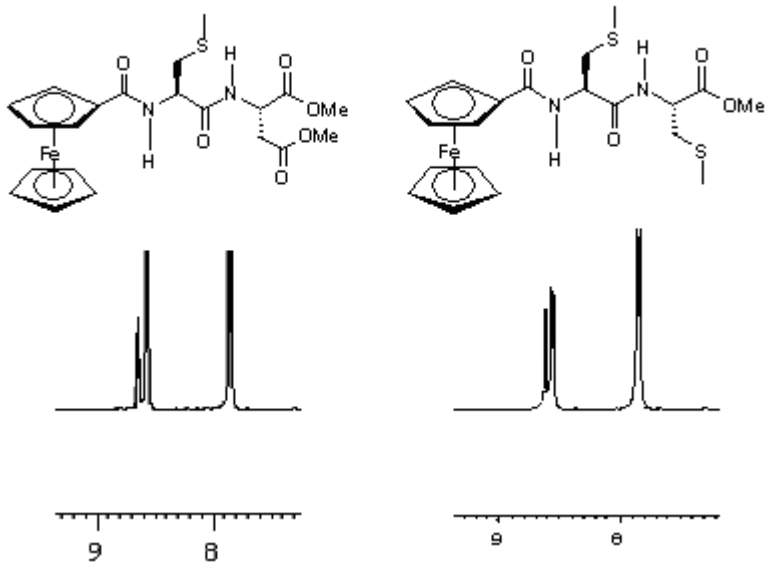

*Fig. 4: The amide proton signals of **103** (right) and **104** (left).*

The exact same pattern of amide proton resonances is observed for **104**, with the more downfield signal appearing as doublets of different intensity. Once again, high temperature ^{1}H-NMR spectra show these two components converging at 80°C. As *table 2* illustrates, these signals appear at almost identical positions in their respective ^{1}H-NMR spectra (7.85 and 8.56/8.67 for **103**, 7.85 and 8.56/8.64 for **104**). These results would suggest that the split amide signal is due to a hydrogen-bonding interaction between the ***C***-termini amide proton, and the sulphur atom of the ***N***-terminal cysteine residue. From a conformational perspective, this would certainly be possible.

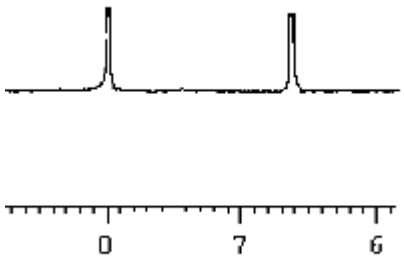

*Fig. 5: The amide protons of **103** recorded* in $CDCl_3$.

In order to confirm this, a ^{1}H-NMR spectrum of **103** was recorded in the non-polar solvent $CDCl_3$, and shows two amide signals at *ca*. 6.6 and 8.0 ppm (although these signals were not resolved into doublets in deuterated chloroform). This confirms the idea that only one of the amide protons is involved in an *intra*-molecular hydrogen bonding interaction. It could therefore be concluded that the sulphur atom of the ***N***-terminal cysteine residue acts as a hydrogen-bonding donor for the ***C***-terminal amide proton in compounds **103** and **104**. Similar results are also observed for compounds **105** and **106**, which have a methionine residue located at their ***N***-termini.

3.4.2: ^{1}H-NMR Spectra of 109-111

The ^{1}H-NMR spectrum of **109** is shown in *fig. 6*. The methylene protons adjacent to the carbonyl groups appear as triplets at 2.4 ppm, while the methylene protons adjacent to the nitrogen atoms of the amide groups appear as triplets at 3.3 ppm. The protons of the unsubstituted Cp ring, and the *meta*- and *ortho*- protons of the substituted Cp ring all appear as

singlets at 4.15, 4.32, and 4.76 ppm respectively. Compounds **110** and **111** also show a similar pattern of signals for their ferrocenoyl protons, as well as for the methylene protons in their peptide backbones. The most striking difference between their respective spectra can be seen in the amide proton signals recorded.

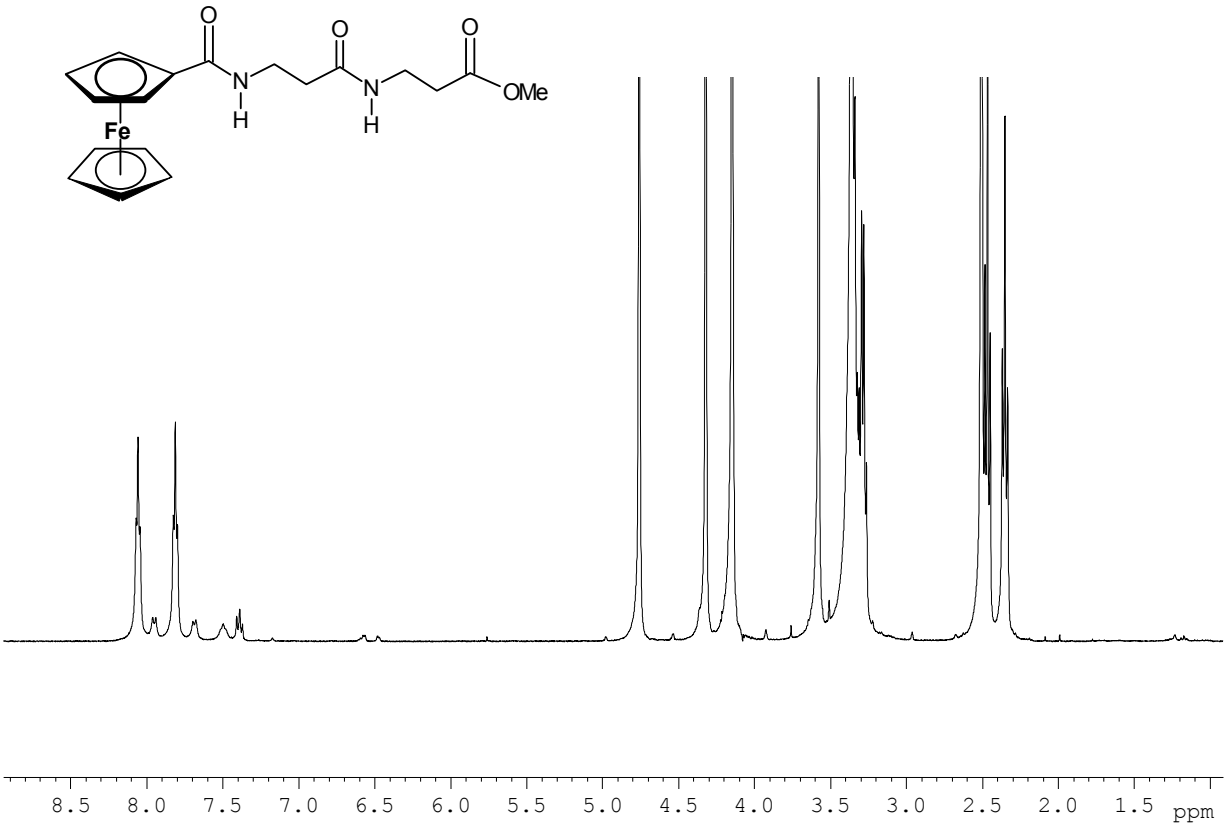

*Fig. 6: The ^{1}H-NMR spectrum of **109** in d^{6} DMSO.*

Two clearly defined triplets can be seen for the amide protons of **109** at 7.79 and 8.05 ppm, while two much more closely grouped triplets are observed for **110** at 7.83 and 7.89 ppm. This is in contrast to the amide signals of **111**, which appear as a convoluted multiplet at 7.8 ppm, as illustrated in *fig. 7*. As the only structural difference between these compounds is in the number of methylene groups in their peptide backbones, between their amide nitrogen atoms and carbonyl groups, it appeared likely that the separation of these amide signals was directly related to their conformational flexibility in solution.

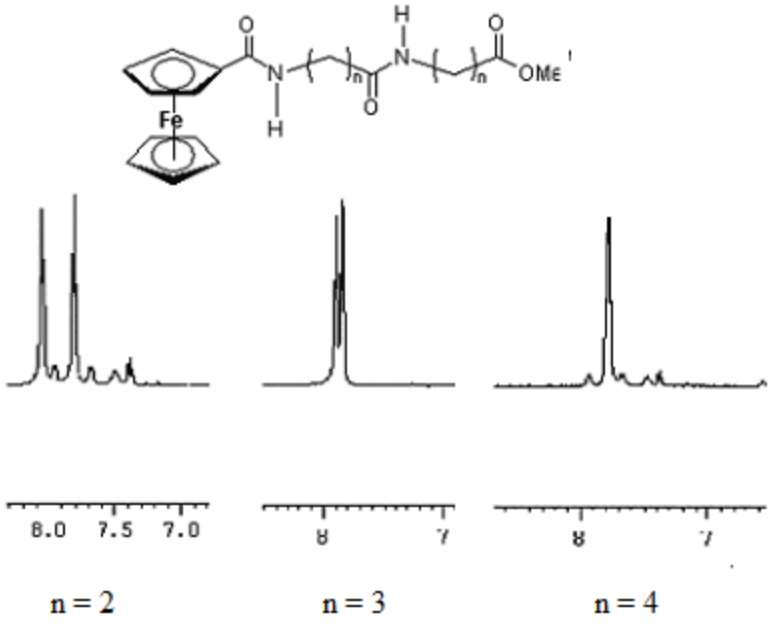

*Fig. 7: The amide protons of **109-111** recorded* in *d^6 DMSO.*

It will be recalled form chapter 2 that among the ***N***-ferrocenoyl amino acid analogues of compounds **109-111**, (**81**, **82** and **88** respectively), the number of methylene groups has an impact on the flexibility of the peptide backbone of the compounds, and hence their ability to form *intra*-molecular hydrogen bonds. In order to gain a clearer picture of the conformations these compounds were able to adopt in solution, it was necessary to record their ^{1}H-NMR spectra in the non-hydrogen bonding solvent, $CDCl_3$.

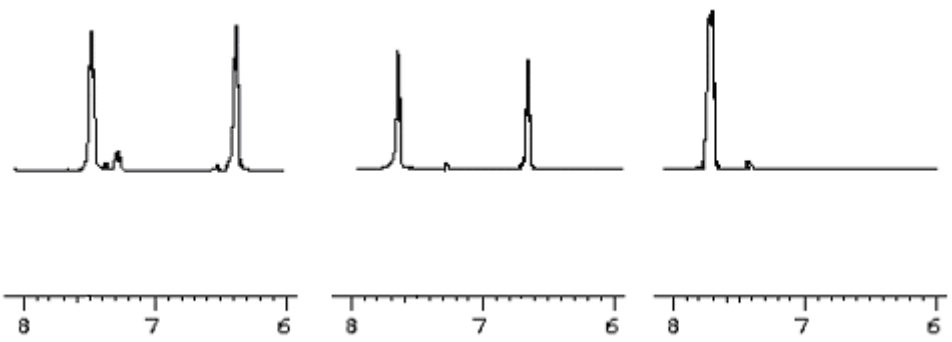

*Fig. 8: The amide protons of **109** (left), **110** (centre) and **111** (right) recorded in $CDCl_3$.*

As can be seen from *fig. 8*, compound **109** shows two amide proton signals (triplets) at *ca*. 6.4 ppm and 7.5 ppm in $CDCl_3$, the latter appearing further downfield in the spectrum due to an *intra*-molecular hydrogen-bonding interaction. A similar situation is observed in the spectrum of **110**, with two amide proton signals being observed at *ca*. 6.7 ppm and 7.7 ppm. Compound **111** shows a multiplet at 7.7 ppm, integrating for two protons, which is almost identical to that which was observed when the spectrum was recorded in d^6 DMSO. These results would suggest that both the amide protons of this compound are involved in an *intra*-molecular hydrogen-bonding interaction in non-polar solution.

3.5: ^{13}C-NMR Spectra of *N*-Ferrocenoyl Monosubstituted Dipeptides

The ^{13}C-NMR spectra of compounds **103-111** show that there are minimal differences between the ***N***-ferrocenoyl monosubstituted dipeptides and their amino acid analogues in terms of the chemical shifts of the ferrocenoyl carbon resonances in their spectra, with the positions of the unsubstituted Cp ring carbons, and the *ortho*, *meta*, and *ipso* carbons of the substituted Cp ring consistent with the spectra of compounds **62-89**. Those compounds which incorporate a chiral α-carbon also show two distinct signals for the *ortho*-carbons, but unlike compounds **62-89**, only one signal is observed for the *meta*-carbons.

Elsewhere in the spectra, the most obvious differences between the mono- and di- substituted compounds is the appearance of a second amide carbon signal *ca*. 170 ppm, and, for compounds **103-108**, a second α-carbon resonance at 52 ppm. A summary of the ^{13}C-NMR data for compounds **103-111** is given in *table 3*.

Compound	**C=O$_{amide}$**	**C=O$_{ester}$**	**Cp$_{unsub.}$**	**C$_{ortho}$**	**C$_{meta}$**	**C$_{ipso}$**
103	169.64	172.65	69.84	68.63	70.42	76.43
	171.38			68.82		
104	169.32	170.79	69.85	68.64	70.44	76.19
	169.58	171.30				
105	169.53	172.60	70.40	68.70	70.57	76.17
	169.61			68.77		
106	169.48	172.32	69.72	68.58	70.04	76.21
	172.18			68.87		

Compound	$C=O_{amide}$	$C=O_{ester}$	$Cp_{unsub.}$	C_{ortho}	C_{meta}	C_{ipso}
104	169.64	172.56	69.73	68.65	70.44	76.25
	171.31			68.78		
105	169.30	172.65	69.69	68.20	70.25	76.24
	171.51			68.93		
106	169.28	172.11	69.69	68.44	70.20	76.95
	170.94					
107	169.16	173.47	69.65	68.44	70.16	77.14
	172.22					
108	169.00	173.61	69.62	68.42	70.12	77.25
	172.20					

*Table 3: The ^{13}C-NMR chemical shifts (δ ppm) of the **N**-ferrocenoyl monosubstituted dipeptide derivatives recorded in d^6 DMSO.*

3.5.1: ^{13}C-NMR Spectrum of 103

The ^{13}C-NMR Spectrum of **103** is shown in *fig. 9*, and is typical of those ***N***-ferrocenoyl monosubstituted dipeptide derivatives which incorporate a chiral centre. Two closely grouped signals for the two methyl groups of the thioether side chains can be seen at 15.5 and 15.6 ppm, with the methylene carbons of the side chain appearing at 35.3 and 35.7 ppm. As expected, these latter carbons appear as negative peaks in the 135DEPT ^{13}C-NMR spectrum (*fig. 10*). The two α-carbon signals are observed at 52 and 52.5 ppm.

Two separate, closely grouped signals for the *ortho*-carbons of the substituted Cp ring are observed at 68.6 and 68.8 ppm, which is almost identical to the positions of these carbons in the spectrum of **87**, the amino acid analogue of **103**. The magnetic non-equivalence of these carbons can once again be attributed to the presence of the chiral centre. The position of the carbons of the unsubstituted Cp ring, which appear at 69.8 ppm, is identical to that of compound **87**, but only one signal for the *meta*-carbons is observed, at 70.4 ppm. The ipso-carbon of the substituted ring appears at 76.4 ppm, while two amide carbon signals appear at 169.6 and 171.3 ppm, while the ester carbon is observed at 172.6 ppm.

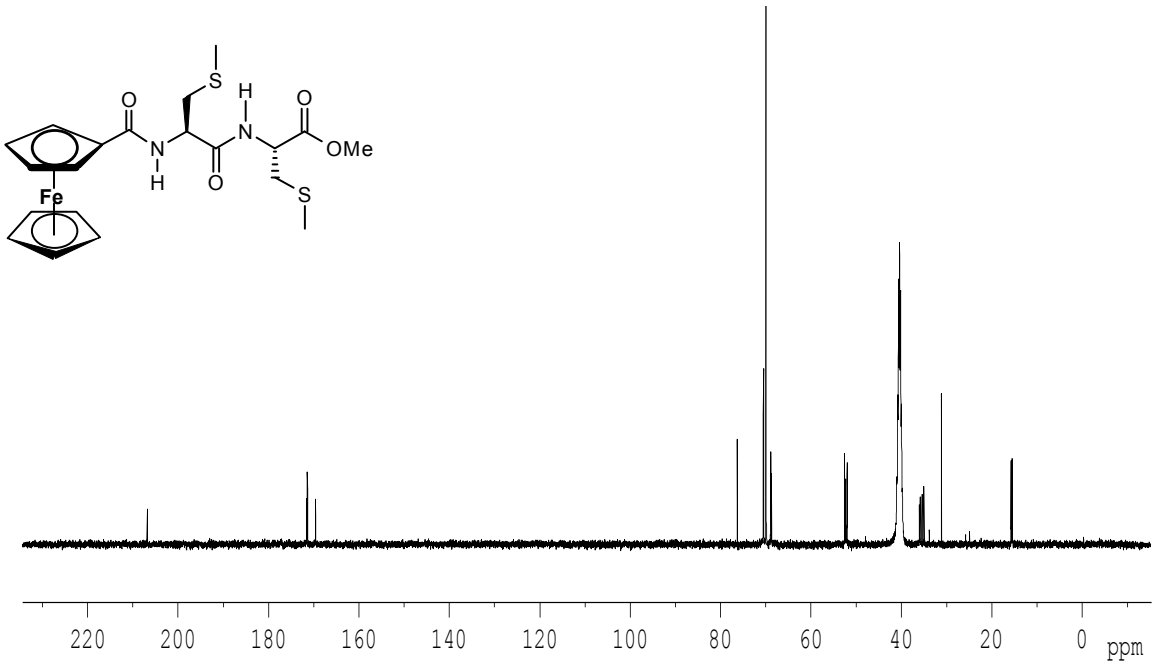

*Fig. 9: The ^{13}C-NMR spectrum of **103** in d^{6} DMSO.*

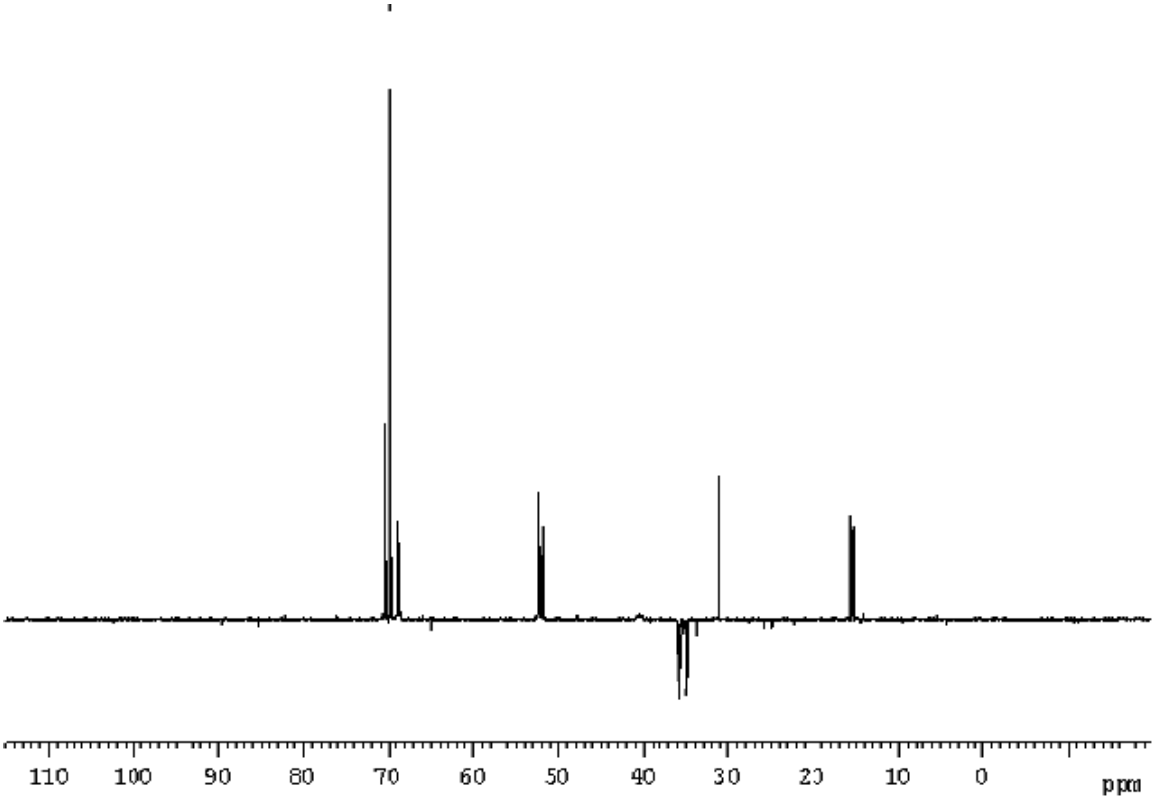

*Fig. 10: The 135DEPT spectrum of **103** in d^{6} DMSO.*

3.5.2: ^{13}C-NMR Spectrum of 109

The ^{13}C-NMR spectrum of compound **109** is shown in *fig. 11*. The four methylene groups of the peptide backbone are observed in the 34–36 ppm region, and appear as negative peaks in the DEPT-135 spectrum. The chiral carbon atoms, which appear in the 50–60 ppm region for compounds **103-108**, are naturally absent from the spectrum. In the absence of a chiral centre, only one signal is observed for the *ortho*-carbons of the substituted Cp ring at 68.4 ppm, while the *ipso*-carbon of the substituted ring appears at a slightly more downfield position in the spectrum, 77 ppm, than the chiral compounds **103-108**. The position of both the unsubstituted Cp ring, 69.7 ppm, and the meta-carbons of the substituted Cp ring are consistent with compounds **103-108**, as are the carbons of both amide groups, 169.2 and 170.9 ppm, and the ester group, 172.1 ppm.

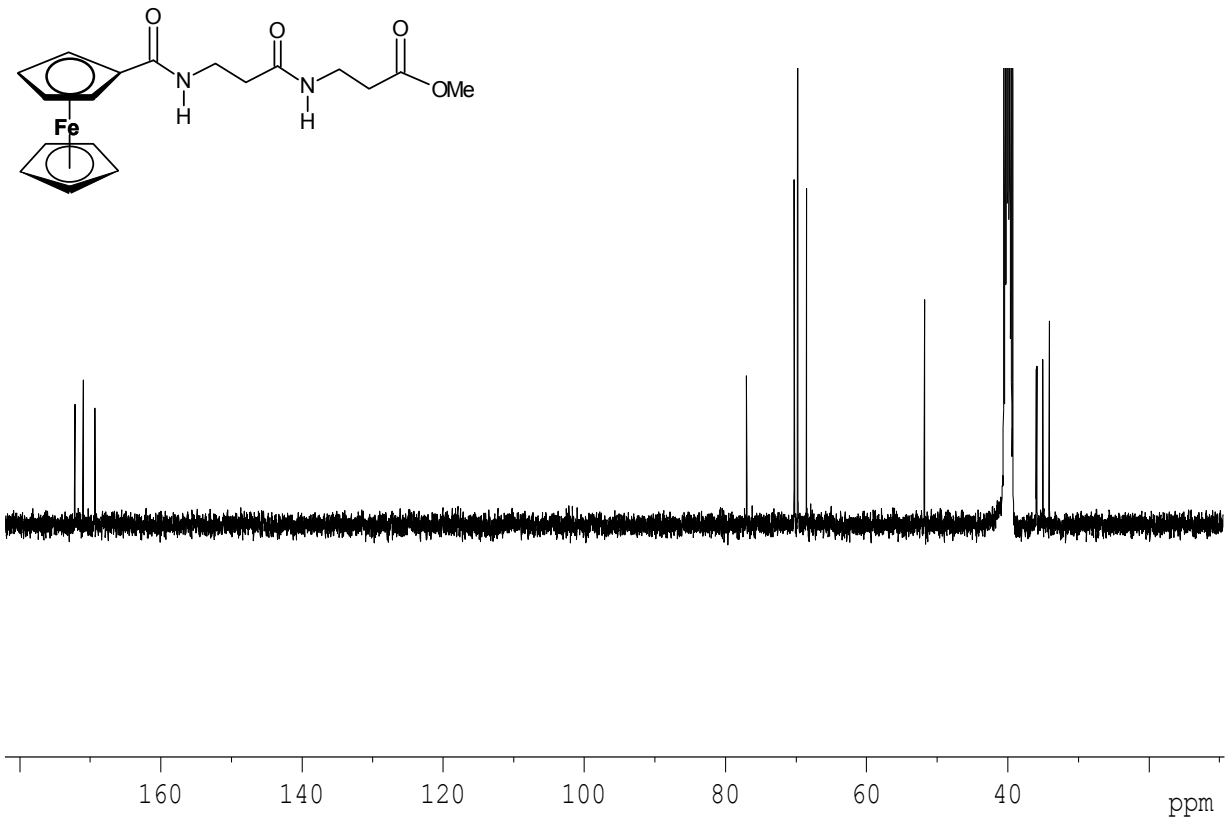

*Fig. 11: The ^{13}C-NMR spectrum of compound **109** in DMSO.*

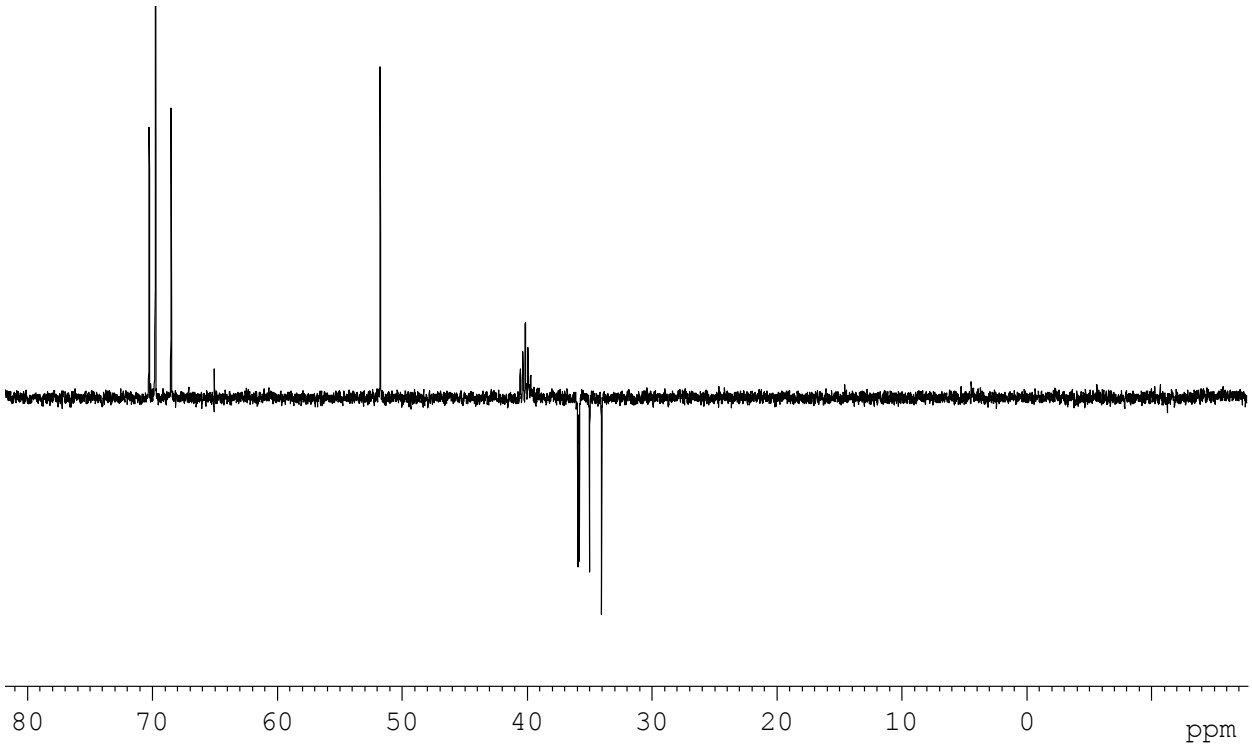

*Fig. 12: The 135DEPT Spectrum of **109** in d^6 DMSO*

3.6: Infrared Spectra of *N*-Ferrocenoyl Monosubstituted Dipeptides

Infrared spectra of compounds **103-111** were recorded both in the solid state (as KBr discs), and in solution (as thin-film methylene chloride solutions). In the solid state, only one broad N-H stretch vibration is observed in the spectra, despite the presence of two amide groups within each of the compounds. The wavenumbers recorded are, however, consistent with those observed for the amino acid analogues **62-89**, and indicate that the amide protons of these compounds are involved in hydrogen-bonding interactions in the solid state. The C=O ester band (or bands in the case of **104**) are observed between 1725 and 1752 cm^{-1}. Two separate C=O amide stretches appear in all spectra recorded, one in the 1625 cm^{-1} region, and a second in the 1655 cm^{-1} region. The former is consistent with that observed for compounds **62-89**, suggesting that this band is due to the amide group adjacent to the ferrocene moiety, while the

latter is due to the ***C***-terminal amide group. A summary of the infrared data recorded for compounds **103-111** is given in *table 4*.

Compound	υ_{N-H}	υ_{COOR}	υ_{CONR}	υ_{N-H} **(CH_2Cl_2)**
103	3280	1749	1656, 1627	3409, 3356
104	3304	1735, 1725	1655, 1628	3416, 3347
105	3285	1746	1656, 1626	3351
106	3277	1744	1655, 1638	3383, 3348
107	3277	1742	1654, 1638	3401
108	3277	1752	1657, 1625	3402
109	3257	1741	1664, 1614	3410, 3367
110	3248	1735	1661, 1619	3412, 3370
111	3268	1742	1659, 1628	3366

*Table 4: Infrared data for **103-111** (cm^{-1}) (as KBr discs unless stated)*

In order to investigate the conformations adopted by these ***N***-ferrocenoyl monosubstituted dipeptides in non-polar solution, thin-film infrared spectra of **103-111** were also recorded. Compounds **103** and **104**, which showed the presence of one hydrogen-bonded and one non-hydrogen-bonded amide proton in their ^{1}H-NMR spectra recorded in $CDCl_3$ (section 3.4.1), and both these compounds also show two υ_{N-H} stretches, one below 3400 cm^{-1} (hydrogen-bonded), the other above 3400 cm^{-1} (non-hydrogen bonded).

A similar situation is observed for the achiral compounds **109** and **110**, which also show the presence of one hydrogen-bonded and one non-hydrogen bonded amide proton in their ^{1}H-NMR spectra recorded in $CDCl_3$, and show two υ_{N-H} stretches, one below 3400 cm^{-1}, with the second above 3400 cm^{-1}. Interestingly, the C=O amide bands of these compounds are both shifted to higher wavenumbers when their spectra are recorded in CH_2Cl_2, while the C=O ester bands remain largely unaltered compared to those observed in the solid state. As discussed in section 3.3, those carbonyl groups, which do not form hydrogen bonds in non-polar solution, tend to appear at lower wavenumbers in the solid state. It is therefore likely that the oxygen atom of the ester group functions as a donor atom for the ***N***-terminal amide proton in non-polar solution for both compounds **109** and **110**.

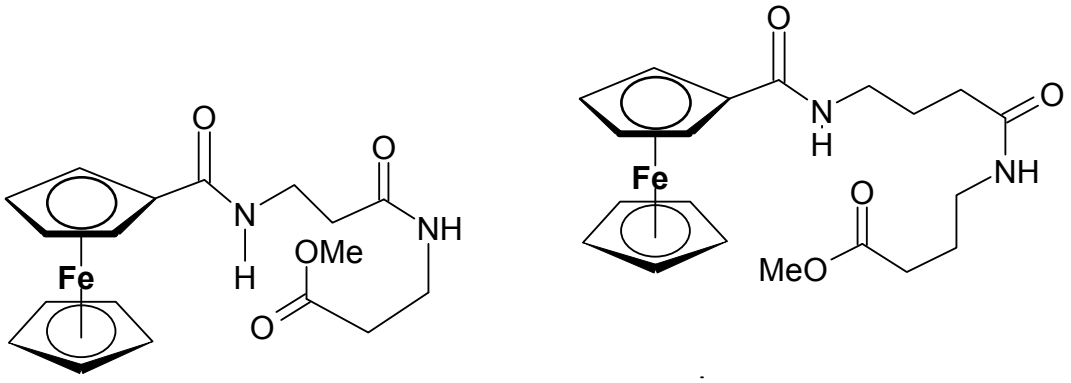

*Fig. 13: Likely conformations in non-polar solution of **109** (left) and **110** (right).*

Compound **111** shows only one N-H stretch in thin film methylene chloride solution, at 3366 cm^{-1}, which would suggest that both amide protons are involved in a hydrogen-bonding interaction. The C=O amide stretch in methylene chloride is not particularly informative, only one broad band being observed ca. 1650 cm^{-1}. The amino acid analogue of this compound, **88**, also forms an *intra*-molecular hydrogen bond in non-polar solution, and based on this observation, the most likely conformation for **111** is shown in *fig. 14*.

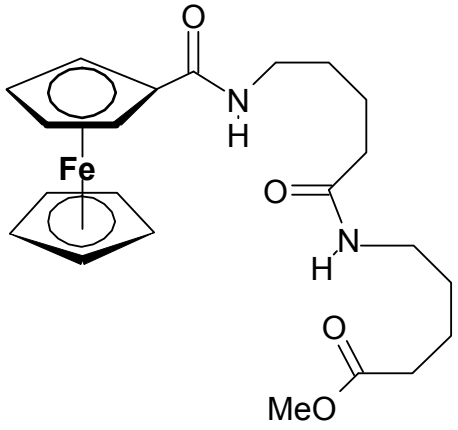

*Fig. 14: Likely conformations in non-polar solution of **111**, with intra-molecular hydrogen bonds accomplished via the formation of two eight-membered rings.*

3.7: UV-Vis Spectra of *N*-Ferrocenoyl Monosubstituted Dipeptides

The UV-Vis spectra of compounds **103**-**111** show minimal differences from those recorded for the ***N***-ferrocenoyl mono peptide derivatives, either in terms of the λ_{max} or the extinction coefficients recorded, i.e. it would appear that modification of the ferrocenoyl peptide at the ***C***-terminal has minimal effect on the electronic properties of the ferrocene moiety. All compounds show two low energy bands in the 440 and 300 nm range, while extinction coefficients are in the 200 M^{-1} cm^{-1} range.

3.8: Cyclic Voltammograms of *N*-Ferrocenoyl Monosubstituted Dipeptides

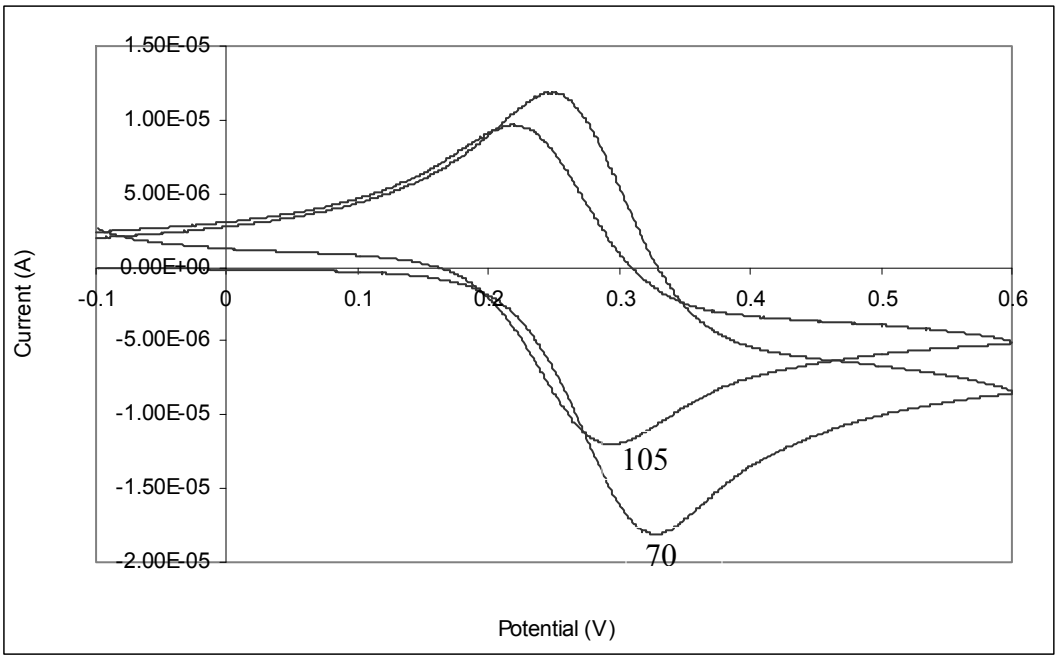

*Fig. 15: The cyclic voltammograms of **70** and **105**.*

The cyclic voltammograms of compounds **103**-**111**, like the ***N***-ferrocenoyl amino acid derivatives, exhibit a reversible, one-electron peak, due to the oxidation of the ferrocenoyl group to the ferricenium cation. What is noticeable is that there does appear to be a cathodic shift of the ferrocenoyl dipeptides relative to the amino acid derivatives, i.e. increasing the length of the peptide chain makes the molecule easier to oxidize. This effect has been previously noted in ferrocenoyl-proline derivatives, although no satisfactory explaination for this could be

elucidated, it was proposed that the alignment of the carbonyl oxygen p-orbitals might be partially responsible, possibly facilitating outer sphere electron transfer [12]. The cyclic voltammograms of compound **105**, ***N***-ferrocenoyl-(L-methionine)$_2$ methyl ester, along with, for comparative purposes, its amino acid analogue **70**, are shown in *fig. 15*.

A summary of the electrochemical and UV-Vis data for compounds **103-111** is given in *table 5*.

Compound	**λ_{max} (nm)**	**ε (M^{-1} cm^{-1})**	**$[\alpha]_D^{20}$**	**$E_{1/2}$(mV)**
103	306, 441	182	-25	175
104	305, 443	220	-18	170
105	306, 444	196	-21	167
106	305, 443	174	-20	162
107	306, 440	199	-24	166
108	302, 441	178	-19	180
109	304, 442	187	-	160
110	306, 442	187	-	155
111	302, 441	187	-	151

Table 5: The electrochemical, UV-Vis, and optical rotation data for compounds **103-111**. *All ε values refer to lowest energy band.*

3.9: Conclusions

Hydrolysis of the ***N***-ferrocenoyl amino acid esters, at 0˚C, using 0.1M NaOH, followed by addition of an equimolar amount of 0.1M HCl, led to the quantitative precipitation of the ***N***-ferrocenoyl free amino acids, which could be then coupled to the free amine of another amino acid ester to yield the ***N***-ferrocenoyl dipeptides. Based on the initial input of ferrocene carboxylic acid, molar yields of > 70% were recorded, which compares very favourably to literature procedures. Catalytic hydrogenation of the ***N***-ferrocenoyl amino acid benzyl esters also yielded the free acids, although in lower yields. Both these routes proved more successful than the coupling of ferrocene carboxylic acid to the pre-prepared dipeptide, where removal of the BOC protecting group from the dipeptide resulted in residual acid adversely affecting peptide coupling.

The ^{1}H-NMR spectra of compounds **103-108** in d^{6} DMSO and in $CDCl_3$, showed the presence of *intra*-molecular hydrogen bonding of one or both of the amide protons to heteroatoms of the side chain of the adjacent residue. Also observed for the chiral compounds **103-108** was the appearance of the *ortho*-protons of the substituted Cp ring as a broadened singlet, as opposed to two sharp singlets observed for the chiral ***N***-ferrocenoyl amino acid derivatives. One possible explanation for this is the presence of more than one conformer in solution at ambient temperature. However, several of these compounds, like their amino acid analogues, show two distinct signals for the *ortho*-carbons in their ^{13}C-NMR spectra. Compounds **109-111** also show the presence of *intra*-molecular hydrogen bonds in solution in their ^{1}H-NMR spectra. The infra-red data for compounds **103-111** is in agreement with the ^{1}H-NMR data recorded in terms of the presence of *intra*-molecular hydrogen bonds in non-polar solution.

Little difference is observed in the UV-Vis spectra between compounds **103-111** and compounds **62-89**, suggesting that modification of the ***N***-ferrocenoyl peptide at the ***C***-terminal has minimal effect on the electronic properties of the ferrocene moiety. However, the electrochemical properties of the ferrocene group does seem to be impacted by this modification, with a noticeable cathodic shift being observed for compounds **103-111** relative to compounds **62-89**, although no definitive explanation for this observation can be given.

3.10: Experimental

Synthesis of Dipeptides

General Procedure

2.5mmol of the ***N***-t-BOC protected amino acid and 2.5mmol of the amino acid ester hydrochloride salt were added a solution of DCC (0.6g, 3.0mmol) and Et_3N (0.4mls, 2.5mmol) in 25mls dichloromethane at 0˚C. The reaction was raised to room temperature after 30 mins, and allowed to proceed for 24 hrs. The precipitated ***N***, ***N*** - dicyclohexylurea was removed by filtration, and the filtrate washed with 5% citric acid, saturated $NaHCO_3$, and water. The organic phase was then dried over $MgSO_4$, and concentrated to *ca*. 5mls in *vacuo*. Subsequent removal of the ***N***-t-BOC group was effected in one of two ways.

(i) The resulting solution was then cooled to 0˚C, and 5mls TFA were added, and the solution stirred at this temperature for 30 mins. Diethyl ether was then added drop-wise,

precipitating the TFA salt as a white solid (only **93** was prepared successfully in this way).

(ii) After cooling to 0˚C, 10mls of a 45% solution of HBr in acetic acid was added drop-wise, and stirred for 30 mins. Diethyl ether was then added drop-wise, precipitating the HBr salt as a white solid, or, in the case of **94** and **96**, the solvent was removed in vacuo, to yield the dipeptides as brown oils.

((S-methyl) L-cysteine)$_2$ methyl ester (93)

0.52g of ***N***-t-BOC-(S-methyl)-L-cysteine and 0.46g of (S-methyl)-L-cysteine methyl ester hydrochloride were used in the synthesis.

Yields: (i) After TFA de-protection 0.73g (77%), (ii) After HBr de-protection, 0.65g (69%), white waxy solid.

^{1}H-NMR (400MHz) δ (*d*^{6} DMSO): 2.01 (3H, s, -SC$\underline{H}_3$), 2.10 (3H, s, -SC$\underline{H}_3$), 2.72-2.80 (2H, m, -C$\underline{H}_2$SCH$_3$), 2.81-2.89 (2H, m, -C$\underline{H}_2$SCH$_3$), 3.68 (3H, s, OC$\underline{H}_3$), 4.40-4.42 (1H, m, NH$_2$C$\underline{H}$-), 4.70-4.71 (1H, m, -NHC$\underline{H}$-), 7.79 (2H, br. s, N$\underline{H}_2$CH-), 8.10 (1H, br. s, -N$\underline{H}$CH-).

(β-alanine)$_2$ methyl ester (94)

0.47g of ***N***-t-BOC-β-alanine and 0.34g of β-alanine methyl ester hydrochloride were used in the synthesis.

Yield 0.50g (80%), brown oil.

^{1}H-NMR (400MHz) δ (*d*^{6} DMSO): 2.33 (2H, t, *J* = 6.8 Hz, NHCH$_2$C$\underline{H}_2$CO-), 2.51 (2H, t, *J* = 6.8 Hz, NHCH$_2$C$\underline{H}_2$CO-), 3.20-3.30 (4H, m, NHC$\underline{H}_2$CH$_2$CO X 2), 3.55 (3H, s, -OC$\underline{H}_3$), 7.69 (2H, br. s, (N$\underline{H}_2$CH$_2$CH$_2$-), 8.00 (1H, t, *J* = 6.4 Hz, N$\underline{H}$CH$_2$CH$_2$-).

(L-methionine)$_2$ methyl ester (95)

0.62g of ***N***-t-BOC-L-methionine and 0.49g of L-methionine methyl ester hydrochloride were used in the synthesis.

Yield 0.66g (71%), white waxy solid.

^{1}H-NMR (400MHz) δ (*d*^{6} DMSO): 1.73-1.99 (10H, m, -C$\underline{H}_2$SC$\underline{H}_3$ x 2), 2.46-2.59 (4H, m, -C$\underline{H}_2$CH$_2$SCH$_3$ x 2), 3.60 (3H, s, -OC$\underline{H}_3$), 4.30-4.31 (1H, m, NH$_2$C$\underline{H}$-), 4.62-4.64 (1H, m, -NHC$\underline{H}$-), 7.65 (2H, br. s, N$\underline{H}_2$CH-), 8.22 (1H, br. s, -N$\underline{H}$CH-).

(γ-aminobutyric acid)$_2$ methyl ester (96)

0.51g of ***N***-t-BOC-γ-aminobutyric acid and 0.39g of γ-aminobutyric acid methyl ester were used in the synthesis.

Yield 0.49g (69%), white waxy solid.

^{1}H-NMR (400MHz) δ (*d*^{6} DMSO): 1.69-1.82 (4H, m, $NHCH_2C\underline{H}_2CH_2CO$ X 2), 2.17 (2H, t, *J* = 7.6 Hz, $NHCH_2CH_2C\underline{H}_2$-), 2.40 (2H, t, *J* = 7.6 Hz, $NHCH_2CH_2C\underline{H}_2$-), 3.03-3.21 (4H, m, $NHC\underline{H}_2CH_2$- X 2), 3.61 (3H, s, $-OC\underline{H}_3$), 7.83 (2H, br. s, $N\underline{H}_2CH_2CH_2$-), 7.99 (1H, t, *J* = 6.4 Hz, $N\underline{H}CH_2CH_2$-).

N-Ferrocenoyl Amino Acids

Route 1, General Procedure

2.5mmol of the appropriate ***N***-ferrocenoyl amino acid ester was slurried in 38mls 0.1M NaOH and 12mls methanol at 0˚C, and the mixture was stirred under N_2 until a deep orange solution was obtained (*ca*. 2 hrs for methyl esters, 4 hrs for ethyl esters). 38mls of 0.1M HCl was then added drop-wise, (a pH of 7 was confirmed with pH paper), precipitating the free acids as orange solids, which were then dried for *ca*. 12 hrs at *ca*. 60˚C. Complete hydrolysis was confirmed by the absence of the ester group protons in the ^{1}H-NMR spectrum, and the appearance of a singlet at 12 ppm. A KBr disc IR spectrum also showed a C=O band at 1715 cm^{-1}, indicative of a carboxyl carbonyl group, and the disappearance of the C=O ester band *at* 1740 cm^{-1}.

Route 2

2.5mmol (1.1g) of ***N***-ferrocenoyl-(S-methyl)-L-cysteine benzyl ester was dissolved in a slurry of 2g of Pd/C in 50mls methanol. A vigorous stream of H_2 was then bubbled through the mixture for 30mins, and the Pd/C was removed by filtration. The solvent was then removed *in vacuo*, and again formation of the free acid was confirmed by the appearance of a singlet at 12 ppm, and the appearance of a C=O band at 1715 cm^{-1} in the KBr disc IR spectrum. Only **97** was prepared by this method.

N-ferrocenoyl-(S-methyl)-L-cysteine (97)

0.72g of -ferrocenoyl-(S-methyl)-L-cysteine benzyl ester was used in the synthesis.

Yields: Route 1, 0.70g (97%). Route 2, 0.88g (80%), orange microcrystalline solid.

^{1}H-NMR (400MHz) δ (d^6 DMSO): 2.10 (3H, s, -SC<u>H</u>$_3$), 2.87 (1H, dd, J_a = 9.6 Hz, J_b = 13.6 Hz, -C<u>H</u>$_2$SCH$_3$), 2.97 (1H, dd, J_a = 4.8 Hz, J_b = 13.6 Hz, -C<u>H</u>$_2$SCH$_3$), 4.20 (5H, s, *unsub*. Cp ring), 4.36 (2H, s, H_{meta} Cp ring), 4.57-4.62 (1H, m, -NHC<u>H</u>-), 4.82 (1H, s, H_{ortho} Cp ring), 4.85 (1H, s, H_{ortho} Cp ring), 8.16 (1H, d, J = 8.0 Hz, -N<u>H</u>CH-), 11.84 (1H, s, -COO<u>H</u>).

_N_-ferrocenoyl-L-methionine (98)

0.78g of **70** was used in the synthesis.

Yield 0.73g (94%), orange microcrystalline solid.

^{1}H-NMR (400MHz) δ (d^6 DMSO): 2.02-2.06 (5H, m, -C<u>H</u>$_2$SC<u>H</u>$_3$), 2.54-2.64 (2H, m, -C<u>H</u>$_2$CH$_2$SCH$_3$), 4.20 (5H, s, *unsub*. Cp ring), 4.41 (2H, s, C_{meta} Cp ring), 4.50-4.54 (1H, m, NHC<u>H</u>-), 4.87 (1H, s, H_{ortho} Cp ring), 4.91 (1H, s, H_{ortho} Cp ring), 8.00 (1H, d, J = 7.6 Hz, N<u>H</u>CH-), 11.91 (1H, s, -COOH).

_N_-ferrocenoyl-L-tyrosine (99)

0.81g of **73** was used in the synthesis.

Yield 0.78g (96%), orange-red crystalline solid.

^{1}H-NMR (400MHz) δ (d^6 DMSO): 2.86-2.95 (1H, m, -NHCH(C<u>H</u>$_2$PhOH), 3.02-3.05 (1H, m, NHCH(C<u>H</u>$_2$PhOH), 4.09 (5H, s, *unsub*. Cp ring), 4.37 (2H, s, H_{meta} Cp ring), 4.57-4.62 (1H, m, NHC<u>H</u>-), 4.80 (1H, s, H_{ortho} Cp ring), 4.86 (1H, s, H_{ortho} Cp ring), 6.68 (2H, d, J = 8.8 Hz, ArH), 7.12 (2H, d, J = 8.8 Hz, ArH), 8.09 (1H, d, J = 8.0 Hz, N<u>H</u>CH-), 9.29 (1H, s, phenolic OH), 11.79 (1H, s, -COO<u>H</u>).

_N_-ferrocenoyl -β-alanine (100)

0.63g of **81** was used in the synthesis.

Yield 0.62g (98%), orange microcrystalline solid.

^{1}H-NMR (400MHz) δ (d^6 DMSO): 2.61 (2H, t, J = 6.6 Hz, NHCH$_2$<u>C</u>H$_2$-), 3.40-3.44 (2H, m, NHC<u>H</u>$_2$CH$_2$-), 4.13 (5H, s, *unsub*. Cp ring), 4.33 (2H, d, J = 2.0 Hz, H_{meta} Cp ring), 4.79 (2H, d, J = 2.0 Hz, C_{ortho} Cp ring), 7.96 (1H, t, J = 6.0 Hz, N<u>H</u>CH$_2$CH$_2$-), 12.01 (1H, s, -COO<u>H</u>).

_N_-ferrocenoyl-γ-aminobutyric acid (101)

0.69g of **82** was used in the synthesis.

Yield 0.64g (94%), orange microcrystalline solid.

^{1}H-NMR (400MHz) δ (d^6 DMSO): 1.81-1.83 (2H, m, $NHCH_2C\underline{H}_2$-), 2.34 (2H, t, J = 5.6 Hz, $NHCH_2CH_2C\underline{H}_2$-), 3.17-3.18 (2H, m, $NHC\underline{H}_2CH_2$-), 4.17 (5H, s, *unsub*. Cp ring), 4.33 (2H, d, J = 2.0 Hz, H_{meta} Cp ring), 4.77 (2H, d, J = 2.0 Hz, C_{ortho} Cp ring), 7.87 (1H, t, J = 5.6 Hz, $N\underline{H}CH_2CH_2$-, 11.98 (1H, s, -COO<u>H</u>).

_N_-ferrocenoyl-valeric acid (102)

0.85g of **88** was used in the synthesis.

^{1}H-NMR (400MHz) δ (d^6 DMSO): 1.50-1.60 (4H, m, $-NHCH_2C\underline{H}_2C\underline{H}_2CH_2CO$-), 2.40 (2H, t, J = 7.2 Hz, $-CH_2C\underline{H}_2CO$-), 3.16-3.20 (2H, m, $-NHC\underline{H}_2CH_2$-), 4.11 (5H, s, *unsub*. Cp ring), 4.37 (2H, s, H_{meta} Cp ring), 4.78 (2H, s, H_{ortho} Cp ring), 7.99 (1H, t, J = 5.6 Hz, -N<u>H</u>CH-), 11.91 (1H, s, -COO<u>H</u>).

***N*-Ferrocenoyl Monosubstituted Dipeptides**

All yields reported are based on the input of ferrocene carboxylic acid. For example, compound **103** was prepared via route 3, the reaction of the O-benzotriazole active ester of ferrocene carboxylic acid, **60**, with the TFA salt of the dipeptide **93**. The yield for the preparation of **60** was 87% (Ch. 2 section 3.7), and the yield for the subsequent coupling to **93** yielded the target molecule in 32% yield, giving an overall yield of 28%. Similarly, preparation of **103** by route 7 was accomplished via the preparation (82%) and subsequent hydrolysis (97%) of **87**, followed by coupling to (S-methyl)-L-cysteine methyl ester (81%), giving an overall yield of 64%. Unless stated, all ***N***-ferrocenoyl monosubstituted dipeptides were prepared by synthetic route 7.

Route 1, General Procedure

1mmol of the appropriate dipeptide ester TFA salt and 0.23 (1mmol) of ferrocene carboxylic acid were added to a solution of 0.14g (1mmol) of 1-hydroxybenzotriazole, 0.19mls (1.2mmol) Et_3N, and 0.24g (1.2mmol) of DCC in 10mls dichloromethane at 0˚C. The reaction was raised to room temperature after 30mins, and allowed to proceed for 24 hrs. The precipitated ***N, N*-** dicyclohexylurea was removed by filtration, and the solvent evaporated *in vacuo*. The crude

product was purified by silica gel column chromatography, using a mobile phase of 2:1 hexane/ethyl acetate.

Route 2, General Procedure

1mmol of the appropriate dipeptide ester TFA salt and 0.23 (1mmol) of ferrocene carboxylic acid were added to a solution of 0.20g (1.2mmol) carbonyldiimidazole and 0.19mls (1.2mmol) Et_3N, in dry tetrahydrofuran at 0˚C. The reaction was raised to room temperature after 30mins, and allowed to proceed for 24 hrs. The solvent evaporated *in vacuo*, and the crude product was eluted from a column of silica gel, using a mobile phase of 2:1 hexane/ethyl acetate.

Route 3, General Procedure

1mmol of the appropriate dipeptide ester TFA salt was added to a solution of **60** (0.35g, 1mmol) and 0.19mls (1.2mmol) Et_3N, in dichloromethane. The reaction was allowed to proceed for 24hrs, and the solvent evaporated *in vacuo*. The crude product was purified by silica gel column chromatography, using a mobile phase of 2:1 hexane/ethyl acetate.

Route 4, General Procedure

1mmol of the appropriate dipeptide ester HBr salt was added to a solution of **60** (0.35g, 1mmol) and 0.19mls (1.2mmol) Et_3N, in dichloromethane. The reaction was allowed to proceed for 24hrs, and the solvent evaporated *in vacuo*. The crude product was purified by silica gel column chromatography, using a mobile phase of 2:1 hexane/ethyl acetate.

Route 5, General Procedure

3mmol of the appropriate amino acid and 0.69g (3mmol) of **60** was added to a solution of 0.42g (3mmol) of 1-hydroxybenzotriazole, 0.57mls (3.6mmol) Et_3N, and 0.72g (3.6mmol) of DCC in 30mls absolute methanol at 0˚C. The reaction was raised to room temperature after 30mins, and allowed to proceed for 24 hrs. The precipitated ***N, N*** - dicyclohexylurea was removed by filtration, and the ***N***-ferrocenoyl amino acid was precipitated via the drop-wise addition of 0.5M HCl.

Route 6, General Procedure

1mmol of the appropriate ***N***-ferrocenoyl amino acid (prepared via hydrogenation of the appropriate ***N***-ferrocenoyl amino acid benzyl ester) and 1mmol of the appropriate amino acid ester hydrochloride salt were added to a solution of 0.14g (1 mmol) of 1-hydroxybenzotriazole, 0.19mls (1.2mmol) Et_3N, and 0.24g (1.2mmol) of DCC in 10mls dichloromethane at 0˚C. The reaction was raised to room temperature after 30mins, and allowed to proceed for 24 hrs. The precipitated ***N, N*** - dicyclohexylurea was removed by filtration, and the filtrate washed with 5% citric acid, saturated $NaHCO_3$, and water. The organic phase was then dried over $MgSO_4$, and evaporated to dryness in *vacuo*, to afford the ***N***-ferrocenoyl monosubstituted dipeptides as orange solids.

Route 7, General Procedure

1mmol of the appropriate ***N***-ferrocenoyl amino acid (prepared via hydrolysis of the appropriate ***N***-ferrocenoyl amino acid alkyl ester) and 1mmol of the appropriate amino acid ester hydrochloride salt were added to a solution of 0.14g (1 mmol) of 1-hydroxybenzotriazole and 0.24g (1.2mmol) of DCC in 10mls dichloromethane at 0˚C. The reaction was raised to room temperature after 30mins, and allowed to proceed for 24 hrs. The precipitated ***N, N*** - dicyclohexylurea was removed by filtration, and the filtrate washed with 5% citric acid, saturated $NaHCO_3$, and water. The organic phase was then dried over $MgSO_4$, and evaporated to dryness in *vacuo*, to afford the ***N***-ferrocenoyl monosubstituted dipeptides as orange solids.

_N_-ferrocenoyl-((S-methyl) L-cysteine)$_2$ methyl ester (103)

0.35g of ***N***-ferrocenoyl-(S-methyl)-L-cysteine and 0.19g of (S-methyl)-L-cysteine methyl ester hydrochloride were used in the synthesis..

Yields: Route 1, 0.09g, (19%). Route 2, 0.11g, (23%). Route 3, 0.15g, (28%). Route 4, 0.22g (41%). Route 5, 0.13g (9%). Route 6, 0.25g (52%). Route 7, 0.30 g (64%), orange solid, m.p. 119-120°C.

$E_{1/2}$ 0.175mV (Vs. Fc/Fc+), $[\alpha]_D^{20}$ -25° (EtOH), UV-Vis (λ_{max}) (EtOH): 306, 441 nm (ε = 182 M^{-1} cm^{-1}), I.R. υ_{max} (KBr): 3280, 2917, 1749, 1656, 1627,1531, 1383, 1215, 819 cm^{-1}.

^{1}H-NMR (400MHz) δ (*d*^{6} DMSO): 2.07 (3H, s, -SC<u>H</u>$_3$), 2.16 (3H, s, -SC<u>H</u>$_3$), 2.72-2.82 (2H, m, -C<u>H</u>$_2$SCH$_3$), 2.84-2.92 (2H, m, -C<u>H</u>$_2$SCH$_3$), 3.63 (3H, s, OC<u>H</u>$_3$), 4.20 (5H, s, *unsub*. Cp ring),

4.35 (2H, s, H_{meta} Cp ring), 4.50-4.55 (1H, m, -NHC<u>H</u>-), 4.68-4.73 (1H, m, -NHC<u>H</u>-), 4.86 (2H, s, H_{ortho} Cp ring), 7.85 (1H, d, *J* = 8.0 Hz, -N<u>H</u>CH-), 8.56, 8.67 (1H, *two doublets*, *J* = 8.0 Hz, -N<u>H</u>CH-).

^{13}C-NMR (100 MHz) δ (*d*^{6} DMSO): 15.53, 15.60, 35.31 (-ve DEPT), 35.73 (-ve DEPT), 51.99, 52.22, 52.48, 68.63, 68.82, 69.84, 70.42, 76.43, 169.64, 171.38, 172.65.

_N_-ferrocenoyl-(S-methyl)-L-cysteine-L-aspartic acid dimethyl ester (104)

0.35g of ***N***-ferrocenoyl-(S-methyl)-L-cysteine and 0.20g of L-aspartic acid dimethyl ester hydrochloride were used in the synthesis.

Yield 0.29g (59%), orange solid. m.p. 131-133°C.

$E_{1/2}$ = 0.170mV (Vs. Fc/Fc+), $[\alpha]_D^{20}$ = - 18° (EtOH), (UV-Vis (λ_{max}) (EtOH): 305, 443 nm (ε = 220 M^{-1} cm^{-1}), I.R. υ_{max} (KBr): 3304, 1735, 1725, 1655, 1628, 1537, 1309, 1230, 818 cm^{-1}.

^{1}H-NMR (400MHz) δ (*d*^{6} DMSO): 2.12 (1H, s, -SC<u>H</u>$_3$), 2.51-2.91 (4H, m, -C<u>H</u>$_2$SCH$_3$ + -C<u>H</u>$_2$COOCH$_3$), 3.60 (3H, s, OC<u>H</u>$_3$), 3.62 (3H, s, OC<u>H</u>$_3$), 4.21 (5H, s, *unsub*. Cp ring), 4.37 (2H, br. s, H_{meta} Cp ring), 4.62-4.71 (2H, m, -NHC<u>H</u>- x 2) 4.86 (2H, s, 2H_{ortho} Cp ring) 7.85 (1H, d, *J* = 8.8 Hz, N<u>H</u>CH-) 8.56, 8.64 (1H, two doublets, *J* = 8.0 Hz, N<u>H</u>CH-).

^{13}C-NMR (100 MHz) δ (*d*^{6} DMSO): 15.34, 35.63 (-ve DEPT), 35.76(-ve DEPT), 49.00, 51.82, 51.92, 52.09, 52.61, 68.64, 69.85, 70.44, 76.19, 169.32, 169.58, 170.79, 171.30.

_N_-ferrocenoyl-(L-methionine)$_2$ methyl ester (105)

0.36 g of ***N***-ferrocenoyl-L-methionine and 0.20g of L-methionine methyl ester hydrochloride were used in the synthesis.

Yields: Route 4, 0.20g (40%). Route 7, 0.31 g, (62%), orange solid. m.p. 119-120°C.

$E_{1/2}$ 0.167mV (Vs. Fc/Fc+), $[\alpha]_D^{20}$ -21° (EtOH), UV-Vis (λ_{max}) (EtOH): 260, 306, 444 nm (ε = 196 M^{-1} cm^{-1}), I.R. υ_{max} (KBr): 3285, 2917, 1746, 1656, 1626,1538, 1214, 1107, 820 cm^{-1}.

^{1}H-NMR (400MHz) δ (*d*^{6} DMSO): 1.83-2.09 (10H, m, -C<u>H</u>$_2$SC<u>H</u>$_3$ x 2), 2.53-2.59 (4H, m, -C<u>H</u>$_2$CH$_2$SCH$_3$ x 2), 3.64 (3H, s, -OC<u>H</u>$_3$), 4.18 (5H, s, *unsub*. Cp ring), 4.36 (2H, s, H_{meta} Cp ring), 4.41-4.46 (2H, m, NHC<u>H</u>-), 4.89 (2H, s, H_{ortho} Cp ring), 7.75-7.80 (1H, m, N<u>H</u>CH), 8.39-8.46 (1H, m, N<u>H</u>CH).

^{13}C-NMR (100 MHz) δ (*d*^{6} DMSO): 14.47, 15.01, 15.07, 29.86 (-ve DEPT), 30.25 (-ve DEPT), 30.78 (-ve DEPT), 31.56 (-ve DEPT), 51.23, 52.13, 52.34, 68.70, 68.77, 70.40, 70.57, 76.17, 169.53, 169.61, 172.60.

_N_-ferrocenoyl-L-methionine-L-tyrosine methyl ester (106)

0.36g of ***N***-ferrocenoyl-L-methionine and 0.23g of L-tyrosine methyl ester hydrochloride were used in the synthesis.

Yield 0.34g (63%), orange solid, m.p. 119-120°C.

$E_{1/2}$ 0.162mV (Vs. Fc/Fc+), $[\alpha]_D^{20}$ -20° (EtOH), UV-Vis (λ_{max}) (EtOH): 305, 443 nm (ε = 174 M^{-1} cm^{-1}), I.R. υ_{max} (KBr): 3277, 2918, 1744, 1655, 1638, 1542, 1401, 1220, 825 cm^{-1}.

^{1}H-NMR (400MHz) δ (*d*^{6} DMSO): 1.94-2.09 (5H, m, -C$\underline{H}_2$SC$\underline{H}_3$), 2.53-2.58 (2H, m, -C$\underline{H}_2$CH$_2$SCH$_3$), 2.79 (2H, m, -NHCH(C$\underline{H}_2$PhOH), 3.40 (3H, s, OC$\underline{H}_3$), 4.17 (5H, s, *unsub*. Cp ring), 4.34-4.44 (3H, m, H_{meta} Cp ring, -NHC$\underline{H}$-), 4.54-4.59 (1H, m, -NHC$\underline{H}$-), 4.88 (2H, br. s, H_{ortho} Cp ring), 6.50 (2H, d, *J* = 8.0 Hz, ArH), 7.00 (2H, d, *J* = 8.0 Hz, ArH), 7.72, 7.76 (1H, *two doublets*, *J* = 8.0 Hz, -N$\underline{H}$CH-), 8.28, 8.36 (1H, *two doublets*, *J* = 8.0 Hz, -N$\underline{H}$CH-), 9.21 (1H, s, PhOH).

^{13}C-NMR (100 MHz) δ (*d*^{6} DMSO): 15.04, 30.21 (-ve DEPT), 31.56 (-ve DEPT), 36.15 (-ve DEPT), 51.95, 52.12, 54.36, 68.58, 68.87, 69.72, 70.04, 76.21, 115.42, 127.25, 130.35, 156.37, 169.48, 172.18, 172.32.

_N_-ferrocenoyl-L-methionine-L-threonine methyl ester (107)

0.36g of ***N***-ferrocenoyl-L-methionine and 0.17g of L-threonine methyl ester hydrochloride were used in the synthesis.

Yield 0.27g (60%), orange solid, m.p 138-141°C.

$E_{1/2}$ = 0.166mV (Vs. Fc/Fc+), $[\alpha]_D^{20}$ -24° (EtOH), UV-Vis (λ_{max}) (EtOH): 306, 440 nm (ε = 199 M^{-1} cm^{-1}), I.R. υ_{max} (KBr): 3277, 2198, 1744, 1654, 1638, 1542, 1401, 1221, 825 cm^{-1}.

^{1}H-NMR (400MHz) δ (*d*^{6} DMSO): 1.05, 1.10 (3H, *two doublets*, *J* = 6.4 Hz, -CH(OH)C$\underline{H}_3$), 1.92-2.08 (5H, m, -C$\underline{H}_2$SC$\underline{H}_3$), 2.53-2.57 (2H, m, - C$\underline{H}_2$CH$_2$SCH$_3$), 3.63 (3H, s, OC$\underline{H}_3$), 4.14-4.19 (6H, m, -C$\underline{H}$(OH)CH$_3$), *unsub*. Cp ring), 4.30-4.32 (1H, m, -NHC$\underline{H}$-), 4.36 (2H, s, H_{meta} Cp ring), 4.61-4.65 (1H, m, -NHC$\underline{H}$-), 4.89 (1H, s, H_{ortho} Cp ring), 4.91 (1H, s, H_{ortho} Cp ring), 5.09

(1H, d, *J* = 5.6 Hz, -CH(OH)CH_3), 7.86 (1H, d, *J* = 8.0 Hz, -NHCH-), 7.92 (1H, d, *J* = 8.8 Hz, -NHCH-).

^{13}C-NMR (100 MHz) δ (*d*^{6} DMSO): 15.04, 20.54, 30.38 (-ve DEPT), 31.62 (-ve DEPT), 52.23, 58.01, 58.12, 66.54, 68.65, 68.78, 69.73, 70.44, 76.25, 169.64, 171.31, 172.56.

_N_-ferrocenoyl-L-tyrosine-(S-methyl)-L-cysteine methyl ester (108)

0.39g of ***N***-ferrocenoyl-L-tyrosine and 0.19g of (S-methyl)-L-cysteine methyl ester hydrochloride were used in the synthesis.

Yield 0.30g (57 %), orange solid, m.p 121-125°C.

$E_{1/2}$ = 0.180mV (Vs. Fc/Fc+), $[\alpha]_D^{20}$ -19° (EtOH), UV-Vis (λ_{max}) (EtOH): 302, 441 nm(ε = 178 M^{-1} cm^{-1}), I.R. υ_{max} (KBr): 3277, 2365, 1752, 1657, 1625, 1516, 1439, 1221, 823 cm^{-1}.

^{1}H-NMR (400MHz) δ (*d*^{6} DMSO): 2.09 (3H, s, -SCH_3), 2.82-2.99 (4H, m, -CH_2PhOH, -CH_2SCH_3), 3.65 (3H, s, OCH_3), 3.96 (5H, s, *unsub*. Cp ring), 4.30 (2H, s, H_{meta} Cp ring), 4.51-4.54 (1H, m, -NHCH-), 4.70-4.74 (3H, m, H_{ortho} Cp ring, -NHCH-), 6.67 (2H, d, *J* = 7.6 Hz, ArH), 7.20 (2H, d, *J* = 7.6 Hz, ArH), 7.76 (1H, d, *J* = 8.0 Hz, -NHCH-), 8.56 (1H, d, *J* = 8.0 Hz, -NHCH-), 9.13 (1H, s, PhOH).

^{13}C-NMR (100 MHz) δ (*d*^{6} DMSO): 15.64, 34.93(-ve DEPT), 36.64(-ve DEPT), 52.29, 52.47, 54.52, 68.20, 68.93, 69.69, 70.25, 76.24, 115.20, 128.79, 130.42, 156.09, 169.30, 171.51, 172.65.

_N_-ferrocenoyl -(β-alanine)$_2$ methyl ester (109)

0.30g of ***N***-ferrocenoyl- β-alanine and 0.14g of β-alanine methyl ester hydrochloride were used in the synthesis.

Yields: Route 4, 0.12g (34%). Route 7, 0.21g, (58%), orange solid, m.p. 150-151°C.

$E_{1/2}$ = 0.160mV (Vs. Fc/Fc+), UV-Vis (λ_{max}) (EtOH): 268, 304, 442 nm (ε =187 M^{-1} cm^{-1}), I.R. υ_{max} (KBr): 3257, 3083, 2931, 1741, 1664, 1614, 1552, 1314, 1107 cm^{-1}.

^{1}H-NMR (400MHz) δ (*d*^{6} DMSO): 2.35 (2H, t, *J* = 6.8 Hz, NHCH_2CH_2CO-), 2.46 (2H, t, *J* = 6.8 Hz, NHCH_2CH_2CO-), 3.26-3.34 (4H, m, NHCH_2CH_2CO X 2), 3.56 (3H, s, -OCH_3), 4.15 (5H, s, *unsub*. Cp ring), 4.32 (2H, s, H_{meta} Cp ring), 4.76 (2H, s, H_{ortho} Cp ring), 7.79 (1H, t, *J* = 6.4 Hz, (NHCH_2CH_2-), 8.05 (1H, t, *J* = 6.4 Hz, NHCH_2CH_2-).

^{13}C-NMR (100 MHz) δ (*d*^{6} DMSO): 34.02 (-ve DEPT), 34.97 (-ve DEPT), 35.79 (-ve DEPT), 35.89 (-ve DEPT), 51.73, 68.44, 69.69, 70.20, 76.95, 169.28, 170.94, 172.11.

***N*-ferrocenoyl-(γ-aminobutyric acid)$_2$ methyl ester (110)**

0.32g of ***N***-ferrocenoyl-γ-aminobutyric acid and 0.15g of γ-aminobutyric acid methyl ester hydrochloride were used in the synthesis.

Yields: Route 4, 0.15g (36%). Route 7, 0.25 g, (60%), orange solid, m.p. 150-151°C.

$E_{1/2}$ = 0.155mV (Vs. Fc/Fc+), UV-Vis (λ_{max}) (EtOH): 306, 442 nm (ε = 187 M^{-1} cm^{-1}), I.R. υ_{max} (KBr): 3329, 3248, 3070, 2935, 2120, 1735, 1661, 1619, 1551, 1445, 1174, 824 cm^{-1}.

^{1}H-NMR (400MHz) δ (*d*^{6} DMSO): 1.65-175 (4H, m, $NHCH_2C\underline{H}_2CH_2CO$ X 2), 2.12 (2H, t, *J* = 7.6 Hz, $NHCH_2CH_2C\underline{H}_2$-), 2.31 (2H, t, *J* = 7.6 Hz, $NHCH_2CH_2C\underline{H}_2$-), 3.03-3.07 (2H, m, $NHC\underline{H}_2CH_2$-), 3.13-3.18 (2H, m, $NHC\underline{H}_2CH_2$-), 3.58 (3H, s, $-OC\underline{H}_3$), 4.15 (5H, s, *unsub*. Cp ring), 4.35 (2H, d, *J* = 2.0 Hz, H_{meta} Cp ring), 4.77 (2H, d, *J* = 2.0 Hz, H_{ortho} Cp ring), 7.83 (1H, t, *J* = 6.4 Hz, $N\underline{H}CH_2CH_2$-), 7.89 (1H, t, *J* = 6.4 Hz, $N\underline{H}CH_2CH_2$-).

^{13}C-NMR (100 MHz) δ (*d*^{6} DMSO): 24.89 (-ve DEPT), 26.08 (-ve DEPT), 31.05 (-ve DEPT), 33.31 (-ve DEPT), 38.09 (-ve DEPT), 38.83 (-ve DEPT), 51.61, 68.44, 69.65, 70.16, 77.14, 169.16, 172.22, 173.47.

***N*-ferrocenoyl-(valeric acid)$_2$ methyl ester (111)**

0.36g of ***N***-ferrocenoyl valeric acid-OH and 0.17g of valeric acid methyl ester hydrochloride were used in the synthesis.

Yield 0.22g (52%), orange solid, m.p. 154-155°C.

$E_{1/2}$ = 0.151V (Vs. Fc/Fc+), UV-Vis (λ_{max}) (EtOH): 302, 441 nm (ε = 187 M^{-1} cm^{-1}).

^{1}H-NMR (400MHz) δ (*d*^{6} DMSO): 1.32-1.57 (8H, m, $-NHCH_2C\underline{H}_2C\underline{H}_2CH_2CO$- x 2), 2.09 (2H, t, *J* = 7.6 Hz, $-CH_2C\underline{H}_2CO$-), 2.28 (2H, t, *J* = 7.6 Hz, $-CH_2C\underline{H}_2CO$-), 3.00-3.01 (2H, m, $-NHC\underline{H}_2CH_2$-), 3.15 (2H, t, *J* = 6.0 Hz, $-NHC\underline{H}_2CH_2$-), 3.57 (3H, s, $-OC\underline{H}_3$), 4.15 (5H, s, *unsub*. Cp ring), 4.33 (2H, br. s, H_{meta} Cp ring), 4.76 (2H, s, H_{ortho} Cp ring), 7.76-7.80 (2H, m, $N\underline{H}CH$- x 2).

^{13}C-NMR (100 MHz) δ (*d*^{6} DMSO): 22.23 (-ve DEPT), 23.23 (-ve DEPT), 24.82 (-ve DEPT), 25.67 (-ve DEPT), 28.94 (-ve DEPT), 33.70 (-ve DEPT), 38.27 (-ve DEPT), 38.76 (-ve DEPT), 51.54, 68.42, 69.62, 70.12, 77.25, 169.00, 172.20, 173.61.

3.11: References

1) S. Maricic, U. Berg, T. Frejd, *Tetrahedron, 58, (2002), 3085*.

2) A. Wieckowska , R. Bilewicz, A. Misicka, M. Pietraszkiewicz, *Chem. Phys. Lett., 350, (2001), 447.*

3) E. Cuignet, C. Sergheraert, A. Tartar, M. Dautrevaux, *J. Organometallic Chem., 195, (1980), 325.*

4) H.B. Kraatz, D.M. Leek, A. Houman, G.D. Enright, *J. Organometallic Chem., 589, (1999), 38.*

5) J. Schnert, A. Hess, N.M. Nolte, *J. Organometallic Chem., 637-639, (2001), 349.*

6) M. Sheehy, *The Design and Synthesis of Novel Peptide Derivatives as Malarial Protease Inhibitors and Electrochemical Anion Sensing Receptors, Ph.D. Thesis, DCU, (1999).*

7) C. Imrie, L. Cook, D. Levendis, *J. Organometallic Chem., 637-639, (2001), 266.*

8) M. Bodansky, A. Bodansky, *Principles of Peptide Synthesis, 2nd ed., Springer-Verlay, (1993).*

9) F.A.Cotton, G. Wilkinson, *Advanced Inorganic Chemistry, 5th ed., Wiley-Interscience.*

10) Y. Xu, H.B. Kraatz*., Tetrahedron Lett., 42, (2001), 75.*

11) P. Saweczko, H.B. Kraatz, *Co-Ord. Chem. Rev., 190-192, (1999), 185.*

12) H.B. Kraatz, Y. Xu, P. Saweczko, *J. Organometallic Chem., 637-639, (2001), 335.*

Chapter IV

The Synthesis and Characterisation of 1, 1'-*N*-Ferrocenoyl Symmetric Dipeptides

4.1: Introduction

Introduction of functional groups on both Cp rings of ferrocene is a well established area of chemical synthesis, although in some cases, more difficult to achieve than mono substitution. For example, due to the electronic communication between the two Cp rings via the central iron atom, the introduction of an electron-withdrawing group onto one ring can significantly deactivate the second ring towards electrophilic aromatic substitution [1].

Developing conformationally constrained molecules which mimic elements of protein secondary structure, i.e. the α-helix, the β-turn, and β-sheet, has been a target of researchers in the last twenty years, as these structural motifs have important implications in terms of biological function [2]. The β-sheet mimetics have proven the most difficult to obtain, primarily because of aggregation problems in solution [3]. Although attempts at overcoming these problems have been addressed by the use of square planar copper complexes and dibenzofuran based amino acids, the ferrocene moiety offers a unique advantage in this respect, as its inter-ring separation of 3.3Å is close to the N-O separation in hydrogen-bonded β-sheets. This fact has been exploited by those groups which have prepared compounds such as **51**-**53** (section 1.3) [4, 5]. In all literature reports, the electrochemical and spectroscopic properties of the disubstituted ferrocenes vary greatly with respect to monosubstituted analogues.

4.2: Synthesis of 1, 1'-*N*-Ferrocenoyl Symmetric Dipeptides

Three different coupling reagents were employed during the synthesis of these compounds, in an attempt to optimise the yields. Despite the difference in reaction stoichiometry employed when preparing disubstituted ferrocenes, yields similar to that recorded for the monosubstituted derivatives were recorded.

4.2.1: Synthetic Route 1

The first attempt at preparation of these compounds involved the use of the DCC/HOBt coupling protocol and ferrocene dicarboxylic acid (**112**), and the same methodology was employed as was used in the synthesis of the monosubstituted compounds discussed in the previous two chapters. The reactions were quenched in all cases after 24 hours, and carried out in the dark, as it was believed that these disubstituted ferrocenes might undergo photochemical decomposition. *Scheme 1* shows the preparation of **131** by this method. Interestingly, all the

chromophoric bands which were eluted from the column before the isolation of **131** were seen to quickly decompose in solution. No mono- or di- substituted ferrocenoyl-OBt intermediate was isolated (there are reports of the former in the literature [6], though the latter could not be found), which would suggest that the bis-OBt intermediates are considerably less stable in solution than the monosubstituted **60** (section 2.4.2).

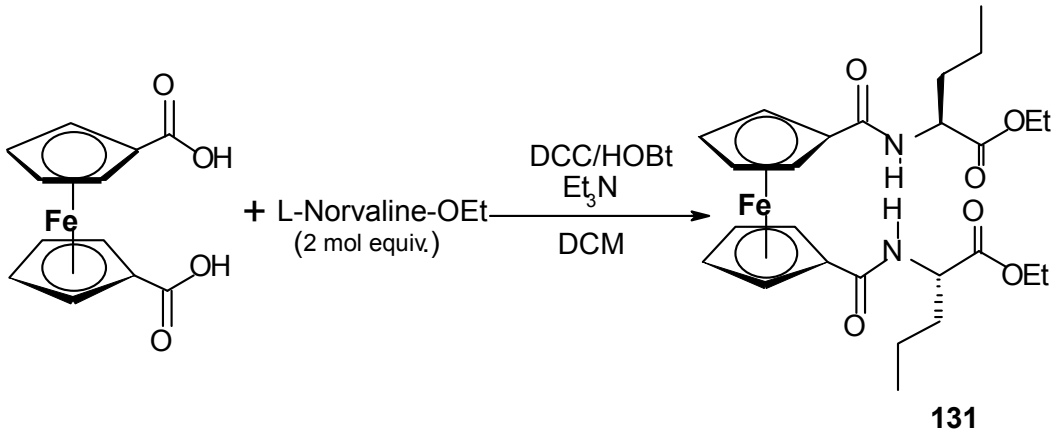

*Scheme 1: Preparation of **131** using the DCC/HOBt protocol.*

4.2.2: Synthetic Route 2

CDI had been employed successfully in the preparation of several monosubstituted ferrocenes (section 2.4.2), and it was thought that it could be used to the same effect when preparing the disubstituted analogues in a similar manner. The reactions were carried out in the dark, and the temperature was maintained at < 15˚C throughout. However, attempts to synthesize **116** and **131** using this route were unsuccessful, and the target molecules were not recovered from the reaction mixtures. TLC analysis, performed at various intervals during the course of the reactions, showed that the desired products were not formed at any stage.

This may possibly be attributable to the formation of a bis-imidazole intermediate when using CDI in conjunction with ferrocene dicarboxylic acid (*fig. 1*). It will be recalled mono-imidazolic ferrocenoyl conjugate (section 2.4.2) was found to decompose readily in solution, and this inherent instability could be accentuated by bis substitution. Certainly, no reports of a bis-ferrocenoyl-imidazolic conjugate could be found in the literature.

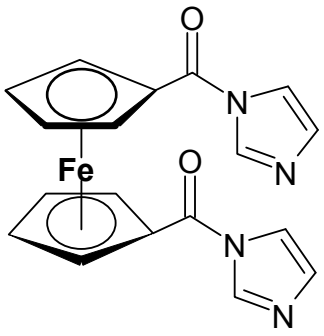

Fig. 1: Bis-imidazole intermediate, whose formation and instability may limit the use of CDI as a coupling reagent for 1, 1'-disubstituted ferrocenes

It may also explain why, during the course of these experiments, the only amino acid ester which failed to yield the desired coupled product with ferrocene dicarboxylic acid, (**112**), was L-histidine methyl ester. It will be recalled from section 2.8 that a ferrocenoyl-imidazolic adduct, **80**, was formed during preparation of compound **74**. It is possible that a bis-ferrocenoyl-imidazolic intermediate may have resulted in decomposition, and hence failure to yield the target molecule.

4.2.3: Synthetic Route 3

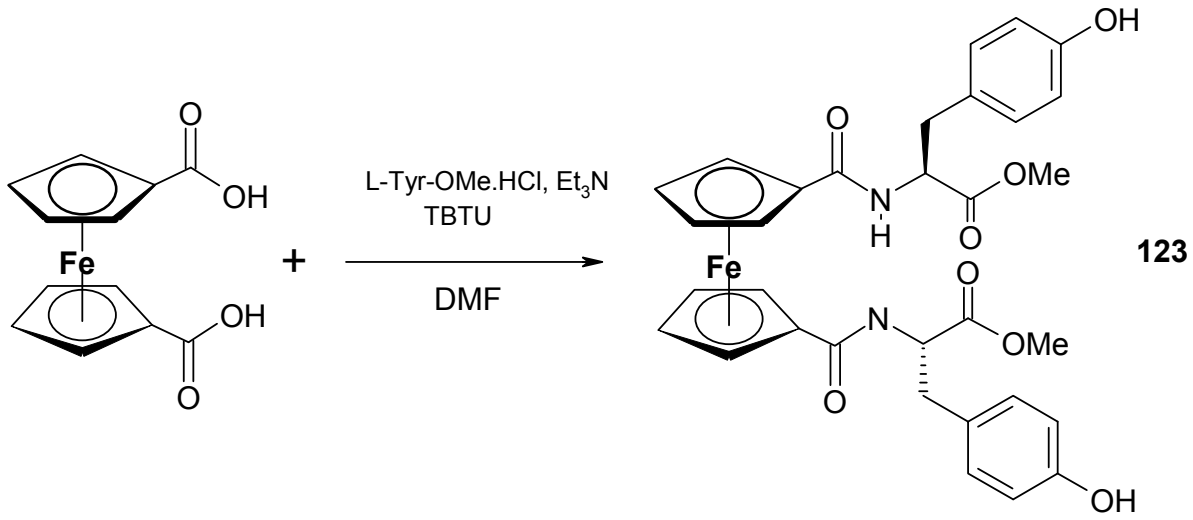

*Scheme 2: Preparation of **123** using TBTU as the coupling reagent*

TBTU had been successfully employed in the synthesis of the monosubstituted compounds. **113** and **131** were both prepared using this reagent, and the yields of these compounds were almost identical to that recorded when DCC/HOBt were used. Given the expensive nature of TBTU, it would appear that DCC is a wiser choice of coupling reagent in the preparation of these disubstituted ferrocenes. The synthesis of **131** is shown in *scheme 2*:

Compound	Name	M.P. (ºC)	Yield (%)
113	1, 1'-***N***-ferrocenoyl-(L-norleucine methyl ester)$_2$	180-182	73
114	1, 1'-***N***-ferrocenoyl-(L-aspartic acid dimethyl ester)$_2$	198-200	68
115	1, 1'-***N***-ferrocenoyl-(L-phenylalanine methyl ester)$_2$	211-213	72
116	1, 1'-***N***-ferrocenoyl-(L-methionine methyl ester)$_2$	220-223	73
117	1, 1'-*N*-ferrocenoyl-(2-isoaminobutyric acid methyl ester)$_2$	201-203	66
118	1, 1'-***N***-ferrocenoyl-(L-leucine methyl ester)$_2$	217-220	70
119	1, 1'-***N***-ferrocenoyl- ((S-methyl)-L-cysteine methyl ester) $_2$	186-187	78
120	1, 1'-***N***-ferrocenoyl-(L-phenylglycine methyl ester)$_2$.	200-203	72
121	1, 1'-***N***-ferrocenoyl-(L-glutamic acid diethyl ester)$_2$	154-157	68
122	1, 1'-***N***-ferrocenoyl-(L-threonine methyl ester)$_2$	189-192	76
123	1, 1'-***N***-ferrocenoyl-(L-tyrosine methyl ester)$_2$	219-221	69
124	1, 1'-***N***-ferrocenoyl-((1S, 2R)-(+)- norephedrine) $_2$	199-201	74
125	1, 1'-***N***-ferrocenoyl-(L-tryptophan methyl ester)$_2$	167-169	64
126	1, 1'-***N***-ferrocenoyl-(glycine ethyl ester)$_2$	213-215	71
127	1, 1'-***N***-ferrocenoyl- (β-alanine methyl ester)$_2$	146-148	68
128	1, 1'-***N***-ferrocenoyl-(γ-aminobutyric acid methyl ester)$_2$	131-132	68
129	1, 1'-***N***-ferrocenoyl-(valeric acid methyl ester)$_2$	161-163	65
130	1, 1'-***N***-ferrocenoyl-[(glycine)$_2$ ethyl ester]$_2$	227-229	66
131	1, 1'-***N***-ferrocenoyl-(L-norvaline ethyl ester)$_2$	168-170	70
132	1, 1'-***N***-ferrocenoyl-(L-serine methyl ester)$_2$	168-170	67
133	1, 1'-***N***-ferrocenoyl-(sarcosine ethyl ester)$_2$	91-93	67

*Table 1: % Yields and melting points of 1, 1'-**N**-ferrocenoyl symmetric dipeptides*

A summary of the yields of the various compounds prepared in this chapter, using synthetic route 1, is given in *table 1*.

4.3: ^{1}H-NMR Spectra of 1, 1'-*N*-Ferrocenoyl Symmetric Dipeptides

There are significant differences in the ^{1}H-NMR spectra of all compounds prepared in this chapter relative to their monosubstituted analogues. The most obvious is the absence in the spectra of the unsubstituted Cp ring proton signal ca. 4.2 ppm. There also appears to be equivalence by symmetry of the amino acid residues attached to each Cp ring, with all signals in the spectra integrating for multiples of two. This equivalence extends to both the ferrocenoyl and amide protons, and recording the spectra in both DMSO and $CDCl_3$, allows for elucidation of the conformation adopted by these molecules in solution. A summary of the ^{1}H-NMR data for the 1'1 ***N***-ferrocenoyl symmetric dipeptides is given in *table 2*.

Compound	**N-H**	**H_{ortho}**	**H_{meta}**	**H_{α}**
113	8.17(d)	4.84, 4.87	4.31-4.38	4.31-4.38
114	8.30 (d)	4.80, 4.82	4.37	4.75
115	8.34(d)	4.49, 4.68	4.10	4.68
116	8.22(d)	4.82, 4.87	4.38, 4.43	4.50-4.54
117	8.09(s)	4.79	4.40	-
118	8.18(d)	4.83	4.43	4.35
119	8.28(d)	4.86, 4.89	4.41, 4.44	4.58-4.59
120	8.56(d)	4.90	4.35, 4.39	5.58
121	8.16(d)	4.83, 4.89	4.38, 4.43	4.38
122	7.62(d)	4.87, 4.97	4.50	4.50
123	8.32(d)	4.48, 4.68	4.13, 4.18	4.53-4.59
124	7.72(d)	4.60, 4.66	4.08-4.14	4.08-4.14
125	8.22(d)	4.51, 4.65	4.01, 4.06	4.67-4.73
126	8.31(t)	4.83	4.44	-
127	7.99(t)	4.70	4.28	-
128	7.94(t)	4.72	4.39	-
129	7.73(t)	4.72	4.34	-

Compound	N-H	H_{ortho}	H_{meta}	H_{α}
130	8.42(t), 8.60(t)	4.79	4.43	-
131	8.12(d)	4.82, 4.87	4.37, 4.43	4.32-4.36
132	7.94(d)	4.83, 4.93	4.41-4.45	4.41-4.45
133	-	4.76	4.50	-

*Table 2: The ^{1}H-NMR chemical shifts (δ ppm) of the 1, 1'-**N**-*ferrocenoyl *symmetric dipeptides recorded in d^{6} DMSO.*

4.3.1 ^{1}H-NMR Spectrum of 131.

The ^{1}H-NMR spectrum of **131** is shown in *fig. 2*, and is typical of those 1, 1'-symmetrically disubstituted dipeptides containing chiral centres, and serves to illustrate the symmetrical nature of the conformation adopted by these compounds in solution, with all signals observed in the spectrum integrating for multiples of two.

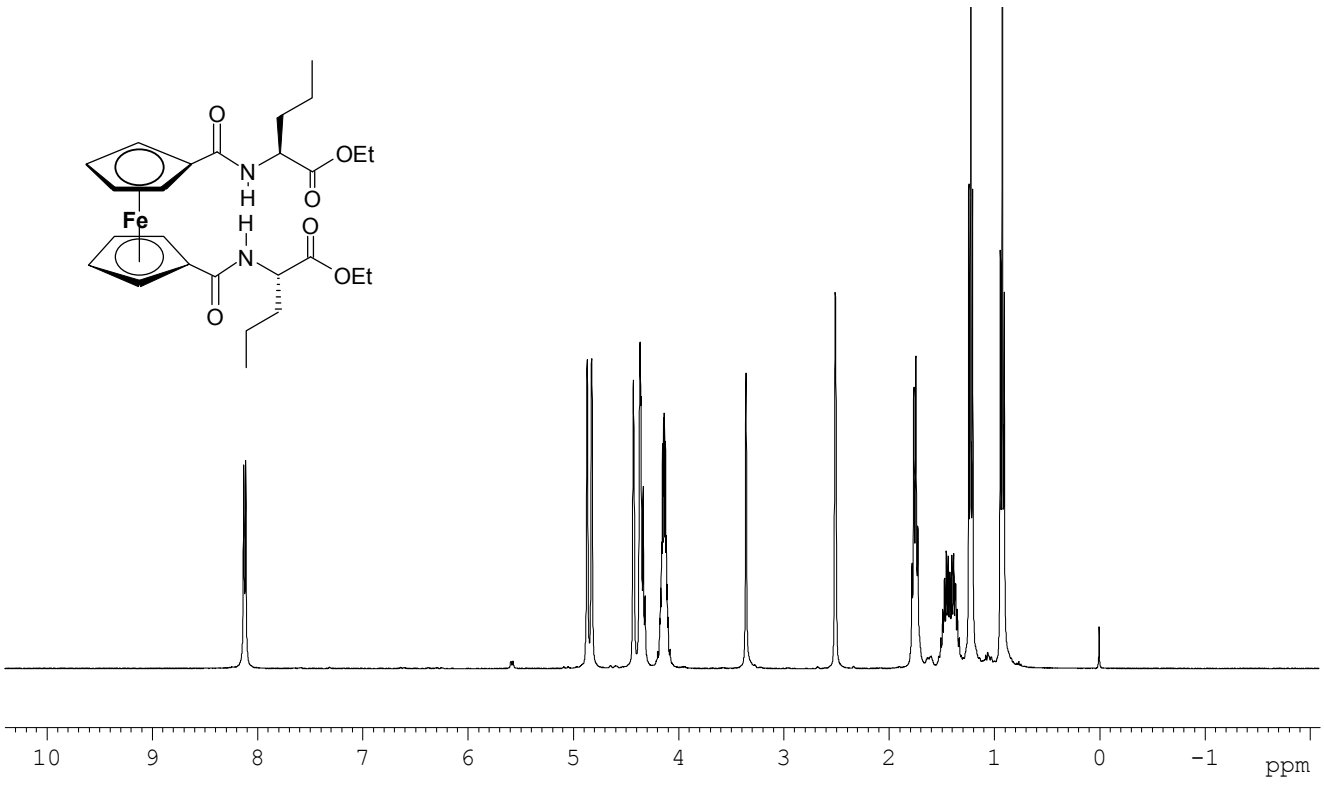

*Fig. 2: The ^{1}H-NMR Spectrum of **131** in d^{6} DMSO.*

Two triplets, each integrating for six protons, are observed at 0.89 and 1.22 ppm, and correspond to the methyl groups of the norvaline side chains and ethyl ester groups respectively. Two multiplets, each integrating for four protons, appear *ca*. 1.4 and 1.75 ppm, and correspond to the two methylene groups of each norvaline side chain. The methylene protons of the ethyl ester groups appear as a quartet at 4.11 ppm, and the protons of each of the chiral α-carbons appear as a multiplet at 4.34 ppm. What is apparent from these results is that corresponding protons of each Cp ring substituent are in the same magnetic environment, an observation which can be expanded upon when other spectroscopic data is considered in subsequent sections.

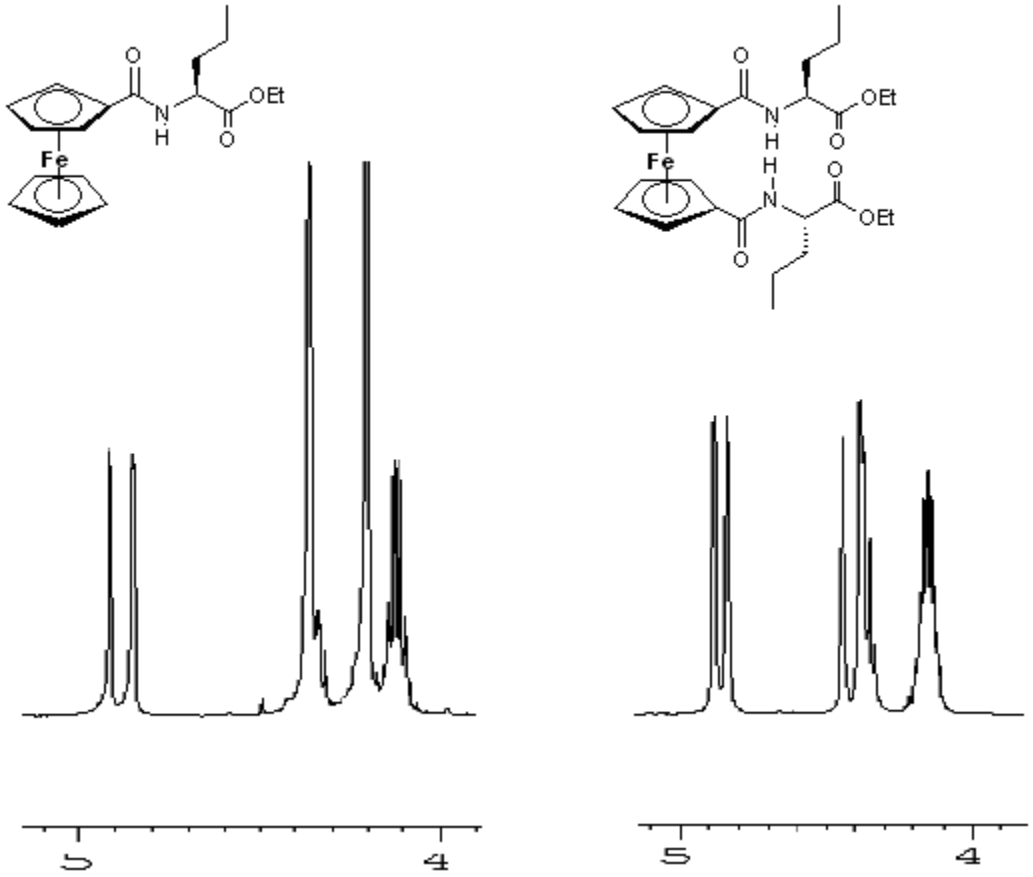

*Fig. 3: The ferrocenoyl protons of **63** (left), and **131** (right). The unsubstituted Cp ring protons ca. 4.2 ppm in the spectrum of **63** are absent from the spectrum of **131**, in which two separate meta-proton signals are observed.*

An interesting contrast can be drawn between the ferrocenoyl protons of **131**, and those of the monosubstituted analogue **63**, as illustrated in *fig. 3*. While the unsubstituted Cp ring protons are naturally absent from the spectrum of **131**, the *meta*-protons of each Cp ring appear as two individual singlets at 4.37 and 4.43 ppm, each integrating for two protons (the former of these overlaps with the protons of the α-carbons, which is also observed in the spectrum of **63**). The *ortho*-protons of the Cp rings appear as two closely grouped singlets, each integrating for two protons, at 4.82 and 4.87 ppm.

There are two possible explanations for this pattern of signals for the ferrocenoyl protons of **131**. The first is that there may be a magnetic non-equivalence between the two Cp rings, and each singlet may correspond to two protons from the same Cp ring. The second is that each of the four ferrocenoyl resonances, all of which integrate for two protons, is composed of a proton from each Cp ring. The latter explanation would seem more likely, given the previously discussed symmetrical aspects of the ^{1}H-NMR spectrum of **131**. The effect of an adjacent chiral centre on the magnetic equivalence of the ferrocenoyl protons (discussed in Ch. 2, section 3.3.1), would appear to extend to the meta-protons of the Cp ring in these disubstituted compounds.

Only one doublet is observed for the two amide protons, at 8.12 ppm, which is slightly more downfield than the resonance observed for the monosubstituted analogue **63** (7.97 ppm). Unlike **63**, however, the amide protons of **131** appear at almost the exact same downfield shift when the spectrum is recorded in $CDCl_3$ (8.10 ppm for **131** vs. 6.34 for **63**). A similar situation is observed for the majority of the 1, 1'-symmetrically disubstituted ferrocenoyl dipeptides, suggesting that an ordered conformation is adopted by these compounds in non-polar solution, via the information of *intra*-molecular hydrogen bonds. This topic is discussed further in subsequent sections, when other spectroscopic data is taken into account.

4.3.2: ^{1}H-NMR Spectra of 126-129.

The achiral compounds **126-129** (*fig. 4*) vary only in terms of the number of methylene groups in their peptide backbones (and of the ester group in the case of **126**). The ^{1}H-NMR spectrum of **127**, recorded in d^6 DMSO, is typical of these compounds, and is shown in *fig. 5*.

As was observed with the chiral 1, 1'-disubstituted compounds, the spectrum of **128** appears to adopt a symmetrical conformation in solution, with all signals integrating for multiplets of two. The protons of the central methylene group of the peptide chains are observed as a multiplet at

1.77 ppm. A triplet, integrating for four protons, and corresponding to the methylene protons adjacent to the ester groups, appears at 2.39 ppm, while the methylene protons adjacent to the amide groups are observed as a multiplet at 3.19 ppm. The methyl protons of each ester group appear as a singlet, integrating for six protons, at 3.62 ppm.

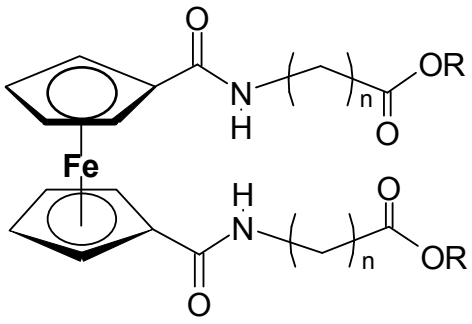

Compound	n =	R =
126	1	Et
127	2	Me
128	3	Me
129	4	Me

*Fig. 4: The structures of compounds **126-129**.*

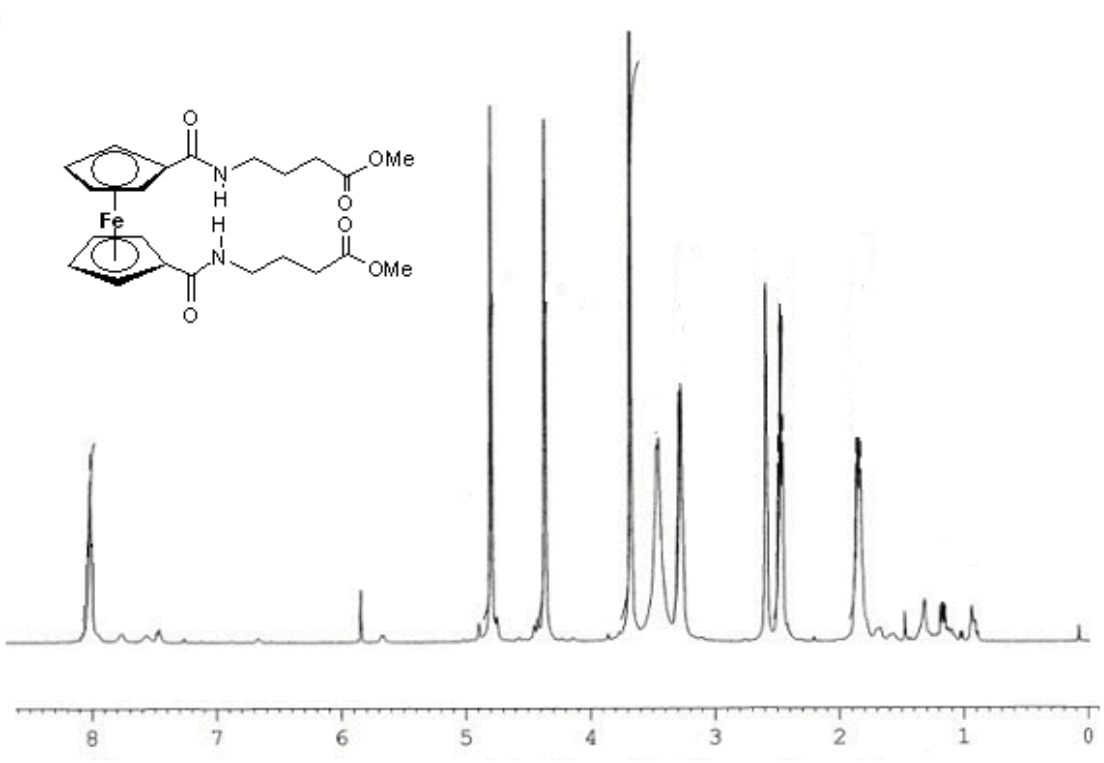

*Fig. 5: The ^{1}H-NMR Spectrum of **128** in d^{6} DMSO.*

In the absence of chiral centres, only two signals are observed for the ferrocenoyl protons. All four of the *meta*-protons appear as a singlet at 4.28 ppm, while the four *ortho*-protons are observed as a singlet at 4.70 ppm. This is in direct contrast to the chiral 1, 1'-disubstituted compounds, where four ferrocenoyl proton signals are observed, and this contrast is illustrated in *fig. 6*, which shows the ferrocenoyl protons of both **128** and the chiral **119**.

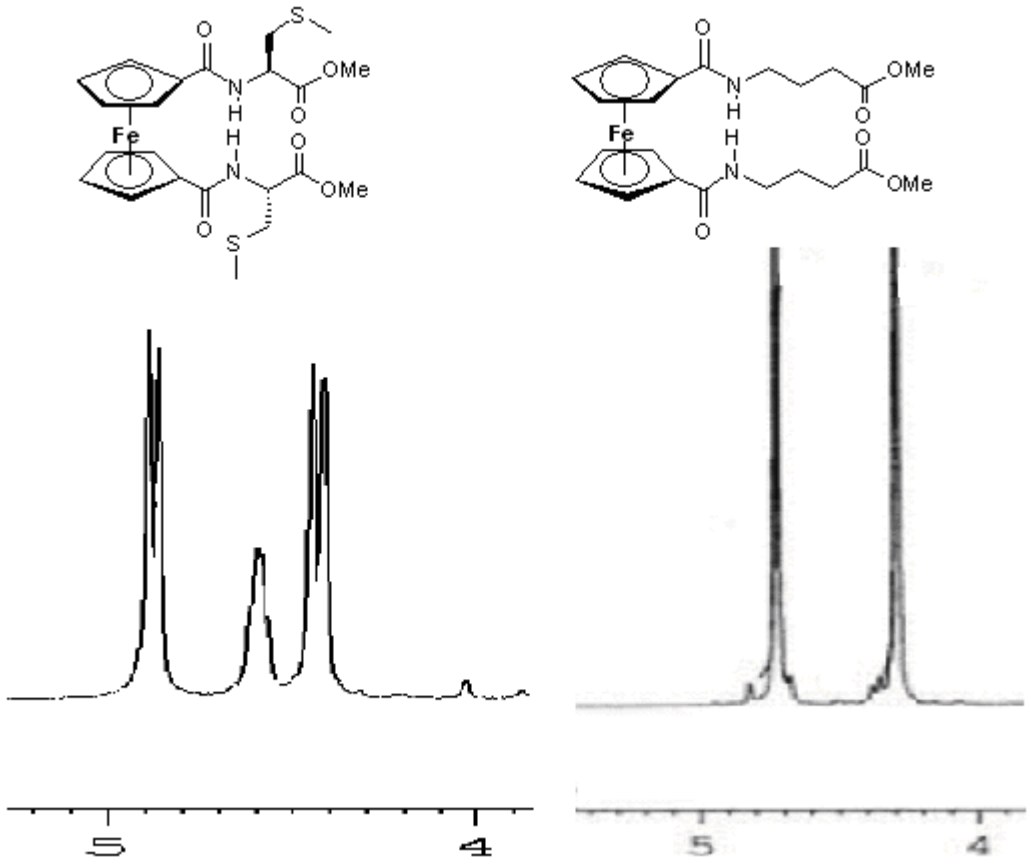

*Fig. 6: Comparison of the ferrocenoyl proton signals of the chiral **119** (left) and achiral **128** (right) in d^6 DMSO.*

The two amide protons of **128** appear as a triplet at 7.94 ppm in d^6 DMSO. Similar chemical shifts were recorded for compounds **126**, **127** and **129**, suggesting that the ability of these compounds to adopt a symmetrical conformation in solution is independent of the length of the peptide backbone.

4.3.3: ^{1}H-NMR Spectrum of 130.

The ^{1}H-NMR spectrum of the tetrapeptide **130**, 1, 1'-***N***-ferrocenoyl-[(glycine)$_2$ ethyl ester]$_2$**,** is shown in *fig. 7*. The methyl protons of both ester groups appear as a triplet integrating for six protons at 1.20 ppm, while the methylene protons of the peptide backbone appear as doublets at 3.84 and 3.92 ppm, both integrating for four protons. The methylene protons of both ester groups appear as a quartet at 4.11 ppm. Only two singlets are observed for the ferrocenoyl protons, at 4.43 (*meta*-) and 4.79 ppm (*ortho*-).

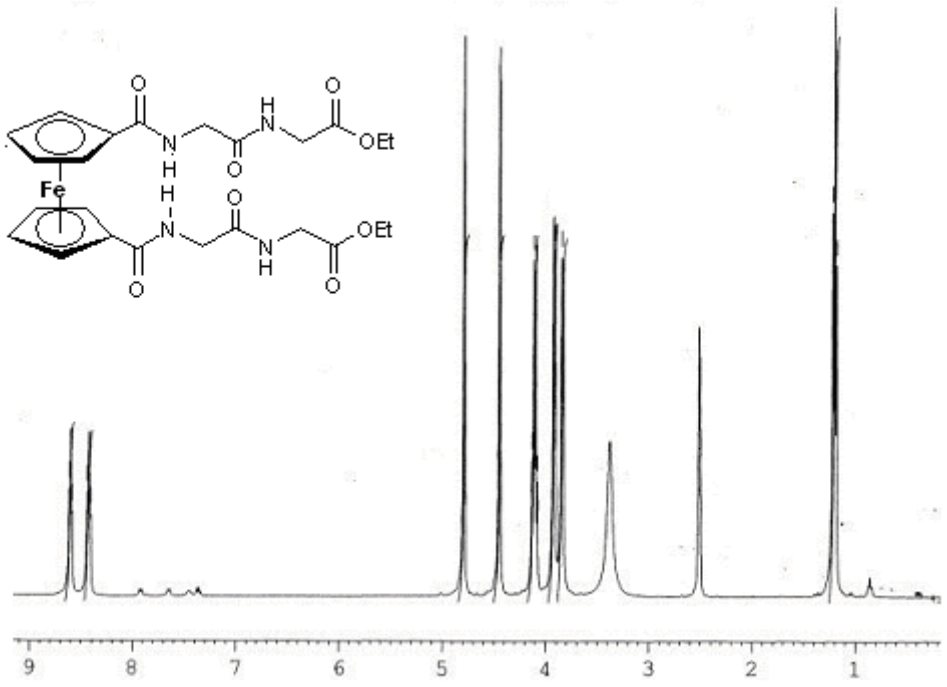

*Fig. 7: The ^{1}H-NMR Spectrum of **130** in d^6 DMSO.*

Two triplets, each integrating for two protons, appear at 8.42 and 8.60 ppm, corresponding to the amide protons. However, when the spectrum of **130** was recorded in $CDCl_3$, a different pattern of signals emerges, as can be seen in *fig. 8*. The amide protons of the compounds discussed so far in this chapter remain largely unaffected in terms of their chemical shifts, whether their spectra is recorded in d^6 DMSO or $CDCl_3$. **130**, however, shows two amide signals in $CDCl_3$, at 6.57 and 8.19 ppm. As was mentioned in section 2.5, in non-polar solution,

hydrogen bonded amide protons tend to appear above 7.5 ppm, while non-hydrogen bonded amide protons appear at lower ppm [7]. It would appear that the conformation adopted by **130** in non-polar solution only allows for the formation of β-sheet-like hydrogen bonding involving the amide groups adjacent to the ferrocenoyl moiety (***N***-terminal). The protons of the ***C***-terminal amide groups may be incapable of forming *intra*-molecular hydrogen bonds for steric reasons.

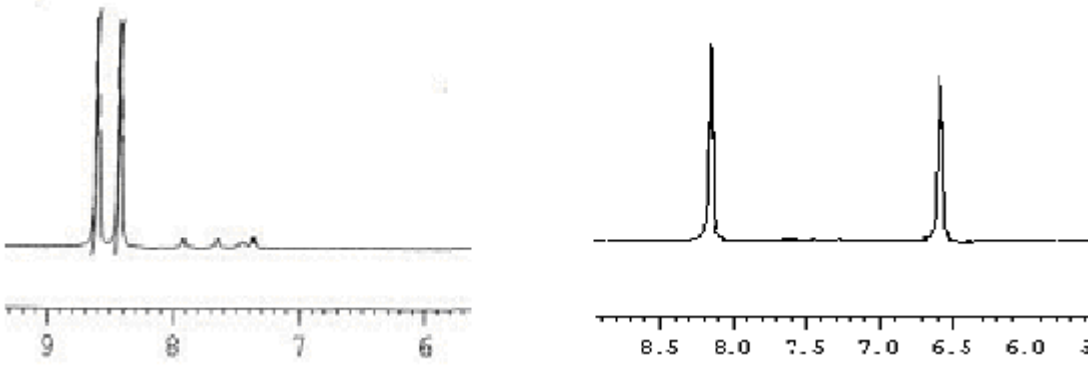

*Fig. 8: The ferrocenoyl protons of **130** in d^6 DMSO (left) and $CDCl_3$ (right).*

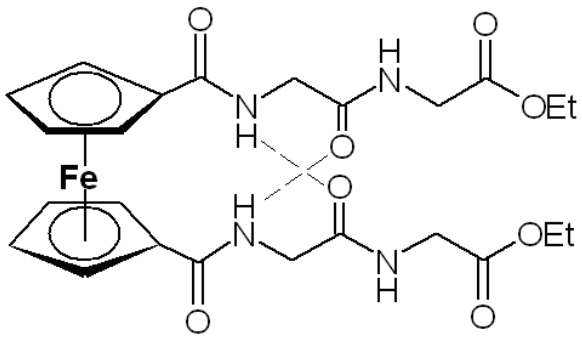

*Fig. 9: Intra-molecular hydrogen bonding of **130** in non-polar solution. The **C**-terminal amide protons do not form such bonds.*

4.3.4: ^{1}H-NMR Spectrum of 124

Compound **124** (*fig. 10*) is unusual in that it is derived from (1S, 2R)-(+)- norephedrine, and hence does not include any ester groups. In d^6 DMSO, the amide protons of **124** appear at 7.72 ppm, while in $CDCl_3$, these protons appear at 6.49 ppm, and hence would appear incapable of forming the hydrogen bonds typical of the compounds discussed so far in this chapter.

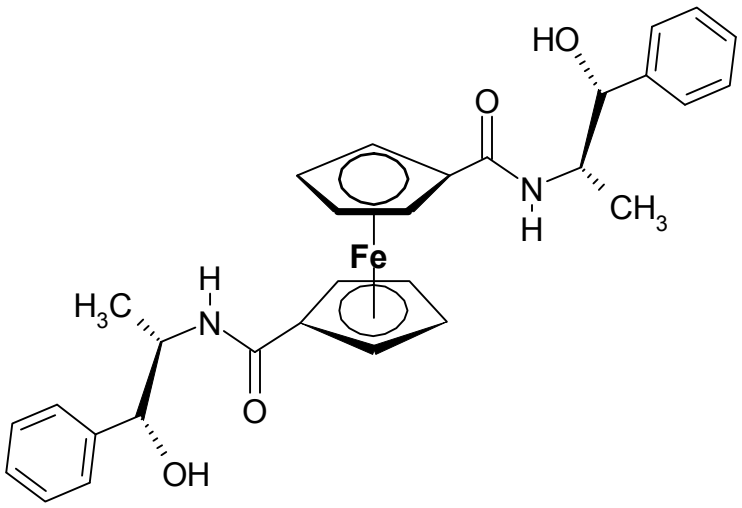

*Fig. 10: the 1, 3 conformation adopted by **124** in solution*

This observation would suggest that the oxygen atoms of the ester groups function as donors in the *intra*-molecular hydrogen bonding in the 1, 1'-disubstituted dipeptides, and that the hydroxy groups of **124** are unable to fulfil a similar function. It would also suggests that **124** is likely to exists in a 1, 3 conformation in solution, rather than the 1, 1'-conformation adopted by those compounds with β-sheet like structures.

4.4: ^{13}C-NMR Spectrum of 1, 1'-*N*-Ferrocenoyl Symmetric Dipeptides

As was inferred from the ^{1}H-NMR data recorded for these compounds, where all signals integrate for multiples of two, the ^{13}C-NMR spectra also suggest a symmetrical conformation in solution, with a maximum of one signal per two carbon atoms being observed. For example, **119** contains twenty-two carbon atoms, and eleven signals are present in its ^{13}C-NMR spectrum. Similarly, **131** contains twenty six carbon atoms, and thirteen signals are present in its spectrum.

A very similar pattern of signals is observed in the ^{13}C-NMR spectra of the chiral 1, 1'-***N***-ferrocenoyl symmetric dipeptides in terms of the ferrocenoyl carbons as well as those of the amide and ester carbonyl carbons. In all cases, two *ortho*-carbon signals (*ca.* 70ppm), two *meta*-carbon signals (*ca.* 72 ppm), and one *ipso*-carbon signal (*ca.* 77ppm) are observed. This data is summarised in *table 3*.

Compound	$C{=}O_{amide}$	$C{=}O_{ester}$	C_{ortho}	C_{meta}	C_{ipso}
113	169.48	173.45	69.63, 70.86	72.19, 72.29	77.13
114	168.96	171.02/171.72	69.91, 70.07	72.62, 72.66	76.71
115	169.60	172.76	68.79, 71.74	71.85, 72.32	76.93
116	169.73	173.07	69.67, 70.83	72.30, 72.46	76.93
117	169.02	174.90	70.36	72.03	77.19
118	169.50	173.76	69.50, 70.95	72.14, 72.23	77.12
119	169.35	171.88	69.73, 70.62	72.55, 72.69	76.92
120	169.32	171.56	69.96, 70.87	72.32, 72.46	76.71
121	169.50	172.37/172.58	69.76, 70.53	72.31, 72.46	76.97
122	169.65	171.67	70.01, 70.18	72.62, 72.71	76.89
123	169.85	172.91	68.75, 71.78	72.05, 72.32	76.95
124	168.14	-	68.97, 71.20	71.38, 71.75	78.21
125	169.54	173.18	69.03, 71.37	71.80, 72.23	76.91
126	169.53	170.59	69.98	72.51	77.00
127	169.05	172.31	69.88	72.05	77.81
128	168.78	173.57	69.82	71.80	78.28
129	167.68	173.69	69.86	73.11	78.87
130	169.32, 169.99	171.17	70.31	71.73	76.98
131	169.49	173.07	69.75, 70.73	72.10, 72.28	77.15
132	169.28	171.61	70.07, 70.29	72.48, 72.52	76.89
133		169.69		72.34	77.62

*Table 3: The ^{13}C-NMR chemical shifts (δ ppm) of the 1, 1'-**N**-*ferrocenoyl *symmetric dipeptides recorded in d^6 DMSO.*

4.4.1: ^{13}C-NMR Spectrum of 131

The ^{13}C-NMR spectrum of **131** is shown in *fig.11*. Two signals, corresponding to the methyl carbons of the side chains and ethyl ester groups, appear at 13.78 and 14.47 ppm respectively, while the methylene carbons of the side chains appear at 29.29 and 32.70 ppm, both of which are seen as negative peaks in the 135DEPT spectrum (*fig. 12*). The chiral α-carbon is observed at 52.34 ppm, while the methylene carbons of the ethyl ester groups appear at 60.86 ppm.

In common with all the chiral 1'1 ***N***-ferrocenoyl symmetric dipeptides discussed in this chapter, the five resonances for the ten ferrocenoyl carbons of **131** are observed in its ^{13}C-NMR spectrum, the *ortho*-carbons at 69.75 and 70.73, the *meta*-carbons at 72.10 and 72.28 ppm, with the *ipso*-carbons at 77.15 ppm. A comparison between this pattern of signals, and that recorded in the case of the monosubstituted analogue **63**, is illustrated in *fig. 13*.

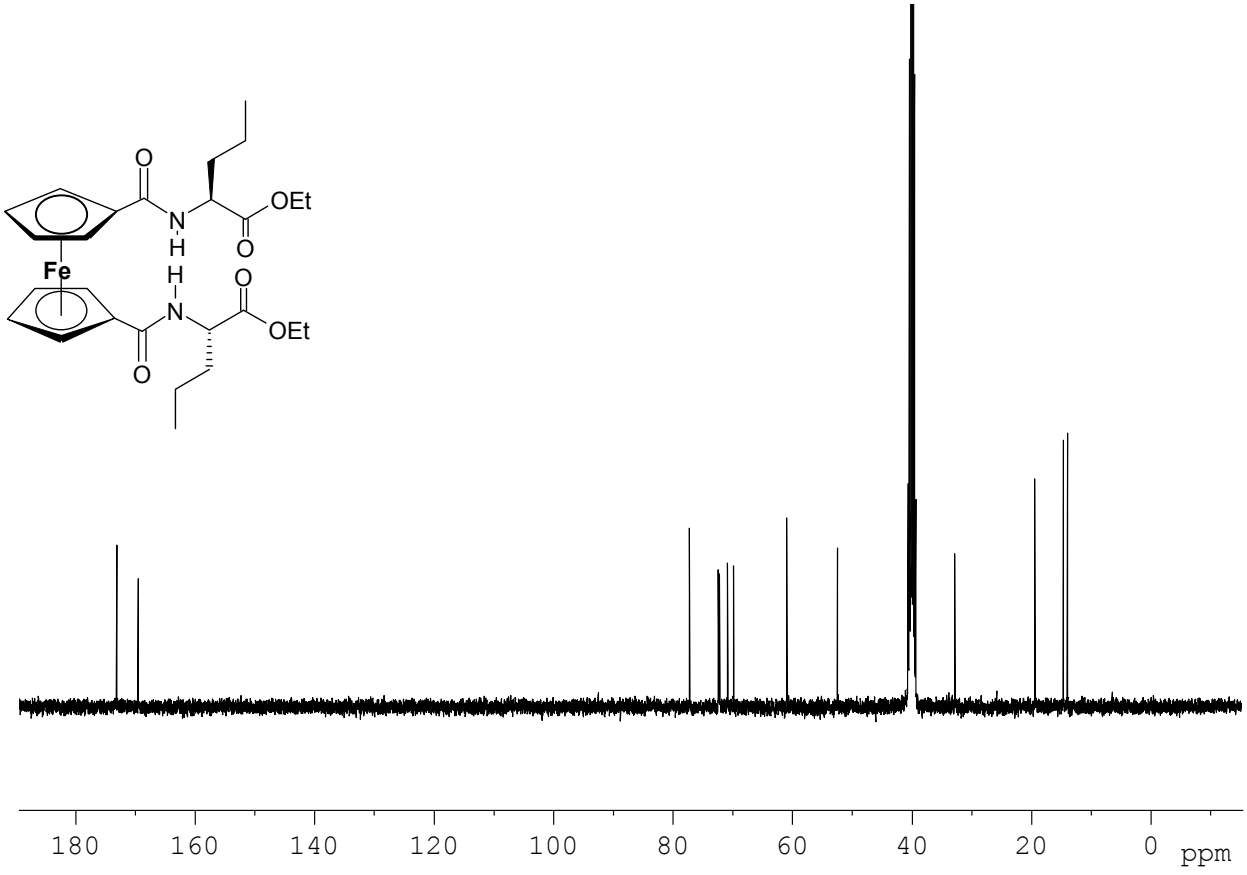

*Fig. 11: The ^{13}C-NMR Spectrum of **131** in d^6 DMSO.*

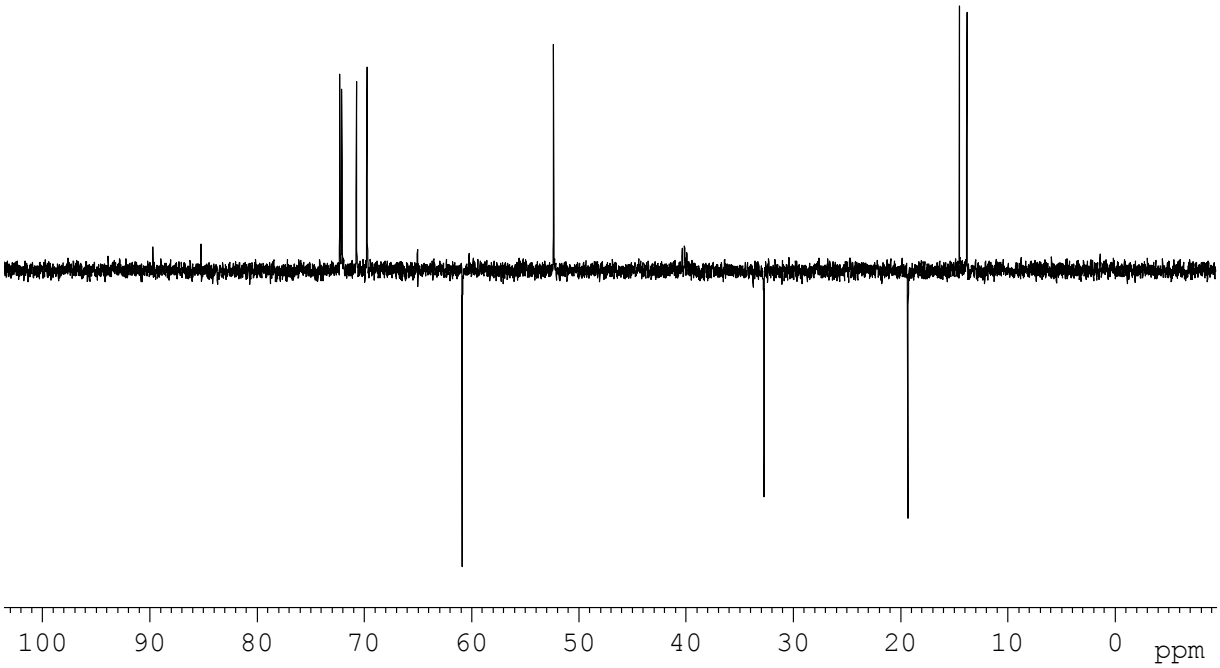

*Fig. 12: The 135DEPT Spectrum of **131** in d^6 DMSO.*

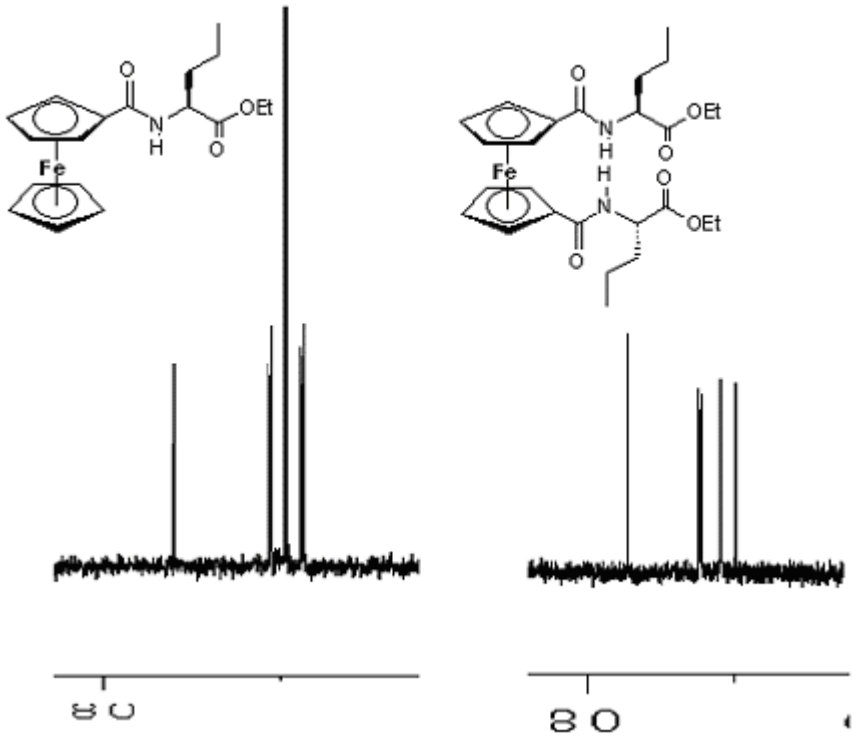

*Fig. 13: The ferrocenoyl carbon resonances of **63** (left) and **131** (right).*

The ^{13}C-NMR spectrum of **63** shows two closely spaced *ortho*-carbon signals at 69 ppm, the unsubstituted Cp ring carbons at 70 ppm, two closely spaced meta-carbon signals at 71 ppm, and the ipso-carbon signal *ca*. 76 ppm. What is noticeable from the comparison of these spectra is the spacing of the *ortho*-carbon signals, which, in the case of **63**, are *ca*. 0.2 ppm apart, while the difference in chemical shift is in the spectrum of **131** is ca. 1 ppm. Clearly, the adjacent chiral centre has a greater effect on the magnetic environment of these carbons in **131** than in **63**. The quaternary carbons of the amide and ester groups appear as signals at 169.49 and 173.07 ppm respectively.

4.4.2: ^{13}C-NMR Spectra of 126-129

The ^{13}C-NMR spectrum of **128** is shown in *fig. 14*. The methylene carbons of the peptide backbone appear as signals at 25.01, 31.09, and 38.43 ppm, while a resonance for methyl carbons of the ester groups is seen at 51.64 ppm.

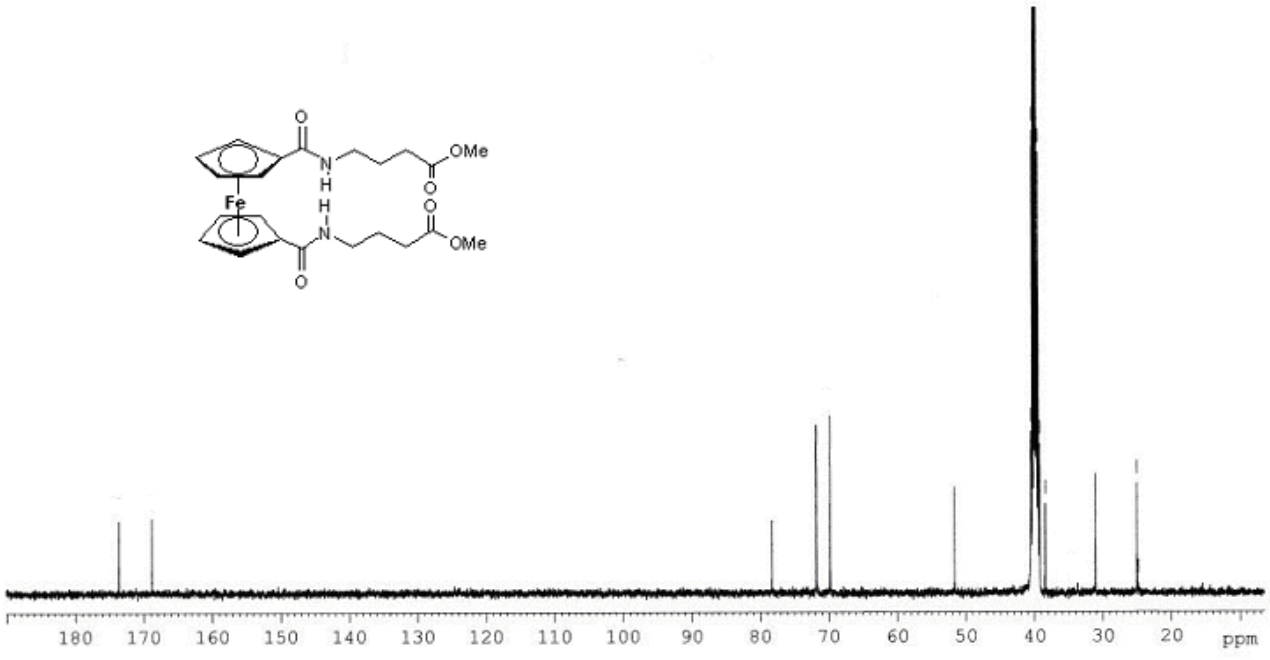

*Fig. 14: The ^{13}C-NMR Spectrum of **128** in d^6 DMSO.*

The pattern of signals corresponding to the ferrocenoyl carbons is typical of the achiral disubstituted ferrocenes **126-129**, with only three signals being observed, with an *ortho*-carbon signal at 69.82 ppm, a meta-carbon signal at 71.80 ppm, and the ipso-carbon signal at 78.28 ppm. The fact that all four *ortho*-carbons appear as one signal shows not only the symmetrical nature of the conformation adopted by **128** in solution, but also further demonstrates the effect of an adjacent chiral centre, as discussed in the previous section. This is illustrated in *fig. 15*, which compares the ferrocenoyl carbon resonances of **128**, and the chiral **119**.

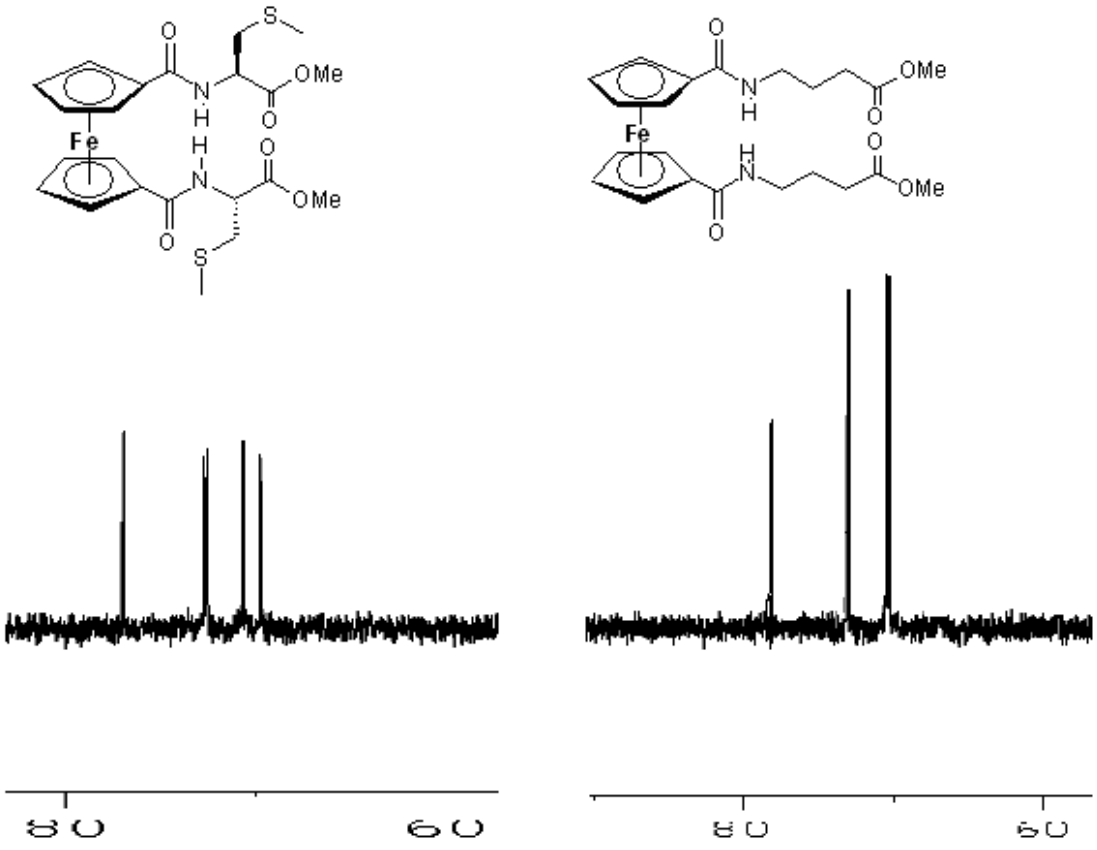

*Fig. 15: The ferrocenoyl carbon resonances of **119** (left) and **128** (right).*

4.5: InfraRed Spectra of 1, 1'-*N*-Ferrocenoyl Symmetric Dipeptides

A summary of the infrared data recorded for compounds **113-133** is given in table 4.

Compound	υ_{N-H}	υ_{COOR}	υ_{CONR}	υ_{N-H} (CH_2Cl_2)
113	3294	1735	1630	3349
114	3302	1739, 1721	1638	3371
115	3285	1740	1632	3362
116	3294	1741	1630	3343
117	3326	1742	1627	3361
118	3326	1742	1633	3349
119	3292	1737	1629	3367
120	3315		1637	3384
121	3332	1720, 1735		3335
122	3361		1635	3366
123	3365	1721	1638	3353
124	3328	-	1628	3411
125	3383	1766	1629	3358
126	3351	1732	1633	3368
127	3292	1737	1633	3354
128	3327	1729	1629	3351
129	3365	1731	1641	3363
130	3300, 3344	1747	1612, 1638	3367, 3409
131	3294	1735	1630	3345
132		1736	1617	3372
133	-	1744	1617	-

*Table 4: Infrared data for **113-133** (cm^{-1}) (as KBr discs unless stated)*

Infrared spectra of compounds **113-133** were recorded, both as KBr discs, and in solution as thin-film methylene chloride solutions, and further serve to illustrate the equivalence by symmetry of the various functional groups within these compounds. Irrespective of whether the spectra were recorded in the solid state or in solution, in general, only one C=O amide band, one

ester C=O band, and one N-H amide band is observed. The latter of these consistently appear below 3400 cm^{-1}, which is diagnostic of hydrogen-bonded amide protons.

Compound **124** has a N-H amide stretch in its CH_2Cl_2 spectrum at 3411 cm^{-1}, which is consistent with the position of its amide proton in the $CDCl_3$ ^1H spectrum (6.49 ppm), and suggests the absence of an ester oxygen atom is responsible for the inability of **124** to adopt a hydrogen bonded conformation in solution. **130** shows two N-H amide stretches in its CH_2Cl_2 spectrum, at 3367 and 3409 cm^{-1}, which further supports the idea that only the ***N***-terminal amide protons are capable of forming hydrogen bonds in solution.

4.6: UV-Vis Spectra of 1, 1'-*N*-Ferrocenoyl Symmetric Dipeptides

The UV-Vis spectra of all the disubstituted ferrocenes discussed in this chapter differ from their mono- substituted analogues in terms of the second low-energy band. Although the lowest energy electronic transition remains unaltered, being observed *ca.* 405nm, the λ_{max} of this second low-energy band undergoes a red shift of ca. 40nm relative to the monosubstituted analogues. It is known that interaction of the Cp rings of ferrocene with other π-systems causes a far greater perturbations to the ligand-based orbitals (e_{1u}, e^*_{2u}) than to the metal-based HOMOs, [9, 10], and results in the low-lying Cp π* orbitals being shifted to lower energy. Substitution of the both Cp rings accentuates this effect. This would explain why this MLCT band is observed at lower energy for the disubstituted compounds. All the extinction coefficients recorded for the lowest energy band are consistent with the values obtained for the monosubstituted analogues.

4.7: Cyclic Voltammogramms of 1, 1'-*N*-Ferrocenoyl Symmetric Dipeptides.

A summary of the UV-Vis and electrochemical data is given in *table 5*. The 1, 1'-disubstituted ferrocenes exhibit a reversible, one-electron peak in their cyclic voltammograms, due to oxidation of the ferrocene moiety to the ferricenium cation, similar to the monosubstituted derivatives. There is, however, a dramatic anodic shift of this peak relative to the monosubstituted derivatives, as can be seen in *fig. 16*, which shows the voltammograms of **131**, and its mono-substitutes analogue **63**.

Compound	λ_{max} (nm)	ε (M^{-1} cm^{-1})	$[\alpha]_D^{20}$	$E_{1/2}$(mV)
113	344, 445	195	- 28°	0.344
114	342, 444	209	- 26°	0.359
115	341, 444	211	- 23°	0.348
116	344, 445	198	- 18°	0.354
117	343, 446	198	-	0.362
118	346, 444	200	- 26°	0.349
119	344, 444	202	- 31°	0.340
120	343, 445	218	- 32°	0.348
121	344, 444	187	- 26°	0.348
122	346, 445	193	- 27°	0.359
123	343, 444	199	- 27°	0.359
124	344, 444	199	21°	0.351
125	345, 444	186	- 18°	0.337
126	344, 445	206	-	0.344
127	342, 446	190	-	0.340
128	344, 444	190	-	0.340
129	345, 441	176	-	0.330
130	340, 442	200	-	0.338
131	344, 445	196	- 22°	0.348
132	345, 442	172	- 19°	0.353
133	345, 446	193	-	0.302

Table 5: The electrochemical, UV-Vis, and optical data for compounds **113-133.** *All ε values refer to lowest energy band.*

Relative to the Fc/Fc^+ couple, the redox potential of **63** was recorded at 187 mV, while that of **131** was determined to be 348mV. The presence of an electron-withdrawing amide group on the second Cp ring obviously has the effect of lowering the energy of the ferrocene e_{2g} orbital even further, thus making the molecule more difficult to oxidize (section 1.4). It has been previously

established that the redox potential of the ferrocene moiety is sensitive to the number of electron-withdrawing substituents [9], and it is therefore not surprising that such an anodic shift should be observed.

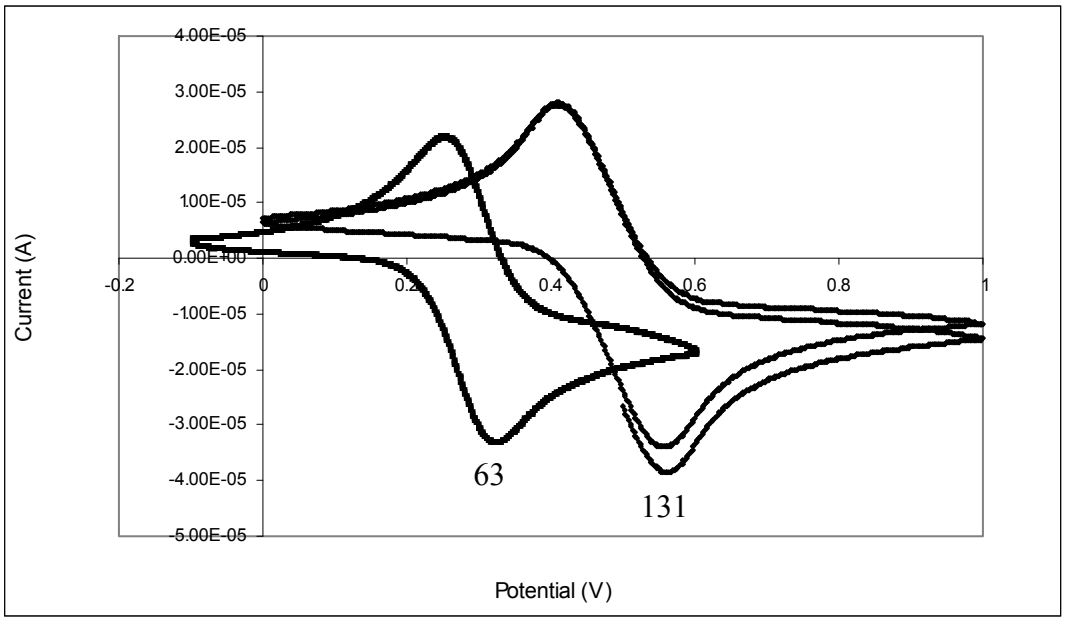

*Fig. 16: The cyclic voltammogramms of **63** and **131**.*

4.8: Conclusions

DCC and TBTU proved effective coupling reagents in the synthesis of compounds **113-133**, although no active esters could be isolated during column chromatography. Despite the difference in reaction stoichiometry, the yields achieved were comparable to those recorded during the preparation of the monosubstituted compounds. Attempts to prepare **116** and **123** using CDI as a coupling reagent failed, possibly due to the formation of a presumably unstable bis-imidazole intermediate.

Both the ^{1}H-NMR and infrared spectra of these compounds clearly show the presence of hydrogen-bonded amide protons, with the ester carbonyl oxygen atom acting as a donor (*fig. 17*), with an anti-parallel, β-sheet-like conformation being adopted in solution (section 1.3.1). Elongation of the peptide backbone, as seen in the case of **126-129**, does not prevent these hydrogen bonds being formed. Addition of further residues to the ***C***-terminal, as in **130**, does not allow for the formation of further anti-parallel hydrogen-bonding, possibly because this would

result in out of plane twisting of the Cp rings. In this respect, the ferrocene moiety may function as a 'constraining' unit, limiting the flexibility of the peptide chain [8].

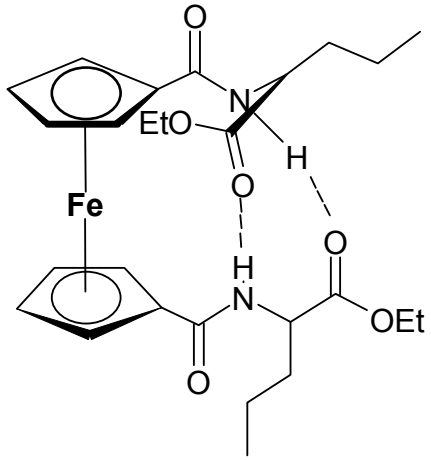

*Fig. 17: β-sheet-like Conformation of **131** in solution.*

Both the ^{1}H and ^{13}C-NMR clearly show a more pronounced influence of an adjacent chiral centre on the magnetic environments of the ferrocenoyl protons and carbon atoms than was observed with the monosubstituted derivatives. There is also a noticeable red shift in the UV-Vis spectra of these compounds, with the second low energy band being observed *ca*. 340 nm (vs. 300 nm for the monosubstituted). Large anodic shifts in the cyclic voltammograms of these compounds are observed, with the redox potential being recorded in the 330-350 mV region (vs. Fc/Fc^{+}).

4.9: Experimental

Synthesis of 1, 1'-Ferrocene dicarboxylic acid (**112**).

9.3g (0.05mol) of ferrocene, 20ml (0.05mol) of a 2.5M solution of n-butyl lithium in hexanes, and 11.3ml (0.075mol) of tetramethylethylenediamine were added to a 500ml round bottomed flask containing 300ml of dry hexane. The solution was kept in the dark and stirred overnight, giving an orange precipitate of the lithiated ferrocene complex. The reaction mixture was then cooled to 0°C, and a vigorous stream of dry CO_2 was bubbled through the mixture for 20

minutes, giving a brown precipitate. The hexane solution was then extracted with water (3 x 250ml), and the aqueous portions were combined, acidified to pH 1-2 with conc. HCl, and the precipitate was collected by vacuum filtration, and dried for ca. 24 hrs at 80°C affording the title product as a light brown powder (*scheme 3*).

Yield 10.14g (74%), m.p. > 300°C.

^{1}H-NMR (400MHz) δ ($CDCl_3$): 4.40 (4H, br. s, H_{meta} Cp ring), 4.77 (2H, s, H_{ortho} Cp ring), 4.89 (2H, s, H_{ortho} Cp ring), 12.11 (2H, br. s, FcCOO<u>H</u>).

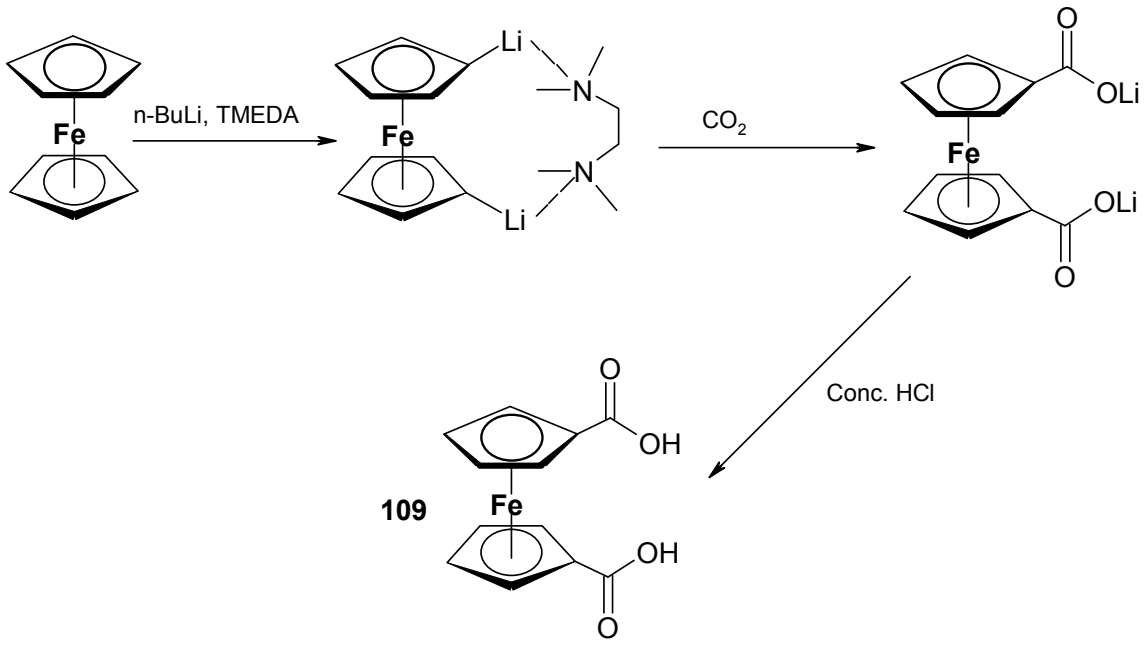

Scheme 3: Preparation of ferrocene dicarboxylic acid.

Synthesis of 1, 1'-*N*-Ferrocenoyl Symmetric Dipeptides

Route 1, General Procedure

DCC (0.4g , 2.4mmol), 2mmol of the appropriate amino acid ester, 0.38mls (2.4mmol) Et_3N and 1-hydroxybenzotriazole (0.14g , 1mmol) were added to a slurry of ferrocene dicarboxylic acid (0.27g, 1 mmol) in 20mls DCM, at 0˚C. The reaction was raised to room temperature after

30 mins, and allowed to proceed for 24 hrs. The precipitated ***N***, ***N*** - dicyclohexylurea was removed by filtration, and the solvent evaporated *in vacuo*. The crude product was then eluted from a column of silica gel, using a mobile phase of 2:1 ethyl acetate/ hexane.

Route 2, General Procedure

2mmol of the appropriate amino acid ester, CDI (0.39g, 2.4mmol), 0.38mls (2.4mmol) Et_3N, were added to a slurry of ferrocene dicarboxylic acid (0.27g, 1 mmol) in 20mls THF, at 0˚C. The reaction was raised to room temperature after 30mins, and allowed to proceed for 24 hrs. No target compounds were recovered using this method.

Route 3, General Procedure

0.83 g of O- (1H-benzotriazol-1-yl) - ***N, N, N', N***', - tetramethyluronium tetrafluoroborate (2.5mmol) and 0.4 ml (2.4mmol) of triethylamine were added to slurry of ferrocene dicarboxylic acid (0.27g, 1mmol) in dimethylformamide (30mls), at ambient temperature. After 30 mins, 2.4mmol of the appropriate amino acid ester hydrochloride salt was added, and stirring was continued for 24 hrs. The solvent evaporated *in vacuo*, and the crude product was purified by silica gel column chromatography using a mobile phase of 2:1 ethyl acetate/hexane.

1, 1'- *N*-ferrocenoyl-(L-norleucine methyl ester)$_2$ (113)

0.36g of L-norleucine methyl ester hydrochloride was used in the synthesis.

Yields: Route 1, 0.41g (73%), Route 2 0.43g (75%), m.p. 180-182°C.

$E_{1/2}$ = 0.344mV (Vs. Fc/Fc+), $[\alpha]_D^{20}$ = - 28° (EtOH), (UV-Vis (λ_{max}) (EtOH): 344, 445 nm (ε = 195 M^{-1} cm^{-1}), I.R. υ_{max} (KBr): 3099, 2972, 1932, 1735, 1630, 1442, 1427, 1413, 1320, 1185, 1140, 1027, 486, cm^{-1}.

^{1}H-NMR (400MHz) δ (*d*^{6} DMSO): 0.90 (6H, t, *J* = 6.0 Hz, -$CH_2CH_2CH_2C\underline{H}_3$ x 2), 1.24-1.41 (8H, m, -$CH_2C\underline{H}_2C\underline{H}_2CH_3$ x 2), 1.69-1.81 (4H, m, -$C\underline{H}_2CH_2CH_2CH_3$ x 2) 3.67 (6H, s, -$OC\underline{H}_3$ x 2), 4.31-4.38 (4H, m, -NHC<u>H</u>- x 2 + H_{meta} Cp ring), 4.43 (2H, s, H_{meta} Cp ring), 4.84 (2H, s, H_{ortho} Cp ring), 4.87 (2H, s, H_{ortho} Cp ring), 8.17 (2H, d, *J* = 7.6 Hz, -N<u>H</u>CH- x 2).

^{13}C-NMR (100 MHz) δ (*d*^{6} DMSO): 14.16, 22.02 (-ve DEPT), 28.22 (-ve DEPT), 30.37 (-ve DEPT), 52.24, 52.46, 69.63, 70.86, 72.19, 72.29, 77.13, 169.48, 173.45.

1, 1'-*N*-ferrocenoyl-(L-aspartic acid dimethyl ester)$_2$ (114)

0.39g of L-aspartic acid dimethyl ester hydrochloride was used in the synthesis.

Yield 0.38g (68%), m.p.198-200°C.

$E_{1/2}$ = 0.359mV (Vs. Fc/Fc+), $[\alpha]_D^{20}$ = - 26° (EtOH), (UV-Vis (λ_{max}) (EtOH): 342, 444 nm (ε = 209 M^{-1} cm^{-1}), I.R. υ_{max} (KBr): 3302, 3102, 2954, 1739, 1638, 1544, 1439, 1310, 1275, 1225, 1002, 663, 507, cm^{-1}.

^{1}H-NMR (400MHz) δ (*d*^{6} DMSO): 2.82 (2H, dd, J_a = 8.0 Hz, J_b = 16.0 Hz, NHCH(C<u>H</u>$_2$-)), 2.96 (2H, dd, J_a = 5.2 Hz, J_b = 16.0 Hz, NHCH(C<u>H</u>$_2$-)), 3.61 (6H, s, -OC<u>H</u>$_3$ x 2), 3.66 (6H, s, -OC<u>H</u>$_3$ x 2), 4.37 (4H, br. s, H_{meta} Cp ring), 4.75 (2H, m, -NHC<u>H</u>- x 2), 4.80 (2H, s, H_{ortho} Cp ring), 4.82 (2H, s, H_{ortho} Cp ring), 8.30 (2H, d, *J* = 7.6 Hz, -N<u>H</u>CH- x 2).

^{13}C-NMR (100 MHz) δ (*d*^{6} DMSO): 29.10 (-ve DEPT), 49.16, 52.05, 52.62, 69.91, 70.07, 72.62, 72.66, 76.71, 168.96, 171.02, 171.72.

1, 1'-*N*-ferrocenoyl-(L-phenylalanine methyl ester)$_2$ (115)

0.43g of L-phenylalanine methyl ester hydrochloride was used in the synthesis.

Yield 0.43g (72%), , m.p. 211-213°C.

$E_{1/2}$ = 0.348mV (Vs. Fc/Fc+), $[\alpha]_D^{20}$ = - 23° (EtOH), (UV-Vis (λ_{max}) (EtOH): 341, 444 nm (ε = 211 M^{-1} cm^{-1}), I.R. υ_{max} (KBr): 3219, 2952, 1740, 1632, 1540, 1271, 1223, 1195, 1097, 1043, 811, 740, 487, cm^{-1}.

^{1}H-NMR (400MHz) δ (*d*^{6} DMSO): 3.04 (2H, dd, J_a = 12.0 Hz, J_b = 12.4 Hz, NHCH(C<u>H</u>$_2$-)), 3.18 (2H, dd, J_a = 11.2 Hz, J_b = 12.4 Hz, NHCH(C<u>H</u>$_2$-)), 3.69 (6H, s, -OC<u>H</u>$_3$ x 2), 4.10 (4H, d, *J* = 7.6 Hz, H_{meta} Cp ring), 4.49 (2H, s, H_{ortho} Cp ring), 4.68 (4H, m, H_{ortho} Cp ring + NHC<u>H</u>- x 2), 7.22-7.35 10H, m, ArH), 8.34 (2H, d, *J* = 8.0 Hz, -N<u>H</u>CH- x 2).

^{13}C-NMR (100 MHz) δ (*d*^{6} DMSO): 36.49 (-ve DEPT), 52.41, 54.09, 68.79, 71.74, 71.85, 72.32, 76.93, 126.90, 128.65, 129.42, 138.19, 169.60, 172.76.

1, 1'-*N*-ferrocenoyl-(L-methionine methyl ester)$_2$ (116)

0.04g of L-methionine methyl ester hydrochloride was used in the synthesis.

Yield 0.41g (73%), m.p. 220-223°C.

$E_{1/2}$ = 0.354mV (Vs. Fc/Fc+), $[\alpha]_D^{20}$ = - 18° (EtOH), (UV-Vis (λ_{max}) (EtOH): 344, 445 nm (ε = 198 M^{-1} cm^{-1}), I.R. υ_{max} (KBr): 1543, 1460, 1381, 1302, 1186, 1027, 671, 487 cm^{-1}.

^{1}H-NMR (400MHz) δ (*d*^{6} DMSO): 2.02-2.07 (10H, m, -C<u>H</u>$_2$SC<u>H</u>$_3$ x 2), 2.54-2.64 (4H, m, -C<u>H</u>$_2$CH$_2$SCH$_3$ x 2), 3.67 (6H, s, -OC<u>H</u>$_3$ x 2), 4.38 (2H, s, H$_{meta}$ Cp ring), 4.43 (2H, s, H$_{meta}$ Cp ring), 4.50-4.54 (2H, m, -NHC<u>H</u>- x 2), 4.82 (2H, s, H$_{ortho}$ Cp ring), 4.87 (2H, s, H$_{ortho}$ Cp ring), 8.22 (2H, d, *J* = 7.2 Hz, -N<u>H</u>CH- x 2).

^{13}C-NMR (100 MHz) δ (*d*^{6} DMSO): 14.86, 30.16 (-ve DEPT), 30.21 (-ve DEPT), 51.43, 52.41, 69.67, 70.83, 72.30, 72.46, 76.93, 169.73, 173.07.

1, 1'-*N*-ferrocenoyl-(2-isoaminobutyric acid methyl ester)$_2$ (117)

0.31g of 2-isoaminobutyric acid methyl ester hydrochloride was used in the synthesis.

Yield 0.31g (66%), orange solid, m.p. 201-203°C.

$E_{1/2}$ = 0.362mV (Vs. Fc/Fc+), (EtOH), UV-Vis (λ_{max}) (EtOH): 343, 446 nm (ε = 198 M^{-1} cm^{-1}), I.R. υ_{max} (KBr): 1538, 1438, 1314, 1277, 1150, 933, 507 cm^{-1}.

^{1}H-NMR (400MHz) δ (*d*^{6} DMSO): 1.44 (12H, s, –NHC(C<u>H</u>$_3$)$_2$- x 2), 3.62 (6H, s, -OC<u>H</u>$_3$ x 2), 4.40 (4H, s, H$_{meta}$ Cp ring), 4.79 (4H, s, H$_{ortho}$ Cp ring), 8.09 (2H, s, –N<u>H</u>C(CH$_3$)$_2$- x 2).

^{13}C-NMR (100 MHz) δ (*d*^{6} DMSO): 25.32, 52.21, 55.68, 70.36, 72.03, 77.19, 169.02, 174.90.

1, 1'-*N*-ferrocenoyl-(L-leucine methyl ester)$_2$ (118)

0.36g of L-leucine methyl ester hydrochloride was used in the synthesis.

Yield 0.37g (70%), orange solid, m.p. 217-220°C.

$E_{1/2}$ = 0.349mV (Vs. Fc/Fc+), $[\alpha]_D^{20}$ = –26° (EtOH), UV-Vis (λ_{max}) (EtOH): 346, 444 (ε = 200 M^{-1} cm^{-1}), I.R. υ_{max} (KBr): 3326 2930, 2363, 2121, 1742, 1633, 1538, 1437, 1301, 1221, 1148, 670, 509 cm^{-1}.

^{1}H-NMR (400MHz) δ (*d*^{6} DMSO): 0.90 (6H, d, *J* = 6.4 Hz, -CH$_2$CH(C<u>H</u>$_3$)$_2$), 0.95 (6H, d, *J* = 6.4 Hz, -CH$_2$CH(C<u>H</u>$_3$)$_2$), 1.22-1.26 (2H, m, -CH$_2$C<u>H</u>(CH$_3$)$_2$ x 2), 1.71-1.77 (4H, m, -C<u>H</u>$_2$CH(CH$_3$)$_2$ x 2), 3.67 (6H, s, -OC<u>H</u>$_3$ x 2), 4.35 (2H, br. s, , -NHC<u>H</u>- x 2), 4.43 (4H, s, H$_{meta}$ Cp ring), 4.83 (4H, s, H$_{ortho}$ Cp ring), 8.18 (2H, d, *J* = 8.0 Hz, -N<u>H</u>CH- x 2).

^{13}C-NMR (100 MHz) δ (*d*^{6} DMSO): 21.31, 23.29, 24.77, 39.44 (-ve DEPT), 52.28, 69.50, 70.95, 72.10, 72.33, 77.12, 169.50, 173.76.

1, 1'-*N*-ferrocenoyl- ((S-methyl)-L-cystine methyl ester))$_2$ (119)

0.37g of (S-methyl)-L-cystine methyl ester hydrochloride was used in the synthesis.

Yield 0.42g (78%), orange microcrystalline solid. m.p. 186-187°C.

$E_{1/2}$ = 0.340mV (Vs. Fc/Fc+), $[\alpha]_D^{20}$ = - 31° (EtOH), (UV-Vis (λ_{max}) (EtOH): 344, 444 nm (ε = 202 M^{-1} cm^{-1}), I.R. υ_{max} (KBr): 3292, 2920, 2366, 1737, 1629, 1545, 1434, 1381, 1312, 1217, 1103, 673, 497 cm^{-1}.

^{1}H-NMR (400MHz) δ (*d*^{6} DMSO): 2.13 (6H, s, -SC<u>H</u>$_3$ x 2), 2.90-3.00 (4H, m, -C<u>H</u>$_2$SCH$_3$ x 2), 3.69 (6H, s, -OC<u>H</u>$_3$ x 2), 4.41 (2H, s, H_{meta} Cp ring), 4.44 (2H, s, H_{meta} Cp ring), 4.58-4.59 (2H, m, –NHC<u>H</u>- x 2), 4.86 (2H, s, H_{ortho} Cp ring), 4.89 (2H, s, H_{ortho} Cp ring), 8.28 (2H, d, *J* = 7.6 Hz, –N<u>H</u>CH- x 2).

^{13}C-NMR (100 MHz) δ (*d*^{6} DMSO): 15.36, 34.61 (-ve DEPT), 51.92, 52.50, 69.73, 70.62, 72.55, 72.69, 76.92, 169.35, 171.88.

1, 1'-*N*-ferrocenoyl-(L-phenylglycine methyl ester)$_2$. (120)

0.40g of L-phenylglycine methyl ester hydrochloride was used in the synthesis.

Yield 0.41g (72%), orange solid, m.p. 200-203°C.

$E_{1/2}$ = 0.348mV (Vs. Fc/Fc+), $[\alpha]_D^{20}$ = - 32° (EtOH), (UV-Vis (λ_{max}) (EtOH): 343, 445 nm (ε = 218 M^{-1} cm^{-1}), I.R. υ_{max} (KBr): 3315, 2953, 2363, 2342, 1637, 1527, 1499, 1219, 1173, 1100, 1026, 698, 506 cm^{-1}.

^{1}H-NMR (400MHz) δ (*d*^{6} DMSO): 3.67 (6H, s, -OC<u>H</u>$_3$ x 2), 4.35 (2H, s, H_{meta} Cp ring), 4.39 (2H, s, H_{meta} Cp ring), 4.90 (4H, br. s, H_{ortho} Cp ring), 5.58 (2H, d, *J* = 5.6Hz, NHC<u>H</u>- x 2), 7.39-7.48 (10H, m, ArH), 8.56 (2H, d, *J* = 5.6 Hz, -N<u>H</u>CH- x 2).

^{13}C-NMR (100 MHz) δ (*d*^{6} DMSO): 52.61, 56.97, 65.29, 69.96, 70.87, 72.32, 72.46, 76.71, 128.54, 128.64, 128.88, 136.64, 169.32, 171.56.

1, 1'-*N*-ferrocenoyl-(L-glutamic acid diethyl ester)$_2$ (121)

0.39g of L-glutamic acid dimethyl ester hydrochloride was used in the synthesis.

Yield 0.38g (68%), orange solid, m.p. 154-157°C.

$E_{1/2}$ = 0.348mV (Vs. Fc/Fc+), $[\alpha]_D^{20}$ = - 26° (EtOH), (UV-Vis (λ_{max}) (EtOH): 344, 444 nm (ε = 187 M^{-1} cm^{-1}), I.R. υ_{max} (KBr): 3332, 3090, 2991, 1735, 1720, 1539, 1291, 1167, 1027, 772, 667, 490 cm^{-1}.

^{1}H-NMR (400MHz) δ (d^6 DMSO): 1.15-1.24 (12 h, m, $OCH_2C\underline{H}_3$ x 4), 1.93-1.96 (2H, m, -$C\underline{H}_2CH_2COOEt$), 2.08-2.10 (2H, m, -$C\underline{H}_2CH_2COOEt$), 2.50 (4H, t, J = 6.8 Hz, -$CH_2C\underline{H}_2COOEt$ x 2), 4.04-4.14 (8H, m, $OC\underline{H}_2CH_3$ x 4), 4.38 (4H, br. s, H_{meta} Cp ring + -NHC<u>H</u>- x 2), 4.43 (2H, br. s, H_{meta} Cp ring), 4.83 (2H, s, H_{ortho} Cp ring), 4.89 (2H, s, H_{ortho} Cp ring), 8.16 (2H, d, J = 7.2 Hz, -N<u>H</u>CH- x 2).

^{13}C-NMR (100 MHz) δ (d^6 DMSO): 14.43, 25.97 (-ve DEPT), 30.49 (-ve DEPT), 51.81, 60.31 (-ve DEPT), 61.02 (-ve DEPT), 69.76, 70.53, 72.31, 72.46, 76.97, 169.50, 172.37, 172.58.

1, 1'-*N*-ferrocenoyl-(L-threonine methyl ester)$_2$ (122)

0.34g of L-threonine methyl ester hydrochloride was used in the synthesis.

Yield 0.38g (76%), orange solid. m.p. 189-192°C.

$E_{1/2}$ = 0.359mV (Vs. Fc/Fc+), $[\alpha]_D^{20}$ = - 27° (EtOH), UV-Vis (λ_{max}) (EtOH): 346, 445 nm (ε = 193 M^{-1} cm^{-1}), I.R. υ_{max} (KBr): 3361, 3096, 2929, 2365, 1677, 1665, 1635, 1543, 1309, 1211, 1192, 1036, 685 cm^{-1}.

^{1}H-NMR (400MHz) δ (d^6 DMSO): 1.16 (6H, d, J = 6.4 Hz, -CH(OH)C<u>H</u>$_3$ x 2), 3.68 (6H, s, -$OC\underline{H}_3$ x 2), 4.50 (6H, br. s, H_{meta} Cp ring + –NHC<u>H</u>- x 2), 4.87 (2H, s, H_{ortho} Cp ring), 4.97 (2H, s, H_{ortho} Cp ring), 5.06 (2H, d, J = 7.6 Hz, -CH(O<u>H</u>)CH_3 x 2), 7.62 (2H, d, J = 8.4 Hz, –N<u>H</u>CH- x 2).

^{13}C-NMR (100 MHz) δ (d^6 DMSO): 20.60, 52.33, 58.69, 66.63, 70.01, 70.18, 72.62, 72.71, 76.89, 169.65, 171.67.

1, 1'-*N*-ferrocenoyl-(L-tyrosine methyl ester)$_2$ (123)

0.46g of L-tyrosine methyl ester hydrochloride was used in the synthesis.

Yields: Route 1 0.43g (69%), Route 30.43g (69%), orange microcrystalline solid. m.p. 219-212°C.

$E_{1/2}$ = 0.359mV (Vs. Fc/Fc+), $[\alpha]_D^{20}$ = - 27° (EtOH), UV-Vis (λ_{max}) (EtOH): 343, 444 nm (ε = 199 M^{-1} cm^{-1}), I.R. υ_{max} (KBr): 3365, 2367, 1721, 1638, 1550, 1517, 1270, 1222, 1109, 1043, 830, 767, 489 cm^{-1}.

^{1}H-NMR (400MHz) δ (d^6 DMSO): 2.91 (2H, dd, J_a = 13.6 Hz, J_b = 12.4 Hz, –NHCH(C<u>H</u>$_2$)-), 3.06 (2H, dd, J_a = 13.6 Hz, J_b = 4.0 Hz, –NHCH(C<u>H</u>$_2$)-), 3.67 (6H, s, -$OC\underline{H}_3$ x 2), 4.13 (2H, s, H_{meta} Cp ring), 4.18 (2H, s, H_{meta} Cp ring), 4.48 (2H, s, H_{ortho} Cp ring), 4.53-4.59 (2H, m, -

NHCH- x 2), 4.68 (2H, s, H_{ortho} Cp ring), 6.72 (4H, d, *J* = 8.4 Hz, ArH), 7.15 (4h, d, *J* = 8.4 Hz, ArH), 8.32 (2H, d, *J* = 8.0 Hz, –NHCH- x 2), 2H, s, Ph-OH x 2).

^{13}C-NMR (100 MHz) δ (*d*^{6} DMSO): 35.73 (-ve DEPT), 52.38, 54.52, 68.75, 71.78, 72.05, 72.32, 76.95, 115.41, 128.15, 130.35, 156.28, 169.85, 172.91.

1, 1'-*N*-ferrocenoyl-((1S, 2R)-(+)- norephedrine)$_2$ (124)

0.37g of norephedrine hydrochloride was used in the synthesis.

Yield 0.40g (74%), orange solid. m.p. 199-201°C.

$E_{1/2}$ = 0.351mV (Vs. Fc/Fc+), $[\alpha]_D^{20}$ = 21° (EtOH), UV-Vis (λ_{max}) (EtOH): 344, 444 nm (ε = 199 M^{-1} cm^{-1}), I.R. υ_{max} (KBr): 3328, 2930, 2854, 2366, 1628, 1543, 1401, 1312, 1281, 1185, 1028, 998, 745, 701, 490 cm^{-1}.

^{1}H-NMR (400MHz) δ (*d*^{6} DMSO): 1.14 (6H, d, *J* = 6.4 Hz, –NHCH(CH_3)-, x 2), 4.08-4.14 (6H, m, H_{meta} Cp ring + –NHCH(CH_3)- x 2), 4.36 (2H, s, H_{ortho} Cp ring), 4.60 (2H, s, H_{ortho} Cp ring), 4.66 (2H, m, –NHCH(CH_3)CH(OH)Ph, x 2), 4.66 (2H, d, *J* = 4.0 Hz, CH(OH)Ph, x 2), 7.23, 2H, d, *J* = 7.6 Hz, ArH), 7.33 - 7.36 (4H, m, ArH), 7.43 (4H, d, *J* = 7.6 Hz, ArH), 7.72 (2H, d, *J* = 8.8 Hz, –NHCH- x 2).

^{13}C-NMR (100 MHz) δ (*d*^{6} DMSO): 16.23, 50.97, 68.97, 71.20, 71.38, 71.75, 75.06, 78.21, 126.81, 127.17, 128.13, 144.38, 168.14.

1, 1'- *N*-ferrocenoyl-(L-tryptophan methyl ester)$_2$ (125)

0.51g of L-tryptophan methyl ester hydrochloride was used in the synthesis.

Yield 0.42g (64%), red microcrystalline solid. m.p. 167-169°C.

$E_{1/2}$ = 0.337mV (Vs. Fc/Fc+), $[\alpha]_D^{20}$ = - 18° (EtOH), UV-Vis (λ_{max}) (EtOH): 345, 444 nm (ε = 186 M^{-1} cm^{-1}), I.R. υ_{max} (KBr): 3383, 2930, 2365, 1766, 1629, 1543, 1437, 1228, 1103, 743, 499, 427 cm^{-1}.

^{1}H-NMR (400MHz) δ (*d*^{6} DMSO): 3.16-3.22 (2H, m, –NHCH(CH_2)-), 3.27-3.32 (2H, m, –NHCH(CH_2)-), 3.69 (6H, s, -OCH_3 x 2), 4.01 (2H, s, H_{meta} Cp ring), 4.06 (2H, s, H_{meta} Cp ring), 4.51 (2H, s, H_{ortho} Cp ring), 4.65 (2H, s, H_{ortho} Cp ring), 4.67-4.73 (2H, m, -NHCH- x 2), 6.99-7.02 (2H, m, H_{indole}), 7.05-7.09 (2H, m, H_{indole}), 7.28 (2H, s, H_{indole}), 7.35 (2H, d, *J* = 8.0 Hz,

H_{indole}), 7.61 (2H, d, *J* = 7.6 Hz, H_{indole}), 8.22 (2H, d, *J* = 7.6 Hz, –N<u>H</u>CH- x 2), 10.92 (2H, s, N-H_{indole}).

^{13}C-NMR (100 MHz) δ (*d*^{6} DMSO): 26.92 (-ve DEPT), 52.38, 53.61, 69.03, 71.37, 71.80, 72.23, 76.91, 110.34, 111.89, 111.89, 121.36, 124.16, 127.36, 136.53, 169.54, 173.18.

1, 1'-*N*-ferrocenoyl-(glycine ethyl ester)$_2$ (126)

0.28g of glycine ester hydrochloride was used in the synthesis.

Yield 0.32g (71%), orange solid, m.p. 213-215°C.

$E_{1/2}$ = 0.344mV (Vs. Fc/Fc+), (UV-Vis (λ_{max}) (EtOH): 344, 445 nm (ε = 206 M^{-1} cm^{-1}), I.R. υ_{max} (KBr): 3351, 3091, 2904, 1732, 1633, 1540, 1432, 1388, 1317, 1167, 1035, 813, 690, 587 cm^{-1}.

^{1}H-NMR (400MHz) δ (*d*^{6} DMSO): 1.23 (6H, t, *J* = 6.0 Hz, -OCH$_2$C<u>H</u>$_3$ x 2), 3.91 (4H, d, *J* = 6.4 Hz, -NHC<u>H</u>$_2$COOEt x 2), 4.15 (4H, q, *J* = 6.0Hz, -OC<u>H</u>$_2$CH$_3$ x 2) 4.44 (4H, s, H_{meta} Cp ring), 4.83 (4H, s, H_{ortho} Cp ring), 8.31 (2H, t, *J* = 6.4Hz, -N<u>H</u>CH$_2$- x 2).

^{13}C-NMR (100 MHz) δ (*d*^{6} DMSO): 14.48, 41.32 (-ve DEPT), 60.86 (-ve DEPT), 69.98, 72.51, 77.00, 169.53, 170.59.

1, 1'-*N*-ferrocenoyl- (β alanine methyl ester)$_2$ (127)

0.29g of β alanine methyl ester hydrochloride was used in the synthesis.

Yield 0.30g (68 %), orange solid. m.p. 146-148°C.

$E_{1/2}$ = 0.340mV (Vs. Fc/Fc+), UV-Vis (λ_{max}) (EtOH): 342, 446 nm (ε = 190 M^{-1} cm^{-1}), I.R. υ_{max} (KBr): 3292, 2301, 1737, 1633, 1549, 1445, 1379, 1327, 1207, 1177, 1085, 678, 484 cm^{-1}.

^{1}H-NMR (400MHz) δ (*d*^{6} DMSO): 2.59 (4H, t, J = 6.0 Hz, -NHCH$_2$C<u>H</u>$_2$CO- x 2), 3.14 (4H, br. s, -NHC<u>H</u>$_2$CH$_2$CO- x 2), 3.62 (6H, s, -OC<u>H</u>$_3$ x 2), 4.28 (4H, s, H_{meta} Cp ring), 4.70 (4H, s, H_{ortho} Cp ring), 7.99 (2H, t, J = 6.0Hz, –N<u>H</u>CH$_2$- x 2).

^{13}C-NMR (100 MHz) δ (*d*^{6} DMSO): 34.14 (-ve DEPT), 35.57 (-ve DEPT), 51.75, 69.88, 72.05, 77.81, 169.05, 172.31.

1, 1'-*N*-ferrocenoyl-(γ-aminobutyric acid methyl ester)$_2$ (128)

0.31g of γ-aminobutyric acid methyl ester hydrochloride was used in the synthesis.

Yield 0.32g (68%), orange solid. m.p. 131-132°C.

$E_{1/2}$ = 0.340mV (Vs. Fc/Fc+), UV-Vis (λ_{max}) (EtOH): 344, 444 nm (ε = 190 M^{-1} cm^{-1}), I.R. υ_{max} (KBr): 3327, 2929, 2851, 2362, 1729, 1629, 1538, 1437, 1229, 1103, 743, 670, 487 cm^{-1}.

^{1}H-NMR (400MHz) δ (*d*^{6} DMSO): 1.75-1.78 (4H, m, -NHCH$_2$C<u>H$_2$</u>CH$_2$CO- x 2), 2.39 (4H, t, *J* = 6.8Hz, -NHCH$_2$CH$_2$C<u>H$_2$</u>CO- x 2), 3.19 (4H, m, -NHC<u>H$_2$</u>CH$_2$CH$_2$CO- x 2), 3.60 (6H, s, -OC<u>H$_3$</u> x 2), 4.39 (4H, s, H_{meta} Cp ring), 4.72 (4H, s, H_{ortho} Cp ring), 7.94 (2H, t, *J* = 5.2 Hz, –N<u>H</u>CH$_2$- x 2).

^{13}C-NMR (100 MHz) δ (*d*^{6} DMSO): 25.01 (-ve DEPT), 31.09 (-ve DEPT), 38.43 (-ve DEPT), 51.64, 69.82, 71.80, 78.28, 168.78, 173.57.

1, 1'-*N*-ferrocenoyl-(valeric acid methyl ester)$_2$ (129)

0.33g of valeric acid methyl ester hydrochloride was used in the synthesis.

Yield 0.33g (65%), orange solid, m.p. 161-163°C.

$E_{1/2}$ = 0.330mV (Vs. Fc/Fc+), (UV-Vis (λ_{max}) (EtOH): 345, 441 nm (ε = 176 M^{-1} cm^{-1}), I.R. υ_{max} (KBr): 3365, 2950, 2343, 1731, 1641, 1519, 1418, 1221, 1101, 1043, 777, 543 cm^{-1}.

^{1}H-NMR (400MHz) δ (*d*^{6} DMSO): 1.40-1.52 (8H, m, -NHCH$_2$C<u>H$_2$</u>C<u>H$_2$</u>CH$_2$CO- x 2), 2.27 (4H, t, *J* = 7.2 Hz, -CH$_2$C<u>H$_2$</u>CO- x 2), 3.06-3.09 (4H, m, -NHC<u>H$_2$</u>CH$_2$- x 2), 3.63 (6H, s, -OC<u>H$_3$</u> x 2), 4.34 (4H, s, H_{meta} Cp ring), 4.72 (4H, s, H_{ortho} Cp ring), 7.73 (2H, t, *J* = 5.6 Hz, -N<u>H</u>CH- x 2).

^{13}C-NMR (100 MHz) δ (*d*^{6} DMSO): 22.31 (-ve DEPT), 29.10 (-ve DEPT), 33.35 (-ve DEPT), 38.64 (-ve DEPT), 51.60, 69.86, 73.11, 78.87, 167.68, 173.69.

1, 1'-*N*-ferrocenoyl-[(glycine)2 ethyl ester]$_2$ (130)

0.39g of glycine-glycine ethyl ester was used in the synthesis.

Yield 0.36g (66%), orange microcrystalline solid. m.p. 227-229°C.

$E_{1/2}$ = 0.338mV (Vs. Fc/Fc+), (UV-Vis (λ_{max}) (EtOH): 340, 442 nm (ε = 200 M^{-1} cm^{-1}), I.R. υ_{max} (KBr): 3449, 3412, 3344, 3300, 2363, 2343, 1747, 1612, 1546, 1416, 1382, 1324, 1184, 1013, 949, 772 cm^{-1}.

^{1}H-NMR (400MHz) δ (*d*^{6} DMSO): 1.20 (6H, t, *J* = 7.6 Hz, -OCH$_2$C<u>H$_3$</u> x 2), 3.84 (4H, d, *J* = 5.6 Hz, -NHC<u>H$_2$</u>CO- x 2), 3.92 (4H, d, *J* = 5.2 Hz, -NHC<u>H$_2$</u>CO- x 2), 4.11 (4H, q, *J* = 7.6 Hz, -OC<u>H$_2$</u>CH$_3$ x 2), 4.43 (4H, s, H_{meta} Cp ring), 4.79 (4H, s, H_{ortho} Cp ring), 8.42 (2H, t, *J* = 5.6 Hz, -N<u>H</u>CH$_2$- x 2) 8.60 (2H, t, *J* = 5.2 Hz, -N<u>H</u>CH$_2$- x 2).

^{13}C-NMR (100 MHz) δ (*d*^{6} DMSO): 14.40, 41.17, 42.07, 60.85, 70.31, 71.73, 76.98, 169.32, 169.99, 171.17.

1, 1'-*N*-ferrocenoyl-(L-norvaline ethyl ester)$_2$ (131)

0.33g of L-norvaline ethyl ester hydrochloride was used in the synthesis.

Yield 0.35g (70%), orange solid, m.p. 168-170°C.

$E_{1/2}$ = 0.348mV (Vs. Fc/Fc+), $[\alpha]_D^{20}$ = - 22° (EtOH), (UV-Vis (λ_{max}) (EtOH): 344, 445 nm (ε = 196 M^{-1} cm^{-1}), I.R. υ_{max} (KBr): 3294, 3099, 2972, 2932, 1735, 1630, 1542, 1185, 1140, 1027, 486 cm^{-1}.

^{1}H-NMR (400MHz) δ (*d*^{6} DMSO): 0.89 (6H, t, *J* = 7.2 Hz, -$CH_2CH_2C\underline{H}_3$ x 2), 1.22 (6H, t, J = 7.6Hz, -$OCH_2C\underline{H}_3$ x 2), 1.35-1.49 (4H, m, -$CH_2C\underline{H}_2CH_3$ x 2) 1.72-1.78 (4H, m, -$C\underline{H}_2CH_2CH_3$ x 2) 4.11 (4H, q, J = 7.6Hz, -$OC\underline{H}_2CH_3$ x 2), 4.32-4.37 (2H, m, -NHC<u>H</u>- x 2), 4.37 (2H, s, H_{meta} Cp ring), 4.43 (2H, s, H_{meta} Cp ring), 4.82 (2H, s, H_{ortho} Cp ring), 4.87 (2H, s, H_{ortho} Cp ring), 8.12 (2H, d, *J* = 7.6 Hz, -N<u>H</u>CH- x 2).

^{13}C-NMR (100 MHz) δ (*d*^{6} DMSO): 13.78, 14.47, 19.29 (-ve DEPT), 32.70 (-ve DEPT), 52.34, 60.86 (-ve DEPT), 69.75, 70.73, 72.10, 72.28, 77.15, 169.49, 173.07.

1, 1'-*N*-ferrocenoyl-(L-serine methyl ester)$_2$ (132)

0.32g of L- serine methyl ester hydrochloride was used in the synthesis.

Yield 0.32g (67%), orange solid, m.p. 168-170°C.

$E_{1/2}$ = 0.353mV (Vs. Fc/Fc+), $[\alpha]_D^{20}$ = - 19° (EtOH), (UV-Vis (λ_{max}) (EtOH): 345, 442 nm (ε = 172 M^{-1} cm^{-1}), I.R. υ_{max} (KBr): 3406, 3112, 2941, 1736, 1617, 1542, 1459, 1341, 1228, 1066, 492 cm^{-1}.

^{1}H-NMR (400MHz) δ (*d*^{6} DMSO): 3.68 (6H, s, -$OC\underline{H}_3$ x 2), 3.79 (4H, br. s, -$C\underline{H}_2OH$ x 2), 4.41-4.45 (6H, m, H_{meta} Cp ring + -NHC<u>H</u>- x 2), 4.83 (2H, s, H_{ortho} Cp ring), 4.93 (2H, s, H_{ortho} Cp ring), 5.11 (2H, t, *J* = 6.0 Hz, -$CH_2O\underline{H}$ x 2), 7.94 (2H, d, *J* = 8.4 Hz, -N<u>H</u>CH- x 2).

^{13}C-NMR (100 MHz) δ (*d*^{6} DMSO): 52.29, 55.47, 61.37 (-ve DEPT), 70.07, 70.29, 72.48, 72.52, 76.89, 169.28, 171.61.

1, 1'-*N*-ferrocenoyl-(sarcosine ethyl ester)$_2$ (133)

0.30g of sarcosine ethyl ester hydrochloride was used in the synthesis.

Yield 0.32g (67%), orange solid, m.p. 91-93°C.

$E_{1/2}$ = 0.302mV (Vs. Fc/Fc+), (UV-Vis (λ_{max}) (EtOH): 345, 446 nm (ε = 193 M^{-1} cm^{-1}), I.R. υ_{max} (KBr): 2938, 2883 2362, 2342, 1744, 1617, 1402, 1200, 1097, 914, 608 cm^{-1}.

^{1}H-NMR (400MHz) δ (*d*^{6} DMSO): 1.21 (6H, t, *J* = 11.2 Hz, -$OCH_2C\underline{H}_3$ x 2), 3.28 (6H, br. s, -$NC\underline{H}_3$ x 2), 4.13 (8H, br. s, $N(CH_3)C\underline{H}_2$- x 2 + -$OC\underline{H}_2CH_3$ x 2), 4.50 (4H, br. s, H_{meta} Cp ring), 4.76 (4H, br. s, H_{ortho} Cp ring).

^{13}C-NMR (100 MHz) δ (*d*^{6} DMSO): 14.44, 38.16, (-ve DEPT), 50.81, 60.85, 72.34, 77.62, 169.69.

4.10: References

1) Metallocenes, N.J. Long, (*1998), Blackwell sciences.*
2) D.P Fairlie, M.L. West, A.K. Wong, *Curr. Med. Chem., 5, (1998), 29.*
3) D.G. Osterman, R. Mora, F. J. Kezdy, E.T. Kaiser, *J. Am. Chem. Soc. 106, (1984), 6845.*
4) R. Herrick, R. Jarret, T. Curran, D. Dragoli, M. Flaherty, S. Lindeyberg, L. Thornton, *Tett. Lett., 37, (1996), 5289.*
5) D. Staveren, T. Weyhermuller, N. Metzler-Nolte, *Dalton Trans., (2003), 210.*
6) H.B. Kraatz, Y. Xu, P. Saweczko, *J. Organometallic Chem., 637-639, (2001), 335.*
7) D.H. Williams, I. Fleming, *Spectroscopic Methods in Organic Chemistry, 4th ed., McGraw-Hill, (1989)*.
8) T. Moriuchi, K. Yoshida., T. Hirao, S. Yamazaki, *J. Organometallic Chem., 637, (2001), 75.*
9) L. Lin, A. Berces, H.B.Kraatz, *J. Organometallic Chem., 556, (1998), 11.*
10) S. Barlow, R.S. Marder, *Chem. Comm., (2000), 1555.*

Chapter V

The Synthesis and Characterisation of 1, 1'-*N*-Ferrocenoyl Asymmetric Dipeptides

5.1: Introduction

The synthesis of asymmetric disubstituted ferrocenes presents a unique synthetic challenge, with complex transformations and low overall yields reported [1]. The most common synthetic methods involve either the stepwise introduction of different functional groups to each of the Cp rings, or selective modification of one of two identical functional groups [2]. As an example of the latter methodology, the group of Li and co-workers have prepared several compounds of the type **134**, via the selective hydrolysis of the corresponding dimethyl ester (*scheme 1*) [3].

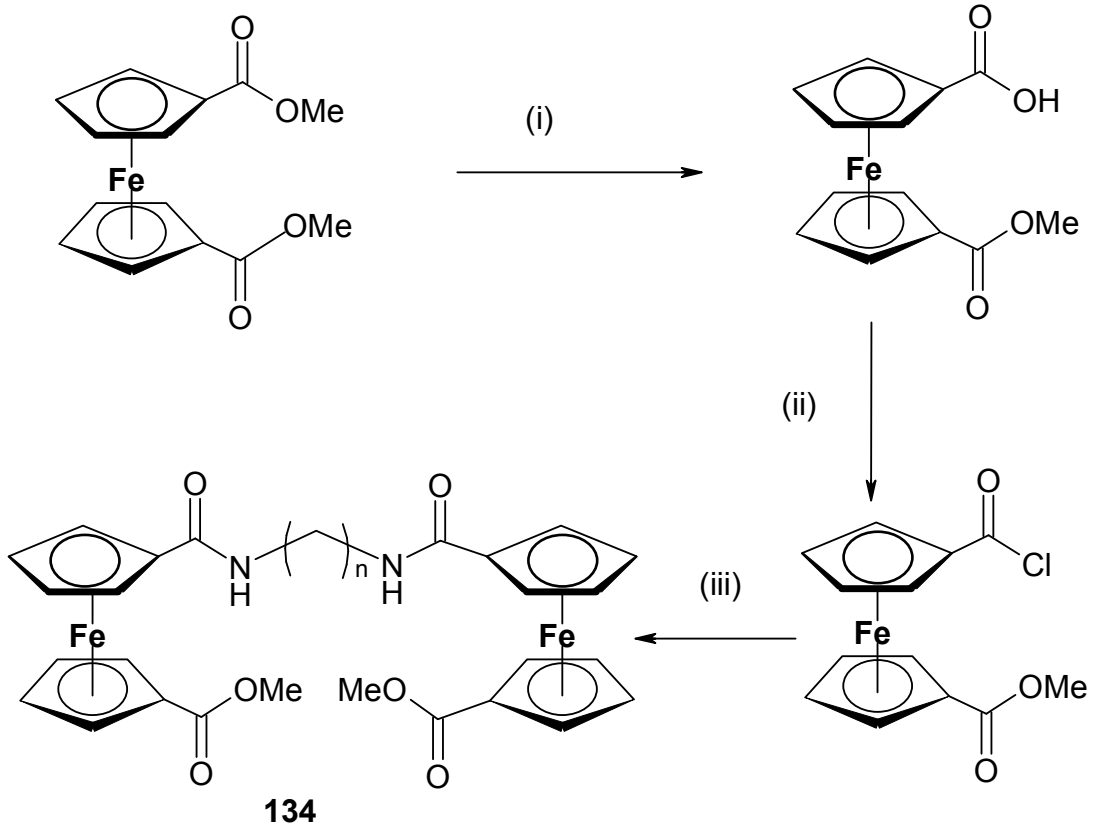

134

(i) NaOH/MeOH (ii) Oxalyl Chloride/MeOH (iii) H_2N-$(CH_2)_n$-NH_2

*Scheme 1: The selective hydrolysis of 1, 1'-ferrocene dimethyl ester, resulting in different functional groups on each of the Cp rings, allowing for the synthesis of **134**.*

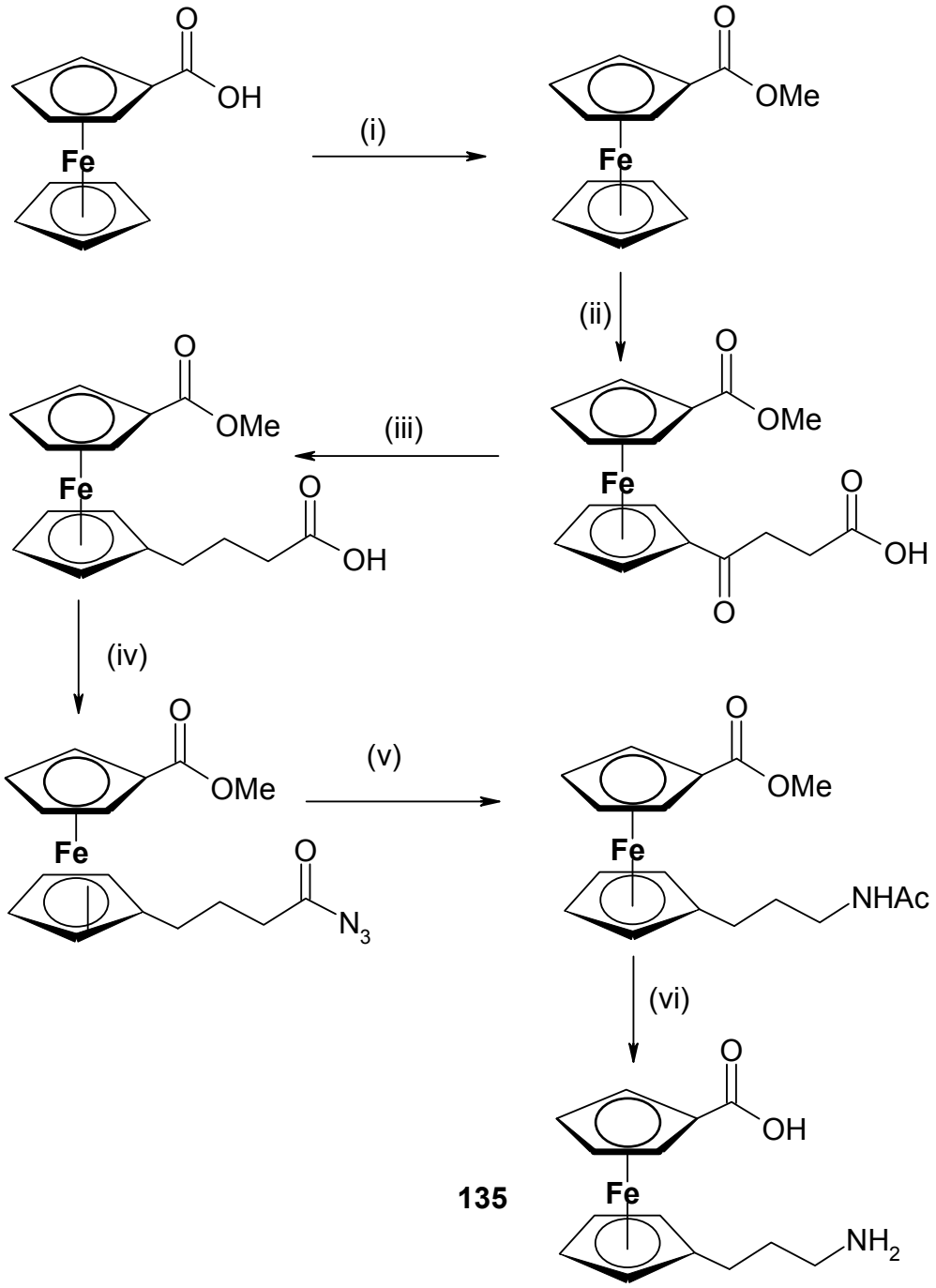

135

(i) $MeOH/BF_3$ (ii) $(COCH_2CH_2COOH)_2O/AlCl_3$ (iii) Zn/Hg, HgOAc (iv) Et_3N, ClCOOEt, NaN_3 (v) Ac_2O (vi) NaOH/EtOH

*Scheme 2: Preparation of **135** from **59**.*

Using a stepwise approach, Barisic *et al*. have reported the synthesis of several ferrocene-amino acid derivatives of the type **135**, using multi-step synthetic procedures, and isolation of all the intermediates, but with overall yields typically under 30% [4].

Many of these unsymmetric ferrocenes reported in the literature are obtained as side products during the preparation of various target molecules. A typical example would be **137**, isolated by Patti *et al*., during the enzymatically-catalysed alcoholysis of **136** (*scheme 3*) [5].

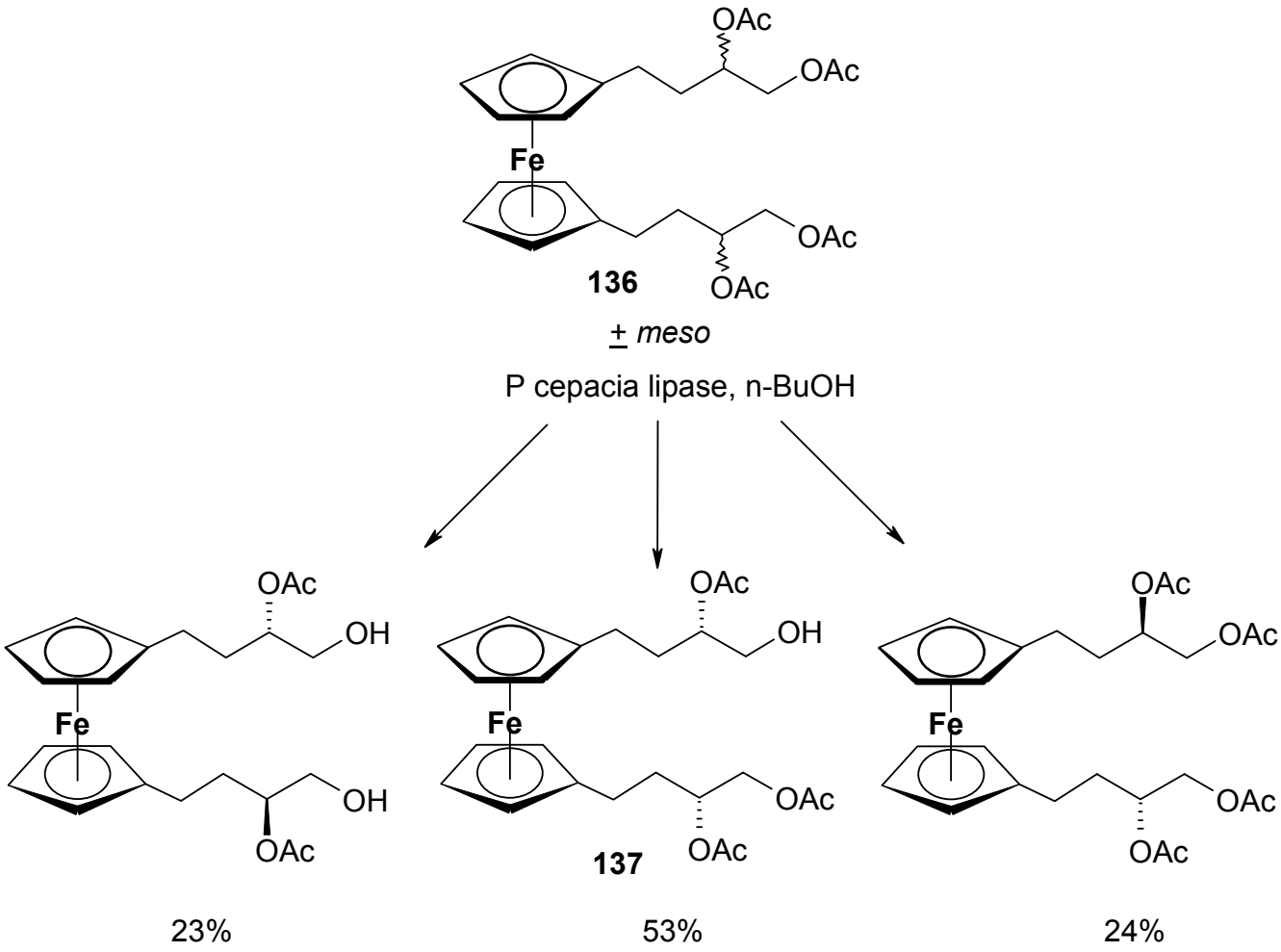

*Scheme 3: The enantiospecific alcoholysis of **136**, resulting in the formation of **137** among the products isolated.*

There are few reports of 1, 1'-***N***-ferrocenoyl asymmetric dipeptides in the literature, and these are only possible with the isolation of unstable intermediates. Typical examples would be the

asymmetric ferrocenoyl oligopeptide **50**, prepared by Xu *et al* [6], and the cyclic ferrocene pentapeptide **57**, prepared by Frejd and co-workers [7] (Ch. 1, 1.7). The following work describes the synthesis of seven novel 1, 1'-***N***-ferrocenoyl asymmetric dipeptides, as well as a convenient one-pot synthetic method for these compounds.

5.2: Synthesis of 1, 1'-*N*-Ferrocenoyl Asymmetric Dipeptides

Three different routes were used to synthesise compound **140**, 1, 1'-***N***-ferrocenoyl-(L-threonine methyl ester)-(L-valine methyl ester), and optimization of these conditions allowed for facile synthesis of the remainder of the unsymmetric ferrocenes (**141**-**146**). In all cases, traces of symmetrically disubstituted ferrocenoyl dipeptides were isolated from the reaction mixtures, although column chromatography on silica gel allowed for facile isolation of the target molecules.

5.2.1: Synthetic Route 1

The first of these synthetic routes was based on the previously reported method of Kraatz et al for stepwise introduction of different peptides onto each Cp ring, which involves the isolation of a mono *O*-benzotriazole active ester [8]. Reaction of ferrocene dicarboxylic with one molar equivalent of L-valine methyl ester hydrochloride using DCC and two molar equivalents of 1-hydroxy benzotriazole in dichloromethane, led to the formation of the active ester **139**, with a yield of 30%, and the product was isolated via silica gel column chromatography. The symmetricly disubstituted 1, 1'-***N***-ferrocenoyl-(L-valine methyl ester)$_2$, **138**, which has previously been reported by Herrick and co-workers, was formed in minor amounts (18%) [9]. The symmetrically disubstituted bis-benzotriazole product was not observed to be formed in any amount, although this could be a function of this compound's stability, either thermal or photochemical. Compound **139** was characterized by ^{1}H-NMR, but its instability in deuterated solvent meant that a clear ^{13}C-NMR spectrum could not be obtained. Even when the ^{13}C-NMR spectrum was recorded immediately after preparation of the sample, decomposition of the product was apparent, with an unsubstituted Cp ring peak appearing *ca*. 70 ppm.

Having isolated the intermediate **139**, this was then reacted with a molar equivalent of L-threonine methyl ester hydrochloride in an attempt to prepare the unsymmetric disubstituted **140**. However, the intermediate **139** proved too unstable in DCM solution, even at 0˚C, to be useful synthetically, and **140** was not isolated from the reaction mixture.

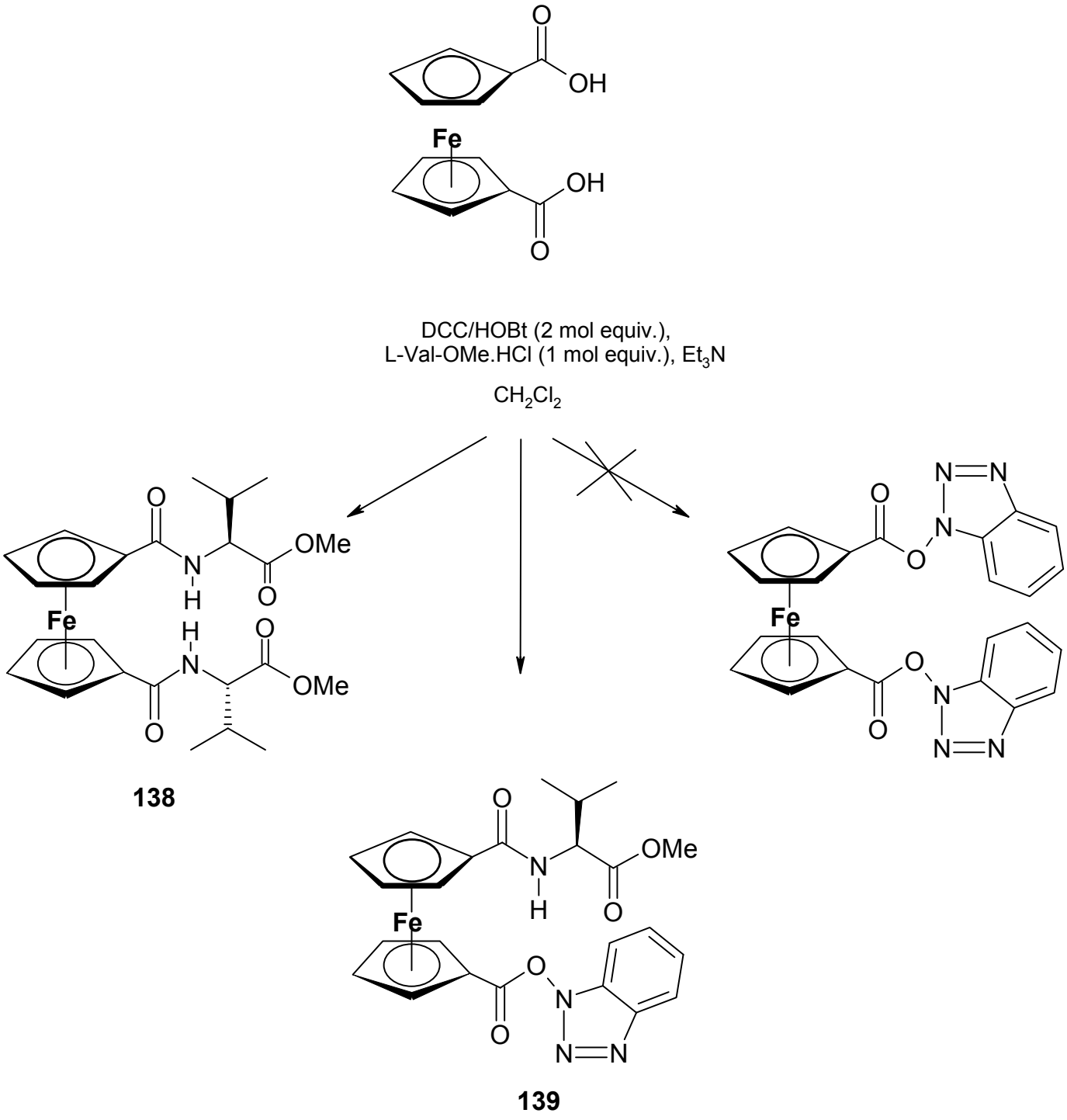

*Scheme 4: Preparation of the active mono-OBt ester **139**.*

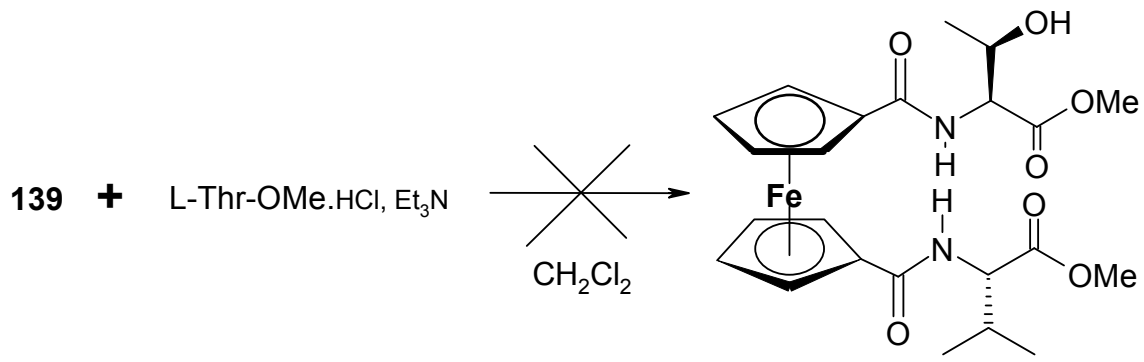

*Scheme 5: Attempted synthesis of **140** using the active ester **139**. The latter proved too unstable in solution to be useful synthetically.*

5.2.2: Synthetic Route 2

Reaction of ferrocene dicarboxylic acid (**112**) with one molar equivalent of L-threonine methyl ester hydrochloride and one molar equivalent of DCC in dichloromethane (i.e. a 2:1 ratio of carboxyl groups to amine groups), it was hoped, would lead to the formation of the mono acid derivative (*scheme 6*). The remaining free carboxyl group could then be coupled to another amino acid. In order to minimize the number of possible side products formed, and hence make the work up more convenient, HOBt was not used in this synthesis. It was hoped that extraction of the dichloromethane reaction mixture into a solution of K_2CO_3, followed by acidification with 0.1M HCl would precipitate the desired compound. Instead, the only product extracted in this way was the starting material **112**. After column chromatography of the remainder of the reaction mixture on silica gel, the symmetricly disubstituted **122** was the only product isolated.

Several attempts were made to prepare the mono acid, and quenching of the reactions over a time range of 12-48 hrs still failed to yield the desired product. No improvement on this situation was observed when CDI was employed as the coupling reagent. Based on these observations, it is possible that the coupling of the first amino acid ester to one of the ferrocene carboxyl groups could be the rate limiting step in such reaction schemes, with coupling of the second amino acid ester being facilitated by forces such as hydrogen bonding in solution.

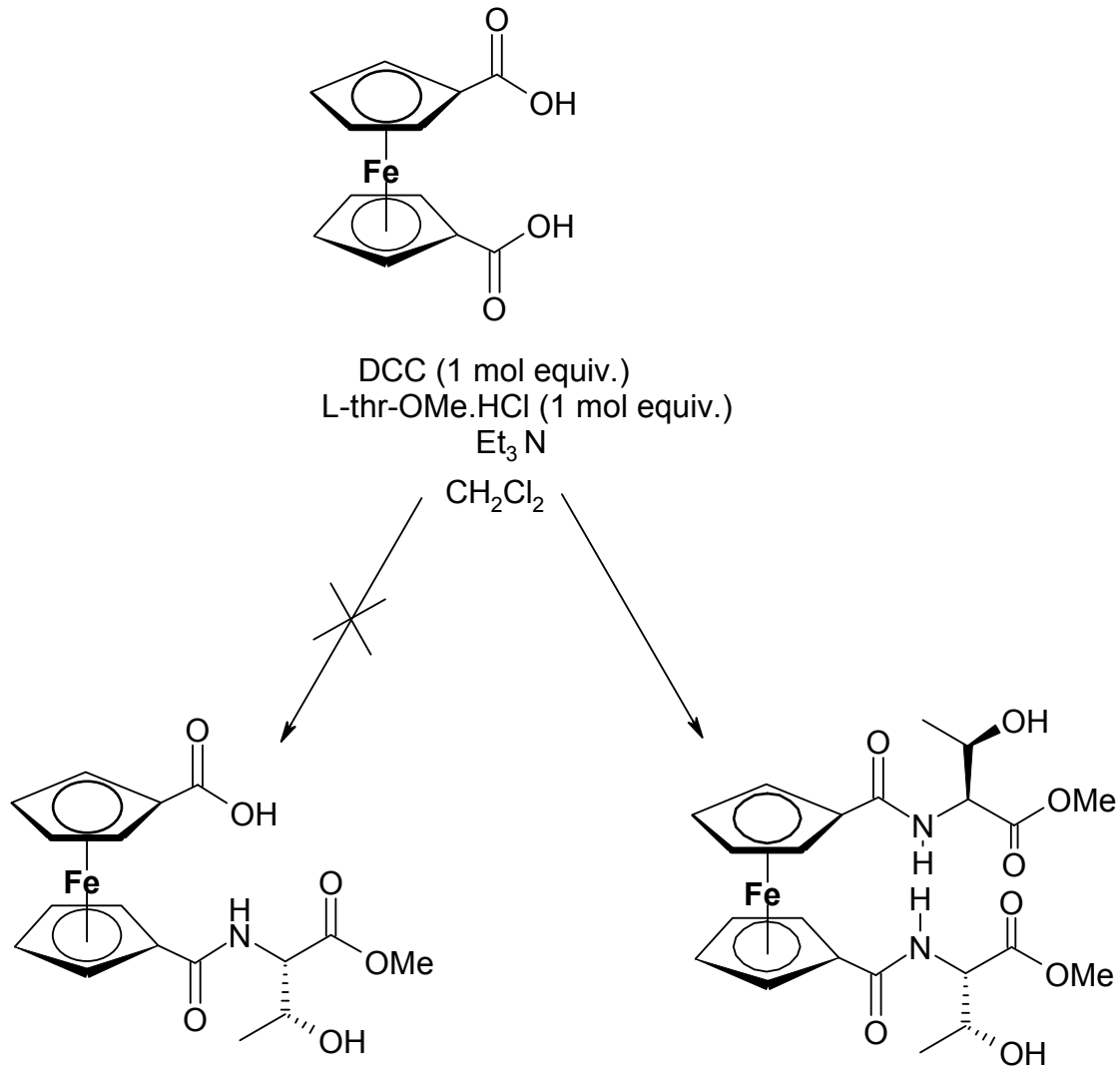

Scheme 6: Attempted preparation of the ferrocenoyl mono acid.

5.2.3: Synthetic Route 3

Reaction of ferrocene dicarboxylic acid with one molar equivalent of L-valine methyl ester hydrochloride in the presence of two molar equivalents of DCC/HOBt in dichloromethane, followed by subsequent addition of a molar equivalent of L-threonine methyl ester hydrochloride (*scheme 7*), gave the unsymmetricly disubstuted ***N***-ferrocenoyl dipeptide **140**, in good yield (50-55%).

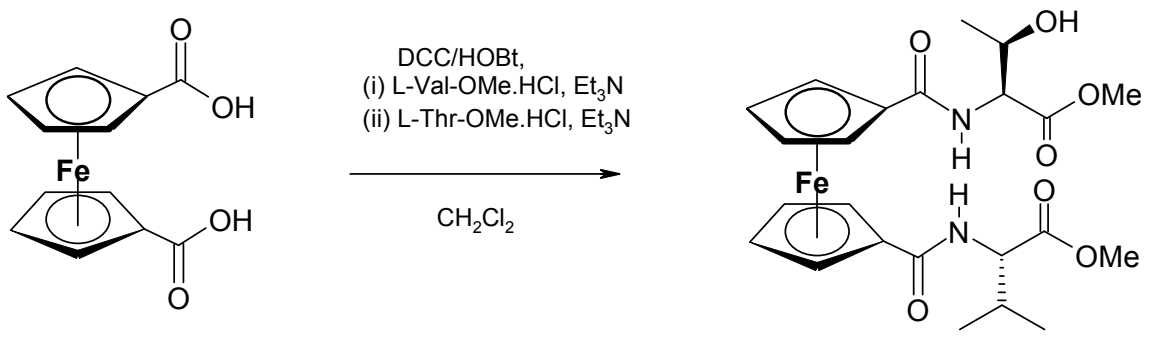

*Scheme 7: Preparation of **140**.*

Fundamental to optimizing the yields in this process was the time difference between the additions of the two amino acid esters to the reaction mixture. *Table 1* shows the effect of 'staggering' their addition on the yield of **140**, as well as the symmetric compounds **138** and **122**. In all cases, the reaction was allowed to proceed for a further 24 hrs after addition of L-threonine methyl ester hydrochloride.

Δ t (hrs)	%Yield **140**	%Yield **122**	%Yield **138**
0	28	13	11
6	34	4	10
12	46	3	10
18	55	<1	9
24	50	<1	12

*Table 1: The effect of staggering the addition of L-valine methyl ester hydrochloride and L-threonine methyl ester hydrochloride on the yield of **140**.*

It was found that 18 hrs was the optimum time to stagger the addition of the two amino acid esters, and this resulted in a yield of 55%, which compares extremely well to any previously reported yields for asymmetric ferrocene peptides, nor could a one-pot synthesis for compounds of this type be found in the literature. All compounds were prepared in similar quantities, with yields in the 50-60% range. A summary of these yields is given in *table 2*.

With the exception of **140** and **146**, which were collected as red solids after evaporation of the hexane/EtOAc mobile phase, these asymmetric compounds were isolated as viscous red oils, and could not be crystallized from the usual solvent combinations.

Compound	Name	M.P. (ºC)	Yield (%)
140	1, 1'-***N***-ferrocenoyl-(L-threonine methyl ester)-(L-valine methyl ester)	90-91	55
141	1, 1'-***N***-ferrocenoyl-(L-serine methyl ester)-(L-norleucine methyl ester)		56
142	1, 1'-***N***-ferrocenoyl-(L-threonine methyl ester)-(L-methionine methyl ester)	-	58
143	1, 1'-***N***-ferrocenoyl-(L-threonine methyl ester)-(L-glutamic acid diethyl ester)	-	51
144	1, 1'-***N***-ferrocenoyl-(L-threonine methyl ester)-(β-alanine methyl ester)	-	54
145	1, 1'-***N***-ferrocenoyl-(L-threonine methyl ester)-(γ-aminobutyric acid methyl ester)	-	59
146	1, 1'-***N***-ferrocenoyl-(L-phenylalanine methyl ester)-(L-aspartic acid dimethyl ester)	100-103	55

*Table 2: % Yields of 1, 1'-**N**-ferrocenoyl asymmetric dipeptides using synthetic route 3, with a Δt of ca. 18 hrs.*

3.3: ^{1}H-NMR Spectra of 1, 1'-*N*-Ferrocenoyl Asymmetric Dipeptides

The ^{1}H-NMR spectrum of the 1, 1'-symmetricly disubstituted compounds are, as would be expected, a good deal more complex than any of those observed for their symmetricly disubstituted analogues. For example, substitution of each of the Cp rings with a different amino acid reside results, in several cases, of four individual signals being observed for the ortho-protons (a maximum of two signals was observed in the case of the symmetric compounds **113-133**). Similarly, two individual and well resolved amide signals were consistently observed, although these could only be unambiguously assigned in compounds incorporating a threonine residue (as this signal invariably appears below 7.7 ppm). The positions of these amide signals in $CDCl_3$ solution, similar to their symmetric analogues, remains largely unaltered relative to that observed in d^6 DMSO.

.

3.3.1: ^{1}H-NMR Spectrum of 140

The ^{1}H-NMR spectrum of **140** is shown in *fig*. 1, and serves to illustrate this complexity of the spectra of the 1, 1'-asymmetricly disubstituted compounds. Three doublets, each integrating for three protons, are observed at 0.87, 0.90, and 1.17 ppm, the first two of which correspond to the two methyl groups of the valine side chain, while the latter corresponds to the methyl group of the threonine side chain. The proton attached to the tertiary carbon of the valine side chain appears as a multiplet *ca*. 2.2 ppm, while the methyl protons of both ester groups appear as a six-proton singlet at 3.68 ppm. The protons of both α-carbons appear as a convoluted multiplet *ca*. 4.2 ppm, while the proton attached to the tertiary carbon of the threonine side chain is observed as a multiplet *ca*. 4.4 ppm.

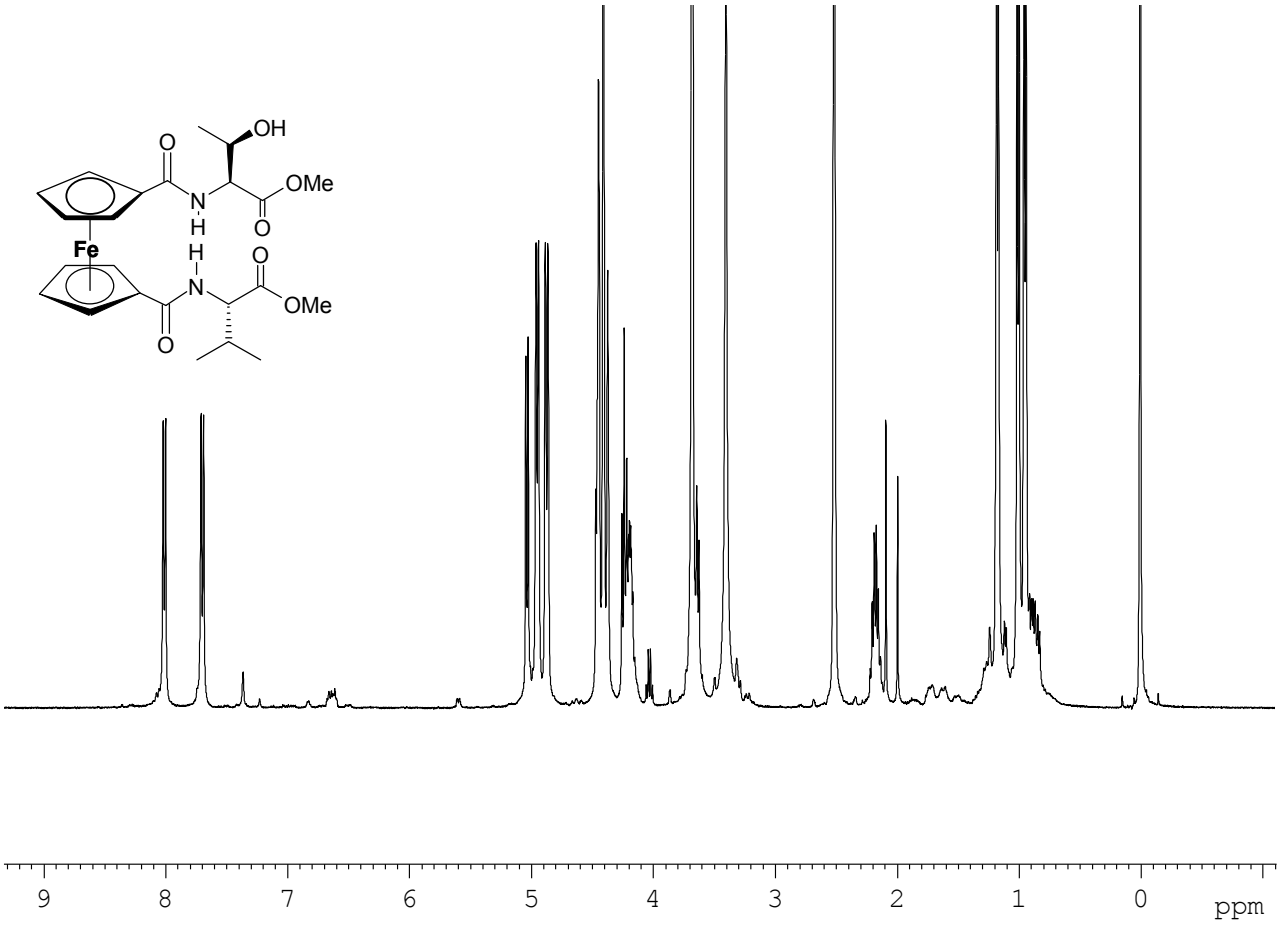

*Fig. 1: The ^{1}H-NMR Spectrum of **140** in d^{6} DMSO.*

The signals observed for the ferrocenoyl protons in the spectrum of **140** serve to illustrate the different effect each individual amino acid can have upon the magnetic environment of the protons of the Cp rings. The meta protons appear as two singlets at 4.41 and 4.45 ppm, each integrating for two protons. This is in contrast to the symmetric threonine derivative, **122**, where the meta protons appear as one singlet, convoluted with the protons of the α-carbons. The *ortho*-protons of **140** appear as four individual, closely grouped singlets *ca*. 4.9 ppm, each integrating for one proton, while only two singlets are observed for **122**. This contrast is illustrated in *fig. 2*.

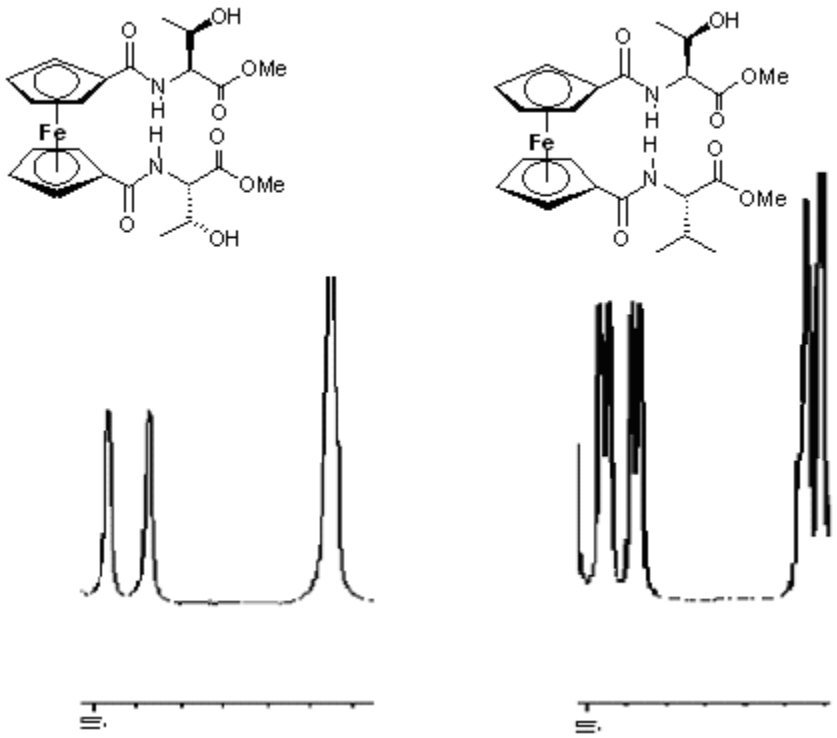

*Fig 2: Comparison of the ferrocenoyl protons of **122** (left) and **140** (right).*

The amide protons of **140** are observed as two doublets, at 7.70 and 8.01 ppm. Given the positions of the amide protons in the spectra of **71** (***N***-ferrocenoyl-L-threonine ethyl ester, 7.46 ppm) and **122** (1, 1'-***N***-ferrocenoyl-(L-threonine methyl ester)$_2$, 7.62 ppm), it is likely that the former of these doublets can be assigned to the amide proton of the threonine residue. One possible reason for the more upfield position of the threonine amide protons could be the shielding effect provided by the lone pairs of the adjacent oxygen atom of the threonine side

chain. Similar large separation of the amide signals are observed for all those 1'1'-***N***-ferrocenoyl asymmetric dipeptides containing a threonine residue. When the spectra of **140** was recorded in $CDCl_3$, the chemical shifts of these protons were observed at 7.68 and 8.00 ppm.

5.3.2: ^{1}H-NMR Spectrum of 144

Compound **144**, 1, 1'-***N***-ferrocenoyl-(L-threonine methyl ester)-(β-alanine methyl ester), incorporates two amino acid esters of unequal length in terms of their respective peptide backbones, which could potentially affect the *intra*-molecular interactions of this compound relative to compounds **140**-**146**. The ^{1}H-NMR spectrum of **144** is shown in *fig*. 3.

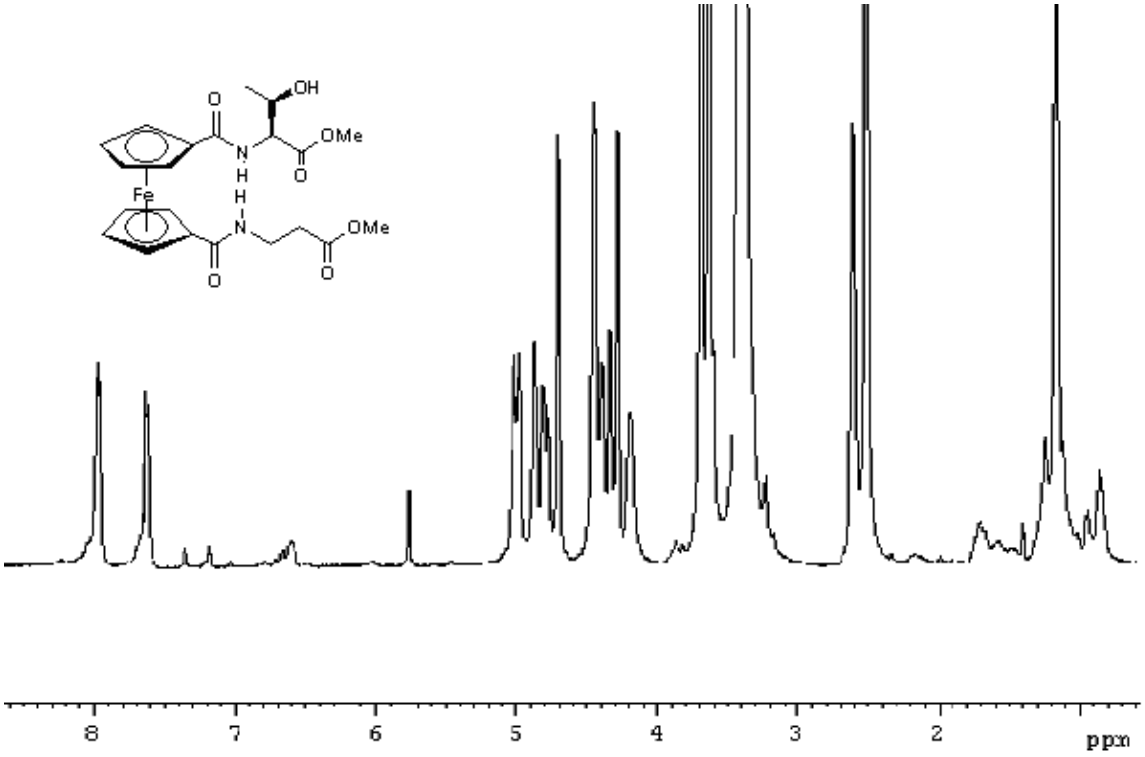

*Fig 3: The ^{1}H-NMR Spectrum of **144** in d^6 DMSO.*

The methyl group protons of the threonine side chain appear as a doublet at 1.17 ppm, while the methylene protons adjacent to the ester functionality of the β-alanine moiety appear as a triplet at 2.60 ppm. The protons of the methylene group adjacent to the amide group of the β-alanine residue are observed as a broadened singlet at 3.27 ppm, and two three-proton singlets,

corresponding to the two methyl ester groups, appear at 3.63 and 3.69 ppm. The proton of the tertiary carbon of the threonine side chain appears as a multiplet at 4.18 ppm.

Two singlets, corresponding to two of the meta protons of the Cp rings, appear at 4.29 and 4.34 ppm, while the other two *meta*- protons are observed as a multiplet *ca*. 4.4 ppm, the signal being convoluted with that corresponding to the α-hydrogen of the threonine residue. The ortho-protons of **144** appear as a one-proton singlet at 4.71 ppm, a two-proton broadened singlet at 4,83 ppm, and a further one proton singlet at 4.97 ppm. The hydroxy proton of the threonine side chain appears as a doublet at 5.02 ppm. The amide proton of the threonine residue is observed as a doublet at 7.63 ppm, while that of the β-alanine residue appears as a triplet at 7.97 ppm. As was observed to be the case with **140**, the positions of these protons are virtually unchanged when the spectrum is recorded in $CDCl_3$, which would suggest that **144** is able to adopt a similar intra-molecular hydrogen bonded conformation to those 1, 1'-disubstituted ferrocenoyl derivatives of α-chiral amino acids.

5.3.3: ^{1}H-NMR Spectrum of 145

Compound **145**, 1, 1'-***N***-ferrocenoyl-(L-threonine methyl ester)-(γ-aminobutyric acid methyl ester), like **144**, incorporates two amino acid esters of unequal length in terms of their peptide backbones. Its ^{1}H-NMR spectrum is shown in *fig*. *4*, and shares many similar features with the spectrum of **144**. The methyl group protons of the threonine side chain appear as a doublet at 1.16 ppm, while the signals for the three methylene groups of the γ-aminobutyric acid residue appear at 1.77, 2.34, and 3.19 ppm. Two three-proton singlets, corresponding to the methyl protons of the ester groups are observed at 3.60 and 3.68 ppm, although, as was the case with **144**, it is not possible to unambiguously assign these peaks. Also in common with the spectrum of **144** is the appearance of the proton of the tertiary carbon of the threonine side chain as a multiplet ca. 4.18 ppm.

The ferrocenoyl signals of **145** are remarkably similar to those of **144**, as can be seen in *fig*. 5, with two singlets being observed for the *meta*-protons of the Cp ring appearing at 4.28 and 4.33 ppm, while the signal for the α-proton of the threonine residue can just about be resolved from the signal for the other two *meta*-Cp protons, the former being observed as a one-proton multiplet at 4.39 ppm, the latter as a broadened singlet at 4.43 ppm. A sharp, one-proton singlet, corresponding to an ortho-proton of a Cp ring is observed at 4.71 ppm, with the other three ortho-protons appearing as a multiplet in the 4.85 ppm region. The hydroxy proton of the

threonine side chain appears as a doublet at 5.00 ppm. The similarities between the spectra of **144** and **145** are shown in *fig*. 5.

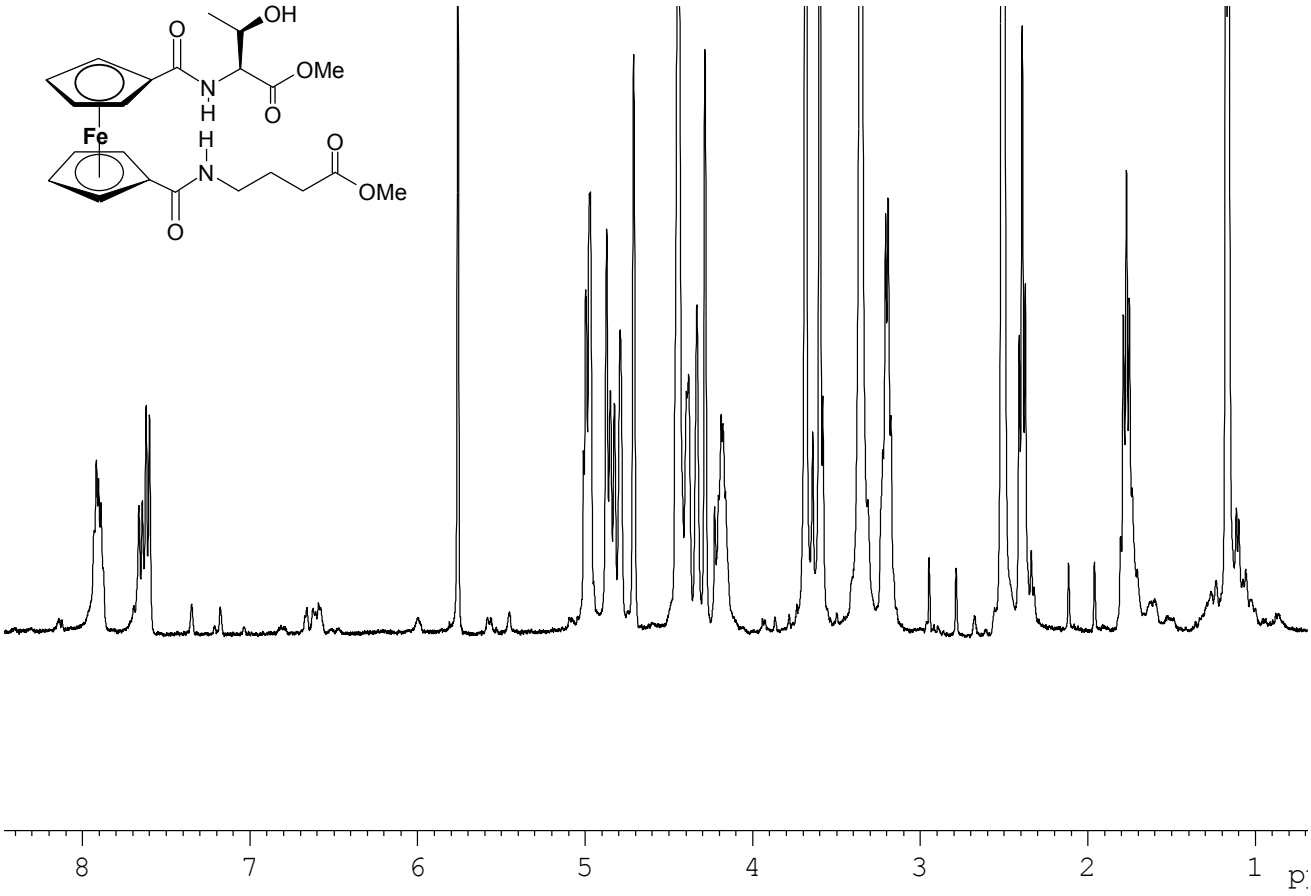

Fig. 4: The ^{1}H-NMR spectrum of **145**.

The signals for the amide protons of **145** differ from those observed in the spectrum of **144**, with two closely grouped doublets, each with J = 8.4 Hz, being observed at 7.65 and 7.69 ppm, between them integrating for one proton, and corresponding to the amide proton of the threonine residue. The signal for the amide proton of the γ-aminobutyric acid residue appears as a triplet at 7.97 ppm. This contrast is illustrated in *fig. 6*.

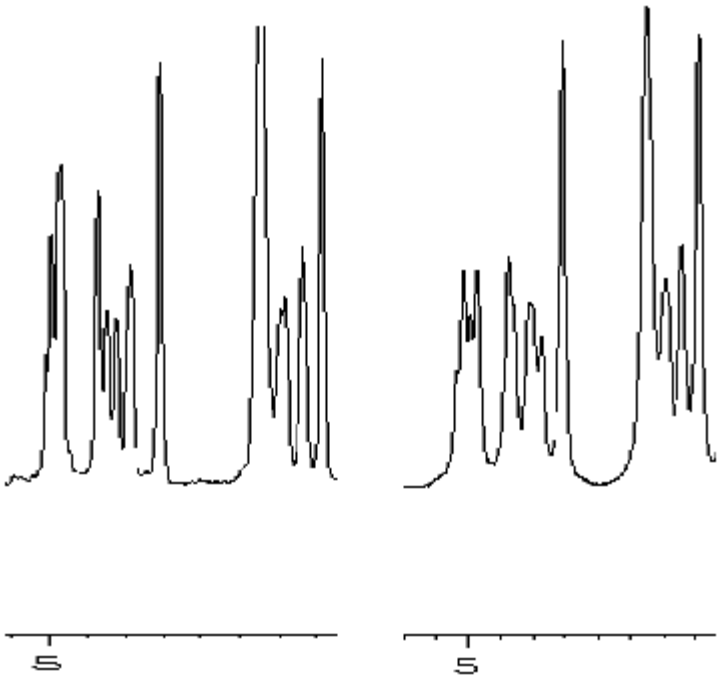

*Fig. 5: The ferrocenoyl protons in the ^{1}H-NMR spectrum of **144** (right) and **145** (left).*

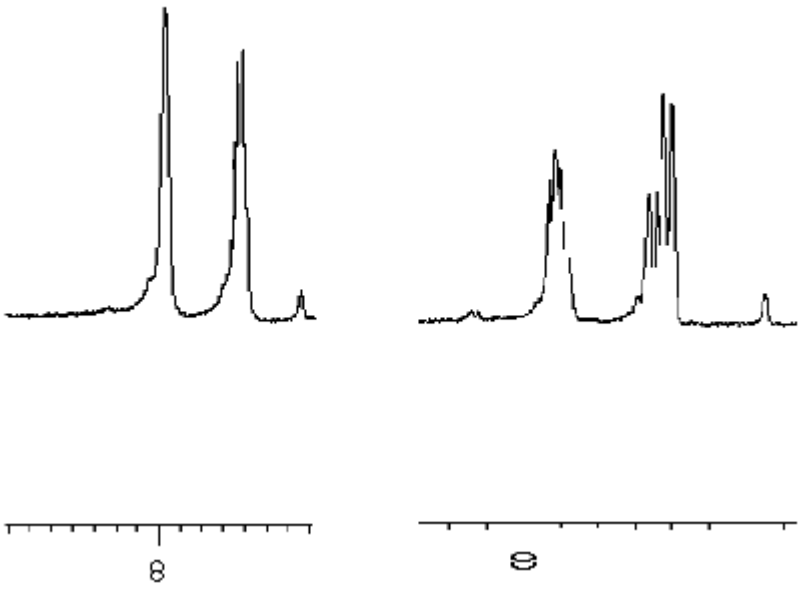

Fig. 6: The amide protons in the ^{1}H-NMR spectrum *of **144** (left) and **145** (right).*

Such 'shoulder' peaks for amide protons were previously observed for several ***N***-ferrocenoyl mono-substituted dipeptides, and were attributed to the presence of more than one particular conformer in d^6 DMSO at ambient temperature (section 3.4.1). In order to confirm this, a spectrum of **145** was recorded at 80˚C, where the two doublets at 7.65 and 7.69 ppm were seen to converge. When the spectrum was recorded in $CDCl_3$, only a broadened singlet was observed at 7.66 ppm. A summary of the ^{1}H-NMR data obtained for these asymmetric compounds is given in *table 3*.

Compound	**N-H**	**H_{ortho}**	**H_{meta}**	**H_{α}**
140	7.70 (d),	4.86, 4.88	4.41, 4.45	4.18-4.25
	8.01 (d)	4.94, 4.96		
141	7.94 (d)	4.82, 4.91	4.34-4.39	4.34-4.39
	8.11 (d)			
142	7.61 (d)	4.83 , 4.86	4.41	4.45-4.48
	8.16 (d)	4.90 , 4.98	4.45-4.48	4.50-4.53
143	7.60 (d)	4.83, 4.88	4.39-4.49	4.39-4.49
	8.16 (d)	4.90, 4.97		
144	7.63 (d)	4.71, 4.83	4.29, 4.34	4.39-4.48
	7.97 (t)	4.97	4.39-4.48	
145	7.65, 7.69 (d)	4.71	4.28, 4.33	4.38-4.43
	7.90 (t)	4.79-4.87	4.38-4.44	
146	8.25 (d)	4.66-4.73	4.10, 4.32	4.66-4.73
	8.32 (d)	4.74-4.76	4.35	4.74-4.76

*Table 3: The ^{1}H-NMR chemical shifts (ppm) of the 1, 1'-**N**-ferrocenoyl asymmetric dipeptide derivatives recorded in d^6 DMSO.*

5.4: ^{13}C-NMR Spectra of 1, 1'-*N*-Ferrocenoyl Asymmetric Dipeptides

As was observed to be the case when the ^{1}H-NMR spectra of these compounds were considered in the preceding sections, the ^{13}C-NMR of these compounds are considerably more detailed than their symmetric analogues. Modification of each of the Cp rings with a different amino acid ester results, in all cases, in two individual signals for both the amide and ester carbonyl carbons

being observed (only one signal was observed for each of these carbons in the spectra of the 1, 1'-symmetricly disubstituted analogues). Also, two individual signals appear for each of the *ipso*- carbons, as well as a considerably more complex pattern of resonances for the ferrocenoyl *meta*- and *ortho*-carbons.

5.4.1: ^{13}C-NMR Spectrum of 140

The ^{13}C-NMR spectrum of compound **140** is shown in *fig. 7*, and incorporates many of the features common to the spectra of these unsymmetric compounds. Two signals for the methyl groups of the valine side chain appear at 18.9 and 19.1 ppm, along with the resonance for the methyl group of the threonine side chain which appears at 20.1 ppm. The tertiary carbon of the valine side chain is observed at 29.1ppm.

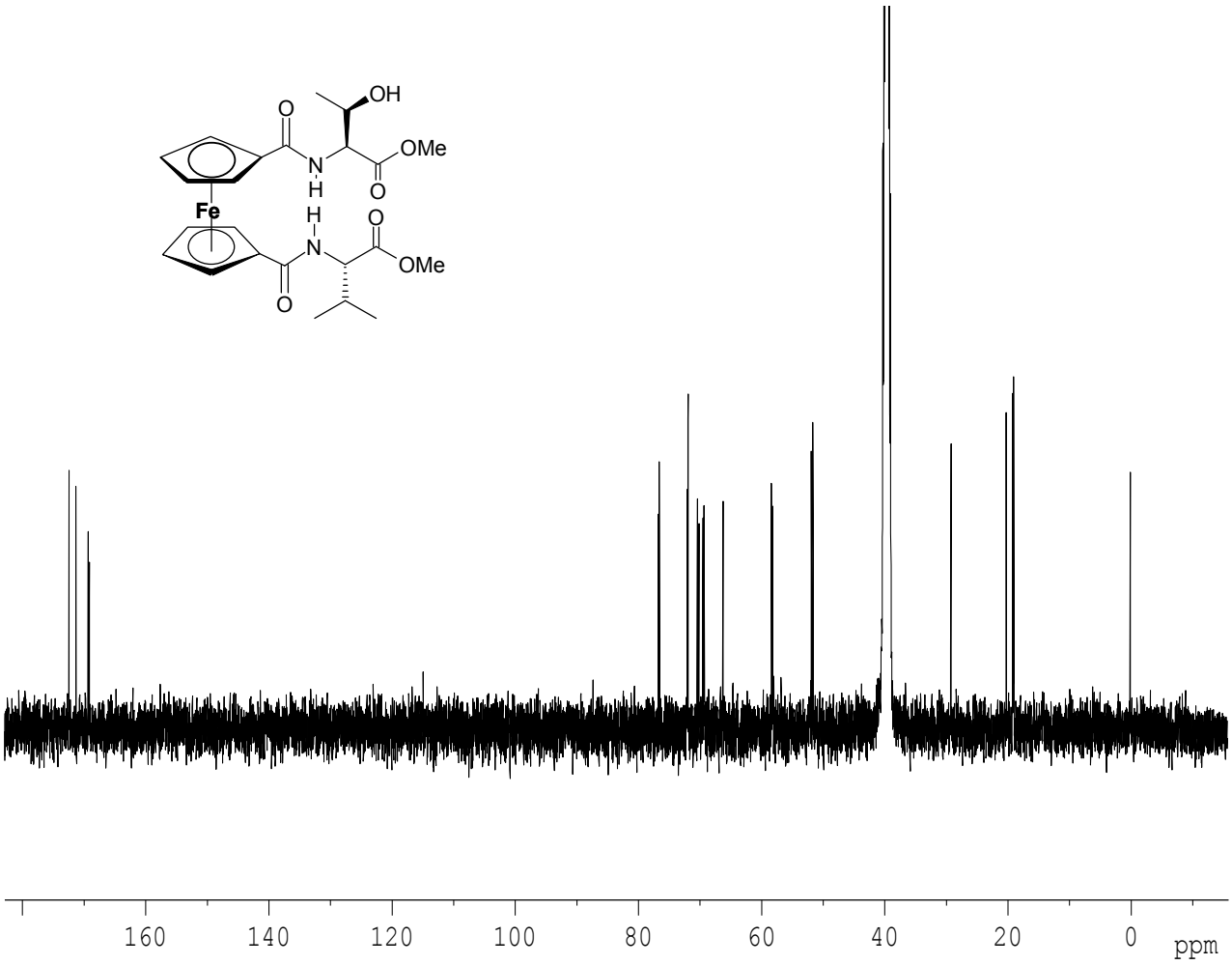

*Fig. 7: The ^{13}C-NMR spectrum of compound **140**.*

Two individual signals appear for each of the methyl carbons of the ester groups, at 51.6 and 51.8 ppm, while the resonances for the chiral α-carbons of the threonine and valine residues are observed at 58.1 and 58.3 ppm. The pattern of signals in the spectrum of **140**, corresponding to the ferrocenoyl carbons, is considerably more detailed than any of the symmetric disubstituted analogues, where a total of five ferrocenoyl carbons were invariably observed in the spectra of chiral compounds (two -*meta*, two -*ortho*, one –*ipso*), and three in that of the achiral analogues (one -*meta*, one -*ortho*, one -*ipso*). This contrast is illustrated in *fig. 8*, which shows the ferrocenoyl carbons of both **140**, and the symmetric **119**.

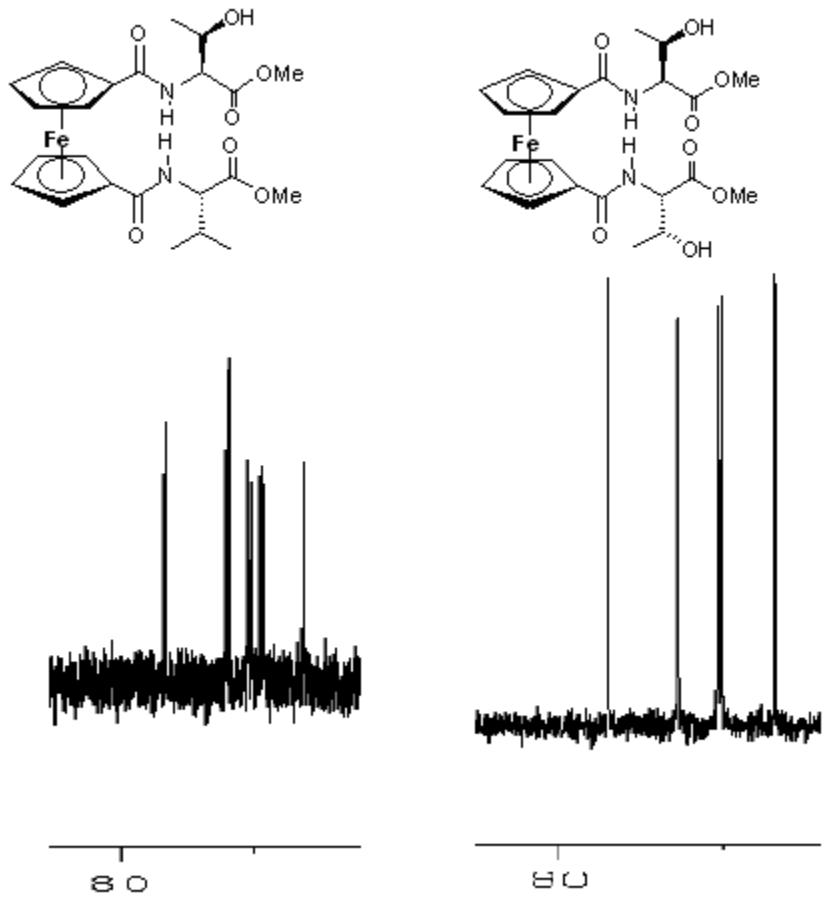

*Fig 8: The ferrocenoyl carbons in the ^{13}C-NMR spectra in d^6 DMSO of **122** (right) and **140**(left).*

Four distinguishable signals, at 69.3, 69.5, 70.1, and 70.3 ppm, corresponding to the ortho-carbons, appear in the spectrum of **140**, while only two signals are observed in the case of **122**.

Like **122**, two individual *meta*-carbon signals are seen in the spectrum of **140**, at 71.8 and 72.0 ppm, but unlike **122**, the quaternary ipso-carbons appear as two individual, narrowly spaced signals at 76.5 and 76.7 ppm. Similarly, a more complex pattern of signals is observed for the other quaternary carbons in the spectrum of **140** relative to that of **122**, with individual signals being recorded for each of the two amide carbonyl carbons at 169.02 and 169.20 ppm, and ester carbonyl carbons at 171.23 and 172.34 ppm, as illustrated in *fig. 9*. All the aforementioned quaternary signals are, as would be expected, absent from the 135DEPT spectrum (*fig. 10*). Also, as **140** includes no methylene carbons, no negative peaks appear.

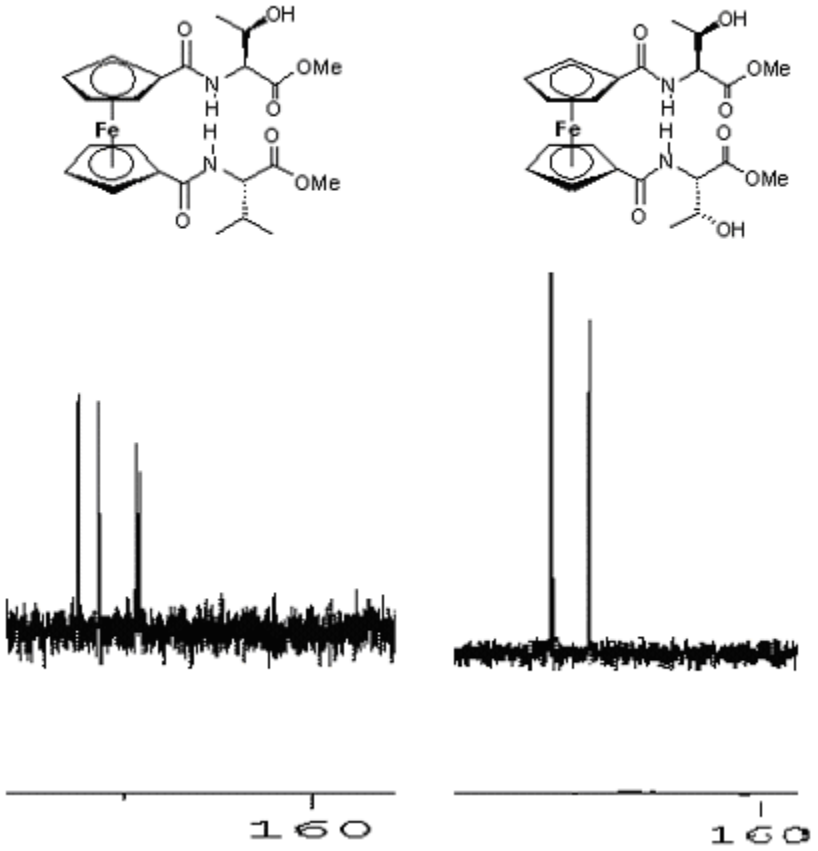

*Fig 9: The quaternary carbonyl carbons in the ^{13}C-NMR spectra in d^6 DMSO of **140** (left) and **122** (right).*

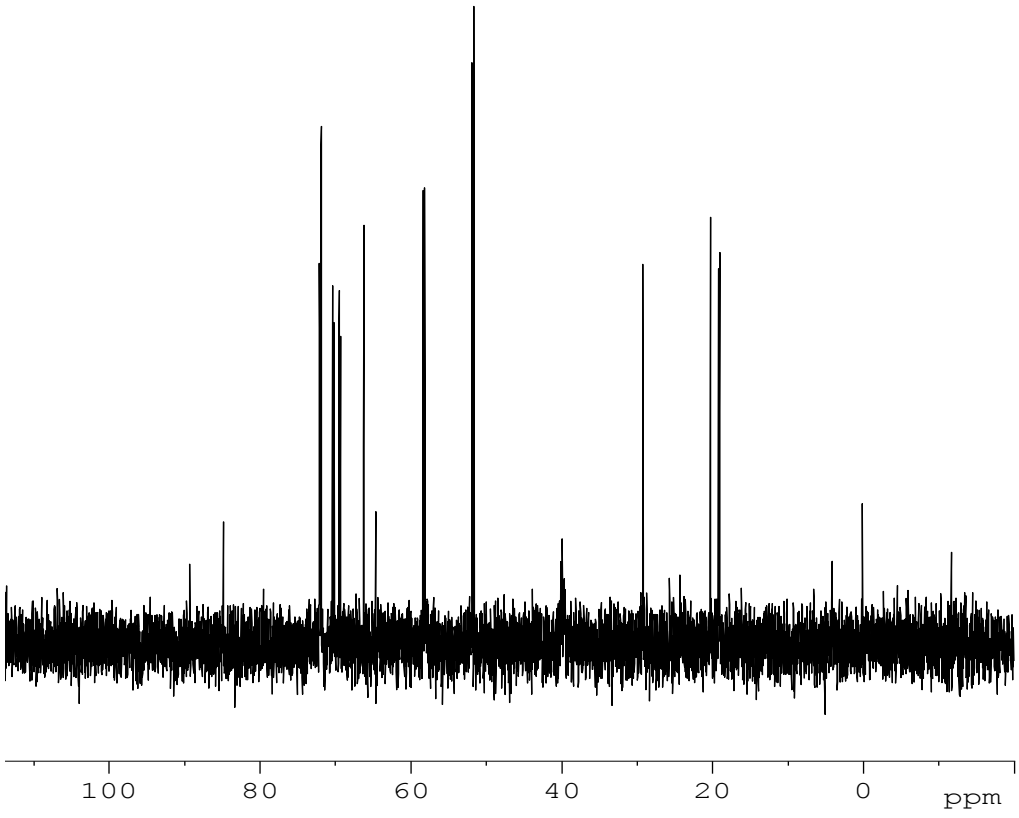

*Fig. 10: The 135DEPT Spectrum of **140** in d^6 DMSO*

What is apparent from the results obtained in *table 4*, is that each individual amino acid ester, when coupled to the Cp ring, has its own particular effect on the chemical shifts on both the ferrocenoyl and the carbonyl carbons. For example, in the ^{13}C-NMR spectrum of **146**, ten individual signals, corresponding to the ten ferrocenoyl carbons (four -*meta*, four -*ortho*, two -*ipso)*, are observed, i.e. each of these carbons is in a different magnetic environment.

Like the all the asymmetric disubstituted ferrocenes discussed in this chapter, the ^{13}C-NMR spectra of compounds **142** (1, 1'-***N***-ferrocenoyl-(L-threonine methyl ester)-(L-methionine methyl ester)) and **143** (1, 1'-***N***-ferrocenoyl-(L-threonine methyl ester)-(L-glutamic acid diethyl ester)) also show two amide and two ester carbonyl carbon resonances, as well as multiple signals for the *ortho*- and *meta*-carbons of the Cp ring. However, as can be seen from *table 4*, only one *ipso*-carbon signal is observed in the spectra of both **142** and **143**, at 76.92 and 76.95 respectively. The symmetric analogues of these compounds, **122** (1, 1'-***N***-ferrocenoyl-(L-threonine methyl ester)$_2$), **116** (1, 1'-*N*-ferrocenoyl-(L-methionine methyl ester)$_2$), and **121** (1, 1'-*N*-ferrocenoyl-(L-glutamic acid diethyl ester)$_2$) all show *ipso*-carbon signals in a very narrow

range, at 76.89, 76.93, and 76.97 ppm respectively. It is therefore likely that the appearance of only one signal in the spectra of **142** and **143** is due to the convolution of the two C_{ipso} resonances due to both these carbons being in equivalent magnetic environments. Certainly, the intensity of the C_{ipso} signals of **142** and **143**, in terms of peak height, is greater than was observed for any of the other asymmetric ferrocenes prepared. This can be seen in *fig. 11*, which compares the C_{ipso} signals of **141** and **142**. A summary of the ^{13}C-NMR data for compounds **140**-**146** is given in *table 4*.

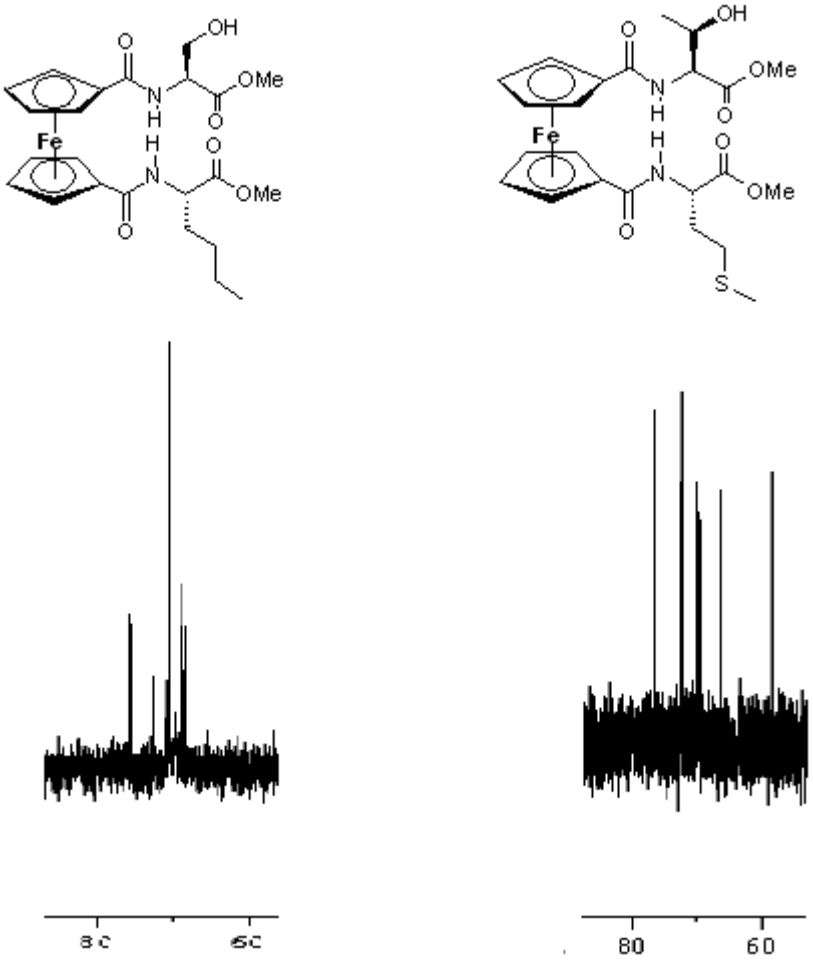

*Fig. 11. The C_{ipso} resonances of **141** (left) and **142(right)** at ca. 77 ppm. They appear in the spectrum of **141** as two closely-grouped signals, while only one signal is observed in the spectrum of **142**.*

Compound	$C=O_{amide}$	$C=O_{ester}$	C_{ortho}	C_{meta}	C_{ipso}
140	169.06	171.23	69.26, 69.46	71.84	76.52
	169.20	172.34	70.10, 70.33	72.02	76.71
141	169.38	172.00	69.14, 69.90	70.99, 71.67	77.68
	169.84	171.38	70.15, 70.26	71.99, 72.09	77.77
142	169.51	171.85	69.83, 69.93	72.39	76.92
	169.62	173.07	70.39	72.58	
143	169.43	171.82	69.85, 69.94	72.38	76.95
	169.58	172.36	70.28/70.35	72.57	
144	168.94	171.73, 172.09	69.87, 70.00	71.97, 72.24	76.69
	169.54	172.27	70.17	72.67	77.93
145	168.76	171.67	69.83, 70.00	71.19	76.99
	169.18	173.12	70.17	72.67	78.31
146	169.18	170.99/171.73	69.32, 69.45	72.31, 72.41	76.59
	169.22	172.73	70.59, 70.78	72.47, 72.60	76.94

*Table 4: The ^{13}C-NMR chemical shifts (ppm) of the 1, 1'-**N**-ferrocenoyl asymmetric dipeptide derivatives recorded in d^6 DMSO.*

5.5: InfraRed Spectra of 1, 1'-*N*-Ferrocenoyl Asymmetric Dipeptides

As the majority of these asymmetric compounds were obtained as oils, only thin-film methylene chloride solution spectra were recorded. In agreement with the ^{1}H and ^{13}C-NMR data reviewed thus far, the infrared spectra of these compounds clearly showed the presence of two distinct C=O amide stretches, two C=O ester stretches, and two υ_{N-H} stretches. This is in contrast to the symmetricly disubstituted compounds, where only one band was observed for each of these groups. The N-H stretches are observed in the 3400-3900 cm^{-1} range, which, as has been discussed in sections 3.6 and 4.6, indicates that each amide proton participates in an intra-molecular hydrogen bonding interaction. It is therefore likely that a similar, β-sheet-like conformation is adopted by these compounds in non-polar solution, as was seen in the case of the 1, 1'-***N***-ferrocenoyl symmetric compounds, with hydrogen bonding occurring in an anti-parallel fashion.

Compound	υ_{N-H}	υ_{COOR}	υ_{CONR}
140	3351, 3375	1729, 1736	1639, 1644
141	3350, 3378	1735, 1725	1631, 1639
142	3359, 3370	1730, 1747	1639, 1645
143	3357, 3371	1740, 1751	1636, 1645
144	3362, 3389	1730, 1742	1641, 1648
145	3349, 3367	1728, 1739	1633, 1641
146	3358, 3390	1740, 1750	1630, 1640

*Table 5: Infrared data for **140-146** (cm^{-1}) (as CH_2Cl_2 thin-film solutions)*

5.6: UV-Vis Spectra of 1, 1'-*N*-Ferrocenoyl Asymmetric Dipeptides

The UV-Vis spectra of compounds **140-146** show minimal differences from those recorded for the symmetricly disubstituted analogues, with similar values for the λ_{max} extinction coefficients being recorded. As has been noted in previous chapters, that modification of the ferrocenoyl group with different amino acid esters, while having a noticeable effect in the NMR spectra, has minimal effect on the electronic behaviour of the ferrocene moiety. It was thought that compounds **141** and **142**, which incorporate two amino acid esters of unequal length in terms of their peptide backbones, might adopt a conformation which resulted in out-of-plane bending of the Cp rings, thus altering the electronic properties of these compounds. This proved not to be the case, with all compounds showing two low energy bands in the 440 and 340nm range, while extinction coefficients are in the 200 A.U. range.

5.7: Cyclic Voltammograms of 1, 1'-*N*-Ferrocenoyl Asymmetric Dipeptides

As was seen to be the case with the symmetrically disubstituted ferrocenes discussed in section 4.8, the presence of an electron-withdrawing amide group on each Cp ring has the effect of lowering the energy of the ferrocenoyl HOMO, making the molecule more difficult to oxidize relative to the mono-substituted derivatives discussed in sections 2.8 and 3.8. The $E_{1/2}$ values are consistent with those obtained for the symmetric analogues, indicating that, as was noted in the previous section, the individual substituent amino acid esters have minimal effect on the electrochemical properties of these compounds. The cyclic voltammogram of compound **140** is

shown in *fig. 12*, and a summary of the electrochemical and UV-Vis data for compounds **140-146** is given in *table 6*.

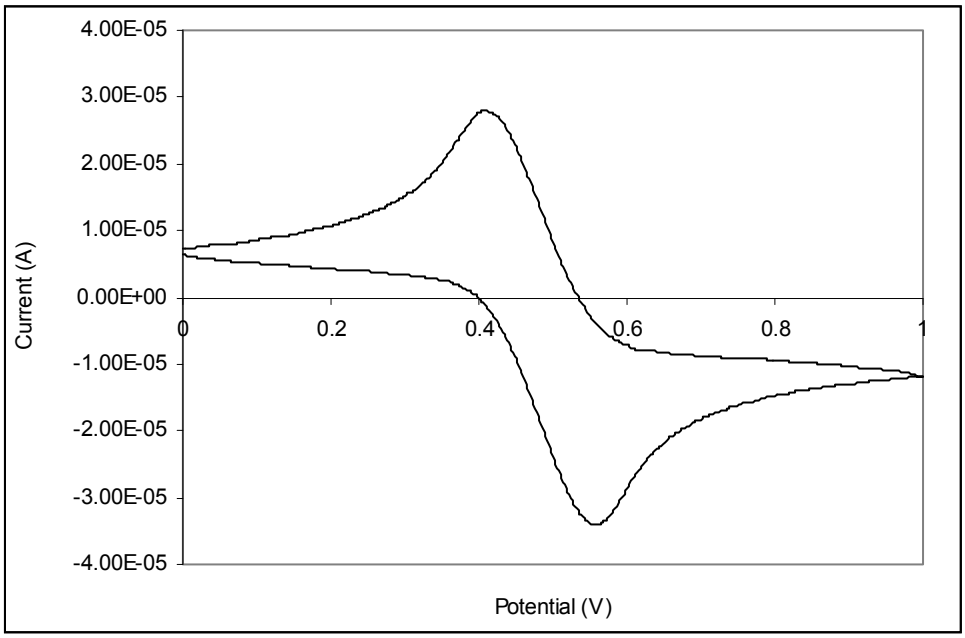

*Fig. 12: The cyclic voltammogram of **140***

Compound	λ_{max} (nm)	ε (M^{-1} cm^{-1})	$[\alpha]_D^{20}$	$E_{1/2}$ (mV)
140	345, 445	168	- 24°	0.341
141	340, 441	196	- 16°	0.338
142	343, 442	189	- 17°	0.344
143	343, 445	189	- 20°	0.350
144	343, 442	189	- 9°	0.334
145	340, 444	163	- 11°	0.328
146	344, 444	212	- 22°	0.352

Table 6: The electrochemical, UV-Vis, and optical rotation data for compounds **140-146**. *All ε values refer to lowest energy band.*

5.8: Conclusions

In a one-pot process, using the DCC/HOBt coupling protocol, 1, 1'-***N***-ferrocenoyl asymmetric dipeptides were prepared in good yield (>50% in all cases) by staggering the addition of the corresponding amino acid esters, and the optimal time difference between the two additions was determined to be 18 hrs. Attempted preparation of these compounds via the isolation of a ferrocenoyl mono O-benzotriazole active ester proved unsuccessful, with this compound proving unstable in solution at room temperature.

The ^{1}H-NMR spectra of all compounds show the presence of two separate amide proton signals, the downfield shift of which in $CDCl_3$ indicate they are involved in intra-molecular hydrogen bonding. The ferrocenoyl protons appear as a complex pattern of signals, with up to four individual *ortho*-proton resonances being observed. Similarly, up to four individual signals are observed for the *ortho*-carbons in the ^{13}C-NMR spectra. The infrared spectra also show the presence of two distinct amide and ester groups within each compound, which appear to be involved, like their symmetric analogues, in a β-sheet-like conformation, forming hydrogen bonds in an anti-parallel fashion.

5.9: Experimental

1, 1'-*N*-ferrocenoyl-(L-valine methyl ester)-(OBt) (139)

0.82g (3mmol) of **122**, 0.84g (6 mmol) of 1-hydroxybenzotriazole, and 1.2g (3.6mmol) DCC were dissolved in 40mls dichloromethane at 0˚C. 0.57mls (3.6mmol) Et_3N, and 0.50 (3mmol) of L-valine methyl ester hydrochloride were then added, and the reaction was brought to room temperature after 30mins, and allowed to proceed for a further 24 hrs. The solvent was evaporated *in vacuo*, and the crude product was then eluted from a column of silica gel, using a mobile phase of 1:1 hexane/ethyl acetate.

Yield 0.33g (22%), red viscous oil.

^{1}H-NMR (400MHz) δ (*d*^{6} dmso): 0.88 (6H, br. s, -CH(C$\underline{H}_3$)$_2$), 2.18 (1H, br. s, -C$\underline{H}$(CH$_3$)$_2$), 3.68 (3H, s, OC$\underline{H}_3$), 4.20-4.25 (1H, m, -NHC$\underline{H}$-), 4.44 (2H, br. s, H_{meta} Cp ring), 4.73 (2H, br. s, H_{meta} Cp ring), 4.90 (2H, br. s, H_{ortho} Cp ring), 5.14 (2H, br. s, H_{ortho} Cp ring), 7.51-7.61 (3H, m, ArH), 8.05 (1H, br. s, N$\underline{H}$CH-), 8.14 (1H, br. s, ArH).

1, 1'-*N*-Ferrocenoyl Asymmetric Dipeptides

General Procedure

0.27g (1mmol) of **112**, 0.28g (2mmol) of 1-hydroxybenzotriazole, and 0.5g (2.4mmol) DCC were dissolved in 15mls dichloromethane at 0˚C. 0.19mls (1.2mmol) Et_3N, and 1mmol of the first amino acid ester hydrochloride were then added, and the reaction allowed to rise to room temperature, and proceed for a further 18hrs. 0.19mls (1.2mmol) Et_3N, and 1mmol of the second amino acid ester hydrochloride were then added, and the reaction allowed to proceed for a further 24 hrs. The solvent was evaporated *in vacuo*, and the crude product was then eluted from a column of silica gel, using a mobile phase of 1:1 hexane/ethyl acetate.

1, 1'-*N*-ferrocenoyl-(L-threonine methyl ester)-(L-valine methyl ester) (140)

0.17g of L-threonine methyl ester hydrochloride and 0.17g of L-valine methyl ester hydrochloride were used in the synthesis.

Yield 0.28g (55%), red solid, m.p. 90-91°C.

$E_{1/2}$ = 0.341mV (Vs. Fc/Fc+), $[\alpha]_D^{20}$ = - 24°, (EtOH) (UV-Vis (λ_{max}) (EtOH): 345, 445 nm (ε = 168 M^{-1} cm^{-1}), I.R. υ_{max} ($CDCl_3$): 3378, 3350, 3193, 2958, 1744, 1731, 1639, 1631, 1547, 1382, 1320, 1261, 1017, 522, 512 cm^{-1}.

^{1}H-NMR (400MHz) δ (*d*^{6} dmso): 0.87 (3H, d, *J* = 6.4 Hz, -CH(C$\underline{H}_3$)$_2$), 0.90 (3H, d, *J* = 6.4 Hz, -CH(C$\underline{H}_3$)$_2$), 1.17 (3H, d, *J* = 6.4 Hz, -CH(OH)C$\underline{H}_3$), 2.15-2.20 (1H, m, -C$\underline{H}$(CH$_3$)$_2$), 3.68 (6H, s, OC$\underline{H}_3$ x 2), 4.18-4.25 (2H, m, -NHC$\underline{H}$- x 2), 4.37-4.40 (1H, m, -C$\underline{H}$(OH)CH$_3$), 4.41 (2H, s, H_{meta} Cp ring), 4.45 (2H, s, H_{meta} Cp ring), 4.86 (1H, s, H_{ortho} Cp ring), 4.88 (1H, s, H_{ortho} Cp ring), 4.94 (1H, s, H_{ortho} Cp ring), 4.96 (1H, s, H_{ortho} Cp ring), 5.03 (1H, d, *J* = 7.6 Hz, -CH(O$\underline{H}$)CH$_3$), 7.70 (1H, d, *J* = 7.6 Hz, N$\underline{H}$CH-), 8.01 (1H, d, *J* = 8.0 Hz, N$\underline{H}$CH-).

^{13}C-NMR (100 MHz) δ (*d*^{6} dmso): 18.95, 19.11, 20.18, 29.14, 51.57, 51.82, 58.08, 58.30, 66.18, 69.26, 69.46, 70.10, 70.33, 71.84, 72.02, 76.52, 76.71, 169.06, 169.20, 171.23, 172.34.

1, 1'-*N*-ferrocenoyl-(L-serine methyl ester)-(L-norleucine methyl ester) (141)

0.16g of L-serine methyl ester hydrochloride and 0.18g of L-norleucine methyl ester hydrochloride were used in the synthesis.

Yield 0.28g (56%), red viscous oil.

$E_{1/2}$ = 0.338mV (Vs. Fc/Fc+), $[\alpha]_D^{20}$ = - 16° (EtOH), (UV-Vis (λ_{max}) (EtOH): 340, 441 nm (ε = 196 M^{-1} cm^{-1}), I.R. υ_{max} ($CDCl_3$): 3375, 3351, 2360, 1736, 1729, 1645, 1639, 1549, 1418, 1350, 1232, 1191, 1040, 485 cm^{-1}.

^{1}H-NMR (400MHz) δ (*d*^{6} dmso): 0.88 (3H, d, *J* = 6.8 Hz, -$CH_2CH_2CH_2C\underline{H}_3$), 1.30-1.37 (4H, m, -$CH_2C\underline{H}_2C\underline{H}_2CH_3$), 1.76-1.79 (2H, m, -$C\underline{H}_2CH_2CH_2CH_3$), 3.61 (6H, s, $OC\underline{H}_3$ x 2), 3.78 (2H, br. s, -$C\underline{H}_2OH$), 4.34-4.39 (6H, m, -NHC<u>H</u>- x 2 + H_{meta} Cp ring), 4.82 (2H, s, H_{ortho} Cp ring), 4.91 (2H, s, H_{ortho} Cp ring), 7.94 (1H, d, *J* = 7.6 Hz, N<u>H</u>CH-), 8.11 (1H, d, *J* = 7.2 Hz, N<u>H</u>CH-).

^{13}C-NMR (100 MHz) δ (*d*^{6} dmso): 18.99, 28.41 (-ve DEPT), 33.21 (-ve DEPT), 36.29 (-ve DEPT), 57.54, 57.78, 60.71 (-ve DEPT), 69.14, 69.90, 70.15, 70.26, 70.99, 71.67, 71.99, 72.09, 77.68, 77.77, 169.38, 169.84, 171.38, 172.00.

1, 1'-*N*-ferrocenoyl-(L-threonine methyl ester)-(L-methionine methyl ester) (142)

0.17g of L-threonine methyl ester hydrochloride and 0.17g of L-methionine methyl ester hydrochloride were used in the synthesis.

Yield 0.31g (58%), red viscous oil.

$E_{1/2}$ = 0.344mV (Vs. Fc/Fc+), $[\alpha]_D^{20}$ = - 17° (EtOH), (UV-Vis (λ_{max}) (EtOH): 343, 442 nm (ε = 189 M^{-1} cm^{-1}), I.R. υ_{max} ($CDCl_3$): 3370, 3359, 3193, 2993, 1747, 1730, 1649, 1639, 1544, 1428, 1336, 1248, 822, 500 cm^{-1}.

^{1}H-NMR (400MHz) δ (*d*^{6} dmso): 1.16 (3H, d, *J* = 6.0 Hz, -CH(OH)$C\underline{H}_3$), 2.02-2.07 (5H, m, -$C\underline{H}_2SC\underline{H}_3$), 2.56-2.64 (2H, m, -$C\underline{H}_2CH_2SCH_3$), 3.69 (6H, s, $OC\underline{H}_3$ x 2), 4.17-4.21 (1H, m, -C<u>H</u>(OH)CH_3), 4.41 (2H, s, H_{meta} Cp ring), 4.45-4.48 (3H, m, H_{meta} Cp ring + -NHC<u>H</u>-), 4.50-4.53 (1H, m, -NHC<u>H</u>-), 4.83 (1H, s, H_{ortho} Cp ring), 4.86 (1H, s, H_{ortho} Cp ring), 4.90 (1H, s, H_{ortho} Cp ring), 4.98 (1H, s, H_{ortho} Cp ring), 5.02 (1H, d, *J* = 7.6 Hz, -CH(O<u>H</u>)CH_3), 7.61 (1H, d, *J* = 8.8 Hz, N<u>H</u>CH-), 8.16 (1H, d, *J* = 8.0 Hz, N<u>H</u>CH-).

^{13}C-NMR (100 MHz) δ (*d*^{6} dmso): 14.89, 20.63, 30.15 (-ve DEPT), 30.26 (-ve DEPT), 51.46, 52.35, 52.42, 58.65, 66.62, 69.83, 69.93, 70.39, 72.39, 72.58, 76.92, 169.51, 169.62, 171.85, 173.07.

1, 1'-*N*-ferrocenoyl-(L-threonine methyl ester)-(L-glutamic acid diethyl ester) (143)

0.17g of L-threonine methyl ester hydrochloride and 0.24g of L-glutamic acid diethyl ester hydrochloride were used in the synthesis.

Yield 0.29g (51%), red viscous oil.

$E_{1/2}$ = 0.350mV (Vs. Fc/Fc+), $[\alpha]_D^{20}$ = - 20° (EtOH), (UV-Vis (λ_{max}) (EtOH): 343, 445 nm (ε = 189 M^{-1} cm^{-1}), I.R. υ_{max} ($CDCl_3$): 3371, 3357, 2989, 1751, 1740, 1645, 1636, 1544, 1429, 1353, 1312, 1220, 814, 528 cm^{-1}.

^{1}H-NMR (400MHz) δ (*d*^{6} dmso): 1.16 (3H, d, *J* = 7.2 Hz, -CH(OH)C<u>H</u>$_3$), 1.19-1.24 (6H, m, -OCH$_2$C<u>H</u>$_3$ x 2) 1.92-1.97 (1H, m, -C<u>H</u>$_2$CH$_2$COOEt), 2.06-2.13 (1H, m, -C<u>H</u>$_2$CH$_2$COOEt), 2.55 (2H, t, *J* = 7.2 Hz, CH$_2$C<u>H</u>$_2$COOEt), 3.68 (3H, s, OC<u>H</u>$_3$), 4.06 (2H, q, *J* = 7.6 Hz, -OC<u>H</u>$_2$CH$_3$), 4.12-4.38 (3H, m, -OC<u>H</u>$_2$CH$_3$ + -C<u>H</u>(OH)CH$_3$), 4.39-4.49 (6H, m, H_{meta} Cp ring + -NHC<u>H</u>- x 2), 4.83 (1H, s, H_{ortho} Cp ring), 4.88 (1H, s, H_{ortho} Cp ring), 4.90 (1H, s, H_{ortho} Cp ring), 4.97 (1H, s, H_{ortho} Cp ring), 5.01 (1H, d, *J* = 7.6 Hz, -CH(O<u>H</u>)CH$_3$), 7.60 (1H, d, *J* = 7.2 Hz, -N<u>H</u>CH-), 8.16 (1H, d, *J* = 8.0 Hz, N<u>H</u>CH-).

^{13}C-NMR (100 MHz) δ (*d*^{6} dmso): 14.44, 20.63, 25.90 (-ve DEPT), 30.49, 51.82, 52.31, 55.27 (-ve DEPT), 58.65, 60.30 (-ve DEPT), 61.04 (-ve DEPT), 66.62, 69.85, 69.94, 70.28, 70.35, 72.38, 72.57, 76.95, 169.43, 169.58, 171.82, 172.09, 172.36.

1, 1'-*N*-ferrocenoyl-(L-threonine methyl ester)-(β-alanine methyl ester) (144)

0.17g of L-threonine methyl ester hydrochloride and 0.14g of β-alanine methyl ester hydrochloride were used in the synthesis.

Yield 0.26g (54%), red viscous oil.

$E_{1/2}$ = 0.334mV (Vs. Fc/Fc+), $[\alpha]_D^{20}$ = - 9° (EtOH), (UV-Vis (λ_{max}) (EtOH): 343, 442 (ε = 189 M^{-1} cm^{-1}), I.R. υ_{max} ($CDCl_3$): 3389, 3362, 3098, 2993, 1742, 1730, 1648, 1641, 1540, 1461, 1310, 1259, 1141, 1011, 689 cm^{-1}.

^{1}H-NMR (400MHz) δ (*d*^{6} dmso): 1.17 (3H, d, *J* = 5.6 Hz, -CH(OH)C<u>H</u>$_3$), 2.60 (2H, t, J = 6.8 Hz, -NHCH$_2$C<u>H</u>$_2$CO-), 3.27 (2H, br. s, -NHC<u>H</u>$_2$CH$_2$CO-), 3.63 (3H, s, OC<u>H</u>$_3$), 3.69 (3H, s, OC<u>H</u>$_3$), 4.16-4.19 (1H, m, -C<u>H</u>(OH)CH$_3$), 4.29 (1H, s, H_{meta} Cp ring), 4.34 (1H, s, H_{meta} Cp ring), 4.39-4.48 (3H, m, H_{meta} Cp ring + -NHC<u>H</u>-), 4.71 (1H, s, H_{ortho} Cp ring), 4.83 (2H, br. s, H_{ortho} Cp ring), 4.97 (1H, s, H_{ortho} Cp ring), 5.02 (1H, d, *J* = 6.8 Hz, -CH(O<u>H</u>)CH$_3$), 7.63 (1H, d, *J* = 8.4 Hz, -N<u>H</u>CH-), 7.97 (1H, t, *J* = 6.0 Hz, -NHC<u>H</u>$_2$-).

^{13}C-NMR (100 MHz) δ (*d*^{6} dmso): 20.64, 34.17 (-ve DEPT), 35.57 (-ve DEPT), 51.73, 52.29, 58.72, 66.64, 69.87, 70.00, 70.17, 71.97, 72.24, 72.67, 76.69, 77.93, 168.94, 169.54, 171.73, 172.27.

1, 1'-*N*-ferrocenoyl-(L-threonine methyl ester)-(γ-aminobutyric acid methyl ester) (145)

0.17g of L-threonine methyl ester hydrochloride and 0.15g of γ-aminobutyric methyl ester hydrochloride were used in the synthesis.

Yield 0.29g (59%), red viscous oil.

$E_{1/2}$ = 0.328mV (Vs. Fc/Fc+), $[\alpha]_D^{20}$ = - 11° (EtOH), (UV-Vis (λ_{max}) (EtOH): 340, 444 nm (ε = 163 M^{-1} cm^{-1}), I.R. υ_{max} ($CDCl_3$): 3367, 3349, 2911, 2362, 1731, 1718, 1641, 1633, 1540, 1441, 1319, 1238, 1160, 1014, 673, 501 cm^{-1}.

^{1}H-NMR (400MHz) δ (*d*^{6} dmso): 1.16 (3H, d, *J* = 6.0 Hz, -CH(OH)C<u>H</u>$_3$), 1.76-1.79 (2H, m, -NHCH$_2$C<u>H</u>$_2$CH$_2$CO-), 2.34 (2H, t, *J* = 7.2 Hz, -NHCH$_2$CH$_2$C<u>H</u>$_2$CO-), 3.19 (2H, m, -NHC<u>H</u>$_2$CH$_2$-), 3.60 (3H, s, OC<u>H</u>$_3$), 3.68 (3H, s, OC<u>H</u>$_3$), 4.18 (1H, m, -C<u>H</u>(OH)CH$_3$), 4.28 (1H, s, H_{meta} Cp ring), 4.33 (1H, s, H_{meta} Cp ring), 4.38-4.42 (1H, m, -NHC<u>H</u>-), 4.43, (2H, br. s, H_{meta} Cp ring), 4.71 (1H, s, H_{ortho} Cp ring), 4.79-4.87 (3H, m, H_{ortho} Cp ring), 5.00 (1H, d, *J* = 4.8 Hz, -CH(O<u>H</u>)CH$_3$), 7.65, 7.69 (1H*, two doublets*, *J* = 8.4 Hz, -N<u>H</u>CH-), 7.90 (1H, t, J = 5.4 Hz, -NHC<u>H</u>$_2$-).

^{13}C-NMR (100 MHz) δ (*d*^{6} dmso): 20.65, 25.02 (-ve DEPT), 31.10 (-ve DEPT), 38.46 (-ve DEPT), 51.64, 52.29, 58.79, 66.63, 69.83, 70.00, 70.17, 71.19, 72.67, 76.99, 78.31, 168.76, 169.18, 171.67, 173.12.

1, 1'-*N*-ferrocenoyl-(L-phenylalanine methyl ester)-(L-aspartic acid dimethyl ester) (146)

0.20g of L-aspartic acid dimethyl ester hydrochloride and 0.22g of L-phenylalanine methyl ester hydrochloride were used in the synthesis.

Yield 0.32g (55%), orange solid, m.p. 100-103°C.

$E_{1/2}$ = 0.352mV (Vs. Fc/Fc+), $[\alpha]_D^{20}$ = - 22° (EtOH), (UV-Vis (λ_{max}) (EtOH): 344, 444 nm (ε = 212 M^{-1} cm^{-1}), I.R. υ_{max} (KBr): 3390, 3358, 2932, 1810, 1750, 1740, 1640, 1630, 1561, 1509, 1408, 1221, 811, 541 cm^{-1}.

^{1}H-NMR (400MHz) δ (d^6 dmso): 2.81 (1H, dd, J_a = 8.4 Hz, J_b = 12.0 Hz, C$\underline{H}_2$COOMe), 2.97 (1H, dd, J_a = 5.4 Hz, J_b = 12.0 Hz, C$\underline{H}_2$COMe), 3.03 (1H, dd, J_a = 11.2 Hz, J_b = 12.8 Hz, -C$\underline{H}_2$Ph), 3.18 (1H, dd, J_a = 4.0 Hz, J_b = 12.8 Hz, -C$\underline{H}_2$Ph), 3.64 (3H, s, OC$\underline{H}_3$), 3.66 (3H, s, OC$\underline{H}_3$), 3.68 (3H, s, OC$\underline{H}_3$), 4.10 (2H, s, H_{meta} Cp ring), 4.32 (1H, s, H_{meta} Cp ring), 4.35 (1H, s, H_{meta} Cp ring), 4.66-4.73 (3H, m, H_{ortho} Cp ring + -NHC$\underline{H}$-), 4.74-4.76 (3H, m, H_{ortho} Cp ring + -NHC$\underline{H}$-), 7.21 (1H, d, J = 6.4 Hz, ArH), 7.30-7.36 (4H, m, ArH), 8.25 (1H, d, J = 7.6 Hz, -N$\underline{H}$CH-), 8.32 (1H, d, J = 8.0 Hz, -N$\underline{H}$CH-).

^{13}C-NMR (100 MHz) δ (d^6 dmso): 35.74 (-ve DEPT), 36.48 (-ve DEPT), 49.21, 52.06, 52.37, 52.62, 53.97, 69.32, 69.45, 70.59, 70.78, 72.31, 72.41, 72.47, 72.60, 76.59, 76.94, 126.63, 128.63, 129.43, 138.17, 169.18, 169.22, 170.99, 171.73, 172.73.

5.10: References

1) T. Dong, L. Li, *J. Organometallic Chem., 509, (1996), 131*
2) G. Iftime, C. Moreau-Bossuet, E. Manoury, G. Balovoine, *Organometallics, 15, (1996), 408.*
3) T. Dong, L. Li, *J. Chem. Soc., Chem. Comm., (1994), 2374.*
4) L. Barisic, V. Rapic, H. Pritskow, G. Pavlovic, I. Nemet, *J. Organometallic Chem., 682, (2003) 131.*
5) A. Patti, G. Nicolosi, *Tetrahedron: Asymmetry, 11, (2000), 3687.*
6) Y. Xu, P. Saweczko, H. B. Kraatz, *J. Organometallic Chem., 637, (2001), 335.*
7) S. Maricic, U. Berg, T. Frejd, *Tetrahedron, 58, (2002), 3085*.
8) Y. Xu, H.B. Kraatz*., Tetrahedron Lett., 42, (2001), 75.*
9) R. Herrick, R. Jarret, T. Curran, D. Dragoli, M. Flaherty, S. Lindeyberg, R. Slate, L. Thornton, *Tetrahedron Lett., 37, (1996), 5289.*

Chapter VI

Anion Binding Studies

6.1: Introduction

Anions are ubiquitous substances in biological and chemical processes, as well as playing a major role in environmental pollution [1]. Not only are the majority of enzyme substrates and co-factors anionic, DNA itself is anionic, and the development of DNA biosensors has, allowed for the successful detection of mutations [2]. The field of anion coordination chemistry has come to prominence in recent years, with electrochemically active anionic receptors of particular interest, as they allow binding of guest anions to be detected by a response at the metal centre [3].

Although the first redox centre-containing receptors were based around the cobaltocenium cation, the bulk of recent work has shifted the emphasis towards ferrocene-based sensors, which offer the possibility to modulate the anion-receptor interaction according to the oxidation state of the iron centre [4]. Structurally, these compounds range from the rather simple ones such as 10 and 11 (section 1.5.2), to larger dendritic structures, such as **147**, prepared by Stone and co-workers [5].

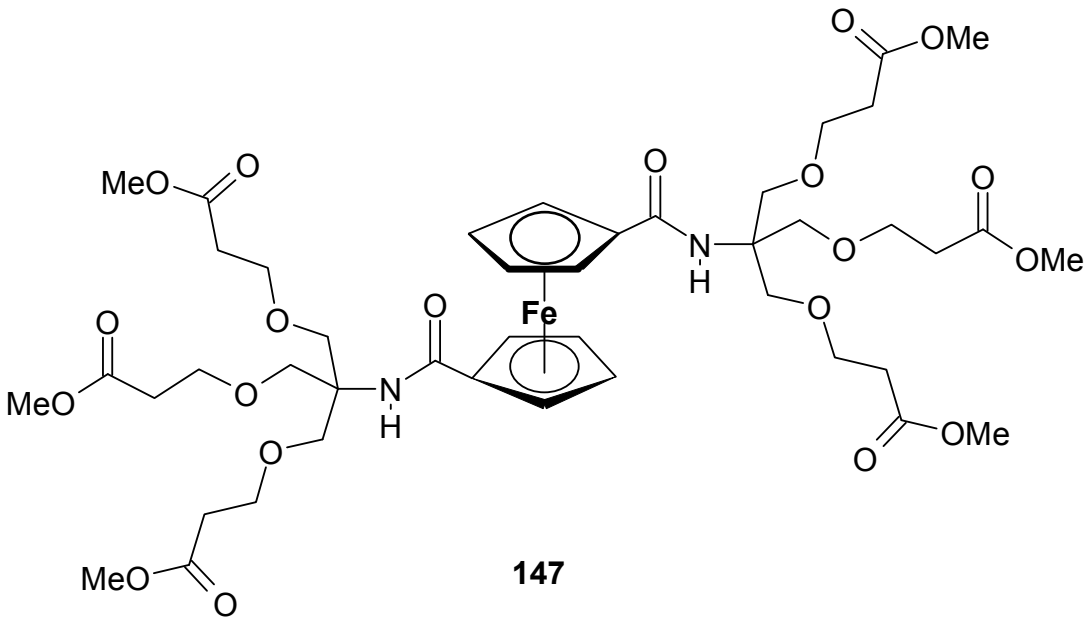

147

The ability of compounds such as **147** to co-ordinate halide anions at the core through hydrogen bonding with the amide protons was poor, due to steric restrictions (determined via ^{1}H-NMR titrations). There was, however, significant anion binding observed in the oxidised ferricenium form, due to electrostatic interactions.

The presence of the amide proton is crucial to the ability of ferrocene-based receptors to coordinate anions, as unsubstituted ferrocene in its neutral form has no inherent attraction for anions, and displays no change in electrochemical behaviour even in the presence of a large excess of anions [6]. Oxidation of amide substituted ferrocenes, however, increases the acidity of the amide proton, making it a better acceptor for electron pairs, and thus there exists a synergy between the electrostatic and hydrogen bonding coordination of guest species [7].

Cyclic amide-substituted ferrocenes such as **148** prepared by Reynes and co-workers, offer a potential advantage in anion sensing, in the respect that they can introduce steric restrictions to the species of anion detected, effectively developing a 'molecular pocket', and hence achieve a greater degree of selectivity [8].

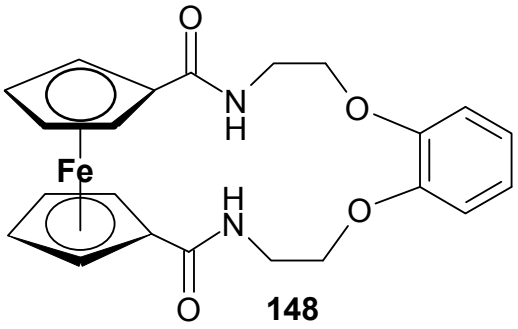

148

The two principal methods of anion detection with ferrocene-based receptors in the literature are ^{1}H-NMR titrations, and cyclic voltammetry, and these techniques were used to determine the effectiveness of the compounds prepared in the previous chapters. As the amide protons of large peptides and proteins are the principal hydrogen bond acceptors in biological systems [9], the choice of ferrocenoyl amino acid derivatives as anionic sensors would seem logical.

6.2: ^{1}H-NMR Titration Studies

As has been discussed in previous chapters, a downfield shift in the ^{1}H-NMR spectrum is observed for amide protons that are involved in hydrogen bonding interactions. Plotting this downfield shift of amide protons against the molar equivalent of anion added can give an indication of the affinity of anionic receptors for various anions. Previous work in this area has indicated that steric factors play an important role here [10], so the compounds chosen

for these experiments were those which have the least bulky substituents vicinal to the amide group.

6.2.1: ^{1}H-NMR Titration Studies of *N*-Ferrocenoyl Amino Acid Derivatives

Three ***N***-ferrocenoyl amino acid derivatives were chosen for this series of experiments, **81**, **82**, and **88**, as these compounds have the least sterically hindered amide protons (*fig. 6*, Ch. 2, section 2.5.3). The downfield shift of their respective amide protons was plotted against the molar equivalent of various anions (Cl^-, Br^-, NO_3^-, HSO_4^-), as their tetra butyl ammonium salts) in $CDCl_3$. *Fig. 1* shows the response of **81**, ***N***-ferrocenoyl-β-alanine methyl ester, to these anions.

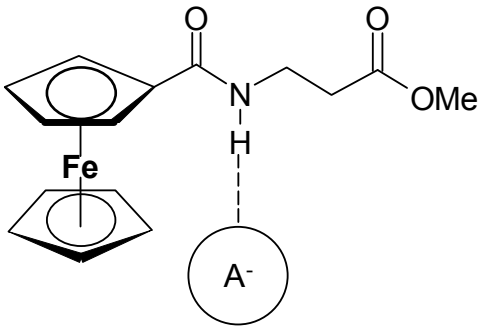

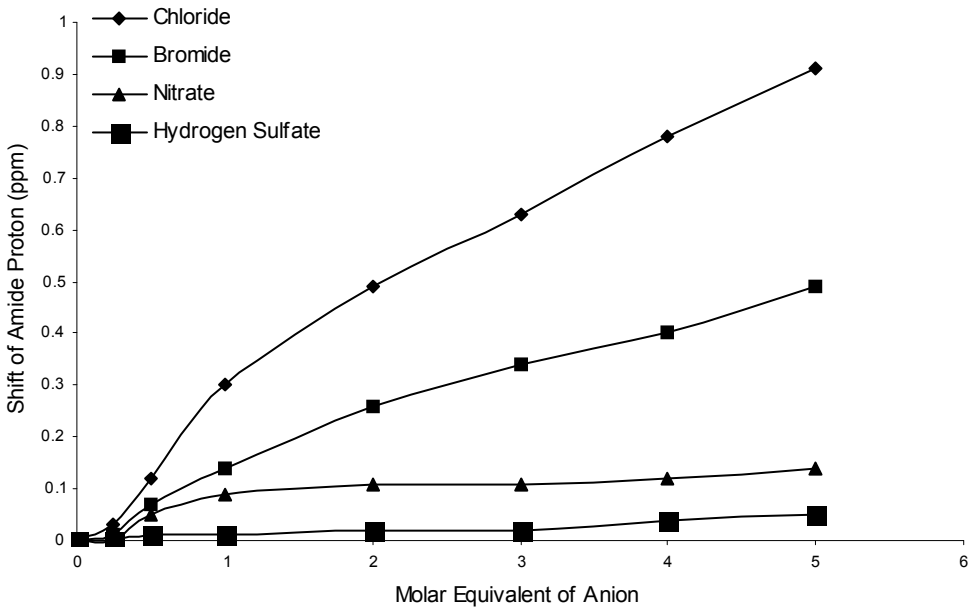

*Fig. 1: The downfield shift of the amide proton of **81** vs. molar equivalent of anion, in $CDCl_3$.*

What is noticeable from *fig. 1* is the far greater response to halide anions than to either nitrate or hydrogen sulphate. Both nitrate and hydrogen sulphate anions are poor bases, and so would have little affinity for the moderately acidic amide proton. The halide anions have a relatively high charge density, and as such are capable of producing a relatively large response in the ^{1}H-NMR spectrum. The chloride ion has a smaller ionic radius relative to bromide, and therefore a higher charge density, and thus produces a greater response. Similar responses to these anions were recorded with compound **82**. What is also noteworthy from *fig. 1* is the absence of a 'plateau' in the response to these anions, and as such, no true selectivity can be claimed for these receptors.

It will be recalled from section 2.5.3 that the amide proton of compound **88** appears at 7.71 ppm in its ^{1}H-NMR spectrum in $CDCl_3$ (vs. 6.26 and 6.29 ppm for **81** and **82** respectively), i.e. this proton is already engaged in *intra*-molecular hydrogen bonding, and as such, the presence of even a five-fold excess of anions produces minimal response in terms of chemical shift. This can be seen in *fig. 2*, which compares the downfield shift of the amide protons of **81**, **82** and **88** to various molar equivalents of chloride anion.

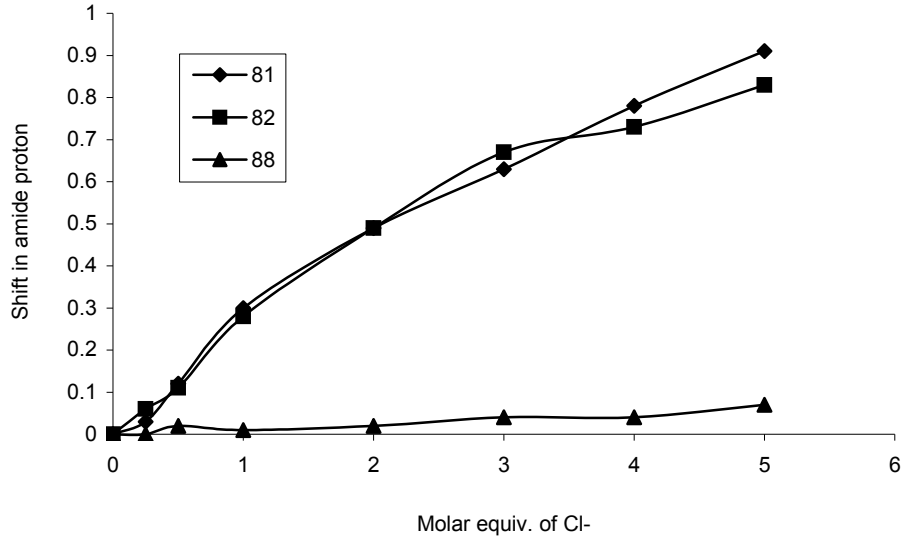

*Fig. 2: The downfield shift of the amide proton of **81**, **82**, and **88** vs. molar equivalent of Cl^-, in $CDCl_3$.*

What is apparent from *fig. 2* is that the stable conformation adopted by **88** in solution is largely unperturbed in the presence of anions, therefore making it a poor candidate for anion binding studies. A summary of the results obtained is given in the experimental section.

6.2.2: ^{1}H-NMR Titration Studies of *N*-Ferrocenoyl Monosubstituted Dipeptides.

For this series of experiments, the dipeptides **109-111** were chosen as candidates for anion receptors. It will be recalled from section 3.4.2 and 3.6 that in $CDCl_3$, the ***N***-terminal amide protons of **109** and **110** form *intra*-molecular hydrogen bonds with the ***C***-terminal ester oxygen atoms, and even in the absence of anions, show considerable downfield shifts (7.5 and 7.7 ppm respectively). In each case, it is only the ***C***-terminal amide proton which shows any response towards various concentrations. *Fig. 3* shows the downfield shift of ***C***-terminal amide proton of **109** in the presence of various concentrations of the same anions as were employed in the previous section.

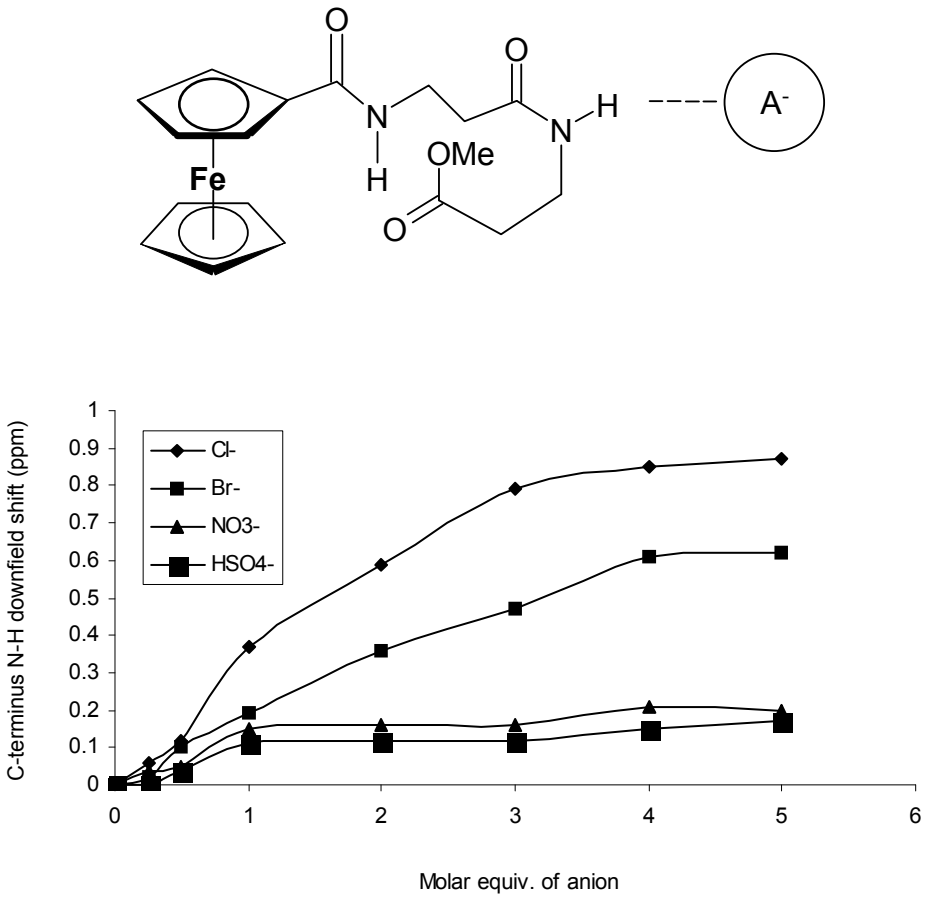

*Fig. 3: The downfield shift of the **C**-terminal amide proton of **109** vs. molar equivalent of anion, in $CDCl_3$.*

The extent to which the chemical shift of each amide proton is affected in the presence of chloride ions can be seen in *fig. 4*.

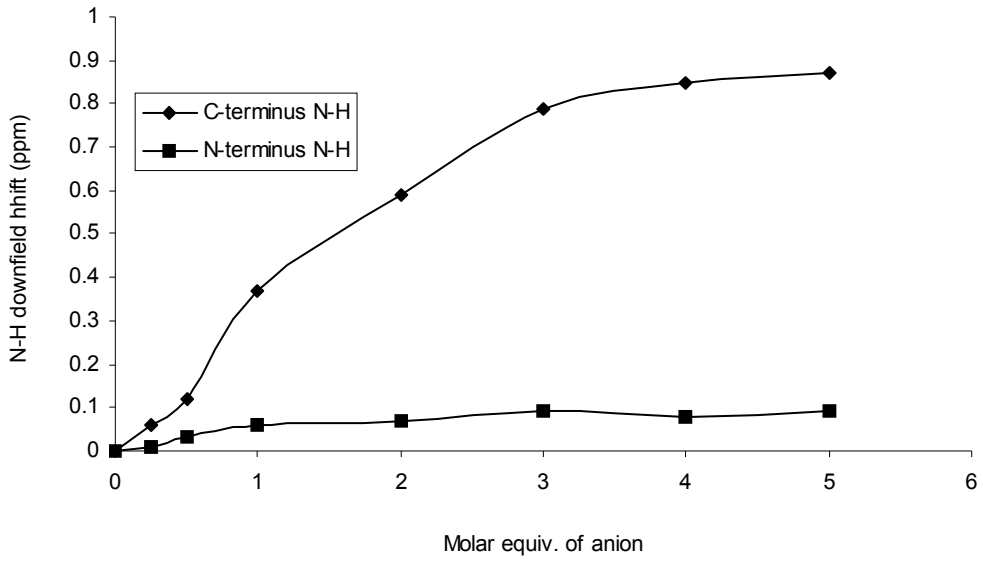

*Fig. 4: The downfield shifts of the **C**- and **N**- terminal amide protons of **109** in the presence of chloride ions.*

Figures 3 and *4* show a clear plateau region in response to both chloride and bromide ions, which is indicative of selectivity towards these species. **110** show a similar response to these anions, with only the ***C***-terminal amide proton showing significant downfield shifts, and plateaus being observed for both the halide ions. Again, both nitrate and hydrogen sulphate anions produce minimal response in the chemical shift.

As discussed in section 3.4.2, the amide protons of **111** appear as a convoluted signal in the ^{1}H-NMR spectrum in $CDCl_3$ at 7.7 ppm, which suggests that they both participate in *intra*-molecular hydrogen bonds. It would appear that, as was the case with the amino acid ester analogue **88**, the conformation adopted by **111** remains unaltered in the presence of these anions, with neither substantial downfield chemical shifts (< 0.12 ppm), nor any divergence of the convoluted signal being recorded.

6.2.3: ^{1}H-NMR Titration Studies of 1, 1'-*N*-Ferrocenoyl Symmetric Dipeptides.

Compounds **126-129**, as well as the tetra-peptide **130**, were chosen for this series of experiments. It will be recalled from section 3.3.3 that the amide protons in **126-129** all appear *ca*. 8 ppm in their ^{1}H-NMR spectrum in $CDCl_3$, i.e. they already form intra-molecular hydrogen bonds, and, without exception, show minimal response to even a ten-fold excess of ions, making them poor candidates for ion recognition.

Only the ***N***-terminal amide protons of the tetra-peptide **130** participate in intra-molecular hydrogen bonds, with those of the ***C***-terminal appearing at 6.57 ppm in its ^{1}H-NMR spectrum in $CDCl_3$. These latter protons show large downfield shifts in the presence of halide ions (> 1.0 ppm), as can be seen in *fig. 5*.

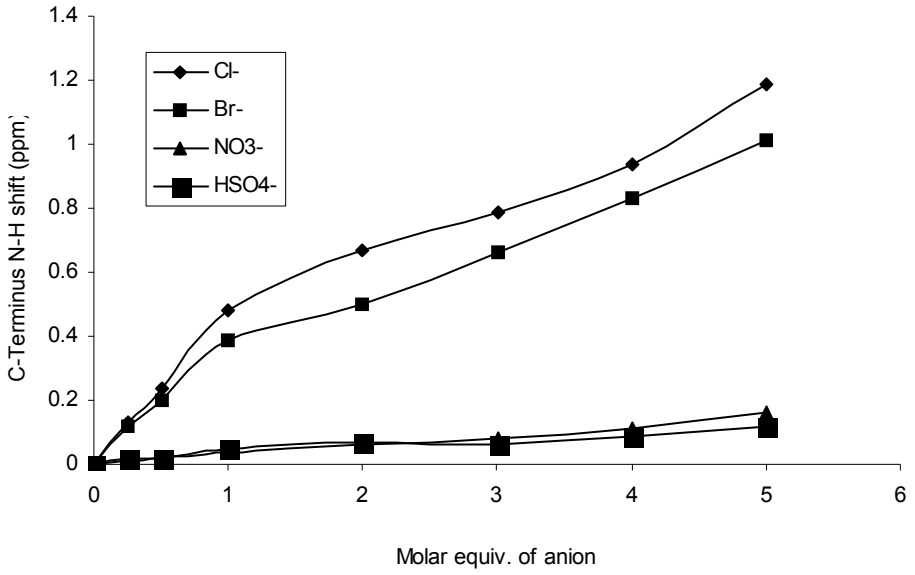

*Fig. 5: The downfield shift of the **C**-terminal amide protons of **130** vs. molar equivalent of anion, in $CDCl_3$.*

The ***C***-terminal amide protons show the greatest response towards halide ions of any compound investigated, although no plateau region is observed for any of the ions used, and as such no selectivity can be claimed for this compound. It should be also noted that in the ^{1}H-NMR spectrum of **130** in $CDCl_3$, ***C***-terminal amide protons appear as one signal integrating for two protons, and this remains the case even in a large excess of halide ions, i.e. both of these ***C***-terminal protons contribute equally toward the binding of anions, and there is no divergence of this signal.

6.3: Electrochemical Anion Binding Studies

As mentioned in section 1.5.2, the Fe^{II}/Fe^{III} redox system can show significant cathodic shifts in the presence of excess amounts of certain simple anions. The same compounds which were used in the ^{1}H-NMR experiments were employed as potential electrochemical sensors in this work. The ions chosen were chloride, nitrate, iodide, tetrafluoroborate, and hydrogen sulphate (as their tetrabutyl ammonium salts). As the redox potential of the bromide anion is too close to that of the ferrocene/ferricenium redox couple, it was not a suitable candidate for these studies.

6.3.1: Electrochemical Anion Binding Studies of *N*-Ferrocenoyl Amino Acid Derivatives

It should be stressed here again that the three ***N***-ferrocenoyl amino acid derivatives selected for these studies, **81**, **82** and **88**, were chosen because their structure in the vicinity of the amide proton would be unlikely to impede anionic complexation. All three showed cathodic shifts *ca*. 40 mV in the presence of a ten-fold excess of chloride and iodide, and minimal response in the presence of nitrate, tetrafluoroborate, and hydrogen sulphate. The results are summarized in *table 1*.

Compound	HSO_4^-	Cl^-	NO_3^-	BF_4^-	I^-
81	-4	-41	+2	+1	-24
82	-6	-40	+5	+4	-20
88	-1	-37	+5	+6	-21

*Table 1: The $\Delta E_{1/2}$ in redox potential of **81**, **82** and **88** in the presence of a ten-fold excess of various ions (cathodic shifts are assigned –ve values).*

The previous anion binding studies performed with ferrocenoyl peptide derivatives only made use of linear sweep voltammetry (i.e. the oxidation wave) [11], and while cathodic shifts in the presence of various anions were noted, the effect on the corresponding reduction wave was not recorded. Disappearance of the reduction wave is indicative of an irreversible oxidation, and hence strong guest-host interaction.

All three compounds showed very similar responses to each anion. The voltammograms of **81**, in the presence of chloride and iodide anions are shown in *fig. 6*. It can be clearly seen from *fig. 6* is that there is a noticeable cathodic shift in the cyclic voltammogram of **81** caused by the presence of chloride anion.

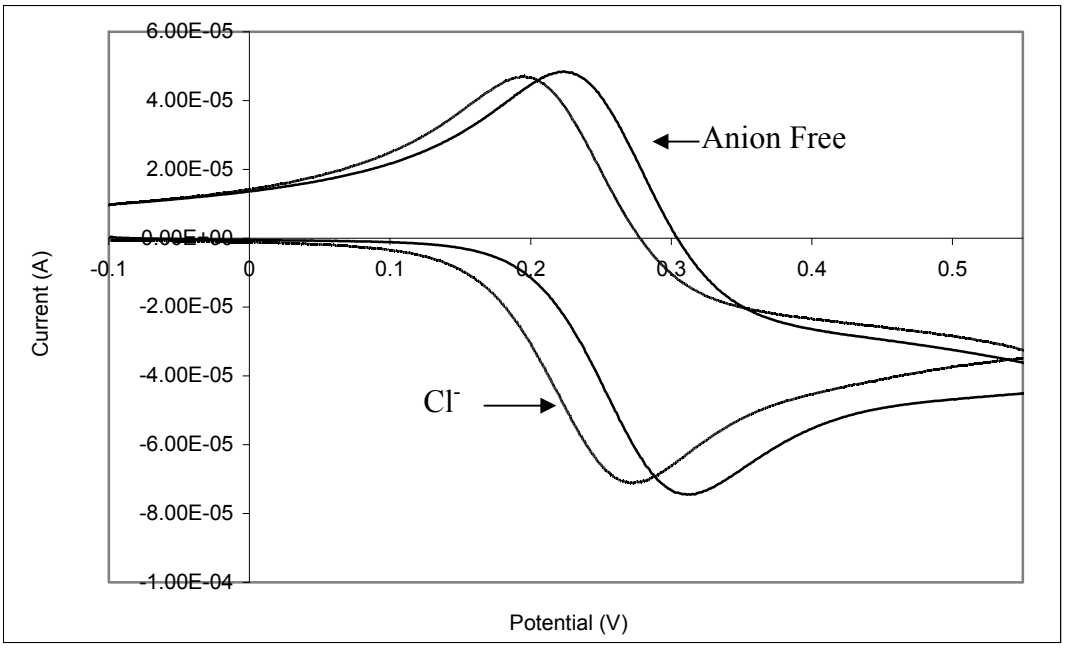

Fig. 6: The cyclic voltammograms of **81***, anion free and in the presence of chloride ions.*

There is little if any reduction in the intensity of the reduction wave (the portion of the wave which gives positive values of the response current). In other words, the one electron oxidation of the ferrocenoyl group remains *reversible* in the presence of these anions, even though an anion would tend to stabilize the ferricenium cation, thus inhibiting reduction. It has previously been reported that anionic sensors incorporating the ferrocene moiety can undergo irreversible oxidation in the presence of anionic species, with a subsequent disappearance of the reduction wave in the cyclic voltammogram [12]. This, however, does not appear to be the case with compounds **81**, **82** and **88**. This would be suggestive of weak guest-host interaction. Chloride ions induce a greater cathodic shift in the voltammograms of **81**, **82** and **88**, than do iodide anions. This is not surprising, due to the smaller chloride anion having a greater charge density than the larger iodide.

Hydrogen sulphate anion had minimal effect on the redox potential of **81**, **82** and **88**. As stated previously, this ion is a poor base, and has less attraction for the amide proton. This is

in agreement with the results recorded during the ^{1}H-NMR titration experiments. These observations would suggest that the amide proton plays a crucial role in 'anchoring' the anionic species in close proximity to the iron centre of the ferrocene moiety, thus inducing a change in its electrochemical behaviour.

An interesting observation in this series of experiments is the induction of a slight *anodic* shift in the cyclic voltammograms of **81**, **82** and **88** by nitrate and tetrafluoroborate anions. A possible explanation for this observation is the fact that not only do these anions have very little affinity for the amide protons of **81**, **82** and **88**, but each of these anions has a central atom with a relatively high positive charge density, the proximity of which to the iron centre could destabilize the ferricenium cation, i.e. make oxidation more difficult.

6.3.2: Electrochemical Anion Binding Studies of *N*-Ferrocenoyl Monosubstituted Dipeptides

It has already been noted that, in the presence of various anions, similar downfield shifts in the ***C***-terminal amide protons were observed in the case of the dipeptides **109-111**, than was recorded for the amino acid derivatives **81**, **82** and **88**, although the ***N***-terminal protons remained largely unaffected. However, the presence of two hydrogen-bond-accepting amide protons can potentially alter the ability of the receptor to complex an anion, and hence affect the electrochemical behaviour of the ferrocene moiety.

The receptors **109-111** showed very similar responses to each anion, with the halides producing significant cathodic shifts in the oxidation portion of their cyclic voltammograms, and these results are summarised in *table 2*. These responses were, however, radically different to that observed the amino acid derivatives, as can be seen in *fig. 7*.

Compound	HSO_4^-	Cl^-	NO_3^-	BF_4^-	I^-
109	-4	-42*	+0	+1	-28*
110	-8	-37*	+4	+4	-26*
111	-1	-39*	+2	+6	-25*

Table 2: The $\Delta E_{1/2\ in}$ redox potential of **109-111***, in the presence of a five-fold excess of various ions (cathodic shifts are assigned –ve values).*

**Values calculated from the difference in oxidation peaks due to loss of reduction peak.*

What is most obvious from these voltammograms is the complete disappearance of the reduction wave caused by the complexation of the halide ions. This is indicative of an irreversible oxidation having taken place. In order to investigate this observation further, the scan rate was reduced from 0.1V/sec to 0.02V/sec. It is known that a reduction in scan rate can, in some cases, cause the reappearance of a reduction wave by allowing the electroactive species more time to diffuse towards the electrode [13]. Even at this reduced scan rate, no reduction wave was observed in the voltammograms of **109-111** in the presence of halide ions. *Fig. 7* shows the voltammograms of **109**, both in the absence and presence of iodide ions.

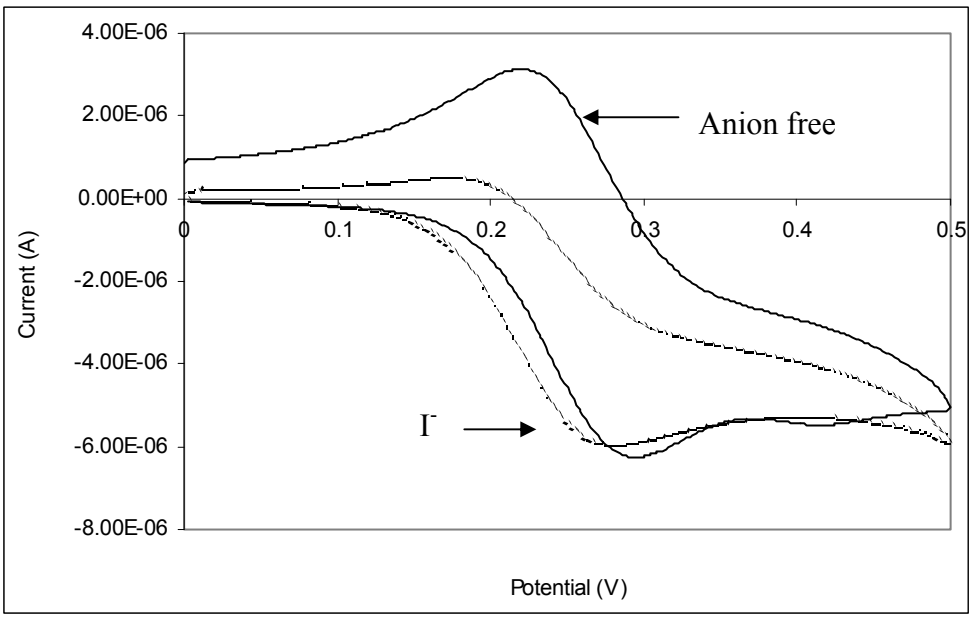

*Fig. 7: The loss in reduction peak in the cyclic voltammogram of **109** in the presence of iodide ions.*

A similar disappearance of the reduction wave was observed in the voltammograms of **110** and **111** in the presence of halide ions. This is indicative of an *EC* mechanism, i.e. after the electron loss upon oxidation, a chemical process occurs whereby reduction is inhibited (e.g. adsorption of the ion pair onto the surface of the working electrode [14]. These results would suggest that the presence of two amide protons does indeed result in much stronger complexation of halide anions with compounds **109-111** than was seen to be the case with their amino acid derivative analogues **81**, **82** and **88**. Previous work in this area has shown the strength of complexation to be sensitive to the number of both ferrocene groups and

amide protons [15]. Although the chemical shifts of the ***N***-terminal amide protons of these dipeptides were shown to remain largely unaltered in the presence of halide ions in the ^{1}H-NMR titration studies, the electrochemical investigations would suggest that they do play a role in the 'anchoring' of the anion close to the ferrocene moiety's iron centre.

What is also apparent is that, given the very similar behaviour of **109-111** in the presence of each individual anion, altering the length of the peptide backbone does not induce any noticeable difference in binding ability of these receptors.

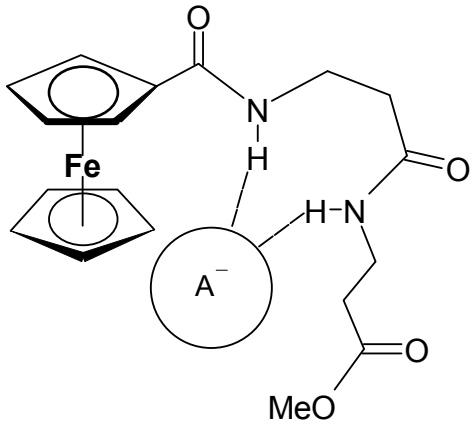

*Fig. 8: Interaction of the two amide protons of **109** with anionic species, which may account for the irreversible oxidation observed in the cyclic voltammograms.*

As was the case with **81**, **82** and **88**, minimal response was observed in the voltammograms of **109-111** in the presence of hydrogen sulphate, nitrate, or tetrafluoroborate anions. Clearly, the presence of the second amide proton does not affect their lack of affinity for complexation. In the case of the latter two anions, once again a small anodic shift is induced in the voltammograms of each ***N***-ferrocenoyl dipeptide.

6.3.3: Electrochemical Anion Binding Studies of 1, 1'-*N*-Ferrocenoyl Symmetric Dipeptides

As is the case with the monosubstituted ***N***-ferrocenoyl dipeptides, the 1, 1'-*N*-ferrocenoyl dipeptides have two amide protons available for hydrogen-bonding to an anion, the difference being their relative spatial arrangement. These protons are located closer to the iron centre of the ferrocenoyl group, and could, in theory, complex anions in such a way as to cause a greater electrochemical response than was observed with **109-111**. It should be

reiterated, however, that none of these compounds showed significant downfield shifts in the presence of anions during the ^{1}H-NMR titration studies. The 1, 1'-***N***-ferrocenoyl derivatives of glycine, β-alanine, γ-aminobutyric acid, and valeric acid methyl esters, **126-129** respectively, were chosen for these investigations. The results obtained are summarised in *table 3*.

Compound	**HSO_4^-**	**Cl^-**	**$NO3^-$**	**$BF4^-$**	**I^-**
126	-1	-32*	+1	+2	-20*
127	-3	-33*	+7	+0	-19*
128	0	-30*	+2	+5	-17*
129	-5	-31*	+0	+4	-21*
130	0	-31*	+1	+1	-19*

Table 3: The $\Delta E_{1/2}$ in redox potential of **126-129** *in the presence of a five-fold excess of various ions (cathodic shifts are assigned –ve values).*

**Values calculated from the difference in oxidation peaks due to loss of reduction peak.*

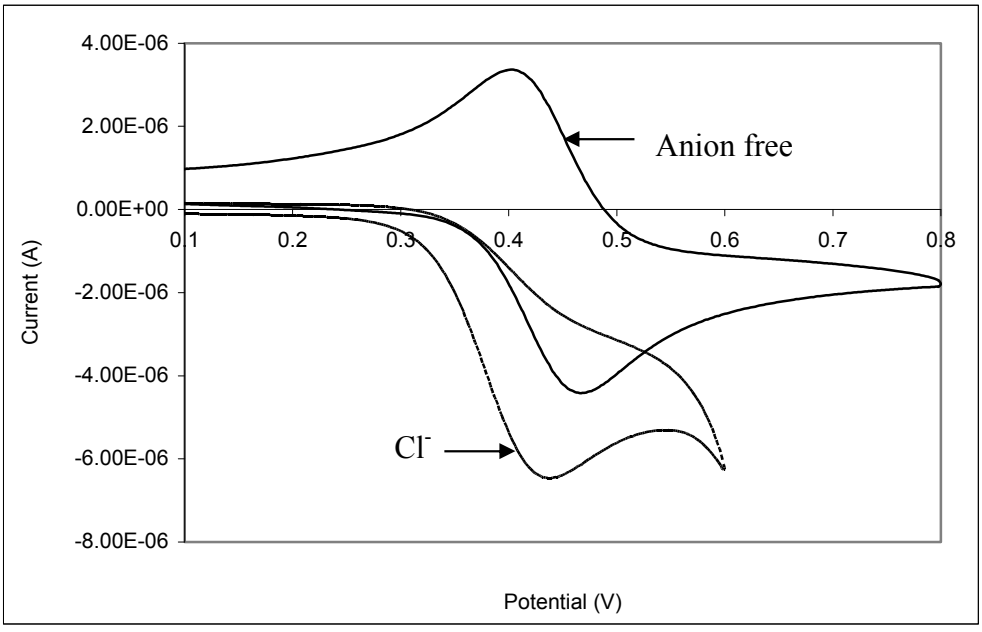

Fig. 9: The loss in reduction peak in the cyclic voltammogram of ***127*** *in the presence of chloride ions.*

The cyclic voltammograms of **127**, on its own and in the presence of chloride ions, is shown in *fig. 9.* As was observed in the case of the monosubstituted ***N***-ferrocenoyl dipeptides, an irreversible oxidation of the ferrocenoyl group occurs in the presence of both chloride and iodide ions. This observation further reinforces the argument that the presence of two amide protons is crucial to the strength of anion complexation. The cathodic shift in the oxidation wave recorded is slightly less pronounced for the 1, 1'-***N***-ferrocenoyl dipeptides than was observed for any of the mono substituted ***N***-ferrocenoyl receptors. These results would suggest that the anion is, upon complexation, not held in as close proximity to the iron centre, due to the spatial arrangement of these amide protons within each receptor. Again, the loss of the reduction portion of the cyclic voltammogram is evidence of an *EC* mechanism.

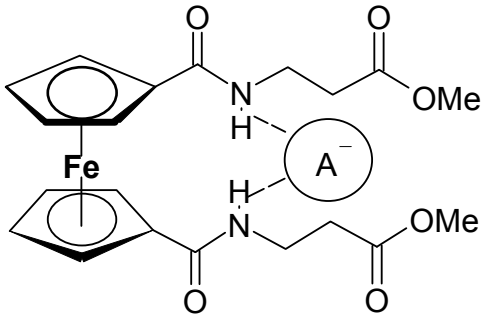

*Fig. 10: Interaction of the two amide protons of **127** with anionic species.*

As previously mentioned, in the ^{1}H-NMR titration experiments, the amide protons of compounds **126-129** appear as one triplet, and remain so, even in the presence of a ten-fold excess of anion. This would suggest that both protons, although relatively unperturbed in terms of their downfield chemical shifts, contribute equally in complexation of the anion. What is likely, however, given the ionic radius of the chloride and iodide anions (1.67 and 2.07 Å respectively [15]), and the spacing of the cyclopentadienyl rings of ferrocene (3.3 Å – the amide protons would be expected to remain roughly co-planar with the Cp rings in solution [16]), is that the 1, 1'-conformation could still be maintained during the binding of these anions to both protons, though exactly what conformation is adopted is difficult to unambiguously assign.

As was the case with the monosubstituted receptors, minimal response was observed in the voltammograms of **109-111** in the presence of hydrogen sulphate, nitrate, or

tetrafluoroborate anions. Clearly, the presence of the second amide proton does not affect their lack of affinity for complexation. This is illustrated in *fig. 11*, which shows the voltammograms of **127**, both in the presence and absence of hydrogen sulfate. In the case of the latter two anions, once again a small anodic shift is induced in the voltammograms of each 1, 1'-***N***-ferrocenoyl dipeptide, as can be seen from *fig. 11*.

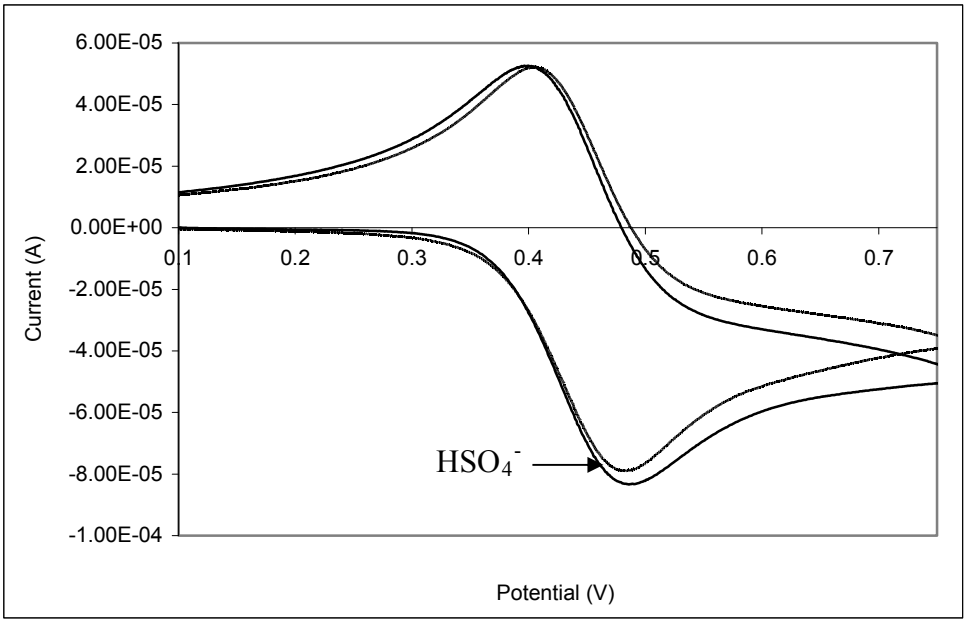

*Fig. 11: The cyclic voltammograms of **127**, both anion free and in the presence of hydrogen sulphate ions.*

The ***N***-ferrocenoyl tetrapeptide **130** shows a very similar pattern of responses to that which is observed for its dipeptide analogue **126**. It was shown during the ^{1}H-NMR titration studies that the ***C***-terminal amide protons clearly interact with halide ions, though anion binding here may occur too far away from the electroactive iron centre to be sensed in the cyclic voltammograms.

6.4: Conclusions

A total of ten potential receptors were tested for their ^{1}H-NMR and voltammetric behaviour in the presence of various anions, and in all cases, only the halide ions produced a significant response. The anions BF_4^-, NO_3^-, and HSO_4^-, being poor bases, appear to have little affinity for the amide protons of these compounds, the net result of which is very weak guest-host interactions.

In the ^{1}H-NMR titration studies, only those amide protons which do not participate in *intra*-molecular hydrogen bonds show any significant downfield shifts in the presence of halide ions. These include the single amide protons of **81** and **82**, and those of the ***C***-terminal of **109** and **111**. The ***C***-terminal protons of compound **130**, 1, 1'-***N***-ferrocenoyl-((glycine)$_2$ ethyl ester)$_2$, show the largest response of all to halide ions, although the only encouraging results in terms of selectivity was found in the case of **109** and **111**, whose titration plots showed a 'plateau' in response to increasing concentration of halide ions.

Halide ions also induce noteworthy perturbations in the cyclic voltammograms of all compounds tested, with cathodic shifts of ca. 40mV being observed for the monosubstituted compounds in the presence of chloride ions, and ca. 30mV for the 1, 1'-disubstituted compounds. Due to its larger ionic radius, and hence more diffuse charge density, iodide ions produced smaller cathodic shifts.

Those compounds which include two amide protons (the ***N***-ferrocenoyl monosubstituted dipeptides and the 1, 1'-***N***-ferrocenoyl symmetric dipeptides) showed a loss of the reduction portion of the wave in their cyclic voltammograms in the presence of halide ions, indicative of irreversible binding and an *EC* mechanism at work. It is clear that these two protons play a crucial role in the complexation of the halides, even if the response is almost undetectable in the ^{1}H-NMR titrations. It is also clear that the number of methylene groups in the peptide backbone has little effect on the ability of these compounds to complex anions, either in terms of voltammetric response, or selectivity of one anion over another.

6.5: References

1) P.D. Beer, *Inorg. Chem., 36, (1997), 2112.*
2) Y. Xu, H.B. Kraatz*., Tetrahedron Lett., 42, (2001), 75.*
3) P.D. Beer, M.I. Ogden, D.B. Crowe, B. Main, *J.C.S. Dalton Trans., (1993), 2107.*
4) R.H. Crabtree*,* K. Kavallieratos, S. Wang, *Inorg. Chem., 38, (1999), 5184.*
5) D.L. Stone, D.K. Smith, *Polyhedron, 22, (2003), 763.*
6) P.D. Beer, M.G.B. Drew, R. Jagessar, *J. Chem. Soc., Dalton Trans.,(1997), 881.*
7) C. Valerio, J.L. Fillaut, C. Valero, J. Ruiz, J. Guitlard, D. Austruc*, J. Am. Chem. Soc., 119, (1997), 2588.*
8) O. Reynes, F. Maillard, J.C. Moutet, G. Royal, *J. Organometallic Chem., 637-639, (2001), 356.*
9) G. Zubay, *Biochemistry, 3rd ed., WCB Publishers, (1993).*

10) M. Sheehy, *The Design and Synthesis of Novel Peptide Derivatives as Malarial Protease Inhibitors and Electrochemical Anion Sensing Receptors, Ph.D. Thesis, DCU, (1999).*
11) J.F. Gallagher, P.T.M. Kenny, M.J. Sheehy, *Inorg. Chem. Comm., 2, (1999), 200.*
12) P.D. Beer*, Co-Ord. Chem. Rev., 205, (2000), 131.*
13) P.W. Atkins, *Phsyical Chemistry, 5th Ed., Oxford University Press, (1994).*
14) P.D. Beer, Z. Chen, A.R. Goulden, S.E. Stokes, *J. Chem. Soc., Chem. Comm., (1992), 270.*
15) D.L. Stone, D.K. Smith, P.T McGrail, *, J. Am. Chem. Soc., 124, (2002), 856.*

Appendix I

Experimental Section:

All reagents were purchased from Sigma/Aldrich, and were used as received without further purification. All solvents were used without drying unless stated. No attempt to exclude air from reactions was made unless stated.

Melting points were determined using a Steward Scientific melting point apparatus. ^{1}H-NMR and ^{13}C NMR spectra were recorded on a Bruker AC 400 NMR spectrometer, operating at 400MHz for ^{1}H-NMR and 100MHz for ^{13}C NMR. All chemical shifts (δ) are reported in ppm relative to tetramethylsilene. Coupling constants (*J*) are reported in Hertz. All infrared spectra were recorded on a Nicolet – Impact 410 FT-IR spectrophotometer.

All UV-Vis spectra were recorded on a Varian Cary 50 Scan UV-Vis spectrophotometer.

All optical rotations were recorded on a Perkin-Elmer polarimeter, model 343, (598nm, 1x 10^{4} ppm in EtOH)

All cyclic voltammogramms were recorded on a CH Instruments electrochemical workstation, model 660, with a 0.1M solution of $TBABF_4$ in CH_3CN as a supporting electrolyte, at a scan rate of 0.1V/sec, using an Ag/Ag^{+} (10mM $AgNO_3$ in CH_3CN) reference electrode.

Appendix II

Abbreviations:

AA	Amino Acid
Ac.	Acetyl
Ar.	Aryl
Bn.	Benzyl
BOC	*tert*-Butyloxycarbonyl
CDI	Carbonyldiimidazole
DCC	Dicyclohexylcarbodiimide
DCM	Dichloromethane
DMF	Dimethylformamide
Conc.	Concentrated
DNA	Deoxyribonucleic Acid
$E_{1/2}$	Half-Wave Potential
Equiv.	Equivalent
Et_3N	Triethylamine
HOBt	1-Hydroxybenzotriazole
HBr	Hydrobromic Acid
HCl	Hydrochloric Acid
hr.	Hour
IR	InfraRed
M	Molar
ml	Millilitre
mmol	Millimole
mol	Mole
m.p.	Melting Point
NMR	Nuclear Magnetic Resonance
RNA	Ribonucleic Acid
r.t.	Room Temperature
SOCl2	Thionyl Chloride
TBTU	O- (1H-benzotriazol-1-yl)-*N, N, N', N*', -tetrmethlyuronium tetrafluoroborate

TFA	Trifluoroacetic Acid
TLC	Thin Layer Chromatography
Z	Benzyloxycarbonyl

The Synthesis, Characterisation, and Application of Novel *N*-Ferrocenoyl Peptide Derivatives

Noel Brennan

Ph.D. 2010

Noel Brennan Ph.D. 2010